UNDERSTANDING THE SPATIAL AND TEMPORAL DISTRIBUTION OF PER- AND POLYFLUORINATED COMPOUNDS IN ATMOSPHERIC DEPOSITION

Daniel Persaud

A dissertation submitted to the Faculty of Graduate studies in partial fulfillment of the requirements for the degree of Doctor of Philosophy

Graduate Program in Chemistry

York University

Toronto, ON

March 2026

Abstract

Per-and polyfluoroalkyl substances (PFAS) are persistent anthropogenic compounds that are distributed globally. However, uncertainties remain regarding dominant sources, long-range transport pathways, and atmospheric deposition mechanisms. This thesis advances the understanding of the spatial and temporal distribution of PFAS by analyzing atmospheric deposition across Arctic, boreal, urban, and tropical environments. To elucidate temporal trends, a 16 meter ice core from the Mt. Oxford icefield, Ellesmere Island provided a continuous 50-year deposition record (1967–2016). Analysis revealed an increase in PFCA deposition after the 1990s. Homologue correlations, molar concentration ratios, and model comparisons suggest that PFCAs are primarily formed through oxidation of volatile precursors. In contrast, PFSAs showed no discernible trend, with episodic deposition observed before 1990, which may be linked to historical Arctic military activities. Spatial patterns in PFAS deposition were examined across the Newfoundland and Labrador Boreal Ecosystem Latitudinal Transect using integrated atmospheric deposition samples collected between 2013–2016. We also quantitively separate wet and dry deposition fluxes for perfluorobutanoic acid (PFBA), perfluorooctanoic acid (PFOA), and perfluorononanoic acid (PFNA). We found that the dry deposition contribution was equal to or greater than the wet deposition flux. This research also specifically focused on trifluoroacetic acid (TFA), a highly persistent and mobile ultrashort chain PFAS. We quantified TFA in total, wet and dry deposition samples in Toronto, Canada between 2018–2024. Seasonal variations showed fluxes peaking in summer months and a decrease in 2020, coinciding with COVID-19 lockdown measures. This work provided the first field-based quantification of TFA in dry deposition, demonstrating that it is a significant and previously underrepresented removal pathway. Finally, a novel hemispheric comparison found substantial TFA deposition at both a tropical site in Georgetown, Guyana (1014–6641 μg m^{-2} a^{-1}) and a temperate residential site in Lambton County, Canada (1969–5863 μg m^{-2} a^{-1}), confirming the global reach of TFA. Collectively, this thesis demonstrates that PFAS distribution by the atmosphere is governed by complex interactions between direct emissions, atmospheric transformation of precursors, and seasonally variable deposition processes.

Acknowledgements

To complete a PhD is a significant undertaking, and it is a journey that cannot be walked alone. It requires a village of individuals to offer support, consolidation, and encouragement along the way. I have been immensely fortunate to have such a community, and I will be forever thankful for the support.

First and foremost, I would be remiss if I did not thank my supervisor Cora J. Young, who took a chance on me as an international student and provided me with the invaluable opportunity to pursue my graduate studies. Her unwavering guidance, immense patience and insightful mentorship have been the cornerstone of my journey. During our talks, I always admired her positive attitude and solution-oriented approach to every challenge; her ability to navigate complexity with optimism not only fostered a resilient research environment but also served as an invaluable lesson in scientific leadership. Thank you for teaching me everything I know about analytical and atmospheric chemistry and beyond.

I would also like to thank the numerous mentors who guided me throughout this journey. My sincere thanks to Dr. Trevor VandenBoer for his support and guidance over the years and for introducing me to the challenge of building custom equipment. Despite the occasional frustration that comes with such intricate work, it taught me resilience and patience. I thank Rob McLaren for your words of advice and always encouraging me to be better. I would like to extend heartfelt thanks to Amila De Silva from the Canadian Centre for Inland waters for introducing me to ice core sectioning and analysis. I am grateful to Hayley Hung, for the incredible opportunity to work at Environment and Climate Change Canada. You have an amazing ability to organize and optimize sampling campaigns. I will always remember our (intense) fieldwork in Quebec City.

I would also like to acknowledge the many contributions from both collaborators and co-authors. Special thanks to Alison Criscitiello for her pivotal role in coordinating field operations and collecting and dating the ice core. I am grateful to Christine Spencer and Cassandra Brinovcar for their assistance with the ice core extraction and analysis. My thanks also go to Heetasmin Singh and the staff of the University of Guyana for all their support with establishing the sampling site. I am also indebted to Derek Muir, Igor

Lehnherr, Sue Ziegler, Kate Edwards, Brian Place and Shira Joudan for input on various manuscripts.

Thank you to the past and present members of the Young and VandenBoer research groups. It was a true honor to work alongside and learn from a such a talented and supportive group of scientists. I am particularly grateful to Jessica, Shira and Mayre for their help with any issues that arise with the IC-MS. Special shout out to my office mate Leyla, whose sound advice both in and out of the lab, was a constant source of guidance and perspective. Also, to my unofficial lab mate, Danial F who is always present, our conversations will not be forgotten. I would also like to recognize my recent colleagues in the Organic Analysis Lab at Environment and Climate Change Canada, especially Alex and Chuba who taught me everything I know about operating the LC-Orbitrap and ensured a seamless transition into my new role.

I would like to thank my family for their unwavering support through my endless studies. The values that you have instilled in me over the years is why I am the man I am today, and I cannot thank you enough. A special and heartfelt thanks must go to my partner, Bhasanie Persaud. You have been my rock, my confidante, and my greatest champion. Your unwavering belief in me, your patience through the long hours and missed weekends, and your incredible strength in shouldering extra responsibilities so I could focus, made this achievement possible. This journey was as much yours as it was mine.

Finally, I would like to thank my daughter, Marie Anayah Persaud. You have been my greatest source of motivation and my most profound joy throughout this demanding journey. Your presence has given me a purpose that extends beyond this PhD. The love and light that you bring into my life have been a constant source of strength during the most challenging times. *This work is dedicated to you* – may it serve as a testament that with perseverance and hard work, no goal is out of reach. I hope one day you will look back on this achievement with pride, knowing that you were my inspiration.

Table of contents

LIST OF FIGURES

CHAPTER 1 Page

CHAPTER 2

CHAPTER 3

LIST OF TABLES

List of Symbols, Nomenclature and Abbreviations

°C	degrees Celsius
°N	degrees north
°W	degrees west
AERS	Anions Electrolytically Regenerated Suppressor
AFFFs	aqueous film forming foams
AMSL	above mean sea level
APFN	ammonium perfluorononanoate
APFO	ammonium perfluorooctanoate
bar	barometric pressure
CCIW	Canada Centre for Inland Waters
CE	current era
CFC	chlorofluorocarbon
CI	confidence interval
cm	centimetre
cm^2	square centimeter
cm^3	cubic centimeter
COF_2	carbonyl fluoride
diPAP	polyfluoroalkyl phosphate diester
ECF	electrochemical fluorination
EE	extraction efficiency
EtFOSA	ethyl perfluorooctane sulfonamide
EtFOSE	ethyl perfluorooctane sulfonamido ethanol
EU	European Union
FASA	perfluoroalkyl sulfonamides
FASE	perfluoroalkyl sulfonamido ethanols
FOSA	perfluorooctane sulfonamide
FT	fluorotelomer
FTACs	fluorotelomer acrylates
FTAL(s)	fluorotelomer aldehydes
FTCA(s)	fluorotelomer carboxylic acids

FTI(s)	fluorotelomer iodides
FTOH(s)	fluorotelomer alcohols
FTOs	fluorotelomer olefins
FTSA	fluorotelomer sulfonic acids
FTUCA	fluorotelomer unsaturated carboxylic acid
g	gram
t½	half-life
HCFCs	hydrochlorofluorocarbons
HF	hydrogen fluoride
HFCs	hydrofluorocarbons
HFE(s)	hydrofluoroethers
HFOs	hydrofluoroolefins
HNO_3	nitric acid
HO_2	hydroperoxyl radical
HPLC	high-performance liquid chromatography
hr	hour
HYSPLIT	HYbrid Single Particle Lagrangian Integrated Trajectory
ICP-MS	inductively coupled plasma mass spectrometry
ICP-OES	inductively coupled plasma optical emission spectroscopy
ICS	ion chromatography system
IDL	instrument detection limit
I.D.	internal diameter
IP	instrument performance standard
IS	internal standard
K_{AW}	air-water partition coefficient
kg	kilogram
km	kilometer
km^2	square kilometer
km^3	cubic kilometer
K_{OC}	organic carbon-water partition coefficient
K_{OW}	octanol-water partition coefficient

kt	kilotonnes
L	litre
LLGHGs	long-lived greenhouse gases
LOD	limit of detection
LOQ	limit of quantitation
LRT	long-range transport
m	metre
m/z	mass-to-charge ratio
m^2	square meter
m^3	cubic meter
MAC	mobile air-conditioning
MDL	method detection limit
ME	matrix effects
MeFBSA	methyl perfluorobutane sulfonamide
MeFOSE	methyl perfluorooctane sulfonamido ethanol
MeOH	methanol
mg	milligram
mL	millilitre
mm	millimetre
mM	millimolar
MRM	multiple reaction monitoring
MS/MS	tandem mass spectrometry
NAFSAs	N-alkyl perfluoroalkane sulfonamides
NAFSEs	N-alkyl perfluoroalkane sulfonamidoethanols
NCAR	National Center for Atmospheric Research
NCEP	National Center for Environmental Protection
ng	nanogram
NH_4OH	ammonium hydroxide
NO	nitric oxide
NOAA	National Oceanic and Atmospheric Administration
NOx	nitrogen oxides

N.M	not measured
nss	non-sea salt
O_3	ozone
ODP	ozone depleting potential
ODSs	ozone-depleting substances
OH·	hydroxyl radical
Pa	pascal
PASFs	perfluoroalkane sulfonyl fluorides
PBSF	perfluorobutane sulfonyl fluoride
PFAAs	perfluoroalkyl acids
PFAI(s)	perfluoroalkyl iodides
PFAL(s)	perfluoroalkyl aldehydes
PFAS	per- and polyfluoroalkyl substances
PFBA	perfluorobutanoic acid
PFBS	perfluorobutanesulfonic acid
PFCAs	perfluoroalkyl carboxylic acids
PFDA	perfluorodecanoic acid
PFDoDA	perfluorododecanoic acid
PFDS	perfluorodecanesulfonic acid
PFECHS	perfluoroethylcyclohexanesulfonate
PFHpA	perfluoroheptanoic acid
PFHpS	perfluoroheptanesulfonic acid
PFHxA	perfluorohexanoic acid
PFHxDA	perfluorohexadecanoic acid
PFHxS	perfluorohexanesulfonic acid
PFNA	perfluorononanoic acid
PFOA	perfluorooctanoic acid
PFOcDA	perfluorooctadecanoic acid
PFOS	perfluorooctanesulfonic acid
PFOs	perfluoroolefins
PFPeA	perfluoropentanoic acid

PFPrA	perfluoropropionic acid
PFSAs	perfluoroalkyl sulfonic acids
PFTeDA	perfluorotetradecanoic acid
PFTrDA	perfluorotridecanoic acid
PFUnDA	perfluoroundecanoic acid
pg	picogram
POPs	persistent organic pollutants
POSF	perfluorooctane sulfonyl fluoride
ppb	parts per billion
ppm	parts per million
ppt	parts per trillion
PTFE	polytetrafluoroethylene
PVDF	polyvinylidene fluoride
r	Pearson correlation coefficient
r^2	coefficient of determination
REACH	Registration, Evaluation, Authorisation and Restriction of Chemicals
RF	radio frequency
RH	relative humidity
RO_2	peroxy radical
rpm	revolutions per minute
RSD	relative standard deviation
s	second
scPFCAs	short-chain perfluoroalkyl carboxylic acids
SD	standard deviation
SE	standard error
S/N	signal-to-noise ratio
SPE	solid phase extraction
SSA	sample spike after
SSB	sample spike before
SSML	sea surface microlayer
TFA	trifluoroacetic acid

TFE	tetrafluoroethylene
U.S.	United States
UPLC-MS/MS	ultra performance liquid chromatography tandem mass spectrometry
US EPA	United States Environmental Protection Agency
V	volt
v/v	volume/volume ratio
w/w	weight per weight
WAX	weak anion exchange
WWTPs	wastewater treatment plants
xFOSEs	N-methyl and N-ethyl perfluorooctane sulfonamidoethanol
yr	year
µg	microgram
µL	microlitre
µm	micrometre

PREFACE

This thesis is comprised of a series of manuscripts that have been published, submitted, or are in preparation for submission to peer-reviewed scientific journals. Consequently, repetition of introductory and experimental details was inevitable. All manuscripts were authored by Daniel Persaud, with critical comments provided by Cora J. Young.

Chapter One: Introduction and Overview

Contributions – Prepared by Daniel Persaud with editorial comments by Cora J. Young

Chapter Two: A 50 year record of perfluoroalkyl acids in the High Arctic: implications for global and local transport.

Accepted: *Environ. Sci.: Processes Impacts*, 2024,26, 1543-1555

Author List: *Daniel Persaud[1], Alison S. Criscitiello[2], Christine Spencer[3], Igor Lehnherr[4], Derek C G. Muir[3], Amila O. De Silva[3], and Cora J. Young[1].*

[1]Department of Chemistry, York University, Toronto, ON

[2]Department of Earth and Atmospheric Sciences, University of Alberta, Edmonton, Alberta, Canada

[3]Aquatic Contaminants Research Division, Environmental and Climate Change Canada, Burlington, Ontario, Canada

[4]Department of Geography, Geomatics and Environment, University of Toronto-Mississauga, Mississauga, Ontario, Canada

Contributions – Alison S. Criscitiello and Igor Lehnherr collected the ice core. Daniel Persaud, Christine Spencer, Cora Young and Amila O De Silva sectioned and performed chemical analysis on ice core sections. Funding was obtained by Cora J Young and Derek C. G. Muir. Daniel Persaud analyzed the data and wrote the manuscript with input from all authors.

Chapter Three: The Occurrence of Legacy Perfluoroalkyl Substances (PFAS) Deposited along a Latitudinal Transect in Newfoundland and Labrador, Canada.

Submitted to: *Environ. Sci.: Processes Impacts*

Author List: *Daniel Persaud[1], Trevor C. VandenBoer[1,2*], Bryan K. Place[3,a], Kate A. Edwards[4,b], Susan E. Ziegler[2], Christine Spencer[5], Amila O. De Silva[5], and Cora J. Young[1,3*].*

[1]Department of Chemistry, York University, Toronto, ON
[2]Department of Earth Science, Memorial University, St. John's, NL
[3]Department of Chemistry, Memorial University, St. John's, NL
[4]Canadian Forest Service, Natural Resources Canada, Corner Brook, NL
[5]Aquatic Contaminants Research Division, Environmental and Climate Change Canada, Burlington, ON

[a]now at: SciGlob Instruments & Services LLC, Columbia, MD, USA
[b]now at: Climate Change Impacts and Adaptation Division, Lands and Minerals Sector, Natural Resources Canada, Ottawa, ON, Canada

Contributions: Susan E. Ziegler, Trevor C. VandenBoer, and Cora J. Young conceived of and designed the experiment. Trevor C. Vandenboer, Bryan K. Place and Kate A. Edwards built and deployed the samplers. Christine Spencer and Amila O De Silva performed the chemical analysis. Daniel Persaud analyzed the data and wrote the manuscript with input from all authors. Funding was acquired by Susan E. Ziegler, Trevor C. VandenBoer and Cora J. Young.

Chapter Four: Atmospheric removal of TFA by dry and wet deposition: a multi year analysis in Toronto

Accepted: *Environ. Sci. Technol. Lett.*

Author List: Daniel Persaud[1], Shira Joudan[1†], Trevor C. VandenBoer[1], and Cora J. Young[1*]

[1]Department of Chemistry, York University, Toronto, ON, M3J1P3
[†]Now at Department of Chemistry, University of Alberta, Edmonton, AB, T6G 2G2

Contributions: Trevor C. VandenBoer and Cora J. Young conceived of and designed the experiment. Daniel Persaud collected and analyzed the samples with assistance from Shira Joudan. Daniel Persaud analyzed the data and wrote the manuscript with input from all authors. Funding was acquired by Trevor C. VandenBoer and Cora J. Young.

Chapter Five: Quantifying the global reach of Trifluoroacetic acid (TFA): Contrasting total deposition between Southern and Northern Hemispheres.

Author List: Daniel Persaud[1], Heetasmin Singh,[2] Trevor C. VandenBoer[1], and Cora J. Young[1*].

[1]Department of Chemistry, York University, Toronto, ON, Canada.
[2]Department of Chemistry, University of Guyana, Turkeyen Campus, Guyana, South America.

Contributions: Cora J. Young and Daniel Persaud conceived and designed the experiment. Heetasmin Singh, Cora J. Young and Trevor C. VandenBoer collected the samples. Daniel Persaud analyzed the sample and collected the data. Daniel Persaud wrote the manuscript with input from all authors. Funding was acquired by Trevor C. VandenBoer and Cora J. Young.

Chapter Six: Conclusions and Future Directions

Contributions – Prepared by Daniel Persaud with editorial comments by Cora J. Young

Other Publications during PhD

1. Young, C. J.; Wong, F. S.; **Persaud, D**. Halogenated Organics in the Cryosphere. In *Chemistry in the Cryosphere*; Advances in Atmospheric Chemistry; WORLD SCIENTIFIC, 2020; Vol. Volume 3, pp 621–648. https://doi.org/10.1142/9789811230134_0012.

2. Pickard, H. M.; Criscitiello, A. S.; **Persaud, D**.; Spencer, C.; Muir, D. C. G.; Lehnherr, I.; Sharp, M. J.; De Silva, A. O.; Young, C. J. Ice Core Record of Persistent Short-Chain Fluorinated Alkyl Acids: Evidence of the Impact From Global Environmental Regulations. *Geophysical Research Letters* **2020**, *47* (10), e2020GL087535. https://doi.org/10.1029/2020GL087535.

3. Colussi, A. A.¨; **Persaud, D**†.; Lao, M.; Place, B. K.; Hems, R. F.; Ziegler, S. E.; Edwards, K. A.; Young, C. J.; VandenBoer, T. C. Cost-Effective off-Grid Automatic Precipitation Samplers for Pollutant and Biogeochemical Atmospheric Deposition. *Atmospheric Measurement Techniques* **2024**, *17* (12), 3697–3718. https://doi.org/10.5194/amt-17-3697-2024.
   †Contributed equally to this work

4. Trinquet, A.; Kasperkiewicz, A.; **Persaud, D**.; Miller, J.; Babin, M.; VandenBoer, T. C.; Shunthirasingham, C.; Galarneau, E.; Hung, H.; Tetreault, G. R.; Lu, Z. Atmospheric Fate and Deposition of Polyhalogenated Carbazoles in Urban Environment. *Environmental Pollution* **2025**, *383*, 126878. https://doi.org/10.1016/j.envpol.2025.126878.

CHAPTER 1

Introduction and Overview

1.1 Defining Per and Polyfluoroalkyl Substances

The definition of PFAS has undergone several modifications since fluorinated chemicals were first introduced in the 1930s. Initially, the term perfluorinated chemicals was used, but has been discontinued due to confusion with perfluorinated carbons and the omission of the polyfluorinated homologues, which were also of interest to the scientific community.[1] The first comprehensive definition was proposed in 2011 by Buck et al., which classified PFAS as a substance that contained two (or more) connected saturated CF_2 groups.[2] However due to limitations of this definition, the Organization for Economic Co-operation and Development (OECD) revised this definition in 2021 to ***"PFAS are defined as fluorinated substances that contain at least one fully fluorinated methyl or methylene carbon atom (without any H/Cl/Br/I atom attached to it, i.e. with a few noted exceptions), any chemical with at least a perfluorinated methyl group (−CF3) or a perfluorinated methylene group (−CF2−) is a PFAS."*** [3] Early research also focused on a limited number of PFAS; with changing definitions and regulations, the number of documented PFAS has been increasing over the past several years. This is compounded with the recent emergence of nontarget "suspect screening" of PFAS by high-resolution mass spectrometry (HRMS).[4] There have been several attempts to concatenate and list the number of known PFAS homologues. These include the OECD list of ~ 4700 PFAS,[5] The National Institute of Standards and Technology (NIST) list of 4948 entries[6] and the United States Environmental Protection Agency (US EPA) PFASMASTER list of 12039 entries as of September 2025.[7]

Within the broad PFAS definition, several subgroups of PFAS exist. The most well-known and studied group are the perfluoroalkyl acids (PFAAs), which include perfluoroalkyl carboxylic acids (PFCAs) and perfluoroalkyl sulfonic acids (PFSAs) (Figure 1-1). Other subgroups include various precursor compounds which can form PFAAs, such as chlorofluorocarbons (CFCs) replacement compounds, fluorotelomer alcohols (FTOHs) and perfluorosulfonamide ethanols (FASEs). A comprehensive list of relevant PFAS homologues is provided in Table 1-1.

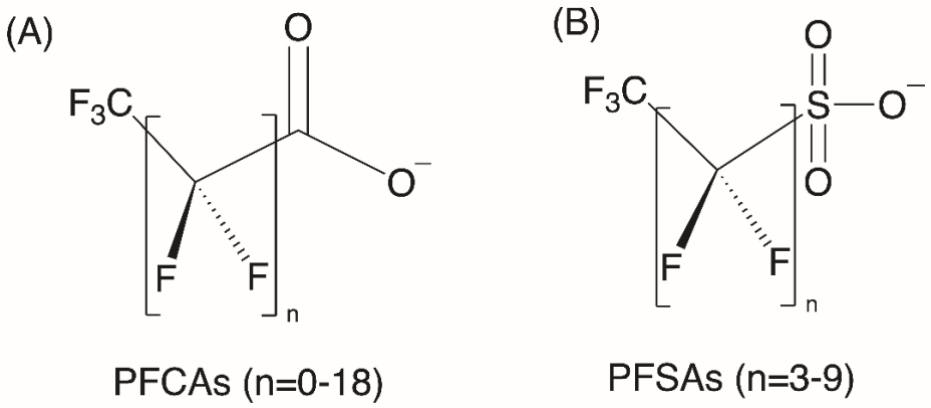

Figure 1-1: General chemical structure of (A) PFCAs and (B) PFSAs

The perfluoroalkyl moiety (C_nF_{2n+1}-) imparts a unique combination of thermal and chemical stability, alongside both hydrophobic and lipophobic properties, which makes them useful in a variety of industrial and commercial applications. The carbon-fluorine bond is extremely strong and stable. Applications of PFAS in the polymer industry include textile stain and soil repellents, as well as non-stick applications.[8] The unparalleled ability of PFAS to lower aqueous surface tension is exploited in key surfactant applications. These include their use in processing aids in fluoropolymer manufacture, coatings, and aqueous film-forming foams (AFFFs) used to extinguish flammable liquid fires.[8,9]

Table 1-1: Overview of PFAS acronyms and formulae

Perfluoroalkylcarboxylic Acids (PFCAs)		
Trifluoroacetic Acid	TFA	CF_3COOH
Perfluoropropionic Acid	PFPrA	$CF_3(CF_2)CO_2H$
Perfluorobutanoic Acid	PFBA	$CF_3(CF_2)_2CO_2H$
Perfluoropentanoic Acid	PFPeA	$CF_3(CF_2)_3CO_2H$
Perfluorohexanoic Acid	PFHxA	$CF_3(CF_2)_4CO_2H$
Perfluoroheptanoic Acid	PFHpA	$CF_3(CF_2)_5CO_2H$
Perfluorooctanoic Acid	PFOA	$CF_3(CF_2)_6CO_2H$
Perfluorononanoic Acid	PFNA	$CF_3(CF_2)_7CO_2H$
Perfluorodecanoic Acid	PFDA	$CF_3(CF_2)_8CO_2H$
Perfluoroundecanoic Acid	PFUnDA	$CF_3(CF_2)_9CO_2H$
Perfluorododecanoic Acid	PFDoDA	$CF_3(CF_2)_{10}CO_2H$
Perfluorotridecanoic Acid	PFTrDA	$CF_3(CF_2)_{11}CO_2H$
Perfluorotetradecanoic Acid	PFTeDA	$CF_3(CF_2)_{12}CO_2H$
Perfluorohexadecanoic Acid	PFHxDA	$CF_3(CF_2)_{14}CO_2H$
Perfluorooctadecanoic Acid	PFOcDA	$CF_3(CF_2)_{16}CO_2H$
Fluorotelomer Alcohols (FTOHs)		
4:2 fluorotelomer alcohol	4:2 FTOH	$CF_3(CF_2)_3(CH_2)_2OH$
6:2 fluorotelomer alcohol	6:2 FTOH	$CF_3(CF_2)_5(CH_2)_2OH$
8:2 fluorotelomer alcohol	8:2 FTOH	$CF_3(CF_2)_7(CH_2)_2OH$
10:2 fluorotelomer alcohol	10:2 FTOH	$CF_3(CF_2)_9(CH_2)_2OH$
12:2 fluorotelomer alcohol	12:2 FTOH	$CF_3(CF_2)_{11}(CH_2)_2OH$
Perfluoroalkylsulfonic Acids (PFSAs)		
Perfluorobutanesulfonic Acid	PFBS	$CF_3(CF_2)_3SO_3H$
Perfluorohexanesulfonic Acid	PFHxS	$CF_3(CF_2)_5SO_3H$
Perfluoroheptanesulfonic Acid	PFHpS	$CF_3(CF_2)_6SO_3H$
Perfluorooctanesulfonic Acid	PFOS	$CF_3(CF_2)_7SO_3H$
Perfluorodecanesulfonic Acid	PFDS	$CF_3(CF_2)_9SO_3H$
Perfluoroethylcyclohexane Sulfonate	PFECHS	$C_6F_{10}(CF_2CF_3)SO_3H$
Perfluoroalkyl ether carboxylic acid (PFECA)		
ADONA	-	$CF_3O(CF_2)_3OCHFCF_2CO_2^-$ $NH4^+$
N-alkyl polyfluoroalkyl sulfonamide (FASA)		
N-methyl perfluorobutane sulfonamide	N-MeFBSA	$CF_3(CF_2)_3SO_2N(CH_3)(CH_3)H$
N-ethyl perfluorobutane sulfonamide	N-EtFBSA	$CF_3(CF_2)_3SO_2N(CH_3)(CH_2CH3)H$
N-methyl perfluorooctanesulfonamide	N-MeFOSA	$CF_3(CF_2)_7SO_2N(CH_3)(CH_3)H$
N-ethyl perfluorooctane sulfonamide	N-EtFOSA	$CF_3(CF_2)_7SO_2N(CH_3)(CH_2CH_3)H$
N-alkyl polyfluoroalkyl sulfonamidoethanol (FASE)		
N-methyl perfluorobutane sulfonamidoethanol	N-MeFBSE	$CF_3(CF_2)_3SO_2N(CH_3)(CH_2CH_2OH)$
N-ethyl perfluorobutane sulfonamidoethanol	N-EtFBSE	$CF_3(CF_2)_3SO_2N(CH_2CH_3)(CH_2CH_2OH)$
N-methyl perfluorooctane sulfonamidoethanol	N-MeFOSE	$CF_3(CF_2)_7SO_2N(CH_3)(CH_2CH2OH)$
N-ethyl perfluorooctane sulfonamidoethanol	N-EtFOSE	$CF_3(CF_2)_7SO_2N(CH_2CH_3)(CH_2CH_2OH)$

1.2 PFAS manufacture

The industrial production of PFAS is primarily achieved through two key synthetic routes: (i) electrochemical fluorination (ECF) and (ii) telomerization. The development of these methods was driven by the unique properties of fluorinated compounds, discovered through both serendipity and targeted research in the 20th century.

The foundational discoveries in organofluoride chemistry date back to the 1930s, with the synthesis of chlorofluorocarbons (CFCs) like Freon-12 (CCl_2F_2) and the accidental discovery of polytetrafluoroethylene (PTFE) by Roy Plunkett in 1938.[10,11] The ECF method was developed during the Manhattan Project (1941-1945) to synthesize coolants, lubricants, and fluoropolymers to assist the production of atomic bombs.[12] This technique was declassified and commercialized in 1949 by the Minnesota Mining and Manufacturing (3M) company.[13] Concurrently, the telomerization process was first reported in 1949 by Hazeldiene, though it was not widely commercialized until 1975.[14] A schematic comparison of these two production routes, including example products and isomer profiles is shown in Figure 1-2.

1.2.1 Electrochemical Fluorination (ECF)

The ECF method involves applying an electric current (5-7 V) across a mixture of an organic precursor dissolved in anhydrous hydrogen fluoride (HF) in a metal cell.[9] This process substitutes all C-H bonds with C-F bonds.[9] From 1949-2002, 3M used ECF to produce perfluorooctane sulfonyl fluoride (POSF, C_8F_{17} SO_2F) and perfluorooctane carbonyl fluoride (POCF, $C_8F_{17}COF$), a key starting material for other PFAS homologues. For example, (i) perfluorooctanesulfonic acid (PFOS) can be produced by hydrolysis of POSF, (ii) methyl perfluorooctane sulfonamide (MeFOSA) and ethyl perfluorooctane sulfonamide (EtFOSA), by reaction of POSF with methyl/ethyl amine and then (iii) MeFOSE and EtFOSE by further reaction with ethylene glycol carbonate. The perfluorooctanoic acid (PFOA) homologue can be produced from the ECF of POCF, followed by hydrolysis.[2]

A notable drawback of the ECF process is its relatively low yield (34-40% for POSF) and the generation of complex mixtures of impurities. The final products contain a significant proportion of linear and branched isomers of PFCAs and PFSAs with varying

chain lengths. For instance, 3M's ECF-derived PFOS contained ~70% linear PFOS, with the remainder being branched isomers and other PFSA, like PFHxS and PFDS.[15] Recently, the ECF process was employed to manufacture shorter chain alternatives such as perfluorobutanesulfonic acid (PFBS), in response to market and regulatory changes.[16]

1.2.2 Telomerization

Telomerization provides an alternative synthesis that builds PFAS chains in C_2 units. The process typically begins with pentafluoroiodoethane (CF_3CF_2I). Under ultraviolet radiation, this compound forms a perfluoroalkyl radical ($CF_3CF_2\cdot$), which undergoes free radical addition with tetrafluoroethylene (TFE, $CF_2=CF_2$).[9] The free radical polymerization successively increases the chain length of the perfluoroalkyl radical. The perfluoroalkyl radical can be reacted with ethene ($CH_2=CH_2$) to form a fluorotelomer iodide (FTI, $F(CF_2)_xCH_2CH_2I$).[9] Like POSF, FTIs are crucial intermediates; hydrolysis of FTIs yields FTOHs, while oxidation and carboxylation yield PFOA and perfluorononanoic acid (PFNA).[17] A key distinction from ECF is the isomer profiles of the products. The telomerization process produces almost exclusively linear(straight-chain) isomers. However, the products still contain chain-length impurities, predominantly even-numbered homologues due to the stepwise addition of TFE monomers.[18]

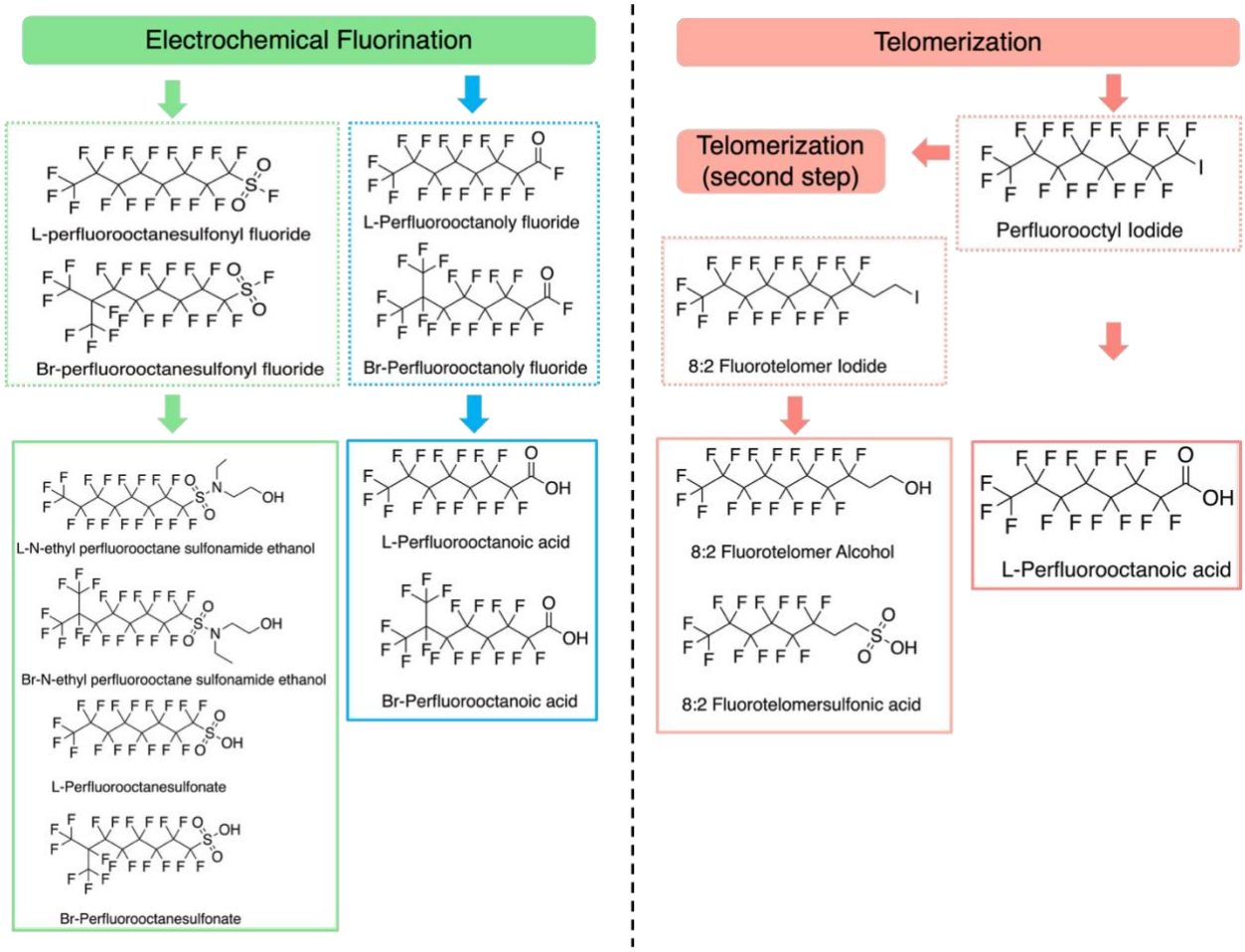

Figure 1-2: Comparison of the two main production techniques for PFAS production techniques: electrochemical fluorination (ECF) and telomerization. A key difference is the structure of the resulting compounds: ECF can result in a mixture of linear (L) and branched (Br) products, whereas telomerization mainly results in linear products (provided that a linear raw material is used). The figure illustrates simplified reaction pathways with example products. An example of an N-alkylated perfluorooctanesulfonamidoethanol, perfluorooctanesulfonamidoethanol is shown to illustrate a perfluorooctanesulfonyl fluoride base product in addition to perfluorooctanesulfonate.

1.3 Physicochemical properties of PFAAs

Despite the widespread global distribution of PFAS, a significant knowledge gap exists regarding the experimental determination of their fundamental physicochemical properties – such as solubility, vapor pressure and partition coefficients, particularly for the environmentally prevalent PFAAs. This gap is primarily due to analytical challenges posed by the inherent amphiphilic nature of PFAAs and the sheer magnitude of the number of individual homologues.[19] Consequently, much of the available data relies on estimated values from computation models or measurements of the neutral acid form,

which is environmentally irrelevant except under highly acidic conditions or in the gas phase. This reliance on uncertain property data introduces errors in fate and transport models, undermining risk assessments and remediation strategies. This section reviews and summarizes selected physicochemical property data for PFAAs, with a focus on the anionic forms relevant to environmental systems.

The environmental behavior of PFAAs is largely governed by their acidic character. Both PFCAs and PFSAs are strong acids with reported pK_a values ranging from <1 to 3.8[20,21]. The low pK_a values ensure that PFAAs exist primarily in a deprotonated, anionic form, which is stabilized by the strong electron-withdrawing effects of the perfluoroalkyl chain fluorine atoms.[19] It is important to note that there has been considerable debate regarding precise pK_a values, especially for PFOA.[22] While the anion form is dominant, PFAAs can, under specific conditions, protonate to a neutral species with distinct physical properties. For example, the protonated neutral form of PFOA exhibits lower water solubility and appreciable vapor pressure, allowing for volatilization from bulk water into air,[23] however, this is highly unlikely. The work of Viekre et al. quantitatively defined these thresholds, demonstrating that complete ionization of PFOS and PFHxS occurred at pH ³ 5.5 and at pH ³ 6.5 for PFOA,[24] confirming that the ionic species prevails in nearly all aqueous environmental systems. The available dissociation constants are provided in Table 1-2.

This anionic nature of PFAAs also dictates their high water solubility, a key determinant of their environmental mobility. The solubility of PFAAs is inversely related to chain length, it is highest for the short-chain PFAAs and decreases with increasing molecular weight and hydrophobic perfluorinated alkyl chain length.[25] Furthermore, the specific functional group also affects the environmental partitioning. The sulfonate moiety of PFSAs has a greater affinity for adsorption in the soil, compared to PFCAs of equivalent chain length.[26] Consequently, short and ultra-short chain PFCAs (e.g., trifluoroacetic acid (TFA)) and (perfluorobutanoic acid (PFBA)) are highly mobile and dominate aqueous phases like groundwater, whereas long-chain PFSAs (e.g., PFOS) are more readily retained in soil and sediments. The PFAAs have very low vapor pressures, which decrease with increasing perfluorinated chain length. As a result, direct emission of

PFCAs and PFSAs should be localized and tend to be released in runoff into nearby oceans and rivers. Solubility of PFAAs is summarized in Table 1-2.

The environmental mobility of PFAAs is predicted using partition coefficients that quantify their distribution between environmental phases. The organic-carbon partitioning coefficient (K_{OC}) and the octanol-water partition coefficient (K_{ow}) are used to estimate the extent to which PFAAs associate with organic matter in soils and sediments during aquatic transport. However, it is impossible to measure the K_{ow} for PFAAs since they accumulate at phase boundaries, forming an interfacial layer rather than partitioning between phases. In general, K_{oc} increases with perfluorinated chain length, reflecting greater hydrophobicity and van der Waals interactions between the fluorinated tail and organic matter.[27] Partition coefficient values for K_{OC} are provided in Table 1-2.

Table 1-2: Summary of selected physicochemical properties of PFAAs. Data from [22,27–33] and references therein.

	Acronym	Dissociation Constant (PK_a)	Water Solubility (g ($mg\ L^{-1}$))	Vapor pressure (Pa)	Log K_{OC}
(PFCAs)	TFA	0.23	Miscible	1×10^4	0.2-1.7
	PFPrA	0.38	N/A	N/A	N/A
	PFBA	2.0×10^{-1} - <1.6	4.9×10^4	2.2×10^{-2} - 2.0×10^3	1.8
	PFPeA	4.0×10^{-1}	9.8×10^3	1.0×10^0 - 2.7×10^3	1.4
	PFHxA	7.0×10^{-1} - <1.6	1.9×10^3	5.1×10^0 - 9.1×10^1	1.9
	PFHpA	-1.5×10^{-1} - 1.9×10^2	1.2×10^2 - 3.6×10^2	3.6×10^4	2.2
	PFOA	-5.0×10^{-1} - 3.8×10^0	1.0×10^{-2} - 9.5×10^3	2.0×10^0 - 1.3×10^3	1.31-2.35
	PFNA	$<1.6 \times 10^0$	11.7×10^0	7.0×10^{-1} - 1.2×10^2	2.39
	PFDA	$<1.6 \times 10^0$ - 2.6×10^1	1.0×10^{-4} - 1.9×10^6	1.0×10^{-1} - 1.0×10^3	2.76
	PFUnDA	$<1.6 \times 10^0$ - 2.6×10^0	5.0×10^{-1} - 92.3×10^0	2.0×10^{-2} - 6.2×10^2	3.30
	PFDoDA	3.1×10^0	7.0×10^{-2} - 5.2×10^1	6.8×10^{-58} - 8.6×10^2	N/A
	PFTrDA	N/A	[a]0.0 - 3.4×10^6	[a]2.0×10^{-2} - 2.1×10^0	N/A
	PFTeDA	[a]-2.1×10^{-1}	2.0×10^{-3} - 3.0×10^{-2}	1.7×10^0	N/A
(PFSAs)	PFBS	$<3.0 \times 10^{-1}$	6.9×10^3	1.3×10^2	1.0
	PFPeS	N/A	[a]8.1×10^0 - 4.3×10^4	[a]3.8×10^{-5}	N/A
	PFHxS	3.0×10^{-1}	2.4×10^2	4.8×10^1	1.8
	PFHpS	N/A	[a]4.0×10^{-2} - 7.1×10^5	[a]4.4×10^{-5}	N/A
	PFOS	<3.0 - <1.0	7.7×10^0 - 9.1×10^2	1.7×10^1	0.5
	PFNS	N/A	[a]2.2×10^{-4} - 1.6×10^6	[a]2.0×10^{-4}	N/A
	PFDS	[a]0.14	[a]1.6×10^{-6} - 2.2×10^6	[a]1.0×10^{-3} – 7.1×10^{-1}	3.5

N/A: Not Available.
[a] value determined by model.

1.3.1 Toxicity and exposure

The understanding of PFAS toxicity was not fully recognized until the early 2000s. However, human exposure to these chemicals was documented much earlier. Pioneering studies by Taves (1968) and Belisle et al. detected organic fluorine in individuals with no occupational exposure.[34,35] This was later reinforced in the 1980s when PFOA was specifically identified in the blood of fluorochemical workers.[36] Decades later, in 2001Giesy and Kannan demonstrated that perfluorooctane sulfonate (PFOS) was globally distributed in wildlife.[37] At the same time, Hansen et al. documented the occurrence of PFOS, perfluorooctanoic acid (PFOA) and additional PFAS homologues in numerous human serum samples obtained from biological supply companies.[38]

The structural similarity of PFAS to endogenous compounds allows them to engage with a diverse array of biological structures, including key transport proteins, nuclear receptors and cell membranes.[39,40] The binding with key biological matrices is considered a crucial pathway for PFAA bioaccumulation.[41] The potential for PFAS to bioaccumulate depends on the specific organisms and the physicochemical properties of PFAS. Historically, long–chain PFAAs (>7C) were considered more bioaccumulative than the short and ultrashort (C2-C3) chain homologues and more likely to biomagnify in aquatic and terrestrial food chains. A strong positive correlation was observed between bioaccumulation/biomagnification and fluoroalkyl chain length of PFAAs.[42] However, extremely long chain homologues (>12 C) generally tend to bioaccumulate less, mainly due to limited bioavailability.[43] More recently, there is growing evidence that some short chain PFAS (e.g., TFA) can be phytoaccumulative, which shifts consideration from classic biomagnification towards plant uptake and plant mediated exposure pathways.

Human exposure to PFAS occurs through oral (e.g., ingestion of contaminated water and food), inhalation and dermal routes.[44] The metabolism and removal of PFAS in humans are complex and depend on the specific type of compounds. A key distinction is that the long-chain homologues (>7C) do not efficiently metabolize in humans, while their precursors can be transformed into stable terminal PFAAs.[45,46] Consequently, the primary route of elimination is through excretion, though other processes, including loss through lactation, parity, menstruation, and blood plasma donations, have been identified as removal mechanisms.[47,48] The PFOS half-life in humans is 3.4 to 5.7 years, whereas

the lifetime of PFOA is 1.5 to 5.1 years.[49] Furthermore, structural properties influence excretion kinetics; branched isomers are excreted more rapidly than the linear isomers[43] and short and ultrashort chain PFAAs are excreted more rapidly than long chain counterparts.[50]

Laboratory studies using animal models have consistently linked PFAS exposure to a spectrum of adverse effects. These experimental findings are corroborated by human epidemiological studies, which have specifically associated PFOS and PFOA exposure with developmental toxicity, immunotoxicity, hepatoxicity, neurotoxicity, tumor induction, endocrine disruption and other carcinogenic effects at high doses.[51] Emerging evidence suggests that PFAS exhibit heightened toxicity in the second generation, a transgenerational effect that challenges traditional toxicological models.[52] Furthermore, studies across various animal models reveal significant sex-specific differences in pharmacokinetics.[53] Consequently, contemporary toxicity evaluations are increasingly accounting for species, sex, and multigenerational impacts. While the bulk of epidemiological research has historically centered on long-chain PFAS like PFOS and PFOA, scientific attention is increasingly turning to their replacements, including short-chain PFAAs (e.g., TFA and PFBA) and fluorotelomer compounds.[54,55] This expanding focus is warranted, given their increasing environmental prevalence in human consumer foods,[56–58] alongside comparatively limited toxicity and epidemiological data for many of these compounds.

1.4 Long-range transport mechanisms of PFAA

The environmental persistence of PFAS is directly responsible for their ubiquitous global detection, including in pristine regions like the High Arctic. PFAAs can be transported to the High Arctic by ocean currents in the bulk dissolved phase as well as the sea surface microlayer (SSML) on the scale of decades.[59,60]. The high water solubility and low volatility of PFAAs suggest that oceans represent a primary sink for PFAAs.[61]

An emerging pathway for long-range transport involves interfacial processes at the sea-air boundary, specifically the generation of marine aerosols. The surfactant nature of PFAAs enables them to be enriched at the air-water interface in the sea surface microlayer.[62] When waves break, the PFAA-enriched microlayer is ejected into the atmosphere, forming sea spray aerosols (SSA) that can be transported over continental

scales by prevailing winds, effectively depositing ocean-derived PFAAs into various terrestrial systems.[62]

The environmental persistence of PFAS is directly responsible for their ubiquitous global detection, including in pristine regions like the High Arctic. PFAAs can be transported to the High Arctic by ocean currents in the bulk dissolved phase as well as the sea surface microlayer (SSML) on the scale of decades.[59,60]. The high water solubility and low volatility of PFAAs suggest that oceans represent a primary sink for PFAAs.[61]

An emerging pathway for long-range transport involves interfacial processes at the sea-air boundary, specifically the generation of marine aerosols. The surfactant nature of PFAAs enables them to be enriched at the air-water interface in the sea surface microlayer.[62] When waves break, the PFAA-enriched microlayer is ejected into the atmosphere, forming sea spray aerosols (SSA) that can be transported over continental scales by prevailing winds, effectively depositing ocean-derived PFAAs into various terrestrial systems.[62]

The atmospheric transport of volatile precursor compounds represents a pathway for the global distribution of PFAAs, particularly in remote regions, including the High Arctic. These precursor compounds, typically neutral and semi-volatile, can undergo oxidative reactions to form stable terminal PFAAs[63] In contrast to the decadal timescale of oceanic advection, the atmospheric transport and transformation of precursors occur on a significantly faster timescale, typically within weeks.[64] For perspective, a precursor compound travelling at the global average wind speed of 13.8 km hr^{-1} could theoretically traverse the ~4,600 km distance from Toronto, Ontario, to Alert, Nunavut, in 14 days.[65] This timeframe is well within the estimated atmospheric lifetime of common precursors like fluorotelomer alcohols (FTOHs), which is about 20 days,[64] confirming the chemical feasibility of this long-range transport pathway. After formation, PFAAs can be subsequently removed from the atmosphere by wet and dry deposition processes, including precipitation, gas-phase deposition and association with atmospheric particles. Direct quantitative evidence for this transport pathway is provided by atmospheric monitoring studies that consistently detect FTOHs and other precursors in Arctic air.[66–72]

It is evident that long-range transport occurs by three distinct mechanisms: (i) direct oceanic transport, (ii) atmospheric oxidative transformations and (iii) SSA. Each of these transport pathways is discussed further in sections 1.4.1 to 1.4.3.

1.4.1 Direct transport of PFAAs

The direct transport mechanism involves the physical translocation of PFAAs in their stable, anionic forms (e.g., carboxylic and sulfonic acid) to remote locations. These compounds enter the environment through primary emission from various industrial and commercial sources, including fluoropolymer dispersion, fluoropolymer manufacture, PFCA manufacture, AFFF usage, and consumer and industrial products.[61] In fact, Prevedouros et al. suggested that the majority (~80%) of PFCAs are direct sources from global fluoropolymer manufacture and use.[61] After release, PFAA contamination should be localized due to the low vapor pressure and high water solubility of PFAAs, followed by removal by wet and dry deposition. This deposition delivers PFAAs directly to the terrestrial and aquatic environment, including the global oceans, which is the primary sink of these compounds.[61]

The global presence of PFAAs in the open oceans is well established, with numerous studies constantly detecting these compounds at parts per trillion concentrations.[60,72–77] Interestingly, elevated levels were observed near coastal regions, suggesting that riverine inputs are an important but overlooked source.[75,78] The horizontal and vertical transport mechanisms have received little attention to date.[60] Marine currents are hypothesized to be the main transport vector to remote locations.[59] These currents (e.g., the Gulf Stream and Kuroshio Current) facilitate the lateral transport of PFAAs from contaminated coastal regions to polar waters over timescales of decades. This process is complemented by the thermohaline circulation[79,80] or “global conveyor belt”, which integrates PFAAs into global deep water masses and ultimately transports them to remote regions, including the Arctic Ocean.[81]

The Arctic Ocean is characterized by its relatively small size, extensive continental shelves (~70% of its area) and significant freshwater inputs.[79] Hydrographic dynamics in the Arctic are dominated by inflows of Atlantic-origin water, which enters via the eastern Fram Strait and the Barents Sea. The water subsequently circulates in a counterclockwise direction – flowing from the Nansen Basin into the Amundsen, Makarov

and Canadian Basin.[60,82] The primary outflow from the Arctic Ocean, which exports these water masses, occurs via the western Fram Strait and the channels of the Canadian Archipelago.[82]

1.4.2 Sea Spray Aerosols (SSA) as a potential source.

The long-range transport of ionic PFAAs can also be facilitated by their enrichment in SSA, the largest natural aerosol by mass.[83] SSA production is driven primarily by wind and wave breaking action and is modulated by factors such as sea-surface temperature, salinity, and surface-active agents (which affect surface tension, density and viscosity).[84] The integral step in SSA formation is when gas bubbles mixed into seawater burst at the surface, releasing SSA into the atmosphere.[85] The bursting of these bubbles generates SSA droplets through two primary mechanisms: (i) the production of larger “jet drops” from the collapse of smaller bubble cavities and (ii) the production of “film drops” from the rupture of the film cap of larger bubbles.[86]

The amphiphilic properties of PFAAs are fundamental to their incorporation into SSA. These properties drive the partitioning of PFAAs from the bulk water to the air-water interface, leading to their enrichment in SSML. This vertical stratification of PFAAs has been confirmed by field measurements, which show higher PFAA concentrations in surface waters compared to deep waters.[59,60] This behavior was corroborated by laboratory simulations showing that selected PFAAs (PFBA, PFOA, PFOS, PFHxS) quickly migrate to the air-water interface from the bulk water region.[87] Consequently, when bubbles burst, they eject SSA droplets directly from the SSML, efficiently transferring PFAAs into the aerosol phase.

Laboratory studies using sea spray simulation chambers were pivotal in confirming the transfer of PFAAs from bulk water to SSA. Early studies by McMurdo et al.[88] found that PFOA (anion) was enriched >80 times in simulated SSA when compared to the bulk water. Similarly, Reth et al.[89] observed an exponential increase in the transfer to SSA with increasing chain length for C6 to C12 PFCAs and PFSAs. Using an identical experimental setup, Sha et al.[62] observed that bulk concentration did not affect the enrichment of PFAAs in SSA, but molecular structure did, with linear PFOA and PFOS being more readily aerosolized than branched isomers. Furthermore, particle size is a critical factor, Johansson et al.[90] observed that particles less than 1.6 μm had PFAAs enhancements

up to ~ 62,000 times greater than in bulk artificial seawater. In a comprehensive analysis, Sha et al.[62] measured 17 PFAAs across 14 aerosol size bins and established that enrichment is highly dependent on chain length and particle size, with enrichment factors ranging from 19 for PFPeA in 2.48 μm particles to 46,000 for perfluorododecanoic acid (PFDoDA) in 0.154 μm particles.

While field measurements of SSA contribution to PFAA transport are scarce, they can be used for validation. Casas et al.[91] presented the first simultaneous measurements of PFAA in bulk seawater, SSML and SSA in the Southern Ocean, reporting that SSA concentrations were 522 to 4960 times greater than in bulk seawater. This was supported by measurements in the Atlantic Ocean by Sha et al., who found that PFAAs were enriched >100,000 times in the SSA relative to seawater concentrations.[92] Further supporting evidence comes from additional field work by Sha et al., who correlated PFAA concentration in aerosol particles collected in two coastal sites in Norway to sodium (Na^+) tracer from seawater (r = 0.4-0.8).[93] More recently, Albers and Voutchkova.[94] analyzed PFAAs in shallow wells on the Danish coast and found elevated levels near the coast, suggesting that SSA transport may be the major contributor. Taken together, laboratory studies and limited field measurements shows a potential for transport by SSA.

1.4.3 Indirect formation and transport of PFAAs

The global distribution of PFAAs is not only governed by direct emission and transport but also by indirect pathways. Among these, the atmospheric oxidation of precursors represents a critical mechanism for the long-range transport and subsequent formation of PFAAs in the environment. These precursors are usually volatile or semi-volatile and originate from several anthropogenic sources. The major source categories include chlorofluorocarbons (CFCs) replacement compounds, and the fluoropolymer industry (including fluorotelomer and POSF-based products).[61,63] The detailed chemistry and mechanism for the oxidation of CFC replacement compounds are provided in Section 1.5.

1.4.3.1 Oxidation of fluoropolymers and related compounds

Within the fluoropolymer industry, several neutral and polyfluorinated precursor compounds can undergo atmospheric oxidation, serving as an indirect source of PFAAs.

These precursor classes could be derived from perfluorooctylsulfonyl fluoride (POSF) based precursors, including FOSEs and perfluorooctane sulfonamide (FOSAs) and fluoropolymer-based precursors such as FTOHs, FTIs, fluorotelomer acrylates (FTACs), and fluorotelomer olefins (FTOs). The atmospheric fate of many of these PFAA precursors has been investigated using smog chamber techniques. As summarized in Figure 1-3, these volatile precursors undergo a series of reactions, often via radical intermediates, to ultimately yield stable terminal PFAAs.

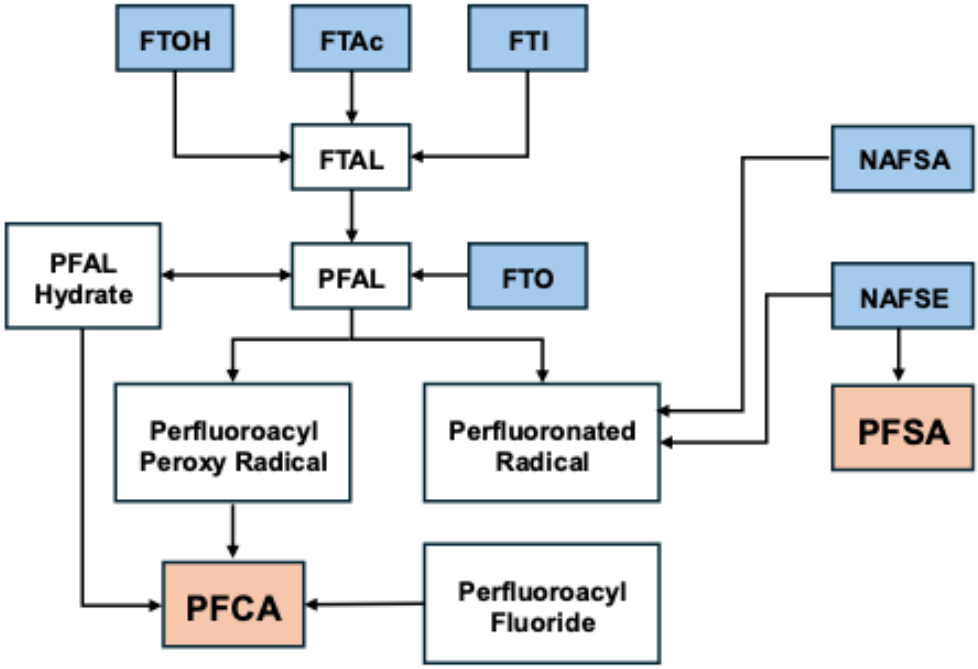

Figure 1-3: Atmospheric transformation pathway of volatile PFAA precursors. Blue-shaded compounds are commercially produced. PFSA and PFCA are the terminal degradation products. Adapted from [63]

1.4.3.2 Atmospheric chemistry of PFAA precursors

The atmospheric lifetime of these precursors is primarily determined by their reactions with the hydroxyl radical. The atmospheric lifetimes of aldehydes (FTALs, PFALs) and FTIs are limited by photolysis.[17] The atmospheric degradation of these precursors occurs primarily through gas-phase reactions, resulting in lifetimes typically ranging from days to weeks (Table 1-3). However, the actual lifetimes and resulting yield of PFAA are variable. They depend on several factors, including seasonal changes of available light, levels of anthropogenic pollution and proximity to the coast or an

anthropogenic chlorine source.[63] Critically, the formation of PFAAs is favored in remote, low-NO_x environments like the Arctic, where the balance between HO_2 and RO_2 to NO_x promotes the formation of PFAAs.[95]

Table 1-3: Summary of atmospheric lifetimes of selected PFAA precursors, calculated with respect to hydroxyl radical degradation

Precursor	Lifetime with respect to hydroxyl radical degradation (days)	Reference
PFAL Hydrate	90	Sulbaek Andersen et al.[96]
PFAL	18	Sulbaek Andersen et al.[97]
FTOHs	20-80	Ellis et al.[64]
FTIs	10	Young et al.[17]
FTACs	1	Butt et al.[98]
FOSEs	2	D'Eon et al.[99]
NAFSA	20-50	Martin et al.[100]
NAFSE	2	D'Eon et al.[99]

The detailed mechanism for the atmospheric reaction of precursors with OH has been elucidated by several studies.[63] The hydroxyl radical initiates the pathway, abstracting a hydrogen atom from the carbon adjacent to the functional group in FTOHs, FTIs and FTAc. The resulting carbon-centered radical rapidly adds an oxygen molecule, forming a peroxy radical that subsequently reacts to produce FTAL as a primary intermediate. FTAL then undergoes further hydroxyl radical initiated oxidation, generating an acyl peroxy radical. This radical can follow branching pathways to form either a fluorotelomer carboxylic acid (FTCA) or, more significantly, the perfluoroalkyl aldehyde (PFAL). The PFAL is the central precursor to PFCAs with more than four carbons. This precursor can also be directly formed from FTOs (Figure 1-4)

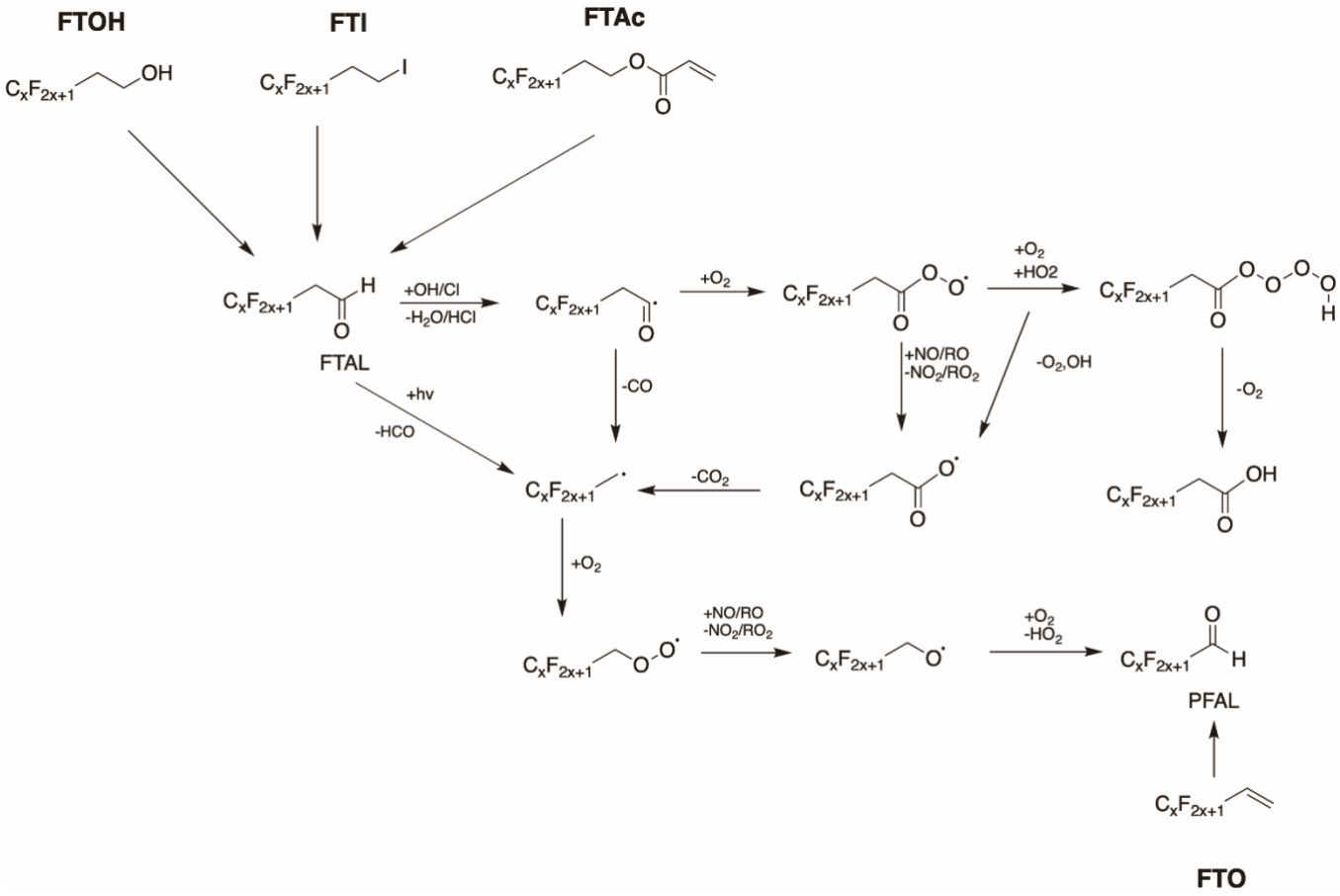

Figure 1-4: Reaction mechanism illustrating the atmospheric oxidation and degradation of FTAL to form PFAL. FTO will form the PFAL through several other steps. Reaction from [63] and references therein.

The conversion of PFAL to terminal PFCAs occurs via three principal mechanisms (Figure 1-5). The first mechanism involves the direct oxidation of PFAL hydrate with hydroxyl and Cl in the absence of NO_x, this reaction will form TFA as the primary product in 100% yield.[63] The second mechanism involves the reaction of perfluoroacyl peroxy radical with HO_2 to form PFCAs.[64] The perfluoroacyl peroxy radical intermediate can also degrade to PFCAs, perfluorinated peracids or perfluoronated acyl oxy radicals. The reaction with HO_2 will most likely occur in remote, low-NOx environments.[95] Finally, the third mechanism involves a radical "unzipping" pathway, initiated by the reaction of the perfluoroacyl peroxy radical with NO, leading to decarboxylation and the formation of a perfluoroalkyl radical.[64] This radical can either decompose to carbonyl fluoride or react

with organic peroxy radicals to form PFCAs. Ultimately, the yield of PFCAs is heavily dependent on the local NO_x concentrations.[101]

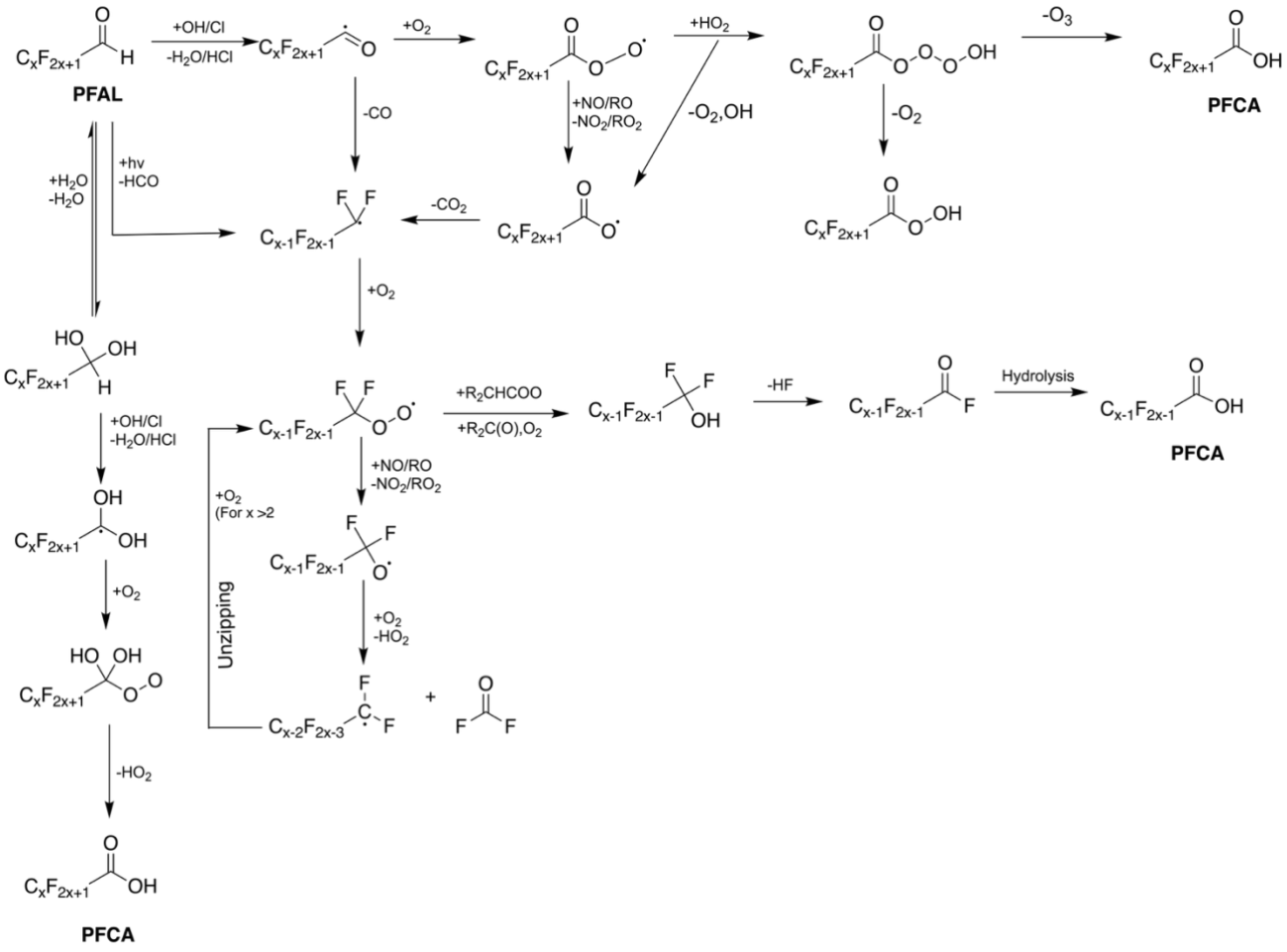

Figure 1-5: Reaction mechanism illustrating the atmospheric degradation pathway of PFAL to form PFCAs. Data from [63,64,96,97].

Evidence for the direct atmospheric formation of PFSAs from precursor compounds, such as perfluoroalkane sulfonamides (FASAs) and their sulfamidoethanols (FASE), is limited but mechanistically established (Figure 1-6) .[99] The primary pathway is initiated by the reaction with the hydroxyl radical. For FASEs like N-methyl perfluorobutanesulfonamidoethanol (N-MeFBSE), oxidation can begin on the ethanol moiety, but the key step for PFSA formation involves the addition of an hydroxyl radical directly to the sulfonyl group, generating a sulfonyl radical intermediate.[99] The intermediate can undergo homolytic cleavage of the carbon-sulfur bond to produce a

perfluoroalkyl radical, which subsequently degrades to form a homologous series of PFCAs or cleavage of the sulfur-nitrogen bond yields PFBS and a nitrogen-centered radical.[99] Smog chamber studies by D'Eon et al. demonstrated that the carbon sulfur bond cleavage is strongly favored over sulfur nitrogen bond cleavage by approximately a factor of 10.[99] An alternative mechanism, potentially relevant for reactions with Cl atoms or for the degradation of non-ethanol based FASA (e.g., N-EtFBSA), may involve hydrogen abstraction from the nitrogen atoms followed by oxygen insertion into the sulfur nitrogen bond, ultimately forming PFSA.[63]

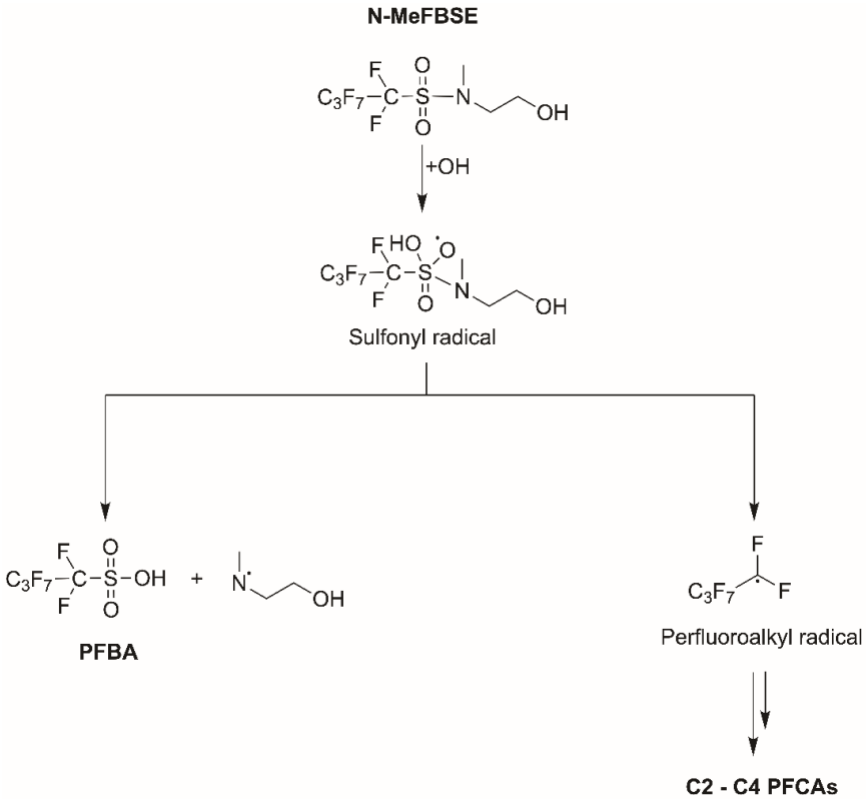

Figure 1-6: Atmospheric oxidation mechanism for N-methyl perfluorobutane-sulfonamidoethanol (N-MeFBSE) producing perfluorobutane sulfonic acid (PFBS) and perfluoroalkyl radicals. Double arrows represent the summation of several steps. Mechanism is adapted from [99].

1.4.3.3 Production changes that affect precursor compounds

The industrial production and regulatory landscape of PFAA and precursor compounds has undergone profound transformations throughout their history, characterized by distinct technological eras, voluntary phase-outs, and an evolving framework of international regulations.

Historically, production was dominated by long chain compounds manufactured primarily in the United States, Western Europe and Japan. The scale of this production was substantial, from 1957-2002, 3M manufactured an estimated 65 kt on POSF, a key precursor to PFOS and its derivatives.[102] Similarly, production of APFO (a PFOA-based product) was estimated at 3.6-5.7 kt during the same time.[61] Additionally, the fluorotelomerization route also contributed, with the production of fluorotelomer alcohols estimated at 11-13 kt per year in 2004.[103]

A pivotal shift began in the early 2000s, driven by the mounting scientific evidence on the environmental persistence, bioaccumulation, toxicity and long-range transport potential of PFAS. This resulted in several regulatory responses, starting with 3M's voluntary phase out of , PFOS and related C8-based chemistry between 2000-2002.[104] This was rapidly followed by coordinated governmental interventions. In 2006, The United States Environmental Protection Agency (US EPA) launched the PFOA stewardship program, securing a commitment from major manufacturers to eliminate PFOA and precursor emissions by 2015.[105] Mirroring this effort, Canada established an Environmental Performance Agreement the same year, achieving a similar phase-out goal.[106] The regulatory scope expanded globally with the 2009 listing of PFOS under Annex B of the Stockholm Convention on Persistent Organic Pollutants, restricting its production and use, followed by the 2019 listing of PFOA under Annex A, mandating its global elimination.[107] This framework was further strengthened in 2022 with the listing of perfluorohexane sulfonic acid (PFHxS) and its salts under Annex A.[107] The regulatory landscape is now advancing towards comprehensive class-based approaches. The most significant development is the European Chemicals Agency's (ECHA) 2023 proposal under the European Union (EU) REACH regulations to restrict the manufacture, placing on the market and the use of all PFAS.[108] This landmark proposal, one of the broadest in

history, aims to manage PFAS as a single class, fundamentally shifting away from a substance-by-substance approach.[108]

These collective actions have not only catalyzed a significant geographical shift of production to Asia but also initiated a strategic transition within the global chemical industry.[109] However, this transition from long-chain substances to shorter-chain homologues and novel fluorinated alternatives presents an ongoing challenge, as the environmental and health profiles of many replacements remain uncertain within this persistently evolving regulatory landscape.

1.5 Chlorofluorocarbon compounds

This section examines the development and atmospheric chemistry of CFC replacements, which undergo atmospheric oxidation to yield the shortest PFCA, TFA. Before the 1930s, common refrigerants included ammonia, chloromethane, carbon tetrachloride, isobutane and propane.[110] These substances were discontinued due to concerns regarding toxicity, flammability and operational hazards, particularly in domestic applications.[110] CFCs were subsequently developed in the 1930s as stable, non-flammable alternatives that revolutionized refrigeration, air conditioning and manufacturing.[111] Their exceptional stability, however, allowed them to accumulate in the atmosphere. Building on James Lovelock's work showing that most CFCs produced up to 1972 had accumulated in the atmosphere,[112] Mario J. Molina and F. Sherwood Rowland proposed that these compounds could reach the stratosphere, where they release chlorine atoms that catalytically destroy ozone,[113] a discovery that, along with Paul J Crutzen's work in atmospheric chemistry earned the 1995 Nobel Prize in Chemistry.[114]

In response, the Montreal Protocol on Substances that Deplete the Ozone Layer was adopted in 1987 and entered into force in 1989, under the Vienna Convention for the Protection of the Ozone Layer, mandating the global phase-out of ozone-depleting substances.[115] CFC replacement products included a range of halogenated substances including hydrochlorofluorocarbons (HCFCs), hydrofluorocarbons (HFCs), hydrofluoroethers (HFEs) and hydrofluoroolefins (HFOs). While few CFCs themselves were defined as PFAS, many of their replacement products fall within this category due to the presence of C-F bonds and their potential to form fluorinated degradation products.

These transitional compounds were introduced under the Montreal Protocol to reduce ozone depletion, but their atmospheric breakdown and climate impacts soon raised new environmental concerns.

1.5.1 Atmospheric chemistry of chlorofluorocarbon compounds

Several HCFCs, HFCs, HFEs and HFOs produce TFA through their atmospheric oxidation as both major and minor products with yields ranging from <10% to 100%.[63] In addition to TFA, oxidation of selected CFC replacement compounds can also form perfluoropropionic acid (PFPrA) and PFBA.[116] The atmospheric lifetime of these replacement compounds are generally dominated by gas-phase OH radical reactions in the troposphere, and the lifetimes are summarized in Table 1-4. Although the OH radical reaction is the dominant degradation pathway, reactions with O_3, Cl and NO_3 can also occur under specific conditions.[117] These compounds can also be transported to the upper atmosphere, but their atmospheric fates will be different.[118] The following discussion focuses on their atmospheric chemistry within the troposphere.

Table 1-4: Tropospheric lifetimes of selected halogenated precursors classes with respect to OH radical degradation. Data taken from [*118–120*]

Precursor	Tropospheric lifetime with respect to OH radical degradation
HCFCs	1-19 years
HFCs	13-228 years
HFEs	3-50 years
HFOs	10-24 days

Considering reaction mechanisms, HCFCs and HFCs primarily undergo initial hydrogen atom abstraction by hydroxyl radicals, forming a carbon-centered radical.[121] This radical subsequently reacts with O_2 and NO, yielding an alkoxy radical, which is further oxidized to a key acyl halide intermediate, trifluoroacetyl chloride from HCFCs or trifluoroacetyl fluoride from HFCs.[121] These acyl halides then hydrolyze to yield TFA. HFEs such as isoflurane and desflurane also react via hydrogen abstraction.[122] However, this process proceeds through the formation of an alkoxy radical that decomposes via C-

C or C-O bond cleavage to directly form perfluoroacyl fluorides, which subsequently hydrolyze to TFA.[122] Although the specific reaction sequence differs slightly depending on molecular structure, the ultimate product is the same. In contrast, HFOs are highly reactive towards hydroxyl radicals due to the unsaturated C=C bond. The reaction proceeds through hydroxyl radical addition to the double bond, forming a fluorinated alkyl radical that undergoes O_2 addition and further reactions to yield a perfluoroacyl fluoride. Hydrolysis of this intermediate produces TFA.[120] This highly efficient addition mechanism is responsible for the characteristically short atmospheric lifetimes of HFOs, which are on the order of days, reflecting their rapid tropospheric reactivity.[120]

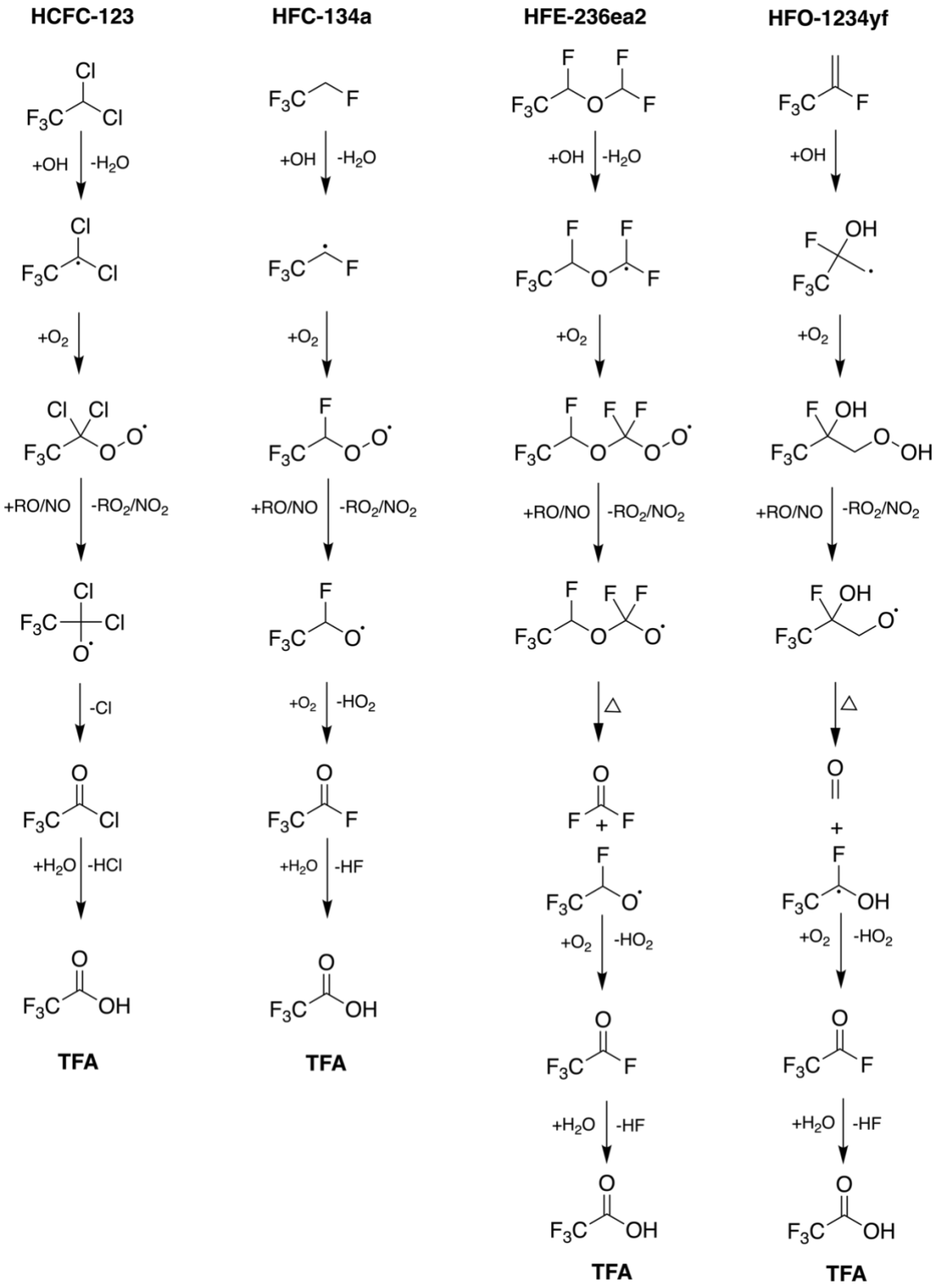

Figure 1-7: Schematic illustration of the atmospheric degradation pathways for HCFC-123, HFC-134a, HFE-236ea2, and HFO-1234yf—leading to the formation of trifluoroacetic acid (TFA).

1.5.2 Chlorofluorocarbon compound regulations and trends

The global implementation of the Montreal Protocol in 1989 initiated a critical transition away from CFCs in the industrial and chemical sectors.[115] This mandated phase-out of CFCs necessitated the rapid development of substitute compounds. This transition, however, has not been a simple linear progression but rather a series of iterative substitutions, each driven by evolving regulations and revealing new environmental tradeoffs.

Initially, HCFCs served as the first transitional substitutes to CFCs. Although these compounds had significantly lower ozone-depleting potential (ODPs) than CFCs, they were still regulated under amendments to the Montreal Protocol from 1990-1999, leading to a complete phase-out in developed countries by 2020 and by 2030 in developing countries.[123] The subsequent shift was to HFCs, which offered the key advantage of zero ODP. Their production in developed nations increased steadily from around 1995, with China becoming the major producer and consumer in the early 2000s.[124] This led to increased emissions of key HFCs, such as HFC-134a, from the 1990s onwards.[125] However, the climate implications of these compounds soon became apparent, as their potent greenhouse gas characteristics and high global warming potentials (GWPs), ranging from 150-8000, represented a significant consequence of the CFC phase-out.[126]

This consequence prompted the next major regulatory intervention: the Kigali Amendment of the Montreal Protocol in 2016. This agreement mandates a global phasedown of HFCs, with developed countries committing to a freeze in 2024 and an 80% reduction by 2043.[127] In response, a new generation of replacement compounds, HFOs, has been developed. With near-zero ODP and GWPs, HFO gases like HFO-1234yf are already being adopted as next-generation refrigerants in mobile air conditioning systems to replace HFC-134a. Production in North America is projected to reach 50-100 kt yr^{-1} in the coming decades.[118]

1.6 Wet and dry deposition of PFAAs

Atmospheric deposition is the dominant removal pathway of PFAA from the atmosphere. While this process acts as a sink, limiting their long-range transport potential, it simultaneously constitutes a direct source of PFAAs to terrestrial and aquatic

ecosystems. This occurs through two distinct mechanisms: (i) wet deposition and (ii) dry deposition.

Wet deposition involves the scavenging of atmospheric contaminants by precipitation (rain and snow). This process includes (i) in-cloud scavenging, where soluble vapors or aerosol particles act as cloud condensation nuclei and become incorporated into cloud or fog droplets and are removed by precipitation and (ii) below-cloud scavenging, where falling raindrops or snowflakes capture gaseous and particulate PFAAs from the air column.[129,130]. Meteorological conditions strongly influence the efficiency of wet deposition by controlling cloud microphysics, precipitation rate, and boundary layer dynamics.[131] For example, field data demonstrate that convective systems, characterized by strong updrafts and boundary layer entrainment, remove atmospheric PFAAs more effectively than stratiform precipitation.[132] The physicochemical properties of PFAAs, including the air-water partitioning coefficient (K_{aw}) and acid dissociation constants (pK_a)[133] also govern removal efficacy. PFAAs with high aqueous affinity that persist in their ionized form partition strongly into cloud and rain droplets. Furthermore, partitioning into snowflakes is favored at low temperature.[134,135] This characteristic, combined with the high specific surface area of snow, makes this deposition process a crucial pathway for the occurrence of PFAAs in polar regions.[134,135]

Dry deposition describes the direct transfer of pollutants to the Earth's surface in the absence of precipitation, and it operates for both particulates and gaseous species. This is a continuous process that occurs through Brownian diffusion, gravitational settling, interception and impaction.[136] The relative importance of these processes depends on particle size, where large particles (>1 μm) mainly deposit by gravitational settling and diffusion acting on smaller particles (<1 μm).[136] Hygroscopic growth, coagulation and particle composition can also move particles between ultrafine to fine mode but not to the coarse mode. Additionally, near-surface transport and surface properties (roughness, vegetation, wetness and chemical affinity) further modulate the net deposition velocity.[137] Generally, gas-phase PFAAs (typically neutral) diffuse to wet or solid surfaces and become retained by surface "scavenging".[138] Conversely, particle-bound PFAAs deposit by gravitational settling and impaction rather than diffusion. The size distribution also vary

by PFAA class, urban measurements of PFAAs in particles found PFCAs associated with ultrafine particles, whereas PFOS was associated with coarse particles.[139,140]

1.7 Measurements of PFAAs in atmospheric deposition

The environmental persistence and long-range transport potential of PFAAs have led to their ubiquitous distribution in air, precipitation and the terrestrial, freshwater and marine environment. This thesis focuses on quantifying PFAS in atmospheric deposition samples, specifically wet deposition and snow (ice cores) (Table 1-5 & 1-6), and these are discussed in sub section 1.7.1 and 1.7.2.

1.7.1 PFAA in wet deposition

Measurements of PFAAs in precipitation confirms that these compounds are globally distributed and strongly suggest that this is a key removal pathway from the atmosphere. Several studies have quantified PFAAs in wet deposition samples across North America, Europe and Asia with concentration ranges from hundreds of pg L^{-1} to several mg L^{-1}.[141–147] However, comparisons between different sampling time and location are complicated since most studies report concentrations instead of deposition flux (mass per unit area per time). To enable robust spatial and temporal comparisons, it is essential to convert concentrations to deposition flux which normalizes for variability in deposition volumes.

Although comprehensive flux measurements remain limited, existing studies suggest that wet deposition is a continuous source of PFAAs to both aquatic and terrestrial environment. Spatial trends show that deposition fluxes are elevated near point sources, such as fluoropolymer manufacturing plants,[148,149] confirming the importance of direct industrial emissions. Beyond localized hotspots, the levels of TFA and perfluoropropionic acid (PFPrA) homologues are consistently found with fluxes an order of magnitude greater than other legacy PFAAs (e.g., PFOA and PFOS).

1.7.2 PFAA in snow and ice cores

Snowfall efficiently scavenges PFAAs from the atmosphere. However, measurements of PFAAs in remote snow are limited mainly due to logistical challenges with sample collection and analysis. Early measurements of PFAAs in surface snow,

snow pit and firn cores established baseline PFAA levels with fluxes ranging from 1-244 ng m^{-2} a^{-1}.[150] The PFBA homologue was detected in the highest fluxes whereas PFOA and PFNA were the most abundant homologues, followed by perfluoroundecanoic acid (PFUnDA), PFOS and perfluorodecanoic acid (PFDA). The advancement of sampling and analytical techniques enabled the use of ice cores to examine temporal trends. Multi-decadal records from the Devon Ice Cap (1977-2015),[116,151] Mt. Oxford icefield (1967-2016) and Lomonosovfonna, Svalbard (2006-2019)[152] have since provided a more comprehensive understanding of PFAA sources and deposition mechanisms. A key finding from these records was the dominance of short-chain homologues, particularly TFA and PFPrA. Additionally, these records suggest an increasing trend of PFAA fluxes, providing critical insights into the continued long-range transport and atmospheric formation of PFAAs.

Table 1-5: Summary of available PFCA deposition flux (ng m^{-2} a^{-1}) in selected atmospheric deposition samples (precipitation, ice cores, surface snow and snow cores). When analytes were not a part of the monitored suite, cells are left empty

		Flux (ng m^{-2} a^{-1})										
Matrix (Time)	**Site (Reference)**	**TFA**	**PFPrA**	**PFBA**	**PFPeA**	**PFHxA**	**PFHpA**	**PFOA**	**PFNA**	**PFDA**	**PFUnDA**	**PFDoDA**
Precipitation (2015-2016)[a]	Corvo, Portugal[153]					99-1278	193-1789	767-4380	803-3431	204-1387	117-325	
	Wuhan, China[153]					840-14600	511-1278	2373-8030	511-1424	88-365	153-657	
	Beijing, China[153]					730-6205	584-6570	4745-32485	1241-10220	402-2628	266-3431	
	Råö, Sweden[153]					80-303	150-420	402-1752	237-767	62-157	29-157	
	Stockholm, Sweden[153]					58-1460	37-2081	120-1898	62-4015	11-767	15-876	
Precipitation 2020[a]	Wisconsin, USA[154]			91-2843	22-1256	110-1591	131-1132	55-1774	44-726	<LOD-380	<LOD-756	<LOD-139
Precipitation 2020-2021	Chongqing, China[155]			200	100	100	100	1400	100	400	300	
Precipitation 2021-2023	Switzerland[156]	410000-1280000										
Precipitation 2016	Mainland, China[149]	43800-5840000	767-98550	2227-34310	2190-34675	913-35040	1168-26645	1424-32850	1862-24090	511-34675	986-28835	803-12775
Precipitation 2018-2019	Germany[147]	91000-401000										
Precipitation 2007-2008	Guangzhou, China[157]	229000										
Ice Core (1967-2016)	Mt. Oxford icefield, Canadian Arctic[158]	29-20100	38-6700	1-303	1-64	1-117	1-139	3-222	1-316	1-40	1-60	1-6
Ice Core (2006-2019)	Lomonsovfonna Ice Core, Svalbard[159]	290-8200	130-1600	41-570	16-570	8-120	5-99	3-59	4-120	2-47	1-79	1-16
Ice Core (1977-2015)	Devon Ice Cap, Canadian Arctic [151]	471-21500	494-29000	2-174	1-37	3-38	6-86	6-80	5-141	0.5-21	0.8-29	1-2
Snow Pit 1995 – 2007	Devon Ice Cap, Canadian Arctic [160]			29-244	7-68	5-60	21-99	25-97	25-219	9-35	4-38	1-4
Snow Pit 1966 – 2006	Devon Ice Cap, Canadian Arctic [150]				3-9			21-81	2-103	1-9	1-10	
Surface Snow 2005	Melville Ice Cap, Canadian Arctic[150]							5	3	1		
Surface Snow 2005	Agassiz Ice Cap, Canadian Arctic[150]							4	3	1		
Snow Core 1980 - 2010	Mt. Muztagata, Tibetan Plateau [161]			<LOD	20-90	7-63		15-154	3-26	2-32	2-6	4-21
Snow Core 1980 – 2010	Mt. Zuoqiupu, Tibetan Plateau[161]			22-62	32-46	6-45		27-188	2-22	30-56		
Firn Core 1996 - 2008	Colle Gnifetti, Swiss/Italian Border [162]			242-545				165-207	86-113		0-53	

[a]denotes instances where annual fluxes were converted from daily flux (ng m^{-2} d^{-1}) to annual flux (ng m^{-2} a^{-1})

Table 1-6: Summary of available PFSA deposition flux (ng m^{-2} a^{-1}) in selected atmospheric deposition samples (precipitation, ice cores, surface snow and snow cores).When analytes were not a part of the monitored suite, cells are left empty

		Flux (ng m^{-2} a^{-1})						
Matrix (Time)	**Site (Reference)**	**PFBS**	**PFHxS**	**PFHpS**	**PFOS**	**PFDS**	**PFECHS**	**FOSA**
Precipitation (2015-2016)[a]	Corvo, Portugal[153]		66-475		675-3687			
	Wuhan, China[153]		55-345		<LOD			
	Beijing, China[153]		164-219		949-2044			
	Råö, Sweden[153]		29-321		438-2701			
	Stockholm, Sweden[153]		7-47		33-1095			
Precipitation 2020[a]	Wisconsin, USA[154]	<LOD	25-161	22-33	37-168	<LOD-73		<LOD-66
Precipitation 2016	Mainland, China[149]	475-47450	208-28105		3650-102200			
Ice Core (1967-2016)	Mt. Oxford icefield, Canadian Arctic[158]	<LOD - 118	<LOD	<LOD	<LOD - 472	<LOD	<LOD - 27	<LOD - 15
Ice Core (2006-2019)	Lomonsovfonna Ice Core, Svalbard[159]		1-9		1-10			1-5
Ice Core (1977-2015)	Devon Ice Cap, Canadian Arctic[151]	<LOD-1	<LOD-2		1-80			<LOD-10
Snow Pit 1995 – 2007	Devon Ice Cap, Canadian Arctic[160]	<LOD-39	<LOD	<LOD	1-4		1-4	2-19
Snow Core 1980 - 2010	Mt. Muztagata, Tibetan Plateau [161]				<LOD			
Snow Core 1980 – 2010	Mt. Zuoqiupu, Tibetan Plateau[161]				21-200			

[a]denotes instances where annual fluxes were converted from daily flux (ng m^{-2} d^{-1}) to annual flux (ng $m^{-2}a^{-1}$)

1.8 Thesis objective

It is evident that the manufacturing and use of PFAS and CFC replacement compounds have led to widespread distribution of PFAAs in various environmental compartments. Despite this ubiquity, there are uncertainties regarding their atmospheric transport and deposition, processes that govern their spatial and temporal distribution. The objective of this thesis is to advance understanding of the spatial and temporal distribution of PFAAs using atmospheric deposition samples collected across Arctic, boreal, urban, and tropical environments.

Environmental monitoring of PFAAs in the High Arctic is useful for improving our understanding of long-range atmospheric transport. However, studies in the Canadian High Arctic remain limited, with only three studies reported to date, these include one snow pit and two ice cores spanning 14 and 38 years from the Devon Ice Cap.[150,151,163] To improve our understanding of PFAA transport and deposition, Chapter 2 presents an extensive 50-year record of PFAAs reconstructed from a 16.5 m ice core collected from Ellesmere island, Nunavut, Canada. This record provides the longest record of PFCAs in the Arctic and the longest record of PFSAs globally. In this work, we (i) quantify temporal variations in PFAA deposition, (ii) identify evidence of both direct emissions and indirect formation via atmospheric precursor oxidation, and (iii) compare observed deposition with available model estimates.

Chapter 3 investigates the spatial distribution of PFAA deposition across the Newfoundland and Labrador Boreal Ecosystem Latitudinal Transect (NL-BELT). This chapter quantifies total, wet and calculated dry deposition fluxes between 2013-2016 to identify dominant removal mechanisms and identify sources of PFAA to this region. Specific objectives include (i) determining concentration and fluxes of PFAAs in total and wet deposition samples, (ii) evaluating the dry deposition contribution, (iii) examining evidence of direct transport, marine aerosol input and indirect formation from precursor oxidation and (iv) comparing observations with chemical transport model predictions.

Chapter 4 shifts focus to an urban environment to examine the atmospheric removal of TFA, through long-term measurements of total and wet deposition samples in Toronto, ON, Canada. This study tests the hypothesis that TFA levels should increase with regulatory changes introduced under the Montreal Protocol and its amendments (i.e.,

introduction of HFOs). These measurements provide critical insights into emission influence, transport mechanisms and deposition processes that govern TFA. This chapter quantifies total, wet and calculated dry deposition fluxes over a period of six years (2018-2024) to determine the dominant removal pathways, evaluate seasonal and interannual variability and compare observed deposition fluxes to existing model estimates. The findings contribute to improved understanding of precursor driven sources, provides the first estimates of dry deposition contribution of TFA and one of the first multi-year field constraints on TFA deposition dynamics in North America.

Finally, Chapter 5 extends the investigation of TFA deposition to a global scale by quantifying TFA deposition across contrasting hemispheres. This chapter compares total deposition between a tropical site in Georgetown, Guyana, and a rural site in Lambton County, Canada, to evaluate the global reach and hemispheric differences in TFA deposition. This study represents the first measurements of TFA deposition near the equator and provides crucial insights for understanding sources, atmospheric transformation processes and the role of climate influencing TFA fluxes. Specific objectives include (i) quantifying and comparing deposition fluxes across the northern and southern hemispheres, (ii) identifying dominant processes and removal mechanisms, and (iii) evaluating model predictions against field measurements to refine our understanding of global TFA deposition.

1.9 References

(1) Gaines, L. G. T. Historical and Current Usage of Per- and Polyfluoroalkyl Substances (PFAS): A Literature Review. *Am. J. Ind. Med.* **2023**, *66* (5), 353–378. https://doi.org/10.1002/ajim.23362.

(2) Buck, R. C.; Franklin, J.; Berger, U.; Conder, J. M.; Cousins, I. T.; Voogt, P. D.; Jensen, A. A.; Kannan, K.; Mabury, S. A.; van Leeuwen, S. P. J. Perfluoroalkyl and Polyfluoroalkyl Substances in the Environment: Terminology, Classification, and Origins. *Integr. Environ. Assess. Manag.* **2011**, *7* (4), 513–541. https://doi.org/10.1002/ieam.258.

(3) OECD. *Reconciling Terminology of the Universe of Per- and Polyfluoroalkyl Substances: Recommendations and Practical Guidance*; OECD Series on Risk Management; 61; 2021; p 23. https://www.oecd.org/chemicalsafety/portal-perfluorinated-chemicals/terminology-per-and-polyfluoroalkyl-substances.pdf (accessed 2025-09-25).

(4) Schymanski, E. L.; Zhang, J.; Thiessen, P. A.; Chirsir, P.; Kondic, T.; Bolton, E. E. Per- and Polyfluoroalkyl Substances (PFAS) in PubChem: 7 Million and Growing. *Environ. Sci. Technol.* **2023**, *57* (44), 16918–16928. https://doi.org/10.1021/acs.est.3c04855.

(5) Wang, Z. S25 | OECDPFAS | List of PFAS from the OECD, 2018. https://doi.org/10.5281/zenodo.2648776.

(6) National Institute of Standards and Technology. Suspect List of Possible Per- and Polyfluoroalkyl Substances (PFAS), 2021. https://catalog.data.gov/dataset/suspect-list-of-possible-per-and-polyfluoroalkyl-substances-pfas (accessed 2025-09-25).

(7) US EPA. *CompTox Chemicals Dashboard | PFASMASTER Chemicals*. https://comptox.epa.gov/dashboard/chemical-lists/PFASMASTER (accessed 2025-09-25).

(8) Kissa, E. *Fluorinated Surfactants: Synthesis, Properties, Applications*; Bioprocess Technology; M. Dekker, 1994.

(9) Kissa, E. *Fluorinated Surfactants and Repellents*; Marcel Dekker, Inc.: New York, 2001.

(10) Plunkett, R. J. Tetrafluoroethylene Polymers. 282437. https://patentimages.storage.googleapis.com/98/41/23/c486d71a8c4ec2/US2230654.pdf (accessed 2025-10-20).

(11) Midgley, T.; Henne, A. L. Organic Fluorides as Refrigerants[1]. *Ind. Eng. Chem.* **1930**, *22* (5), 542–545. https://doi.org/10.1021/ie50245a031.

(12) Goldwhite, H. The Manhattan Project. *J. Fluor. Chem.* **1986**, *33* (1–4), 109–132. https://doi.org/10.1016/S0022-1139(00)85273-2.

(13) Simons, J. H. Production of Fluorocarbons. *J. Electrochem. Soc.* **1949**, *95* (2), 47. https://doi.org/10.1149/1.2776733.

(14) Haszeldine, R. N. 603. The Reactions of Fluorocarbon Radicals. Part I. The Reaction of Iodotrifluoromethane with Ethylene and Tetrafluoroethylene. *J. Chem. Soc. Resumed* **1949**, 2856. https://doi.org/10.1039/jr9490002856.

(15) Benskin, J. P.; De Silva, A. O.; Martin, J. W. Isomer Profiling of Perfluorinated Substances as a Tool for Source Tracking: A Review of Early Findings and Future Applications. In *Reviews of Environmental Contamination and Toxicology Volume 208*; De Voogt, P., Ed.; Reviews of Environmental Contamination and Toxicology; Springer New York: New York, NY, 2010; Vol. 208, pp 111–160. https://doi.org/10.1007/978-1-4419-6880-7_2.

(16) Renner, R. The Long and the Short of Perfluorinated Replacements. *Environ. Sci. Technol.* **2006**, *40* (1), 12–13. https://doi.org/10.1021/es062612a.

(17) Young, C. J.; Hurley, M. D.; Wallington, T. J.; Mabury, S. A. Atmospheric Chemistry of 4:2 Fluorotelomer Iodide (*n* -C_4 F_9 CH_2 CH_2 I): Kinetics and Products of Photolysis and Reaction with OH Radicals and Cl Atoms. *J. Phys. Chem. A* **2008**, *112* (51), 13542–13548. https://doi.org/10.1021/jp807322x.

(18) De Silva, A. O.; Muir, D. C. G.; Mabury, S. A. Distribution of Perfluorocarboxylate Isomers in Select Samples from the North American Environment. *Environ. Toxicol. Chem.* **2009**, *28* (9), 1801–1814. https://doi.org/10.1897/08-500.1.

(19) Leung, S. C. E.; Wanninayake, D.; Chen, D.; Nguyen, N.-T.; Li, Q. Physicochemical Properties and Interactions of Perfluoroalkyl Substances (PFAS) - Challenges and Opportunities in Sensing and Remediation. *Sci. Total Environ.* **2023**, *905*, 166764. https://doi.org/10.1016/j.scitotenv.2023.166764.

(20) Musegades, L. J.; Curtin, O. P.; Cyran, J. D. Determining the Surface p K_a of Perfluorooctanoic Acid. *J. Phys. Chem. C* **2024**, *128* (5), 1946–1951. https://doi.org/10.1021/acs.jpcc.3c07235.

(21) Balasuryia, D.; Queral-Beltran, A.; Vick, T.; Simpson, S.; Lacorte, S.; Aga, D. S.; Hoepker, A. C. Experimental Determination of p K_a for 10 PFAS, Mono-, Di-, and Trifluoroacetic Acid by^{19} F-NMR. *Environ. Sci. Technol. Lett.* **2025**, *12* (9), 1238–1246. https://doi.org/10.1021/acs.estlett.5c00688.

(22) Wang, Z.; MacLeod, M.; Cousins, I. T.; Scheringer, M.; Hungerbühler, K. Using COSMOtherm to Predict Physicochemical Properties of Poly- and Perfluorinated Alkyl Substances (PFASs). *Environ. Chem.* **2011**, *8* (4), 389. https://doi.org/10.1071/EN10143.

(23) Webster, E.; Ellis, D. A.; Reid, L. K. Modeling the Environmental Fate of Perfluorooctanoic Acid and Perfluorooctanoate: An Investigation of the Role of Individual Species Partitioning. *Environ. Toxicol. Chem.* **2010**, *29* (7), 1466–1475. https://doi.org/10.1002/etc.181.

(24) Vierke, L.; Berger, U.; Cousins, I. T. Estimation of the Acid Dissociation Constant of Perfluoroalkyl Carboxylic Acids through an Experimental Investigation of Their Water-to-Air Transport. *Environ. Sci. Technol.* **2013**, *47* (19), 11032–11039. https://doi.org/10.1021/es402691z.

(25) Chambers, W. S.; Hopkins, J. G.; Richards, S. M. A Review of Per- and Polyfluorinated Alkyl Substance Impairment of Reproduction. *Front. Toxicol.* **2021**, *3*, 732436. https://doi.org/10.3389/ftox.2021.732436.

(26) Christensen, E. R.; Wang, Y.; Huo, J.; Li, A. Properties and Fate and Transport of Persistent and Mobile Polar Organic Water Pollutants: A Review. *J. Environ. Chem. Eng.* **2022**, *10* (2), 107201. https://doi.org/10.1016/j.jece.2022.107201.

(27) Naidu, R.; Mallavarapu, M.; Liu, Y.; Umeh, A. *Per- and Polyfluorinated Alkyl Substances: Occurrence, Toxicity and Remediation of PFAS*; Walter de Gruyter GmbH & Co KG, 2025.

(28) *Per- and Polyfluoroalkyl Substances (PFAS)*. ITRC. https://itrcweb.org/pfas-guidance/ (accessed 2025-10-11).

(29) Rayne, S.; Forest, K. Congener Specific Organic Carbon Normalized Soil and Sediment-Water Partitioning Coefficients for the C1 through C8 Perfluorinated Alkylsulfonic and Alkylcarboxylic Acids. *Nat. Preced.* **2009**. https://doi.org/10.1038/npre.2009.3011.1.

(30) Fabregat-Palau, J.; Vidal, M.; Rigol, A. Examining Sorption of Perfluoroalkyl Substances (PFAS) in Biochars and Other Carbon-Rich Materials. *Chemosphere* **2022**, *302*, 134733. https://doi.org/10.1016/j.chemosphere.2022.134733.

(31) Milinovic, J.; Lacorte, S.; Vidal, M.; Rigol, A. Sorption Behaviour of Perfluoroalkyl Substances in Soils. *Sci. Total Environ.* **2015**, *511*, 63–71. https://doi.org/10.1016/j.scitotenv.2014.12.017.

(32) Podder, A.; Sadmani, A. H. M. A.; Reinhart, D.; Chang, N.-B.; Goel, R. Per and Poly-Fluoroalkyl Substances (PFAS) as a Contaminant of Emerging Concern in Surface Water: A Transboundary Review of Their Occurrences and Toxicity Effects. *J. Hazard. Mater.* **2021**, *419*, 126361. https://doi.org/10.1016/j.jhazmat.2021.126361.

(33) Torralba-Sanchez, T. L.; Di Toro, D. M.; Dmitrenko, O.; Murillo-Gelvez, J.; Tratnyek, P. G. Modeling the Partitioning of Anionic Carboxylic and Perfluoroalkyl Carboxylic and Sulfonic Acids to Octanol and Membrane Lipid. *Environ. Toxicol. Chem.* **2023**, *42* (11), 2317–2328. https://doi.org/10.1002/etc.5716.

(34) TAVES, D. R. Evidence That There Are Two Forms of Fluoride in Human Serum. *Nature* **1968**, *217* (5133), 1050–1051. https://doi.org/10.1038/2171050b0.

(35) Belisle, J. Organic Fluorine in Human Serum: Natural Versus Industrial Sources. *Science* **1981**, *212* (4502), 1509–1510. https://doi.org/10.1126/science.7233235.

(36) Ubel, F. A.; Sorenson, S. D.; Roach, D. E. Health Status of Plant Workers Exposed to Fluorochemicals - a Preliminary Report. *Am. Ind. Hyg. Assoc. J.* **1980**, *41* (8), 584–589. https://doi.org/10.1080/15298668091425310.

(37) Giesy, J. P.; Kannan, K. Global Distribution of Perfluorooctane Sulfonate in Wildlife. *Environ. Sci. Technol.* **2001**, *35* (7), 1339–1342. https://doi.org/10.1021/es001834k.

(38) Hansen, K. J.; Clemen, L. A.; Ellefson, M. E.; Johnson, H. O. Compound-Specific, Quantitative Characterization of Organic Fluorochemicals in Biological Matrices. *Environ. Sci. Technol.* **2001**, *35* (4), 766–770. https://doi.org/10.1021/es001489z.

(39) Zhao, L.; Teng, M.; Zhao, X.; Li, Y.; Sun, J.; Zhao, W.; Ruan, Y.; Leung, K. M. Y.; Wu, F. Insight into the Binding Model of Per- and Polyfluoroalkyl Substances to Proteins and Membranes. *Environ. Int.* **2023**, *175*, 107951. https://doi.org/10.1016/j.envint.2023.107951.

(40) Chen, R.; Muensterman, D.; Field, J.; Ng, C. Deriving Membrane–Water and Protein–Water Partition Coefficients from In Vitro Experiments for Per- and Polyfluoroalkyl Substances (PFAS). *Environ. Sci. Technol.* **2025**, *59* (1), 82–91. https://doi.org/10.1021/acs.est.4c06734.

(41) Ng, C. A.; Hungerbühler, K. Bioaccumulation of Perfluorinated Alkyl Acids: Observations and Models. *Environ. Sci. Technol.* **2014**, *48* (9), 4637–4648. https://doi.org/10.1021/es404008g.

(42) Conder, J. M.; Hoke, R. A.; Wolf, W. D.; Russell, M. H.; Buck, R. C. Are PFCAs Bioaccumulative? A Critical Review and Comparison with Regulatory Criteria and Persistent Lipophilic Compounds. *Environ. Sci. Technol.* **2008**, *42* (4), 995–1003. https://doi.org/10.1021/es070895g.

(43) Ahrens, L.; Bundschuh, M. Fate and Effects of Poly- and Perfluoroalkyl Substances in the Aquatic Environment: A Review. *Environ. Toxicol. Chem.* **2014**, *33* (9), 1921–1929. https://doi.org/10.1002/etc.2663.

(44) Sunderland, E. M.; Hu, X. C.; Dassuncao, C.; Tokranov, A. K.; Wagner, C. C.; Allen, J. G. A Review of the Pathways of Human Exposure to Poly- and Perfluoroalkyl Substances (PFASs) and Present Understanding of Health Effects. *J. Expo. Sci. Environ. Epidemiol.* **2019**, *29* (2), 131–147. https://doi.org/10.1038/s41370-018-0094-1.

(45) Haug, L. S.; Huber, S.; Becher, G.; Thomsen, C. Characterisation of Human Exposure Pathways to Perfluorinated Compounds — Comparing Exposure Estimates with Biomarkers of Exposure. *Environ. Int.* **2011**, *37* (4), 687–693. https://doi.org/10.1016/j.envint.2011.01.011.

(46) Vestergren, R.; Cousins, I. T.; Trudel, D.; Wormuth, M.; Scheringer, M. Estimating the Contribution of Precursor Compounds in Consumer Exposure to PFOS and PFOA. *Chemosphere* **2008**, *73* (10), 1617–1624. https://doi.org/10.1016/j.chemosphere.2008.08.011.

(47) Genuis, S. J.; Birkholz, D.; Ralitsch, M.; Thibault, N. Human Detoxification of Perfluorinated Compounds. *Public Health* **2010**, *124* (7), 367–375. https://doi.org/10.1016/j.puhe.2010.03.002.

(48) Ma, J.; Zhu, H.; Kannan, K. Fecal Excretion of Perfluoroalkyl and Polyfluoroalkyl Substances in Pets from New York State, United States. *Environ. Sci. Technol. Lett.* **2020**, *7* (3), 135–142. https://doi.org/10.1021/acs.estlett.9b00786.

(49) Rosato, I.; Bonato, T.; Fletcher, T.; Batzella, E.; Canova, C. Estimation of Per- and Polyfluoroalkyl Substances (PFAS) Half-Lives in Human Studies: A Systematic Review and Meta-Analysis. *Environ. Res.* **2024**, *242*, 117743. https://doi.org/10.1016/j.envres.2023.117743.

(50) Stahl, T.; Mattern, D.; Brunn, H. Toxicology of Perfluorinated Compounds. *Environ. Sci. Eur.* **2011**, *23* (1), 38. https://doi.org/10.1186/2190-4715-23-38.

(51) DeWitt, J. C. *Toxicological Effects of Perfluoroalkyl and Polyfluoroalkyl Substances*; Springer, 2015.

(52) Coperchini, F.; Teliti, M.; Greco, A.; Croce, L.; Rotondi, M. Per-Polyfluoroalkyl Substances (PFAS) as Thyroid Disruptors: Is There Evidence for Multi-Transgenerational Effects? *Expert Rev. Endocrinol. Metab.* **2024**, *19* (4), 307–315. https://doi.org/10.1080/17446651.2024.2351885.

(53) Kim, S.-J.; Shin, H.; Lee, Y.-B.; Cho, H.-Y. Sex-Specific Risk Assessment of PFHxS Using a Physiologically Based Pharmacokinetic Model. *Arch. Toxicol.* **2018**, *92* (3), 1113–1131. https://doi.org/10.1007/s00204-017-2116-5.

(54) Solan, M. E.; Lavado, R. The Use of in Vitro Methods in Assessing Human Health Risks Associated with Short-chain Perfluoroalkyl and Polyfluoroalkyl Substances (PFAS). *J. Appl. Toxicol.* **2022**, *42* (8), 1298–1309. https://doi.org/10.1002/jat.4270.

(55) Sodani, K.; Ter Braak, B.; Hartvelt, S.; Boelens, M.; Jamalpoor, A.; Mukhi, S. Toxicological Mode-of-Action and Developmental Toxicity of Different Carbon Chain Length PFAS. *Toxicol. Lett.* **2025**, *405*, 59–66. https://doi.org/10.1016/j.toxlet.2025.02.003.

(56) Freeling, F.; Scheurer, M.; Koschorreck, J.; Hoffmann, G.; Ternes, T. A.; Nödler, K. Levels and Temporal Trends of Trifluoroacetate (TFA) in Archived Plants: Evidence

for Increasing Emissions of Gaseous TFA Precursors over the Last Decades. *Environ. Sci. Technol. Lett.* **2022**, *9*, 400–405. https://doi.org/10.1021/acs.estlett.2c00164.

(57) Hawley, A. S.; Winne, M.; Cahill, T. M. Trifluoroacetic Acid Concentrations in Consumer Foods. *J. Agric. Food Chem.* **2025**, *73* (50), 32250–32254. https://doi.org/10.1021/acs.jafc.5c07390.

(58) Scheurer, M.; Nödler, K. Ultrashort-Chain Perfluoroalkyl Substance Trifluoroacetate (TFA) in Beer and Tea – An Unintended Aqueous Extraction. *Food Chem.* **2021**, *351*, 129304. https://doi.org/10.1016/j.foodchem.2021.129304.

(59) Yamashita, N.; Kannan, K.; Taniyasu, S.; Horii, Y.; Petrick, G.; Gamo, T. A Global Survey of Perfluorinated Acids in Oceans. *Mar. Pollut. Bull.* **2005**, *51* (8–12), 658–668. https://doi.org/10.1016/j.marpolbul.2005.04.026.

(60) Yeung, L. W. Y.; Dassuncao, C.; Mabury, S.; Sunderland, E. M.; Zhang, X.; Lohmann, R. Vertical Profiles, Sources, and Transport of PFASs in the Arctic Ocean. *Environ. Sci. Technol.* **2017**, *51* (12), 6735–6744. https://doi.org/10.1021/acs.est.7b00788.

(61) Prevedouros, K.; Cousins, I. T.; Buck, R. C.; Korzeniowski, S. H. Sources, Fate and Transport of Perfluorocarboxylates. *Environ. Sci. Technol.* **2006**, *40* (1), 32–44. https://doi.org/10.1021/es0512475.

(62) Sha, B.; Johansson, J. H.; Benskin, J. P.; Cousins, I. T.; Salter, M. E. Influence of Water Concentrations of Perfluoroalkyl Acids (PFAAs) on Their Size-Resolved Enrichment in Nascent Sea Spray Aerosols. *Environ. Sci. Technol.* **2021**, *55* (14), 9489–9497. https://doi.org/10.1021/acs.est.0c03804.

(63) Young, C. J.; Mabury, S. A. Reviews of Environmental Contamination and Toxicology Perfluorinated Alkylated Substances. In *Reviews of Enviromental Contamination and Toxicology*; edited by de Voogt, P., Ed.; Springer New York: New York, NY, 2010; Vol. 208.

(64) Ellis, D. A.; Martin, J. W.; Mabury, S. A.; Hurley, M. D.; Sulbaek Andersen, M. P.; Wallington, T. J. Atmospheric Lifetime of Fluorotelomer Alcohols. *Environ. Sci. Technol.* **2003**, *37* (17), 3816–3820. https://doi.org/10.1021/es034136j.

(65) Archer, C. L.; Jacobson, M. Z. Evaluation of Global Wind Power. *J. Geophys. Res. Atmospheres* **2005**, *110* (D12). https://doi.org/10.1029/2004JD005462.

(66) Wong, F.; Shoeib, M.; Katsoyiannis, A.; Eckhardt, S.; Stohl, A.; Bohlin-Nizzetto, P.; Li, H.; Fellin, P.; Su, Y.; Hung, H. Assessing Temporal Trends and Source Regions of Per- and Polyfluoroalkyl Substances (PFASs) in Air under the Arctic Monitoring and Assessment Programme (AMAP). *Atmos. Environ.* **2018**, *172* (June 2017), 65–73. https://doi.org/10.1016/j.atmosenv.2017.10.028.

(67) Wong, F.; Hung, H.; Dryfhout-Clark, H.; Aas, W.; Bohlin-Nizzetto, P.; Breivik, K.; Mastromonaco, M. N.; Lundén, E. B.; Ólafsdóttir, K.; Sigurðsson, Á.; Vorkamp, K.; Bossi, R.; Skov, H.; Hakola, H.; Barresi, E.; Sverko, E.; Fellin, P.; Li, H.; Vlasenko, A.; Zapevalov, M.; Samsonov, D.; Wilson, S. Time Trends of Persistent Organic Pollutants (POPs) and Chemicals of Emerging Arctic Concern (CEAC) in Arctic Air from 25 Years of Monitoring. *Sci. Total Environ.* **2021**, *775* (January). https://doi.org/10.1016/j.scitotenv.2021.145109.

(68) Ahrens, L.; Shoeib, M.; Del Vento, S.; Codling, G.; Halsall, C. Polyfluoroalkyl Compounds in the Canadian Arctic Atmosphere. *Environ. Chem.* **2011**, *8* (4), 399. https://doi.org/10.1071/EN10131.

(69) Stock, N. L.; Furdui, V. I.; Muir, D. C. G.; Mabury, S. A. Perfluoroalkyl Contaminants in the Canadian Arctic: Evidence of Atmospheric Transport and Local Contamination. *Environ. Sci. Technol.* **2007**, *41* (10), 3529–3536. https://doi.org/10.1021/es062709x.

(70) Rauert, C.; Shoieb, M.; Schuster, J. K.; Eng, A.; Harner, T. Atmospheric Concentrations and Trends of Poly- and Perfluoroalkyl Substances (PFAS) and Volatile Methyl Siloxanes (VMS) over 7 Years of Sampling in the Global Atmospheric Passive Sampling (GAPS) Network. *Environ. Pollut.* **2018**, *238*, 94–102. https://doi.org/10.1016/j.envpol.2018.03.017.

(71) Shoeib, M.; Harner, T.; Vlahos, P. Perfluorinated Chemicals in the Arctic Atmosphere. *Environ. Sci. Technol.* **2006**, *40* (24), 7577–7583. https://doi.org/10.1021/es0618999.

(72) Cai, M. M.; Zhao, Z.; Yin, Z.; Ahrens, L.; Huang, P.; Cai, M. M.; Yang, H.; He, J.; Sturm, R.; Ebinghaus, R.; Xie, Z. Occurrence of Perfluoroalkyl Compounds in Surface Waters from the North Pacific to the Arctic Ocean. *Environ. Sci. Technol.* **2012**, *46* (2), 661–668. https://doi.org/10.1021/es2026278.

(73) Benskin, J. P.; Muir, D. C. G.; Scott, B. F.; Spencer, C.; De Silva, A. O.; Kylin, H.; Martin, J. W.; Morris, A.; Lohmann, R.; Tomy, G.; Rosenberg, B.; Taniyasu, S.; Yamashita, N. Perfluoroalkyl Acids in the Atlantic and Canadian Arctic Oceans. *Environ. Sci. Technol.* **2012**, *46* (11), 5815–5823. https://doi.org/10.1021/es300578x.

(74) Busch, J.; Ahrens, L.; Xie, Z.; Sturm, R.; Ebinghaus, R. Polyfluoroalkyl Compounds in the East Greenland Arctic Ocean. *J. Environ. Monit.* **2010**, *12* (6), 1242. https://doi.org/10.1039/c002242j.

(75) Muir, D.; Miaz, L. T. Spatial and Temporal Trends of Perfluoroalkyl Substances in Global Ocean and Coastal Waters. *Environ. Sci. Technol.* **2021**, *55* (14), 9527–9537. https://doi.org/10.1021/acs.est.0c08035.

(76) Miranda, D. D. A.; Leonel, J.; Benskin, J. P.; Johansson, J.; Hatje, V. Perfluoroalkyl Substances in the Western Tropical Atlantic Ocean. *Environ. Sci. Technol.* **2021**, *55* (20), 13749–13758. https://doi.org/10.1021/acs.est.1c01794.

(77) Yu, J.; Fu, Y.; Zhu, J.; Chen, X.; Zhong, Y.; Pan, Y.; Ma, Y. Marine Transport Barrier for Traditional and Emerging Per- and Polyfluoroalkyl Substances in the Southeast Indian Ocean and Antarctic Marginal Seas. *Environ. Sci. Technol.* **2025**, *59* (10), 5283–5292. https://doi.org/10.1021/acs.est.4c13574.

(78) Tansel, B. Geographical Characteristics That Promote Persistence and Accumulation of PFAS in Coastal Waters and Open Seas: Current and Emerging Hot Spots. *Environ. Chall.* **2024**, *14*, 100861. https://doi.org/10.1016/j.envc.2024.100861.

(79) *The Freshwater Budget of the Arctic Ocean*; Lewis, E. L., Jones, E. P., Lemke, P., Prowse, T. D., Wadhams, P., Eds.; Springer Netherlands: Dordrecht, 2000. https://doi.org/10.1007/978-94-011-4132-1.

(80) Li, K.-Y.; Liu, W. Weakened Atlantic Meridional Overturning Circulation Causes the Historical North Atlantic Warming Hole. *Commun. Earth Environ.* **2025**, *6* (1), 416. https://doi.org/10.1038/s43247-025-02403-0.

(81) National Oceanic and Atmospheric Administration. *The Global Conveyor Belt - Currents: NOAA's National Ocean Service Education*. https://oceanservice.noaa.gov/education/tutorial_currents/05conveyor2.html (accessed 2025-10-03).

(82) Fahrbach, E.; Meincke, J.; Østerhus, S.; Rohardt, G.; Schauer, U.; Tverberg, V.; Verduin, J. Direct Measurements of Volume Transports through Fram Strait. *Polar Res.* **2001**, *20* (2), 217–224. https://doi.org/10.3402/polar.v20i2.6520.

(83) Andreae, M. O.; Rosenfeld, D. Aerosol–Cloud–Precipitation Interactions. Part 1. The Nature and Sources of Cloud-Active Aerosols. *Earth-Sci. Rev.* **2008**, *89* (1–2), 13–41. https://doi.org/10.1016/j.earscirev.2008.03.001.

(84) Saliba, G.; Chen, C.-L.; Lewis, S.; Russell, L. M.; Rivellini, L.-H.; Lee, A. K. Y.; Quinn, P. K.; Bates, T. S.; Haëntjens, N.; Boss, E. S.; Karp-Boss, L.; Baetge, N.; Carlson, C. A.; Behrenfeld, M. J. Factors Driving the Seasonal and Hourly Variability of Sea-Spray Aerosol Number in the North Atlantic. *Proc. Natl. Acad. Sci.* **2019**, *116* (41), 20309–20314. https://doi.org/10.1073/pnas.1907574116.

(85) de Leeuw, G.; Andreas, E. L.; Anguelova, M. D.; Fairall, C. W.; Lewis, E. R.; O'Dowd, C.; Schulz, M.; Schwartz, S. E. Production Flux of Sea Spray Aerosol. *Rev. Geophys.* **2011**, *49* (2). https://doi.org/10.1029/2010RG000349.

(86) Lewis, R.; Schwartz, E. *Sea Salt Aerosol Production: Mechanisms, Methods, Measurements and Models—A Critical Review*; Geophysical Monograph Series; American Geophysical Union: Washington, D. C., 2004; Vol. 152. https://doi.org/10.1029/GM152.

(87) Yuan, S.; Wang, X.; Jiang, Z.; Zhang, H.; Yuan, S. Contribution of Air-Water Interface in Removing PFAS from Drinking Water: Adsorption, Stability, Interaction and Machine Learning Studies. *Water Res.* **2023**, *236*, 119947. https://doi.org/10.1016/j.watres.2023.119947.

(88) McMurdo, C. J.; Ellis, D. A.; Webster, E.; Butler, J.; Christensen, R. D.; Reid, L. K. Aerosol Enrichment of the Surfactant PFO and Mediation of the Water−Air Transport of Gaseous PFOA. *Environ. Sci. Technol.* **2008**, *42* (11), 3969–3974. https://doi.org/10.1021/es7032026.

(89) Reth, M.; Berger, U.; Broman, D.; Cousins, I. T.; Nilsson, E. D.; McLachlan, M. S. Water-to-Air Transfer of Perfluorinated Carboxylates and Sulfonates in a Sea Spray Simulator. *Environ. Chem.* **2011**, *8* (4), 381–388. https://doi.org/10.1071/EN11007.

(90) Johansson, J. H.; Salter, M. E.; Acosta Navarro, J. C.; Leck, C.; Nilsson, E. D.; Cousins, I. T. Global Transport of Perfluoroalkyl Acids via Sea Spray Aerosol. *Environ. Sci. Process. Impacts* **2019**, *21* (4), 635–649. https://doi.org/10.1039/c8em00525g.

(91) Casas, G.; Martínez-Varela, A.; Roscales, J. L.; Vila-Costa, M.; Dachs, J.; Jiménez, B. Enrichment of Perfluoroalkyl Substances in the Sea-Surface Microlayer and Sea-Spray Aerosols in the Southern Ocean. *Environ. Pollut.* **2020**, *267*, 115512. https://doi.org/10.1016/j.envpol.2020.115512.

(92) Sha, B.; Johansson, J. H.; Salter, M. E.; Blichner, S. M.; Cousins, I. T. Constraining Global Transport of Perfluoroalkyl Acids on Sea Spray Aerosol Using Field Measurements. *Sci. Adv.* **2024**, *10* (14), eadl1026. https://doi.org/10.1126/sciadv.adl1026.

(93) Sha, B.; Johansson, J. H.; Tunved, P.; Bohlin-Nizzetto, P.; Cousins, I. T.; Salter, M. E. Sea Spray Aerosol (SSA) as a Source of Perfluoroalkyl Acids (PFAAs) to the Atmosphere: Field Evidence from Long-Term Air Monitoring. *Environ. Sci. Technol.* **2022**, *56* (1), 228–238. https://doi.org/10.1021/acs.est.1c04277.

(94) Albers, C. N.; Voutchkova, D. Sea Spray Aerosols Can Be a Source of PFAS Pollution in Coastal Aquifers. *Environ. Sci. Adv.* **2025**, 10.1039.D5VA00181A. https://doi.org/10.1039/D5VA00181A.

(95) Hurley, M. D.; Misner, J. A.; Ball, J. C.; Wallington, T. J.; Ellis, D. A.; Martin, J. W.; Mabury, S. A.; Sulbaek Andersen, M. P. Atmospheric Chemistry of CF_3 CH_2 CH_2 OH: Kinetics, Mechanisms and Products of Cl Atom and OH Radical Initiated Oxidation in the Presence and Absence of NO_x . *J. Phys. Chem. A* **2005**, *109* (43), 9816–9826. https://doi.org/10.1021/jp0535902.

(96) Sulbaek Andersen, M. P.; Toft, A.; Nielsen, O. J.; Hurley, M. D.; Wallington, T. J.; Chishima, H.; Tonokura, K.; Mabury, S. A.; Martin, J. W.; Ellis, D. A. Atmospheric Chemistry of Perfluorinated Aldehyde Hydrates (n -C_x F_{2x+1} $CH(OH)_2$, x = 1, 3, 4): Hydration, Dehydration, and Kinetics and Mechanism of Cl Atom and OH Radical Initiated Oxidation. *J. Phys. Chem. A* **2006**, *110* (32), 9854–9860. https://doi.org/10.1021/jp060404z.

(97) Sulbaek Andersen, M. P.; Stenby, C.; Nielsen, O. J.; Hurley, M. D.; Ball, J. C.; Wallington, T. J.; Martin, J. W.; Ellis, D. A.; Mabury, S. A. Atmospheric Chemistry of *n*-

$C_x F_{2x+1} CHO$ (x = 1, 3, 4): Mechanism of the $C_x F_{2x+1} C(O)O_2 + HO_2$ Reaction. *J. Phys. Chem. A* **2004**, *108* (30), 6325–6330. https://doi.org/10.1021/jp048849f.

(98) Butt, C. M.; Young, C. J.; Mabury, S. A.; Hurley, M. D.; Wallington, T. J. Atmospheric Chemistry of 4:2 Fluorotelomer Acrylate [$C_4 F_9 CH_2 CH_2 OC(O)CH{=}CH_2$]: Kinetics, Mechanisms, and Products of Chlorine-Atom- and OH-Radical-Initiated Oxidation. *J. Phys. Chem. A* **2009**, *113* (13), 3155–3161. https://doi.org/10.1021/jp810358k.

(99) D'eon, J. C.; Hurley, M. D.; Wallington, T. J.; Mabury, S. A. Atmospheric Chemistry of *N* -Methyl Perfluorobutane Sulfonamidoethanol, $C_4 F_9 SO_2 N(CH_3)CH_2 CH_2 OH$: Kinetics and Mechanism of Reaction with OH. *Environ. Sci. Technol.* **2006**, *40* (6), 1862–1868. https://doi.org/10.1021/es0520767.

(100) Martin, J. W.; Ellis, D. A.; Mabury, S. A.; Hurley, M. D.; Wallington, T. J. Atmospheric Chemistry of Perfluoroalkanesulfonamides: Kinetic and Product Studies of the OH Radical and Cl Atom Initiated Oxidation of N-Ethyl Perfluorobutanesulfonamide. *Environ. Sci. Technol.* **2006**, *40* (3), 864–872. https://doi.org/10.1021/es051362f.

(101) Wallington, T. J.; Hurley, M. D.; Xia, J.; Wuebbles, D. J.; Sillman, S.; Ito, A.; Penner, J. E.; Ellis, D. A.; Martin, J.; Mabury, S. A.; Nielsen, O. J.; Sulbaek Andersen, M. P. Formation of $C_7 F_{15} COOH$ (PFOA) and Other Perfluorocarboxylic Acids during the Atmospheric Oxidation of 8:2 Fluorotelomer Alcohol. *Environ. Sci. Technol.* **2006**, *40* (3), 924–930. https://doi.org/10.1021/es051858x.

(102) Armitage, J. M.; Schenker, U.; Scheringer, M.; Martin, J. W.; MacLeod, M.; Cousins, I. T. Modeling the Global Fate and Transport of Perfluorooctane Sulfonate (PFOS) and Precursor Compounds in Relation to Temporal Trends in Wildlife Exposure. *Environ. Sci. Technol.* **2009**, *43* (24), 9274–9280. https://doi.org/10.1021/es901448p.

(103) Lindstrom, A. B.; Strynar, M. J.; Libelo, E. L. Polyfluorinated Compounds: Past, Present, and Future. *Environ. Sci. Technol.* **2011**, *45* (19), 7954–7961. https://doi.org/10.1021/es2011622.

(104) Wang, Z.; Cousins, I. T.; Scheringer, M.; Hungerbühler, K. Fluorinated Alternatives to Long-Chain Perfluoroalkyl Carboxylic Acids (PFCAs), Perfluoroalkane Sulfonic Acids (PFSAs) and Their Potential Precursors. *Environ. Int.* **2013**, *60*, 242–248. https://doi.org/10.1016/j.envint.2013.08.021.

(105) *US EPA PFOA Stewardship Program Baseline Year Summary Report*. https://www.epa.gov/assessing-and-managing-chemicals-under-tsca/pfoa-stewardship-program-baseline-year-summary-report#contents (accessed 2022-06-10).

(106) Environment and Climate Change Canada; Health Canada. *State of per- and polyfluoroalkyl substances (PFAS) report*. https://publications.gc.ca/collections/collection_2025/eccc/En84-395-2025-eng.pdf (accessed 2025-03-29).

(107) Land, M.; De Wit, C. A.; Cousins, I. T.; Herzke, D.; Johansson, J.; Martin, J. W. What Is the Effect of Phasing out Long-Chain per- and Polyfluoroalkyl Substances on the Concentrations of Perfluoroalkyl Acids and Their Precursors in the Environment? A Systematic Review Protocol. *Environ. Evid.* **2015**, *4* (1), 1–13. https://doi.org/10.1186/2047-2382-4-3.

(108) *ECHA*. https://echa.europa.eu (accessed 2025-11-10).

(109) Wang, Z.; Cousins, I. T.; Scheringer, M.; Buck, R. C.; Hungerbuhler, K. Global Emission Inventories for C4-C14 Perfluoroalkyl Carboxylic Acid (PFCA) Homologues from 1951 to 2030, Part II: The Remianing Pieces of the Puzzle. *Environ. Int.* **2014**, *69*, 166–176. https://doi.org/10.1016/j.envint.2014.04.006.

(110) McLinden, M. O.; Huber, M. L. (R)Evolution of Refrigerants. *J. Chem. Eng. Data* **2020**, *65* (9), 4176–4193. https://doi.org/10.1021/acs.jced.0c00338.

(111) McCulloch, A. CFC and Halon Replacements in the Environment. *J. Fluor. Chem.* **1999**, *100* (1–2), 163–173. https://doi.org/10.1016/S0022-1139(99)00198-0.

(112) Lovelock, J. E.; Maggs, R. J.; Wade, R. J. Halogenated Hydrocarbons in and over the Atlantic. *Nature* **1973**, *241* (5386), 194–196. https://doi.org/10.1038/241194a0.

(113) Molina, M. J.; Rowland, F. S. Stratospheric Sink for Chlorofluoromethanes: Chlorine Atom-Catalysed Destruction of Ozone. *Nature* **1974**, *249* (5460), 810–812. https://doi.org/10.1038/249810a0.

(114) Zurer, P. CHEMISTRY NOBEL PRIZES Three Win for Ozone Depletion Research. *Chem. Eng. News Arch.* **1995**, *73* (42), 4–5. https://doi.org/10.1021/cen-v073n042.p004.

(115) UNEP. *"The Montreal Protocol on Substances That Deplete the Ozone Layer, as Adjusted and/or Amended in London 1990, Copenhagen 1992, Vienna 1995, Montreal 1997, Beijing 1999, Montreal 2007, Kigali 2016", Ozone Secretariat, United Nations Environment Programme*; 2000.

(116) Pickard, H. M.; Criscitiello, A. S.; Persaud, D.; Spencer, C.; Muir, D. C. G.; Lehnherr, I.; Sharp, M. J.; De Silva, A. O.; Young, C. J. Ice Core Record of Persistent Short-Chain Fluorinated Alkyl Acids: Evidence of the Impact From Global Environmental Regulations. *Geophys. Res. Lett.* **2020**, *47* (10), e2020GL087535. https://doi.org/10.1029/2020GL087535.

(117) Paul, S.; Deka, R. C.; Gour, N. K. Kinetics, Mechanism, and Global Warming Potentials of HFO-1234yf Initiated by O3 Molecules and NO3 Radicals: Insights from Quantum Study. *Environ. Sci. Pollut. Res.* **2018**, *25* (26), 26144–26156. https://doi.org/10.1007/s11356-018-2633-7.

(118) Burkholder, J. B.; Cox, R. A.; Ravishankara, A. R. Atmospheric Degradation of Ozone Depleting Substances, Their Substitutes, and Related Species. *Chem. Rev.* **2015**, *115* (10), 3704–3759. https://doi.org/10.1021/cr5006759.

(119) Young, C. J.; Hurley, M. D.; Wallington, T. J.; Mabury, S. A. Atmospheric Chemistry of Perfluorobutenes (CF3CFCFCF3 and CF3CF2CFCF2): Kinetics and Mechanisms of Reactions with OH Radicals and Chlorine Atoms, IR Spectra, Global Warming Potentials, and Oxidation to Perfluorocarboxylic Acids. *Atmos. Environ.* **2009**, *43* (24), 3717–3724. https://doi.org/10.1016/j.atmosenv.2009.04.025.

(120) Hurley, M. D.; Ball, J. C.; Wallington, T. J. Atmospheric Chemistry of the Z and E Isomers of CF_3 CFCHF; Kinetics, Mechanisms, and Products of Gas-Phase Reactions with Cl Atoms, OH Radicals, and O_3. *J. Phys. Chem. A* **2007**, *111* (39), 9789–9795. https://doi.org/10.1021/jp0753530.

(121) Kotamarthi, V. R.; Rodriguez, J. M.; Ko, M. K. W.; Tromp, T. K.; Sze, N. D.; Prather, M. J. Trifluoroacetic Acid from Degradation of HCFCs and HFCs: A Three-Dimensional Modeling Study. *J. Geophys. Res.* **1998**, *103* (D5), 5747–5758. https://doi.org/10.1029/97JD02988.

(122) Sulbaek Andersen, M. P.; Nielsen, O. J.; Karpichev, B.; Wallington, T. J.; Sander, S. P. Atmospheric Chemistry of Isoflurane, Desflurane, and Sevoflurane: Kinetics and

Mechanisms of Reactions with Chlorine Atoms and OH Radicals and Global Warming Potentials. *J. Phys. Chem. A* **2012**, *116* (24), 5806–5820. https://doi.org/10.1021/jp2077598.

(123) Velders, G. J. M.; Fahey, D. W.; Daniel, J. S.; Andersen, S. O.; McFarland, M. Future Atmospheric Abundances and Climate Forcings from Scenarios of Global and Regional Hydrofluorocarbon (HFC) Emissions. *Atmos. Environ.* **2015**, *123*, 200–209. https://doi.org/10.1016/j.atmosenv.2015.10.071.

(124) Fang, X.; Velders, G. J. M.; Ravishankara, A. R.; Molina, M. J.; Hu, J.; Prinn, R. G. Hydrofluorocarbon (HFC) Emissions in China: An Inventory for 2005–2013 and Projections to 2050. *Environ. Sci. Technol.* **2016**, *50* (4), 2027–2034. https://doi.org/10.1021/acs.est.5b04376.

(125) Carpenter, L. J.; Reimann, S.; Burkholder, J. B.; Clerbaux, C.; Hall, B. D.; Hossaini, R.; Laube, J. C.; Yvon-Lewis, S. A. *Update on Ozone-Depleting Substances (ODSs) and Other Gases of Interest to the Montreal Protocol*; World Meteorological Organization, Geneva, Switzerland, 2014; p 1.1-1.101. https://orbi.uliege.be/handle/2268/175647 (accessed 2025-11-03).

(126) Federico, S. C.; Salvador, C.; Stevenson, L.; Dolislager, F.; Armstrong, A.; Power, S.; Mathews, T.; Yana Motta, S. *Critical Literature Review of Low Global Warming Potential (GWP) Refrigerants and Their Environmental Impact*; ORNL/TM--2024/3638, 2573502; 2024; p ORNL/TM--2024/3638, 2573502. https://doi.org/10.2172/2573502.

(127) Birmpili, T. Montreal Protocol at 30: The Governance Structure, the Evolution, and the Kigali Amendment. *Comptes Rendus Géoscience* **2018**, *350* (7), 425–431. https://doi.org/10.1016/j.crte.2018.09.002.

(128) Tang, X.; Wilson, S. R.; Solomon, K. R.; Shao, M.; Madronich, S. Changes in Air Quality and Tropospheric Composition Due to Depletion of Stratospheric Ozone and Interactions with Climate. *Photochem. Photobiol. Sci.* **2011**, *10* (2), 280–291. https://doi.org/10.1039/c0pp90039g.

(129) Flossmann, A. I.; Hall, W. D.; Pruppacher, H. R. A Theoretical Study of the Wet Removal of Atmospheric Pollutants. Part I: The Redistribution of Aerosol Particles Captured through Nucleation and Impaction Scavenging by Growing Cloud Drops. *J.*

Atmospheric Sci. **1985**, *42* (6), 583–606. https://doi.org/10.1175/1520-0469(1985)042%3C0583:ATSOTW%3E2.0.CO;2.

(130) Zhao, S.; Yu, Y.; He, J.; Yin, D.; Wang, B. Below-Cloud Scavenging of Aerosol Particles by Precipitation in a Typical Valley City, Northwestern China. *Atmos. Environ.* **2015**, *102*, 70–78. https://doi.org/10.1016/j.atmosenv.2014.11.051.

(131) Ohata, S.; Moteki, N.; Mori, T.; Koike, M.; Kondo, Y. A Key Process Controlling the Wet Removal of Aerosols: New Observational Evidence. *Sci. Rep.* **2016**, *6* (1), 34113. https://doi.org/10.1038/srep34113.

(132) Olney, S.; Jones, M.; Rockwell, C.; Collins, R. D.; Bryant, J. D.; Occhialini, J. Influence of Convective and Stratiform Precipitation Types on Per- and Polyfluoroalkyl Substance Concentrations in Rain. *Sci. Total Environ.* **2023**, *890*, 164051. https://doi.org/10.1016/j.scitotenv.2023.164051.

(133) Barton, C. A.; Kaiser, M. A.; Russell, M. H. Partitioning and Removal of Perfluorooctanoate during Rain Events: The Importance of Physical-Chemical Properties. *J. Environ. Monit.* **2007**, *9* (8), 839–846. https://doi.org/10.1039/b703510a.

(134) Casal, P.; Cabrerizo, A.; Vila-Costa, M.; Pizarro, M.; Jiménez, B.; Dachs, J. Pivotal Role of Snow Deposition and Melting Driving Fluxes of Polycyclic Aromatic Hydrocarbons at Coastal Livingston Island (Antarctica). *Environ. Sci. Technol.* **2018**, *52* (21), 12327–12337. https://doi.org/10.1021/acs.est.8b03640.

(135) Lei, Y. D.; Wania, F. Is Rain or Snow a More Efficient Scavenger of Organic Chemicals? *Atmos. Environ.* **2004**, *38* (22), 3557–3571. https://doi.org/10.1016/j.atmosenv.2004.03.039.

(136) Farmer, D. K.; Boedicker, E. K.; DeBolt, H. M. Dry Deposition of Atmospheric Aerosols: Approaches, Observations, and Mechanisms. *Annu. Rev. Phys. Chem.* **2021**, *72* (1), 375–397. https://doi.org/10.1146/annurev-physchem-090519-034936.

(137) Hicks, B. B.; Saylor, R. D.; Baker, B. D. Dry Deposition of Particles to Canopies—A Look Back and the Road Forward. *J. Geophys. Res. Atmospheres* **2016**, *121* (24), 14,691-14,707. https://doi.org/10.1002/2015JD024742.

(138) Faust, J. A. PFAS on Atmospheric Aerosol Particles: A Review. *Environ. Sci. Process. Impacts* **2022**, *25* (2), 133–150. https://doi.org/10.1039/d2em00002d.

(139) Ge, H.; Yamazaki, E.; Yamashita, N.; Taniyasu, S.; Ogata, A.; Furuuchi, M. Particle Size Specific Distribution of Perfluoro Alkyl Substances in Atmospheric Particulate Matter in Asian Cities. *Environ. Sci. Process. Impacts* **2017**, *19* (4), 549–560. https://doi.org/10.1039/C6EM00564K.

(140) Dreyer, A.; Kirchgeorg, T.; Weinberg, I.; Matthias, V. Particle-Size Distribution of Airborne Poly- and Perfluorinated Alkyl Substances. *Chemosphere* **2015**, *129*, 142–149. https://doi.org/10.1016/j.chemosphere.2014.06.069.

(141) Pike, K. A.; Edmiston, P. L.; Morrison, J. J.; Faust, J. A. Correlation Analysis of Perfluoroalkyl Substances in Regional U.S. Precipitation Events. *Water Res.* **2021**, *190*, 116685. https://doi.org/10.1016/j.watres.2020.116685.

(142) Li, X.; Wang, Y.; Cui, J.; Shi, Y.; Cai, Y. Occurrence and Fate of Per- and Polyfluoroalkyl Substances (PFAS) in Atmosphere: Size-Dependent Gas-Particle Partitioning, Precipitation Scavenging, and Amplification. *Environ. Sci. Technol.* **2024**, *58* (21), 9283–9291. https://doi.org/10.1021/acs.est.4c00569.

(143) Olney, S.; Jones, M.; Rockwell, C.; Collins, R. D.; Bryant, J. D.; Occhialini, J. Influence of Convective and Stratiform Precipitation Types on Per- and Polyfluoroalkyl Substance Concentrations in Rain. *Sci. Total Environ.* **2023**, *890*, 164051. https://doi.org/10.1016/j.scitotenv.2023.164051.

(144) Taniyasu, S.; Yamashita, N.; Moon, H.-B.; Kwok, K. Y.; Lam, P. K. S.; Horii, Y.; Petrick, G.; Kannan, K. Does Wet Precipitation Represent Local and Regional Atmospheric Transportation by Perfluorinated Alkyl Substances? *Environ. Int.* **2013**, *55*, 25–32. https://doi.org/10.1016/j.envint.2013.02.005.

(145) Scott, B. F.; Spencer, C.; Mabury, S. A.; Muir, D. C. G. Poly and Perfluorinated Carboxylates in North American Precipitation. *Environ. Sci. Technol.* **2006**, *40* (23), 7167–7174.

(146) Chen, H.; Zhang, L.; Li, M.; Yao, Y.; Zhao, Z.; Munoz, G.; Sun, H. Per- and Polyfluoroalkyl Substances (PFASs) in Precipitation from Mainland China: Contributions of Unknown Precursors and Short-Chain (C2 C3) Perfluoroalkyl Carboxylic Acids. *Water Res.* **2019**, *153*, 169–177. https://doi.org/10.1016/j.watres.2019.01.019.

(147) Freeling, F.; Behringer, D.; Heydel, F.; Scheurer, M.; Ternes, T. A.; Nödler, K. Trifluoroacetate in Precipitation: Deriving a Benchmark Data Set. *Environ. Sci. Technol.* **2020**, *54* (18), 11210–11219. https://doi.org/10.1021/acs.est.0c02910.

(148) D'Ambro, E. L.; Pye, H. O. T.; Bash, J. O.; Bowyer, J.; Allen, C.; Efstathiou, C.; Gilliam, R. C.; Reynolds, L.; Talgo, K.; Murphy, B. N. Characterizing the Air Emissions, Transport, and Deposition of Per- And Polyfluoroalkyl Substances from a Fluoropolymer Manufacturing Facility. *Environ. Sci. Technol.* **2021**, *55* (2), 862–870. https://doi.org/10.1021/acs.est.0c06580.

(149) Chen, H.; Yao, Y.; Zhao, Z.; Wang, Y.; Wang, Q.; Ren, C.; Wang, B.; Sun, H.; Alder, A. C.; Kannan, K. Multimedia Distribution and Transfer of Per- and Polyfluoroalkyl Substances (PFASs) Surrounding Two Fluorochemical Manufacturing Facilities in Fuxin, China. *Env. Sci Technol* **2018**, *52* (15), 8263–8271. https://doi.org/10.1021/acs.est.8b00544.

(150) Young, C. J.; Furdui, V. I.; Franklin, J.; Koerner, R. M.; Muir, D. C. G.; Mabury, S. A. Perfluorinated Acids in Arctic Snow: New Evidence for Atmospheric Formation. *Environ. Sci. Technol.* **2007**, *41* (10), 3455–3461. https://doi.org/10.1021/es0626234.

(151) Pickard, H. M.; Criscitiello, A. S.; Spencer, C.; Sharp, M. J.; Muir, D. C. G.; De Silva, A. O.; Young, C. J. Continuous Non-Marine Inputs of per- and Polyfluoroalkyl Substances to the High Arctic: A Multi-Decadal Temporal Record. *Atmospheric Chem. Phys.* **2018**, *18* (7), 5045–5058. https://doi.org/10.5194/acp-18-5045-2018.

(152) Hartz, W. F.; Björnsdotter, M. K.; Yeung, L. W. Y.; Hodson, A.; Thomas, E. R.; Humby, J. D.; Day, C.; Jogsten, I. E.; Kärrman, A.; Kallenborn, R. Levels and Distribution Profiles of Per- and Polyfluoroalkyl Substances (PFAS) in a High Arctic Svalbard Ice Core. *Sci. Total Environ.* **2023**, *871*, 161830. https://doi.org/10.1016/j.scitotenv.2023.161830.

(153) Johansson, J. H.; Shi, Y.; Salter, M.; Cousins, I. T. Spatial Variation in the Atmospheric Deposition of Perfluoroalkyl Acids: Source Elucidation through Analysis of Isomer Patterns. *Environ. Sci. Process. Impacts* **2018**, *20* (7), 997–1006. https://doi.org/10.1039/C8EM00102B.

(154) Pfotenhauer, D.; Sellers, E.; Olson, M.; Praedel, K.; Shafer, M. PFAS Concentrations and Deposition in Precipitation: An Intensive 5-Month Study at

National Atmospheric Deposition Program – National Trends Sites (NADP-NTN) across Wisconsin, USA. *Atmos. Environ.* **2022**, *291*, 119368. https://doi.org/10.1016/j.atmosenv.2022.119368.

(155) Wang, F.; Wang, W.; Zhao, D.; Liu, J.; Lu, P.; Rose, N. L.; Zhang, G. Source Apportionment and Wet Deposition of Atmospheric Poly- and per-Fluoroalkyl Substances in a Metropolitan City Centre of Southwest China. *Atmos. Environ.* **2022**, *273*, 118983. https://doi.org/10.1016/j.atmosenv.2022.118983.

(156) Henne, S.; Storck, F. R.; Wöhrnschimmel, H.; Leuenberger, M.; Vollmer, M. K.; Reimann, S. Trifluoroacetate (TFA) in Precipitation and Surface Waters in Switzerland: Trends, Source Attribution, and Budget. EGUsphere [Preprint] June 27, 2025. https://doi.org/10.5194/egusphere-2025-2861.

(157) Wang, Q.; Wang, X.; Ding, X. Rainwater Trifluoroacetic Acid (TFA) in Guangzhou, South China: Levels, Wet Deposition Fluxes and Source Implication. *Sci. Total Environ.* **2014**, *468–469*, 272–279. https://doi.org/10.1016/j.scitotenv.2013.08.055.

(158) Persaud, D.; Criscitiello, A. S.; Spencer, C.; Lehnherr, I.; Muir, D. C. G.; De Silva, A. O.; Young, C. J. A 50 Year Record for Perfluoroalkyl Acids in the High Arctic: Implications for Global and Local Transport. *Environ. Sci. Process. Impacts* **2024**, *26* (9), 1543–1555. https://doi.org/10.1039/D4EM00219A.

(159) Hartz, W. F.; Björnsdotter, M. K.; Yeung, L. W. Y.; Hodson, A.; Thomas, E. R.; Humby, J. D.; Day, C.; Jogsten, I. E.; Kärrman, A.; Kallenborn, R. Levels and Distribution Profiles of Per- and Polyfluoroalkyl Substances (PFAS) in a High Arctic Svalbard Ice Core. *Sci. Total Environ.* **2023**, No. 5, 161830. https://doi.org/10.1016/j.scitotenv.2023.161830.

(160) Macinnis, J. J.; French, K.; Muir, D. C. G.; Spencer, C.; Criscitiello, A.; De Silva, A. O.; Young, C. J. Emerging Investigator Series: A 14-Year Depositional Ice Record of Perfluoroalkyl Substances in the High Arctic. *Environ. Sci. Process. Impacts* **2017**, *19* (1), 22–30. https://doi.org/10.1039/c6em00593d.

(161) Wang, X.; Halsall, C.; Codling, G.; Xie, Z.; Xu, B.; Zhao, Z.; Xue, Y.; Ebinghaus, R.; Jones, K. C. Accumulation of Perfluoroalkyl Compunds in Tibetan Mountain Snow: Temporal Patterns from 1980 to 2010. *Environ. Sci. Technol.* **2014**, *48* (1), 173–181. https://doi.org/10.1021/es4044775.

(162) Kirchgeorg, T.; Dreyer, A.; Gabrieli, J.; Kehrwald, N.; Sigl, M.; Schwikowski, M.; Boutron, C.; Gambaro, A.; Barbante, C.; Ebinghaus, R. Temporal Variations of Perfluoroalkyl Substances and Polybrominated Diphenyl Ethers in Alpine Snow. *Environ. Pollut.* **2013**, *178* (3), 367–374. https://doi.org/10.1016/j.envpol.2013.03.043.

(163) MacInnis, J. J.; French, K.; Muir, D. C. G.; Spencer, C.; Criscitiello, A.; Silva, A. O. D.; Young, C. J. Emerging Investigator Series: A 14-Year Depositional Ice Record of Perfluoroalkyl Substances in the High Arctic. *Environ. Sci. Process. Impacts* **2017**, *19* (1), 22–30. https://doi.org/10.1039/C6EM00593D.

CHAPTER 2

A 50-year record for perfluoroalkyl acids in the High Arctic: Implications for global and local transport

Daniel Persaud[1], Alison S. Criscitiello[2], Christine Spencer[3], Igor Lehnherr[4], Derek C G. Muir[3], Amila O. De Silva[3], and Cora J. Young[1].

[1]Department of Chemistry, York University, Toronto, ON
[2]Department of Earth and Atmospheric Sciences, University of Alberta, Edmonton, Alberta, Canada
[3]Aquatic Contaminants Research Division, Environmental and Climate Change Canada, Burlington, Ontario, Canada
[4]Department of Geography, Geomatics and Environment, University of Toronto-Mississauga, Mississauga, Ontario, Canada

Published: *Environ. Sci. Processes Impacts, 2024, 1543-1555, DOI:* 10.1039/D4EM00219A

Author Contributions:
Alison S. Criscitiello and Igor Lehnherr collected the ice core. Daniel Persaud, Christine Spencer, Cora Young and Amila O De Silva sectioned and performed chemical analysis on ice core sections. Funding was obtained by Cora J Young and Derek C. G. Muir. Daniel Persaud analyzed the data and wrote the manuscript with input from all authors.

2.1 Introduction

Per- and polyfluoroalkyl substances (PFAS,C_nF_{2n+1}-R) describe a diverse class of anthropogenic compounds that have been produced since the 1950s.[1] A perfluoroalkyl moiety (C_nF_{2n+1}-) imparts unique properties when compared to its hydrocarbon counterparts including the ability to lower surface tension, form stable foams, as well as exceptional chemical and thermal stability.[2,3] Thus, these compounds have numerous consumer and industrial applications including fluoropolymer-coated cookware, clothing, metal plating, and aqueous film-forming foams (AFFF).[2] While many useful applications exist, they are highly persistent in the environment,[4] bioaccumulative,[5] toxic,[6] and can undergo long-range transport.[3] These are all hallmark characteristics of persistent organic pollutants (POPs), which prompted manufacturers and regulatory bodies to phase out and restrict the use of selected PFAS.[7]

PFAS exists in several subgroups, the most widely known and studied is the perfluoroalkyl acids (PFAAs) which include both the perfluoroalkylcarboxylic acids (PFCAs) and perfluoroalkyl sulfonic acids (PFSAs).[1] Due to the ubiquitous nature of PFAAs, they are frequently detected in remote locations, including the Arctic.[8–13] Two major pathways have been suggested to explain their long-range transport: direct transport and indirect formation in the atmosphere.[3] With direct transport, PFAAs are released and transported in the stable carboxylic (PFCA) or sulfonic acid (PFSA) form after manufacture and use. This transport mechanism can occur in the gas phase, on particles (including marine aerosols) or by ocean currents.[3,10] With indirect formation, PFAAs are formed through chemical transformation of volatile precursors in the atmosphere.[14] Samples collected in remote locations can be used to investigate these different transport mechanisms. Ice caps and glaciers receive deposition primarily from the atmosphere due to their isolation from local sources and high elevation, in which a record of contamination can be preserved.[9,10,15–17]

Temporal variations over multiple decades can elucidate source and precursor contributions to long-range transport that can be used to understand the deposition mechanisms of PFAAs. Previously, ice core records from the Arctic have been measured, where PFAAs were detected in most samples with a few exceptions described elsewhere.[8–10] To further improve our knowledge of PFAA deposition and transport

mechanism in the High Arctic, we collected an ice core from Mt. Oxford icefield, located on Ellesmere Island, Nunavut, Canada. This ice core is geographically closer to possible emission sources highlighted in a previous study from Devon Ice Cap that recorded 38 years of deposition.[10] Because Mt. Oxford icefield receives less precipitation annually than the Devon Ice Cap,[18] an ice core of similar length from Mt. Oxford icefield records over an additional decade of deposition. This 50-year record represents the longest yet recorded for PFAS in the northern hemisphere and the longest for PFSAs globally. Here, we use the ice core record to examine: (1) PFAA depositional profiles; (2) temporal variations; (3) evidence of indirect and aerosol transport; and (4) causes of episodic pulses of high deposition.

2.2 Methods

2.2.1 Ice core collection and sectioning

Details of sampling procedures were described previously.[10,19] Briefly, a 16.5 m ice core was collected from the summit of the Mt. Oxford icefield, Nunavut (82.19°N, 72.96°W, 1784 m above sea level) in May 2017 (Figure A-1). Ice core sections were retrieved using a 3-inch (7.7 cm) diameter aluminum and stainless-steel Kovacs ice drill. The ice core was drilled in one meter sections, packaged in polyethylene bags, and shipped frozen to the Canada Centre for Inland Waters (CCIW) in Burlington, ON, Canada.

An age-depth scale was created using oxygen stable isotopes and ion chemistry measured in a co-located core that was drilled simultaneously within 5 m. Details of the dating methods have been previously described.[20–22] The 16.5 m ice core represented 50 years of deposition (1967 – 2017) with a total dating error of ±1 years; further details can be found in the SI. The ice core was sectioned into discrete samples corresponding to individual years in a cold room (0 to -10°C) using methanol (MeOH) rinsed stainless steel tools, with each section transferred to pre-cleaned high density polyethylene bottles. Samples were kept frozen (-30°C) prior to sectioning, melting, extraction, and analysis. Data for the partial year of sample collection (2017) was not included in our analysis.

2.2.2 Sample preparation and extraction

Details of sample extraction have been described previously.[10] We analyzed PFCAs (C5-C16), PFSAs (C4, C6, C8), perfluorooctanesulfonamide (FOSA), perfluoroethylcyclohexanesulfonate (PFECHS) and hexafluoropropylene oxide dimer acid (HFPO-DA), commonly known as GenX (See Table A-1 for full analyte list). Measurement of PFCAs with four or fewer carbons in this ice core was reported previously.[19] Samples were thawed prior to extraction and aliquoted to at least 500 mL melted volume which was required for solid phase extraction (SPE).[9,10] Samples were shaken, sonicated for 10 minutes, and held for 30 minutes at room temperature.

Samples were concentrated using OASIS® weak anion exchange SPE cartridges (6 cm^3, 150 mg, 30 µm). Before extraction, each cartridge was conditioned with 5 mL 0.1% NH_4OH/MeOH, followed by 5 mL MeOH and 5 mL SPE-cleaned HPLC grade water. Following sample concentration, cartridges were rinsed with 25 mM ammonium acetate buffer acidified to pH 4 with acetic acid and centrifuged at 4000 rpm for 2 minutes to remove any residual water. Elution was done in two fractions: the first fraction was eluted with 6 mL of MeOH for FOSA, while the second fraction was eluted with 8 mL of 0.1% NH_4OH/MeOH for other PFAAs. Extracts were evaporated to dryness under a gentle stream of nitrogen and reconstituted in 0.5 mL 50/50 methanol-water containing the surrogate mixture (Table A-2), which was used to monitor matrix effects. Reconstituted samples were sonicated for 5 min, vortexed, and transferred to polypropylene vials for analysis.

2.2.3 Instrumental Analysis

Extracts were analyzed using an Acquity UPLC I class liquid chromatography coupled to a XEVO® TQ-S tandem mass spectrometer in electrospray negative ionization mode (Waters Corporation, Massachusetts, USA). Analytes were separated using an Acquity UPLC BEH C18 column (Waters Acquity UPLC® BEH, 2.1 x 50 mm,1.7 μm) with a water-methanol 2 mM ammonium acetate gradient method (Table A-3 and A-4) and quantified based on relative response to isotopically labelled internal standards (Wellington Laboratories, Guelph, ON).

Subsamples were also analyzed for major cations (Li^+, Na^+, K^+, NH_4^+, Al^{3+}, Ca^{2+}, Mg^{2+}) and anions (F^-, Cl^-, SO_4^{2-}, PO_4^{2-}, NO_3^-) by ion chromatography with conductivity detection. Separation was achieved using Dionex CS19 and AS11 columns for cations and anions, respectively (further details in the SI).

2.2.4 Quality assurance and quality control

Our previous findings suggest that environmental exposure and shipping do not contribute to PFAS contamination.[10] Cartridge blanks were analyzed to verify the integrity of the extraction procedure. A mixture of isotopically labelled standards was also used to determine analyte recoveries and matrix effects (Table A-5). The accuracy of the method was evaluated by spiking an Arctic freshwater composite (n=4) with native analytes before or after extraction (Table A-7). Limits of detection (LOD) were based on signal to noise ratios of 3, while method detection limits were based on average plus 3 times the standard deviation of method blanks (Table A-8). All QA/QC data can be found in Section 1.5 in the SI.

2.2.5 Statistical Analysis

Statistical analyses were performed using RStudio (Version 1.4.1106) with R version 4.3.0. Annual fluxes of PFAAs and ions were logarithm-transformed [$\log_{10}$ PFAA,ions] to approximate normality before Pearson's correlation (r) analysis using the lmodel2 package. [23] The significance threshold was set at $p<0.05$. Values below the detection limit were excluded from all statistical tests. Further details are provided in the SI.

2.3 Results and Discussion

2.3.1 PFAA concentrations and fluxes on the Mt Oxford Icefield

Annual concentrations were measured in the ice core samples dating from 1967 – 2016 for PFAAs and FOSA. Generally, PFCAs from PFPeA (C5) to PFDoDA (12) were detected on Mt. Oxford icefield. The PFCAs from PFHxA to PFDA (C6-C10) were detected in 98% of samples, whereas PFPeA (C5), PFUnDA (C11) and PFDoDA (C12) were detected in 92, 88, and 66% of samples, respectively. The concentrations of individual PFCAs ranged from <LOD to 2.33 ng L^{-1} (Table A-9), with PFOA (C8) and PFNA (C9)

being the major contributors. The presence of C13-C16 and C18 PFCAs, as well as HFPO-DA, were sought but were <LOD for the entire 50-year record. HFPO-DA was introduced as a PFOA alternative and has been produced since 2009.[24] Since its introduction, several studies have detected HFPO-DA within a few hundred kilometers of fluorochemical production facilities,[25–27] as well as in precipitation samples in the United States.[28] The lack of detection of HFPO-DA on Mt. Oxford icefield may be because (i) the compound is present at levels below our current detection limits; (ii) no known precursors exist to facilitate indirect transport; and/or (iii) not enough time has passed since its introduction for direct transport via ocean currents to the remote Canadian Arctic to occur.[29] HFPO-DA was detected in surface water samples from Europe to the Arctic along two transects within the Fram Strait, with a concentration range of <MDL to 26 pg/L.[30] The concentration of HFPO-DA displayed a sequential decrease from Europe to the Fram Strait[30] which aligns with our hypothesis that insufficient time has elapsed for a direct transport mechanism to the High Arctic. Moreover, HFPO-DA was never registered for use in Canada.[31]The PFSAs detected were PFBS (C4), PFOS (C8), and PFECHS (cyclic C8), as well as FOSA with individual concentrations ranging from <LOD to 4.16 ng L^{-1} (Table A-10). PFHxS (C6) and PFDS (C10) were <LOD in all samples. PFBS was the dominant homologue with a detection frequency of 98%, whereas PFOS, PFECHS, and FOSA were detected in 90, 94, and 84% of samples, respectively. The detection of PFECHS is not consistent among previous studies in the Canadian Arctic. The Devon Ice Cap summit was sampled in 2008 and 2015.[9,10] In the 2008 study, PFECHS was detected up to 20 pg L^{-1} in snow pit samples whereas all PFECHS were <0.94 pg L^{-1} in the ice core record collected in 2015. The concentration of PFECHS on Mt Oxford icefield is greater (142 pg L^{-1}) than the maximum observed in the 2008 Devon Ice Cap study.

Concentrations (ng L^{-1}) were converted to fluxes (ng m^{-2} a^{-1}) to determine the annual deposition of PFAAs on Mt. Oxford icefield (Tables A-11, A-12). Fluxes of individual PFCAs were up to 316 ng m^{-2} a^{-1} and were consistently higher than other Arctic and sub-Arctic deposition measurements, but lower than lower-latitude precipitation samples[9,10,32–36] (Table A-13). Fluxes of PFSAs were generally lower than PFCAs, averaging 13 ng m^{-2} a^{-1}, but elevated levels of PFOS and PFBS up to 471 ng m^{-2} a^{-1} were observed in a few years before the 1990s, which will be discussed below.

2.3.2 PFAA temporal variations

Variations in PFAA deposition over time are useful to elucidate source and precursor contributions to the High Arctic. We do not expect the integrity of the temporal record to be affected by post depositional effects based on the detection of solstice peaks of major ions in the aforementioned co-located ice core (Figure A-2). Nevertheless, to circumvent any possible errors associated with sectioning, dating, and post-depositional processes, we conservatively report fluxes as five-year moving averages for the full temporal record.

In general, all fluxes of PFCAs were observed to be constant or increasing with time, with the increases being more prominent after 1985 (Figures 2-1A, A-3). Before this period, fluxes were relatively constant except for episodes of elevated levels of C6-12 PFCAs in the 1970s, which will be discussed below. The C8 (PFOA) and C9 (PFNA) homologues were the dominant PFCAs observed at Mt. Oxford icefield, similar to previous observations.[10] Contrary to the deposition trends at Devon Ice Cap, in which C8 (PFOA) and C9 (PFNA) plateaued after 1995, we observe a consistent increase for these two homologues. Additionally, PFOA fluxes were at least an order of magnitude higher at Mt. Oxford icefield compared to Devon Ice Cap and the Lomonsovfonna Ice Cap in Svalbard[16] (Figure 2-2), suggesting potential differences in sources. Our observations are generally consistent with air measurements[37] of several neutral PFAS and ionic PFAAs further north on Ellesmere Island at Alert, where an exponential increase of the 8:2 FTOH from 2006 to 2015 was observed, as well as doubling times of PFBA, PFOS, PFBS and PFOS from 2.5 to 3.7 years.[37]

In 2006, the United States Environmental Protection Agency PFOA Stewardship program invited the eight major fluoropolymer and fluorotelomer manufacturers to voluntary eliminate emissions and production of PFOA, its precursor compounds, and the related longer chain homologues.[26] Meanwhile in Canada, four participating companies agreed to eliminate residual PFOA, long chain PFCAs, and their precursors by 2015.[27] Other manufacturers in Japan and Western Europe also implemented similar regulations. These regulations prompted a geographical shift in sources of PFCAs, as manufacturers that were not participants in the reduction programs (mainly in China and India) increased or began production of several classes of PFAS and its precursors.[38] Ellesmere Island,

where Mt. Oxford icefield is located, is influenced less by North American airmasses and more by Eurasian airmasses compared to more southern areas of the Canadian Arctic.[39] Thus, we would expect that the more southern Devon Ice Cap might be more influenced by the reduction in emissions, while deposition to the more northern Mt. Oxford icefield would be more affected by continuing global production. This is consistent with our observations of PFCAs at Mt. Oxford icefield and the previous observations at Devon Ice Cap.

Fluxes of FOSA generally increased from 1980 to 2000 followed by a decrease over the next decade (Figures 2-1B, A-4). This decrease is likely the effect of the voluntary phase out by 3M of POSF-based chemistry (including PFOS and its precursors) by 2002.[40] A similar temporal variation was observed at the Devon Ice Cap.[10] However, at that location the decline happened over a faster timescale of ~2 years. Following the decrease, FOSA fluxes at Mt. Oxford icefield remained higher than those at Devon Ice Cap. No discernible trend with time was observed in the deposition of the other PFSAs. There were several years with deposition fluxes above 100 ng m^{-2} a^{-1} of the C8 PFSA (PFOS) and 10 ng m^{-2} a^{-1} of the C4 PFSA (PFBS) before 1995. Deposition events were isolated in time, suggesting episodic events that resulted in the deposition of these two homologues. This will be discussed further below.

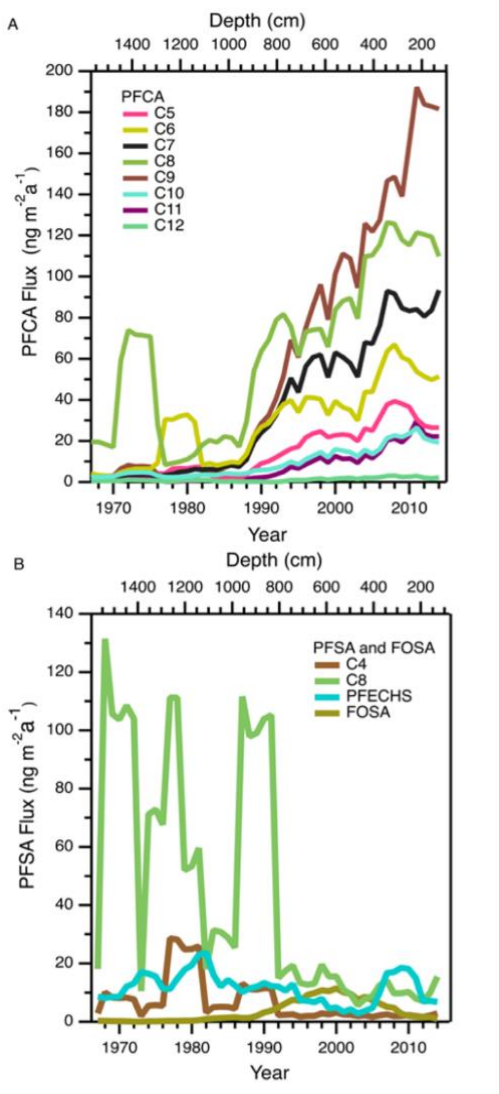

Figure 2-1: Five year moving averages of PFAA deposition flux on Mt. Oxford icefield: (A) PFCAs (C5 - C12) and (B) PFSAs (C4, C8, PFECHS) and FOSA for the period 1967 – 2016.

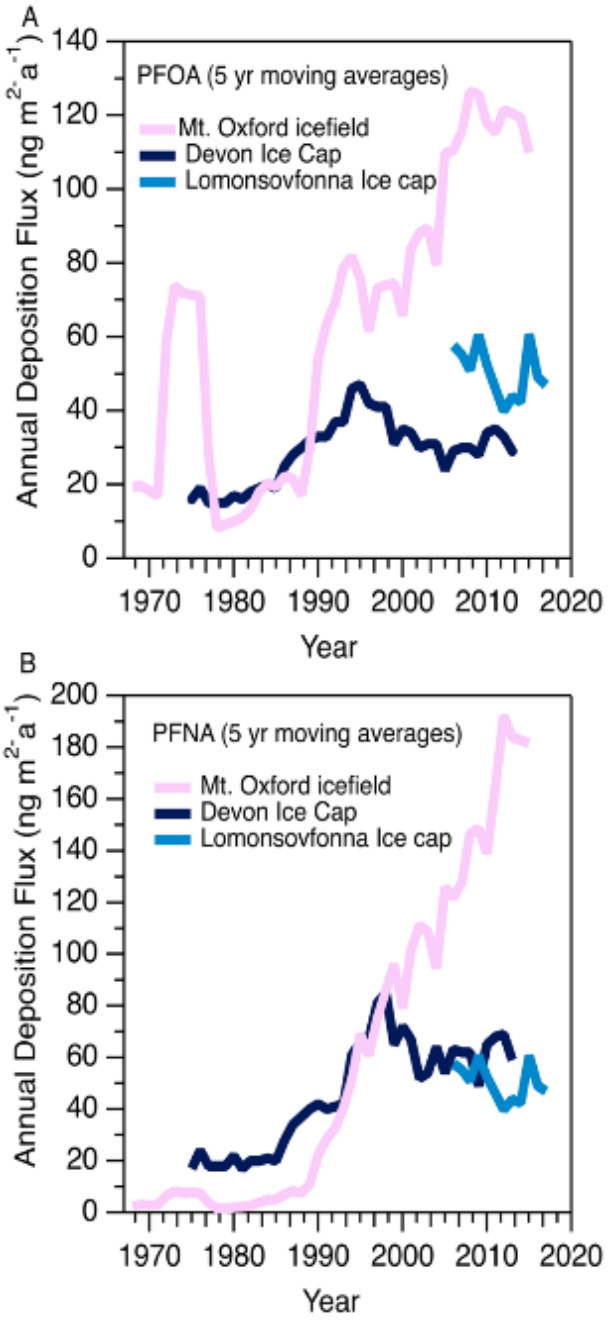

Figure 2-2: Five year moving averages of (A) PFOA and (B) PFNA deposition at Mt. Oxford icefield (1967-2016), Devon Ice Cap (1977 – 2015),[11] and Lomonsovfonna Ice Cap (2006 – 2019).[30]

2.3.3 Evidence for indirect transport of PFAAs

Indirect sources of PFAS may contribute to their presence and distribution to the Arctic. Laboratory chamber studies and chemical modelling demonstrated that volatile and semi-volatile precursor compounds including fluorotelomer alcohols (FTOHs), perfluoroalkane sulfonamides, and N-alkane perfluoroalkane sulfonamidoethanols can undergo OH-initiated oxidation in the gas phase to produce PFAAs.[41–43] If a common indirect source exists, then PFAA homologues are expected to vary through time together. To explore this, we compared fluxes of PFAAs (Figure 2-3, Table A-14).[19,28] Generally, all PFCA homologue pairs showed statistically significant moderate to very strong correlations (r: 0.5 – 0.96, $p < 0.05$). Weak but statistically significant correlations were also observed between FOSA and C5 – C10 PFCAs (r: 0.34 – 0.46, $p < 0.05$). This correlation is unique to this study but is expected since sulfonamide precursors have been identified as atmospheric sources of PFCAs with ≤ 8 carbons.[43,44] This strongly suggests that most PFCAs originate from common sources and/or have experienced similar precursor oxidation and deposition processes. This is consistent with expected PFCA homologue production by gas phase atmospheric oxidation of fluorotelomer compounds.[41] These results are also consistent with observations from other remote terrestrial locations where atmospheric deposition has been shown as a dominant source of PFCAs.[9,10,16,17,33]

Molar concentration ratios of even-odd homologue pairs are useful to discern the contribution of fluorotelomer atmospheric oxidation in PFCA deposition. Smog chamber studies suggest that the degradation of X:2 fluorotelomer compound yields PFCAs with X and X+1 carbons.[41] There will be some variability in the molar ratio of the even-odd PFCA pair depending on the atmospheric levels of NO_x ($NO + NO_2$) and peroxy radicals.[14] If fluorotelomer oxidation is indeed a major pathway for PFCA formation, then sequential homologue pairs are expected to be present in roughly equal molar quantities (i.e., 1:1).[10,45] Molar concentration ratios were calculated for three pairs of PFCAs: C6-C7, C8-C9, and C10-C11 (with the even carbon PFCA in the numerator and the odd carbon PFCA in the denominator), which represent the major PFCA oxidation products of 6:2, 8:2, and 10:2 fluorotelomers, respectively. Most flux ratio measurements were clustered around a 1:1 ratio within a factor of ± 2 after 1990 (i.e., between 2:1 and 1:2, Figure A-5),

comparable to previous measurements in the Arctic.[10,16] Detection of the odd PFCA homologues close to the detection limits resulted in higher molar ratios before 1990.

The available evidence from homologue correlations and molar concentration ratios strongly suggests that most PFCAs are formed indirectly through the oxidation of volatile precursors. We can therefore use these data as an observational test of a recent GEOS-CHEM model (Figure A-6)[46] that includes oxidation chemistry of fluorotelomer compounds as well as deposition and transport of precursors and intermediates. Comparing the modelled and measured fluxes we found that modelled fluorotelomer oxidation can account for < 50 % of C9 – C12 PFCAs and 3 – 46 % of C5-C8 PFCAs, respectively, after the 1990s. Discrepancies between modelled and measured PFCA deposition highlight uncertainty in emission inventories used by the model[47] and that gas-particle partitioning, which could contribute to the transport of PFCAs,[46] has not yet been parameterized in model calculations. Thus, further work in chemical modeling of PFCA atmospheric formation and fate is needed.

In contrast to the PFCAs, pairs of PFSAs were not generally correlated with each other or with any PFCAs (Figure 2-3, Table A-14). This is consistent with the previous record from Devon Ice Cap, but inconsistent with a record from Svalbard, where correlation was observed between C8 PFSA (PFOS) and C2 PFCA (TFA).[10,16] We observed a very strong, statistically significant correlation for the PFOS-PFBS pair (C8-C4, r: 0.90, $p < 0.001$). A similar observation was made at Devon Ice Cap (r^2: 0.31, $p < 0.05$).[10] These two compounds can be formed through the atmospheric oxidation of perfluoroalkane sulfonamido substances.[42] Chamber experiments demonstrated that oxidation of N-methyl perfluorobutane sulfonamido ethanol (N-MeFBSE, C4 homologue) yields C2-C4 PFCAs and the C4 PFSA (PFBS). Similarly, the oxidation of N-methyl perfluorooctane sulfonamido ethanol (N-MeFOSE, C8 homologue) would be expected to yield the C8 PFSA (PFOS) and C2-C8 PFCAs. These precursors may co-occur in commercial products[48] and may be emitted from similar sources.[49] Both C4 and C8 PFSA precursors have been detected in Arctic environments.[50,51] If this indirect formation were a significant source, we might expect to see correlations between C8 PFSA (PFOS) with one of its measured potential precursors, FOSA, and with C8 PFCA. We would also expect to see a correlation between C4 PFSA (PFBS) with the C4 PFCA. As discussed

above, no correlations between any of these species were observed (Figure 2-3). Thus, we have no substantive evidence that PFBS and PFOS found on Mt Oxford icefield were a result of indirect transport. However, another possibility for the correlation of PFBS and PFOS could be the use of these two homologues in AFFF formulations, where they could be released and subsequently transported to the Arctic. Potential impacts of local usage will be discussed in the next section.

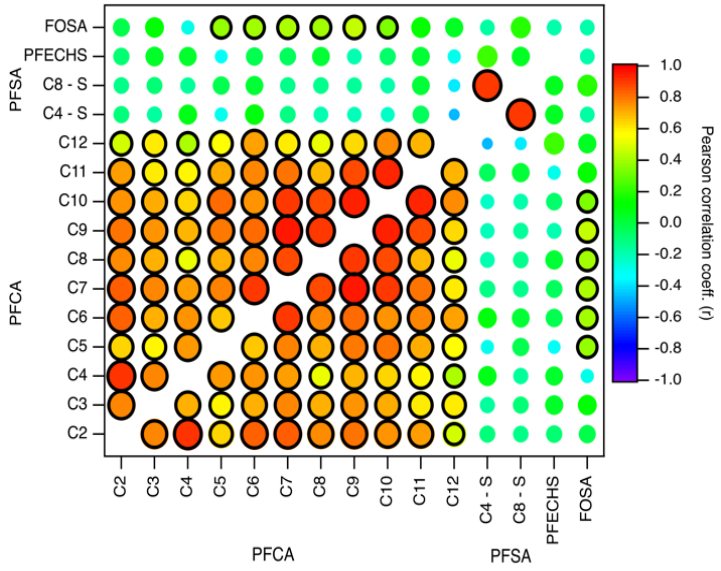

Figure 2-3: Pearson correlation map of log transformed PFCA, PFSA, and FOSA deposition fluxes on Mt. Oxford icefield for the entire sampling period (1967-2016). The strength of the correlation is illustrated by the colour and size of the circle, where larger circles denote a strong correlation based on the magnitude of r. The black outline represents a statistically significant correlation (p-value <0.05). Data for C2 – C4 PFCAs from Pickard et al.[19]

2.3.4 Evidence for aerosol transport of PFAAs

Aerosol transport may also contribute to PFAA deposition on the Mt. Oxford icefield. Depending on the PFAA homologue and the aerosol source, transport on aerosols could be attributed to both direct and indirect sources. Most previous studies in remote regions have not observed clear evidence for marine aerosol-mediated long-range transport of PFAAs.[9,16,17] While high volume atmospheric sampling has measured several PFAAs in aerosols (e.g., Wong et al.,2018, 2021),[37,52] this sampling approach cannot accurately distinguish between gaseous and particulate PFAAs.[53,54] The ice core record from Devon Ice Cap suggested a role for aerosols, in which there was some

evidence for transport by mineral dust.[10] Major ion analysis can be useful to determine the influence of sea spray, biomass burning, mineral dust, and anthropogenic aerosol contributions to the High Arctic.[10,55]

To assess the contribution of marine aerosols to PFAA deposition, we compared the PFAA homologue profiles in the ice core to the surrounding ocean samples and conducted correlation analysis on individual PFAAs with a marine aerosol tracer (Na^+). Consistent with other studies, the molar ratios are distinct to the typical ratios in oceans (Figure A-7). The contribution of marine aerosols to PFAA deposition was also assessed by comparing the PFAA homologue profiles in the ice core and surrounding ocean samples (Figure A-8).[10,9] This transport mechanism is highly dependent on the concentration of the analyte in bulk seawater, which is expected to change with time, as well as the enrichment factor in marine aerosols.[56,57] Enrichment is larger for PFSAs and increases with perfluorinated chain length.[56,58] Thus, if a marine source is important, an icefield homologue profile relatively enriched in longer-chain homologues and PFSAs is expected.[9] Consistent with previous observations from the Canadian Arctic[10] and the Antarctic,[17] we did not observe this (Figure A-8). Instead, we observed a relative enrichment of short chain homologues and a lower abundance of PFSAs on the icefield when compared to the surrounding oceans.

Correlation with Na^+ was also used to assess marine aerosol contributions to individual PFAA deposition. The ocean around Ellesmere Island is icebound for most of the year, with minimum sea ice in September.[59] Despite this, evidence from measurements and simulations suggest that marine aerosols can be generated from salty blowing snow from sea ice surfaces and/or transport by frost flowers.[60–64] In fact, model simulations estimate sea ice produces an order of magnitude more marine aerosols than the same unit area of open ocean under similar conditions.[60,65] Polynyas also exist in the Canadian Arctic Archipelago year-round due to tidal currents and tidal mixing (e.g., North Water and Hell Gate polynya).[66] Recently, the polynyas within Arctic Canada and the Canadian Basin of the Arctic Ocean were identified as a possible source of marine aerosols to Ellesmere Island.[21] Correlation analysis revealed weak to moderate correlations ($p < 0.05$) between individual PFAA homologues and Na^+ (Figure 2-4A, Table A-18, Figure A-10). The C5 – C10 and C12 PFCAs were all positively correlated with Na^+

(r: 0.35 – 0.52, $p < 0.05$), while the C11 (PFUnDA) homologue showed no relationship with Na^+ (r: 0.11, p=0.54). Among the PFSAs, PFECHS was the only homologue that had a statistically significant correlation with Na^+ ($r = 0.52$, $p < 0.00001$), whereas the other PFSAs (C4 and C8) and FOSA failed to show any correlations (r: -0.04 – 0.03, p: 0.83 – 0.84). This suggests transport by marine aerosols may be a contributing source of selected PFAAs to Mt. Oxford icefield.

Although the ocean vertical distribution and composition profiles of PFAAs are variable, several studies have found enhanced PFAA concentrations near the air-sea interface.[30,67] Recently, Garnett et al.[68] investigated the distribution of PFAAs in seawater and sea ice compartments in the European High Arctic. They found elevated levels of PFAAs at the surface of sea ice and under-ice seawater, and, using salinity profiles and $d^{18}O_{H2O}$ composition, found a strong atmospheric source of PFAAs.[68] It is possible that PFAAs are deposited to seawater or sea ice compartments through atmospheric transformation of precursors, followed by the subsequent transport to the terrestrial environment by marine aerosols.[68] A similar association was made during a long-term air monitoring study in Norway, which found PFCAs and PFSAs significantly correlated with Na^+ (r: 0.4–0.8, $p < 0.05$).[58] However, that study collected particulate PFAA in low-lying sampling locations that were close to the ocean (~1.3 and 20 km to open water)[58] whereas Mt. Oxford icefield is located ~ 100 km from the Arctic Ocean and at ~1.8 km elevation. Interestingly, the results from our study are inconsistent with results from two other Arctic sites (Devon Ice Cap and Lomonsovfonna Ice Cap)[10,16] where no correlation with Na^+ was observed, although both sites can be influenced by marine aerosols.[16,21] This may be due to competing sources other than marine aerosol transport (e.g., oxidation of volatile precursors). To the best of our knowledge, our observations represent the first evidence for marine aerosol transport contributing to PFAA loading on a remote polar terrestrial environment.

Among the statistically significant correlations between PFAAs and Na^+, the C12 PFCA (PFDoDA) and PFECHS were most strongly correlated (r: 0.52 for both, $p < 0.05$, Figure 4), which provides further evidence of marine aerosol transport. PFDoDA, with its long perfluorinated carbon chain, is one of the most surface-active PFCAs and has a higher enrichment factor in marine aerosols than other PFCAs.[56,57,69] The transport of

PFECHS must be driven by direct processes since no known precursors exist. Because PFECHS is permitted to be used as an abrasion inhibitor in aircraft hydraulic fluids,[70] hydraulic fluid leakage from aircraft and airport activities may increase Arctic PFECHS concentrations. Multiple studies have linked PFECHS use in aviation to local environmental contamination (e.g., [71,72]). It is plausible that Arctic airport activity on and around Ellesmere Island (e.g., Canadian Forces Station Alert, located 162 km from Mt. Oxford icefield) could have led to elevated concentrations of PFECHS in the surrounding ocean. Though we cannot confirm our hypothesis since no measurements exist, this would be consistent with local contamination measurements elsewhere, and could explain this unusual observation.

Long range transport by mineral dust aerosols may also be a pathway for transport of PFAAs to this region. One previous study has suggested a role for PFAA transport mediated by mineral dust.[10] Correlation with non-sea salt (nss) Ca^{2+} and nssMg^{2+} suggests either that a mechanistic relationship between PFAAs and mineral dust exists or that PFAAs and mineral dust are being transported within the same airmass. Other strong atmospheric acids are known to accumulate on dust and undergo long-range transport.[73] Since PFAAs are strong acids, a similar mechanism could lead to their transport. To assess the potential role of this pathway, we examined correlations between PFAAs and typical indicators of mineral dust, nssCa^{2+} and nssMg^{2+}.[74] No correlations were observed when applied on a multidecadal scale, with the exception of PFECHS, which showed a moderate correlation with nssCa^{2+} ($r = 0.49$, $p < 0.05$). This is in contrast to the observations of Pickard et al.[10] at the Devon Ice Cap where nssCa^{2+} and nssMg^{2+} were correlated with several PFAAs.

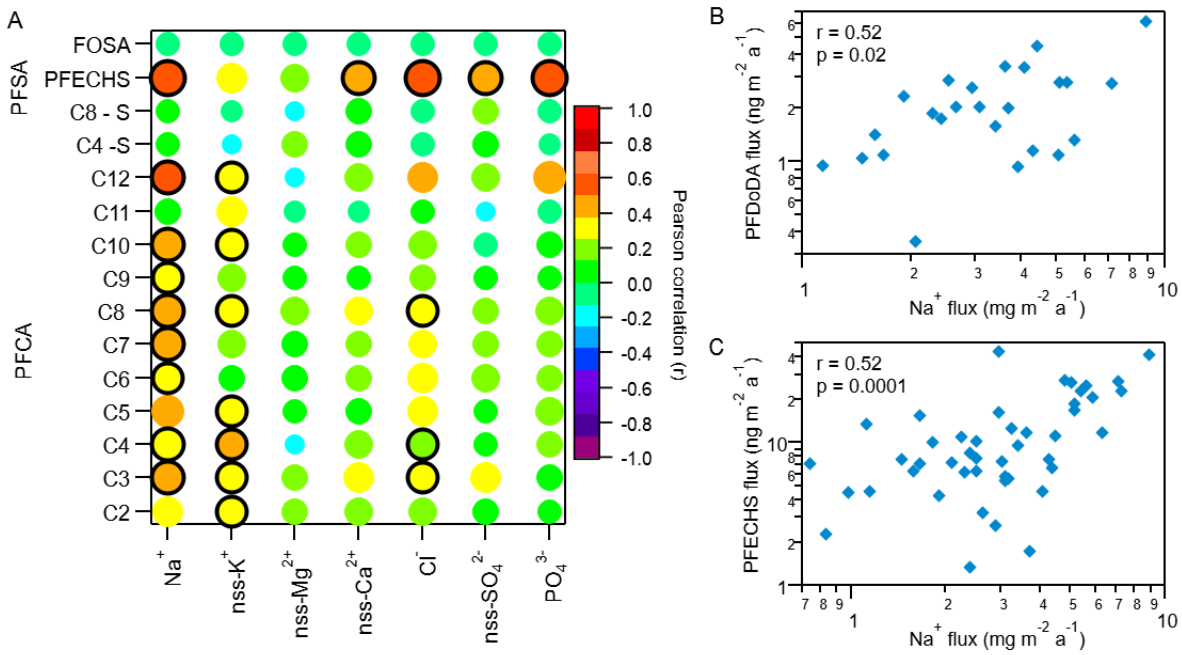

Figure 2-4: Correlations log transformed PFAA deposition fluxes and major ions on Mt. Oxford icefield for the entire sampling period (1967-2016). (A) Correlation matrix where the strength of the correlation is illustrated by the colour and size of the circle, where larger circles denote a strong correlation (larger Pearson correlation coefficient). The black outline represents a statistically significant correlation (p-value <0.05). (B) Correlation between Na^+ and PFDoDA fluxes.(C) Correlation between Na^+ and PFECHS fluxes (1967-2016). For (B) and (C), the Pearson correlation (r) and p-value for the line of best fit are also included.

2.3.5 Episodic PFAA transport pathways

This ice core uniquely recorded several episodes of elevated deposition for PFSAs and PFCAs (Figure 1); since the seasonal record is robust, we additionally reported the annual fluxes to highlight the episodic nature of deposition (Figure 2-5). Episodic detection was based on at least two consecutive samples (e.g., 1973 and 1974), indicating the observations were not caused by contamination of a single sample. In previous ice core records, episodic deposition has not been observed, with the exception of one episode of elevated C8 PFSA (PFOS) on Devon Ice Cap in 2013.[10] Because these events differed from the rest of the temporal record, they were examined separately to assess whether they could be attributed to different transport pathways.

Prior to 1980, we observed two distinct periods of PFCA increases (Figure 2-5A). One episode occurred during 1973-1974, where C6-C12 PFCA deposition fluxes showed more than a three-fold increase. Among these, C8 (PFOA) demonstrated the largest increase, rising by more than 34 times from the prior year. Another episode occurred in 1979, where C6 (PFHxA) deposition flux increased 100 times. The correlation analysis between PFCAs and aerosol tracers was repeated for the period 1967-1979 to determine if any relationship existed. We observed statistically significant correlations between C8-C10 PFCAs and Na^+ (r: 0.55 - 0.70, $p < 0.05$) and moderate to strong correlations between C7-C10 PFCAs and $nssCa^{2+}$ and $nssMg^{2+}$ (r: 0.54 - 0.87, $p < 0.05$, Table A-18). These correlations were driven by the co-occurrence of elevated cation deposition during the 1973 episode, which may indicate a role for marine aerosols and/or mineral dust in the deposition events observed pre-1980. The long-range transport of mineral dust to the Arctic has been investigated to understand impacts on regional climate. Recently, Zhao et al.[75] analyzed dust events in China during 2011 – 2015 and found two major transport routes to the Arctic: (i) mostly over land transport with a short duration (4-8 d), which was observed in Barrow, Alaska; and (ii) long-duration transport event (7-10 d) originating from the Gobi desert, passing through China, Korea, Japan, and the North Pacific ocean (where mixing with marine aerosols is possible) and finally deposited at Alert.[75] Long-duration transport events could be consistent with our observation of elevated PFCAs along with Na^+, $nssCa^{2+}$, and $nssMg^{2+}$ during the 1970s. The cation profile also shows high concentration of Ca^{2+} which is typical of Asian mineral dust,[73] providing additional evidence for a synoptic scale event leading to enhanced transport from that region.[76] Taken together, the evidence presented here suggests that direct transport during the period 1967-1980 may be responsible for the observed episodes of elevated PFCA deposition.

We also observed episodes of elevated PFSAs, with the C4 (PFBS) and C8 (PFOS) elevated in 1970, 1976, 1979, 1985, and 1989 (Figure 2-5B). In all episodes, deposition fluxes of C8 were more than 74 times greater than the previous year, whereas the deposition fluxes of C4 increased 2 to 84 times. As discussed above, we have no clear evidence for C4 and C8 PFSA indirect formation or transport by marine aerosols or mineral dust. In the absence of other evidence, we hypothesize that episodic deposition

may be related to direct release of AFFF from military Arctic activities. First developed in the 1960s, AFFF is primarily used to extinguish hydrocarbon fuelled fires at oil refineries, military bases, airports and firefighter training facilities.[77] It is documented that AFFF was stored and used in military fire suppressant training at Thule Air Base, Qaanaaq, Greenland[78] and in Alert, Canada.[79,80] As of 2017, Thule Air Base was the only US Air Force base that still had AFFF stockpiles on site and had not transitioned to newer formulations that are typically characterized by shorter chain PFAS or the absence of fluorinated chemicals.[78] The composition of commercially produced AFFF is proprietary and is known to vary between manufacturer and production time.[81] While we cannot know for sure what formulations of AFFF were used at Alert and Thule, analysis of archived AFFF samples from military bases found that C8 (PFOS) was the dominant homologue in the formulation, with lesser contributions of other PFSAs, as well as PFCAs.[82] The archived samples represented AFFF formulations from 1989 to 2001—well after our observed events—but represent the oldest AFFF characterizations available.[77] Unfortunately, very little is known about emissions to air from AFFF, with the few studies that exist focusing on modern AFFF formulations.[83,84] Given these uncertainties, our measurements are generally consistent with a possible legacy AFFF source.[83,84] Air mass back trajectory analysis for two years (2011 and 2013) revealed that some of the air mass impacting Mt Oxford icefield originated from the Arctic Ocean and the western coast of Greenland (Figure A-11), which is in close proximity to Thule Air Base. We caution that annual average air mass back trajectories may not capture source regions for sporadic long-range transport episodes that convey materials long distances to the Arctic; rather they are intended to identify possible source regions. It is also possible that anomalous events, such as those that have been shown to be responsible for the long-range transport of dust and pollen to the Arctic,[76,85] could contribute to the transport of PFSAs.

Additionally, episodic pulses were observed for two organophosphate ester contaminants in Mt. Oxford icefield measured in a separate core sampled at the same time as this study.[22] In that paper, pulses of tris(isobutyl)phosphate and tris-(1-chloro-2-propyl)phosphate were observed in several years between 1975 and 1992. These peaks were not coincident with the temporal profile at the Devon Ice Cap and were unique to

Mt. Oxford icefield.[22] Taken together, this may suggest a combination of local activity with climate episodes can result in depositional pulses.

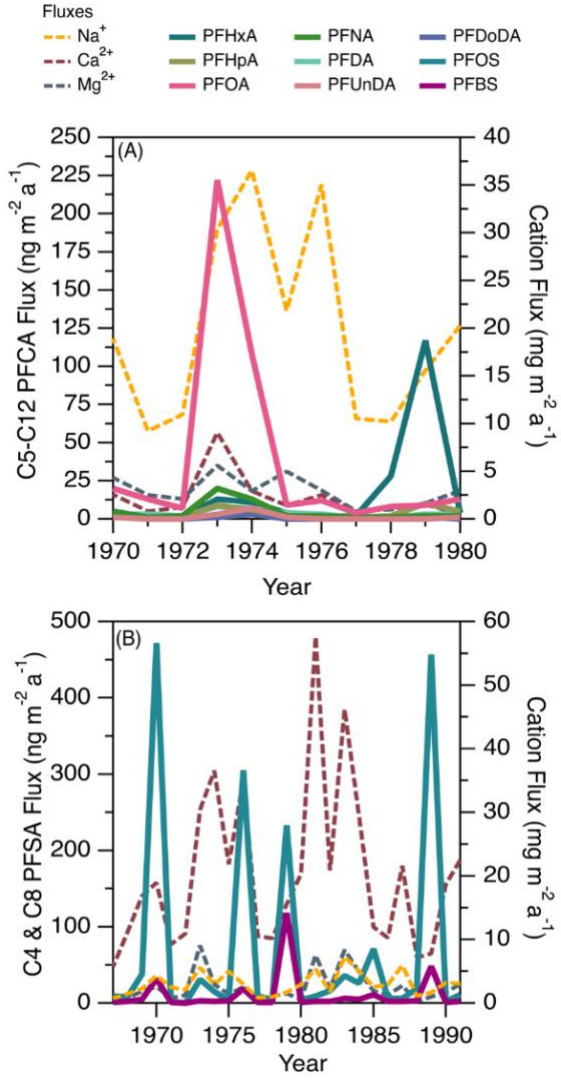

Figure 2-5: Annual deposition fluxes for (A) C6 – C12 PFCAs (ng m^{-2} a^{-1}, left) and Na^{+}, $nssCa^{2+}$, and $nssMg^{2+}$ (mg m^{-2} a^{-1}, right) for the period 1970 – 1980 and (B) C4 and C8 PFSAs (ng m^{-2} a^{-1}, left) and Na^{+}, $nssCa^{2+}$ and $nssMg^{2+}$ (mg m^{-2} a^{-1}, right) for the period 1967-1991. The PFAAs are represented by solid lines while major ions are represented by broken lines and are presented on different scales.

2.4 Conclusions

Monitoring deposition of organic contaminants in remote pristine environments is an invaluable tool to help us understand the impacts of changing production, as well as

different transport mechanisms. It is well established that PFAS can undergo long-range transport to remote locations;[9,10,17,55] however, the mechanisms that facilitate this transport are not fully understood. This study emphasizes the power of ice cores to aid in understanding long-range transport of contaminants. To gain new insight into possible transport mechanisms, we presented the most extensive temporal record of PFCAs in the Northern Hemisphere, as well as the longest temporal record of PFSAs globally.

Our results indicate that most PFAAs are present and there is evidence of increasing deposition of PFCAs over the past 50 years at Mt. Oxford icefield. Using homologue correlations, molar concentration ratios and model comparisons, we confirmed that PFCAs deposited at Mt. Oxford icefield are formed primarily through the long-range atmospheric transport and oxidation of volatile precursors in the atmosphere. The PFCA deposition was greater than observed deposition at Devon Ice Cap, which suggests a greater influence from Europe and Continental Asia. We also highlighted the importance of measuring supplementary analytes for source elucidation. Correlation analysis between marine and mineral dust tracers yielded two unique findings exclusive to this ice core: (i) marine aerosols have been identified as a possible transport mechanism for selected PFAAs to the terrestrial environment during specific time periods; and (ii) mineral dust was associated with an unusual deposition event of PFCAs observed during the 1970s.

The extended temporal record of this ice core allowed unique observations that were not possible in other previous studies. We observed episodic elevated deposition pulses for several PFAAs. Notably, C8 (PFOS) and C4 (PFBS) PFSAs were elevated in five (5) years prior to 1990. While one pulse of C8 PFSA was observed at the Devon Ice Cap in 2013 (70 ng m^2 a^{-1}), the deposition fluxes observed in the current study (up to 471 ng m^2 a^{-1}) are several times greater. We postulate that these events may be evidence of direct transport of AFFF used in nearby military Arctic activities. Further work is needed to better understand the causes of these historic pulses.

Ice caps represent a natural record of contaminant concentration, which is useful to discern trends and sources that may change over time. Ice cores provide particular utility for understanding PFAAs in remote locations, for which there are multiple potential

long-range transport mechanisms. While ice cores can improve our understanding of long-range transport sources and mechanisms of PFAAs, as well as the efficacy of regulation, this valuable resource is disappearing as a result of climate change.[86,87] Therefore, there is an urgent need to prioritize further research efforts to collect ice cores to discern temporal trends and possible sources.

2.5 References

(1) Buck, R. C.; Franklin, J.; Berger, U.; Conder, J. M.; Cousins, I. T.; Voogt, P. D.; Jensen, A. A.; Kannan, K.; Mabury, S. A.; van Leeuwen, S. P. J. Perfluoroalkyl and Polyfluoroalkyl Substances in the Environment: Terminology, Classification, and Origins. *Integrated Environmental Assessment and Management* **2011**, *7* (4), 513–541. https://doi.org/10.1002/ieam.258.

(2) Glüge, J.; Scheringer, M.; Cousins, I. T.; Dewitt, J. C.; Goldenman, G.; Herzke, D.; Lohmann, R.; Ng, C. A.; Trier, X.; Wang, Z. An Overview of the Uses of Per- And Polyfluoroalkyl Substances (PFAS). *Environmental Science: Processes and Impacts* **2020**, *22* (12), 2345–2373. https://doi.org/10.1039/d0em00291g.

(3) Prevedouros, K.; Cousins, I. T.; Buck, R. C.; Korzeniowski, S. H. Sources, Fate and Transport of Perfluorocarboxylates. *Environmental Science and Technology* **2006**, *40* (1), 32–44. https://doi.org/10.1021/es0512475.

(4) Frömel, T.; Knepper, T. P. Biodegradation of Fluorinated Alkyl Substances. *Reviews of environmental contamination and toxicology* **2010**, *208*, 161–177. https://doi.org/10.1007/978-1-4419-6880-7_3.

(5) Conder, J. M.; Hoke, R. A.; De Wolf, W.; Russell, M. H.; Buck, R. C. Are PFCAs Bioaccumulative? A Critical Review and Comparison with Regulatory Criteria and Persistent Lipophilic Compounds. *Environmental Science and Technology* **2008**, *42* (4), 995–1003. https://doi.org/10.1021/es070895g.

(6) Lau, C.; Anitole, K.; Hodes, C.; Lai, D.; Pfahles-Hutchens, A.; Seed, J. Perfluoroalkyl Acids: A Review of Monitoring and Toxicological Findings. *Toxicological Sciences* **2007**, *99* (2), 366–394. https://doi.org/10.1093/toxsci/kfm128.

(7) Land, M.; De Wit, C. A.; Cousins, I. T.; Herzke, D.; Johansson, J.; Martin, J. W. What Is the Effect of Phasing out Long-Chain per- and Polyfluoroalkyl Substances on the Concentrations of Perfluoroalkyl Acids and Their Precursors in the Environment? A Systematic Review Protocol. *Environmental Evidence* **2015**, *4* (1), 1–13. https://doi.org/10.1186/2047-2382-4-3.

(8) Young, C. J.; Furdui, V. I.; Franklin, J.; Koerner, R. M.; Muir, D. C. G.; Mabury, S. A. Perfluorinated Acids in Arctic Snow: New Evidence for Atmospheric Formation.

Environmental Science and Technology **2007**, *41* (10), 3455–3461. https://doi.org/10.1021/es0626234.

(9) MacInnis, J. J.; French, K.; Muir, D. C. G.; Spencer, C.; Criscitiello, A.; De Silva, A. O.; Young, C. J. A 14-Year Depositional Ice Record of Perfluoroalkyl Acids in the High Arctic. *Environmental Science Processes and Impacts* **2017**, *19*, 22–30. https://doi.org/10.1039/C6EM00593D.

(10) Pickard, H. M.; Criscitiello, A. S.; Spencer, C.; Sharp, M. J.; Muir, D. C. G.; De Silva, A. O.; Young, C. J. Continuous Non-Marine Inputs of per- and Polyfluoroalkyl Substances to the High Arctic: A Multi-Decadal Temporal Record. *Atmospheric Chemistry and Physics* **2018**, *18* (7), 5045–5058. https://doi.org/10.5194/acp-18-5045-2018.

(11) Muir, D.; Bossi, R.; Carlsson, P.; Evans, M.; De Silva, A.; Halsall, C.; Rauert, C.; Herzke, D.; Hung, H.; Letcher, R.; Rigét, F.; Roos, A. Levels and Trends of Poly- and Perfluoroalkyl Substances in the Arctic Environment – An Update. *Emerging Contaminants* **2019**, *5*, 240–271. https://doi.org/10.1016/j.emcon.2019.06.002.

(12) Chen, Y.; Fu, J.; Ye, T.; Li, X.; Gao, K.; Xue, Q.; Lv, J.; Zhang, A.; Fu, J. Occurrence, Profiles, and Ecotoxicity of Poly- and Perfluoroalkyl Substances and Their Alternatives in Global Apex Predators: A Critical Review. *Journal of Environmental Sciences (China)* **2021**, *109*, 219–236. https://doi.org/10.1016/j.jes.2021.03.036.

(13) Xie, Z.; Kallenborn, R. Legacy and Emerging Per- and Polyfluoroalkyl Substances in Polar Regions. *Current Opinion in Green and Sustainable Chemistry* **2023**, *42*, 100840. https://doi.org/10.1016/j.cogsc.2023.100840.

(14) Young, C. J.; Mabury, S. A. *Atmospheric Perfluorinated Acid Precursors: Chemistry, Occurrence and Impacts*; 2010; Vol. 208. https://doi.org/10.1007/978-1-4419-6880-7_1.

(15) Kwok, K. Y.; Yamazaki, E.; Yamashita, N.; Taniyasu, S.; Murphy, M. B.; Horii, Y.; Petrick, G.; Kallerborn, R.; Kannan, K.; Murano, K.; Lam, P. K. S. Transport of Perfluoroalkyl Substances (PFAS) from an Arctic Glacier to Downstream Locations: Implications for Sources. *Science of the Total Environment* **2013**, *447*, 46–55. https://doi.org/10.1016/j.scitotenv.2012.10.091.

(16) Hartz, W. F.; Björnsdotter, M. K.; Yeung, L. W. Y.; Hodson, A.; Thomas, E. R.; Humby, J. D.; Day, C.; Jogsten, I. E.; Kärrman, A.; Kallenborn, R. Levels and Distribution Profiles of Per- and Polyfluoroalkyl Substances (PFAS) in a High Arctic Svalbard Ice Core. *Science of The Total Environment* **2023**, No. 5, 161830. https://doi.org/10.1016/j.scitotenv.2023.161830.

(17) Garnett, J.; Halsall, C.; Winton, H.; Joerss, H.; Mulvaney, R.; Ebinghaus, R.; Frey, M.; Jones, A.; Leeson, A.; Wynn, P. Increasing Accumulation of Perfluorocarboxylate Contaminants Revealed in an Antarctic Firn Core (1958-2017). *Environmental Science and Technology* **2022**, *56* (16), 11246–11255. https://doi.org/10.1021/acs.est.2c02592.

(18) Maxwell, J. B. Climatic Regions of the Canadian Arctic Islands. *Arctic* **1981**, *34* (3), 225–240. https://doi.org/10.14430/arctic2525.

(19) Pickard, H. M.; Criscitiello, A. S.; Persaud, D.; Spencer, C.; Muir, D. C. G.; Lehnherr, I.; Sharp, M. J.; De Silva, A. O.; Young, C. J. Ice Core Record of Persistent Short-Chain Fluorinated Alkyl Acids: Evidence of the Impact From Global Environmental Regulations. *Geophysical Research Letters* **2020**, *47* (10). https://doi.org/10.1029/2020GL087535.

(20) Arienzo, M. M.; McConnell, J. R.; Chellman, N.; Criscitiello, A. S.; Curran, M.; Fritzsche, D.; Kipfstuhl, S.; Mulvaney, R.; Nolan, M.; Opel, T.; Sigl, M.; Steffensen, J. P. A Method for Continuous 239Pu Determinations in Arctic and Antarctic Ice Cores. *Environmental Science and Technology* **2016**, *50* (13), 7066–7073. https://doi.org/10.1021/acs.est.6b01108.

(21) Criscitiello, A. S.; Geldsetzer, T.; Rhodes, R. H.; Arienzo, M.; McConnell, J.; Chellman, N.; Osman, M. B.; Yackel, J. J.; Marshall, S. Marine Aerosol Records of Arctic Sea-Ice and Polynya Variability From New Ellesmere and Devon Island Firn Cores, Nunavut, Canada. *Journal of Geophysical Research: Oceans* **2021**, *126* (9), 1–20. https://doi.org/10.1029/2021JC017205.

(22) De Silva, A. O.; Young, C. J.; Spencer, C.; Muir, D. C. G.; Sharp, M.; Lehnherr, I.; Criscitiello, A. Canadian High Arctic Ice Core Records of Organophosphate Flame Retardants and Plasticizers. *Environmental Science: Processes and Impacts* **2023**, 2001–2014. https://doi.org/10.1039/d3em00215b.

(23) Legendre, P. *lmodel2: Model II Regression. R package version 1.7-3.*

(24) *DuPont GenX Processing Aid for Making Fluoropolymer Resins*.

(25) Gebbink, W. A.; Van Asseldonk, L.; Van Leeuwen, S. P. J. Presence of Emerging Per- and Polyfluoroalkyl Substances (PFASs) in River and Drinking Water near a Fluorochemical Production Plant in the Netherlands. *Environmental Science and Technology* **2017**, *51* (19), 11057–11065. https://doi.org/10.1021/acs.est.7b02488.

(26) Sun, M.; Arevalo, E.; Strynar, M.; Lindstrom, A.; Richardson, M.; Kearns, B.; Pickett, A.; Smith, C.; Knappe, D. R. U. Legacy and Emerging Perfluoroalkyl Substances Are Important Drinking Water Contaminants in the Cape Fear River Watershed of North Carolina. *Environmental Science and Technology Letters* **2016**, *3* (12), 415–419. https://doi.org/10.1021/acs.estlett.6b00398.

(27) Galloway, J. E.; Moreno, A. V. P.; Lindstrom, A. B.; Strynar, M. J.; Newton, S.; May, A. A.; May, A. A.; Weavers, L. K.; Weavers, L. K. Evidence of Air Dispersion: HFPO-DA and PFOA in Ohio and West Virginia Surface Water and Soil near a Fluoropolymer Production Facility. *Environmental Science and Technology* **2020**, *54* (12), 7175–7184. https://doi.org/10.1021/acs.est.9b07384.

(28) Pike, K. A.; Edmiston, P. L.; Morrison, J. J.; Faust, J. A. Correlation Analysis of Perfluoroalkyl Substances in Regional U.S. Precipitation Events. *Water Research* **2021**, *190*. https://doi.org/10.1016/j.watres.2020.116685.

(29) Macdonald, R. W.; Barrie, L. A.; Bidleman, T. F.; Diamond, M. L.; Gregor, D. J.; Semkin, R. G.; Strachan, W. M. J.; Li, Y. F.; Wania, F.; Alaee, M.; Alexeeva, L. B.; Backus, S. M.; Bailey, R.; Bewers, J. M.; Gobeil, C.; Halsall, C. J.; Harner, T.; Hoff, J. T.; Jantunen, L. M. M.; Lockhart, W. L.; Mackay, D.; Muir, D. C. G.; Pudykiewicz, J.; Reimer, K. J.; Smith, J. N.; Stern, G. A.; Schroeder, W. H.; Wagemann, R.; Yunker, M. B. *Contaminants in the Canadian Arctic: 5 Years of Progress in Understanding Sources, Occurrence and Pathways*; 2000; Vol. 254. https://doi.org/10.1016/S0048-9697(00)00434-4.

(30) Joerss, H.; Xie, Z.; Wagner, C. C.; Von Appen, W. J.; Sunderland, E. M.; Ebinghaus, R. Transport of Legacy Perfluoroalkyl Substances and the Replacement Compound HFPO-DA through the Atlantic Gateway to the Arctic Ocean - Is the Arctic

a Sink or a Source? *Environmental Science and Technology* **2020**, *54* (16), 9958–9967. https://doi.org/10.1021/acs.est.0c00228.

(31) Gewurtz, S. B.; Auyeung, A. S.; De Silva, A. O.; Teslic, S.; Smyth, S. A. Per- and Polyfluoroalkyl Substances (PFAS) in Canadian Municipal Wastewater and Biosolids: Recent Patterns and Time Trends 2009 to 2021. *Science of The Total Environment* **2024**, *912*, 168638. https://doi.org/10.1016/j.scitotenv.2023.168638.

(32) Young, C. J.; Furdui, V. I.; Franklin, J.; Koerner, R. M.; Muir, D. C. G.; Mabury, S. A. Perfluorinated Acids in Arctic Snow: New Evidence for Atmospheric Formation. *Environmental Science and Technology* **2007**, *41* (10), 3455–3461. https://doi.org/10.1021/es0626234.

(33) Wang, X.; Halsall, C.; Codling, G.; Xie, Z.; Xu, B.; Zhao, Z.; Xue, Y.; Ebinghaus, R.; Jones, K. C. Accumulation of Perfluoroalkyl Compunds in Tibetan Mountain Snow: Temporal Patterns from 1980 to 2010. *Environmental Science and Technology* **2014**, *48* (1), 173–181. https://doi.org/10.1021/es4044775.

(34) Kirchgeorg, T.; Dreyer, A.; Gabrieli, J.; Kehrwald, N.; Sigl, M.; Schwikowski, M.; Boutron, C.; Gambaro, A.; Barbante, C.; Ebinghaus, R. Temporal Variations of Perfluoroalkyl Substances and Polybrominated Diphenyl Ethers in Alpine Snow. *Environmental Pollution* **2013**, *178* (3), 367–374. https://doi.org/10.1016/j.envpol.2013.03.043.

(35) Kwok, K. Y.; Taniyasu, S.; Yeung, L. W. Y.; Murphy, M. B.; Lam, P. K. S.; Horii, Y.; Kannan, K.; Petrick, G.; Sinha, R. K.; Yamashita, N. Flux of Perfluorinated Chemicals through Wet Deposition in Japan, the United States, and Several Other Countries. *Environmental Science and Technology* **2010**, *44* (18), 7043–7049. https://doi.org/10.1021/es101170c.

(36) Scott, B. F.; Spencer, C.; Mabury, S. A.; Muir, D. C. G. Poly and Perfluorinated Carboxylates in North American Precipitation. *Environmental Science and Technology* **2006**, *40* (23), 7167–7174.

(37) Wong, F.; Shoeib, M.; Katsoyiannis, A.; Eckhardt, S.; Stohl, A.; Bohlin-Nizzetto, P.; Li, H.; Fellin, P.; Su, Y.; Hung, H. Assessing Temporal Trends and Source Regions of Per- and Polyfluoroalkyl Substances (PFASs) in Air under the Arctic Monitoring and

Assessment Programme (AMAP). *Atmospheric Environment* **2018**, *172* (June 2017), 65–73. https://doi.org/10.1016/j.atmosenv.2017.10.028.

(38) Wang, Z.; Cousins, I. T.; Scheringer, M.; Buck, R. C.; Hungerbuhler, K. Global Emission Inventories for C4-C14 Perfluoroalkyl Carboxylic Acid (PFCA) Homologues from 1951 to 2030, Part II: The Remianing Pieces of the Puzzle. *Environment International* **2014**, *69*, 166–176. https://doi.org/10.1016/j.envint.2014.04.006.

(39) Goto-Azuma, K.; Koerner, R. M. Ice Core Studies of Anthropogenic Sulfate and Nitrate Trends in the Arctic. *Journal of Geophysical Research Atmospheres* **2001**, *106* (D5), 4959–4969. https://doi.org/10.1029/2000JD900635.

(40) Weppner, W. *Letter by William Weppner, 3M, to Charles Auer, EPA OPPT, Regarding the Phase-out Plan for POSF-Based Products;US EPA Public Docket EPA-HQ-OPPT-2002−0043−0009;3M General Offices; St. Paul, MN.*; 2000; p US EPA Public Docket EPA-HQ-OPPT-2002−0043−0009;3M.

(41) Ellis, D. A.; Martin, J. W.; De Silva, A. O.; Mabury, S. A.; Hurley, M. D.; Sulbaek Andersen, M. P.; Wallington, T. J. Degradation of Fluorotelomer Alcohols: A Likely Atmospheric Source of Perfluorinated Carboxylic Acids. *Environmental Science and Technology* **2004**, *38* (12), 3316–3321. https://doi.org/10.1021/es049860w.

(42) D'Eon, J. C.; Hurley, M. D.; Wallington, T. J.; Mabury, S. A. Atmospheric Chemistry of N-Methyl Perfluorobutane Sulfonamidoethanol, C4F9SO2N(CH3)CH2CH2OH: Kinetics and Mechanism of Reaction with OH. *Environmental Science & Technology* **2016**, *40*, 1862–1868. https://doi.org/10.1021/es0520767.

(43) Young, C. J.; Mabury, S. A. Reviews of Environmental Contamination and Toxicology. In *Reviews of Enviromental Contamination and Toxicology*; edited by de Voogt, P., Ed.; Springer New York: New York, NY, 2010; Vol. 208.

(44) Martin, J. W.; Ellis, D. A.; Mabury, S. A.; Hurley, M. D.; Wallington, T. J. Atmospheric Chemistry of Perfluoroalkanesulfonamides: Kinetic and Product Studies of the OH Radical and Cl Atom Initiated Oxidation of N-Ethyl Perfluorobutanesulfonamide. *Environmental Science and Technology* **2006**, *40* (3), 864–872. https://doi.org/10.1021/es051362f.

(45) Macinnis, J. J.; French, K.; Muir, D. C. G.; Spencer, C.; Criscitiello, A.; De Silva, A. O.; Young, C. J. Emerging Investigator Series: A 14-Year Depositional Ice Record of

Perfluoroalkyl Substances in the High Arctic. *Environmental Science: Processes and Impacts* **2017**, *19* (1), 22–30. https://doi.org/10.1039/c6em00593d.

(46) Thackray, C. P.; Selin, N. E.; Young, C. J. A Global Atmospheric Chemistry Model for the Fate and Transport of PFCAs and Their Precursors. *Environmental Science: Processes and Impacts* **2019**, *22* (2), 285–293. https://doi.org/10.1039/c9em00326f.

(47) Wang, Z.; Cousins, I. T.; Scheringer, M.; Buck, R. C.; Hungerbühler, K. Global Emission Inventories for C4-C14 Perfluoroalkyl Carboxylic Acid (PFCA) Homologues from 1951 to 2030, Part I: Production and Emissions from Quantifiable Sources. *Environment International* **2014**, *70*, 62–75. https://doi.org/10.1016/j.envint.2014.04.013.

(48) Titaley, I. A.; Khattak, J.; Dong, J.; Olivares, C. I.; Diguiseppi, B.; Lutes, C. C.; Field, J. A. Neutral Per- and Polyfluoroalkyl Substances, Butyl Carbitol, and Organic Corrosion Inhibitors in Aqueous Film-Forming Foams: Implications for Vapor Intrusion and the Environment. *Environmental Science and Technology* **2022**, *56* (15), 10785–10797. https://doi.org/10.1021/acs.est.2c02349.

(49) Lin, H.; Lao, J.-Y. Y.; Wang, Q.; Ruan, Y.; He, Y.; Lee, P. K. H.; Leung, K. M. Y.; Lam. Paul K.S; Lam, P. K. S. Per- and Polyfluoroalkyl Substances in the Atmosphere of Waste Management Infrastructures: Uncovering Secondary Fluorotelomer Alcohols, Particle Size Distribution, and Human Inhalation Exposure. *Environment International* **2022**, *167* (April), 107434. https://doi.org/10.1016/j.envint.2022.107434.

(50) Shoeib, M.; Harner, T.; Vlahos, P. Perfluorinated Chemicals in the Arctic Atmosphere. *Environmental Science and Technology* **2006**, *40* (24), 7577–7583. https://doi.org/10.1021/es0618999.

(51) Stock, N. L.; Furdui, V. I.; Muir, D. C. G.; Mabury, S. A. Perfluoroalkyl Contaminants in the Canadian Arctic: Evidence of Atmospheric Transport and Local Contamination. *Environmental Science and Technology* **2007**, *41* (10), 3529–3536. https://doi.org/10.1021/es062709x.

(52) Wong, F.; Hung, H.; Dryfhout-Clark, H.; Aas, W.; Bohlin-Nizzetto, P.; Breivik, K.; Mastromonaco, M. N.; Lundén, E. B.; Ólafsdóttir, K.; Sigurðsson, Á.; Vorkamp, K.; Bossi, R.; Skov, H.; Hakola, H.; Barresi, E.; Sverko, E.; Fellin, P.; Li, H.; Vlasenko, A.; Zapevalov, M.; Samsonov, D.; Wilson, S. Time Trends of Persistent Organic Pollutants

(POPs) and Chemicals of Emerging Arctic Concern (CEAC) in Arctic Air from 25 Years of Monitoring. *Science of the Total Environment* **2021**, *775* (January). https://doi.org/10.1016/j.scitotenv.2021.145109.

(53) Faust, J. A. PFAS on Atmospheric Aerosol Particles: A Review. *Environmental Science: Processes and Impacts* **2022**, *25* (2), 133–150. https://doi.org/10.1039/d2em00002d.

(54) Tao, Y.; VandenBoer, T. C.; Ye, R. X.; Young, C. J. Exploring Controls on Perfluorocarboxylic Acid (PFCA) Gas-Particle Partitioning Using a Model with Observational Constraints. *Environmental Science: Processes and Impacts* **2022**, 264–276. https://doi.org/10.1039/d2em00261b.

(55) MacInnis, J. J.; Lehnherr, I.; Muir, D. C. G.; St. Pierre, K. A.; St. Louis, V. L.; Spencer, C.; De Silva, A. O. Fate and Transport of Perfluoroalkyl Substances from Snowpacks into a Lake in the High Arctic of Canada. *Environmental Science and Technology* **2019**, *53* (18), 10753–10762. https://doi.org/10.1021/acs.est.9b03372.

(56) Johansson, J. H.; Salter, M. E.; Acosta Navarro, J. C.; Leck, C.; Nilsson, E. D.; Cousins, I. T. Global Transport of Perfluoroalkyl Acids via Sea Spray Aerosol. *Environmental Science: Processes and Impacts* **2019**, *21* (4), 635–649. https://doi.org/10.1039/c8em00525g.

(57) Reth, M.; Berger, U.; Broman, D.; Cousins, I. T.; Nilsson, E. D.; McLachlan, M. S. Water-to-Air Transfer of Perfluorinated Carboxylates and Sulfonates in a Sea Spray Simulator. *Environmental Chemistry* **2011**, *8* (4), 381–388. https://doi.org/10.1071/EN11007.

(58) Sha, B.; Johansson, J. H.; Tunved, P.; Bohlin-Nizzetto, P.; Cousins, I. T.; Salter, M. E. Sea Spray Aerosol (SSA) as a Source of Perfluoroalkyl Acids (PFAAs) to the Atmosphere: Field Evidence from Long-Term Air Monitoring. *Environmental Science and Technology* **2022**, *56* (1), 228–238. https://doi.org/10.1021/acs.est.1c04277.

(59) Cavalieri, D. J.; Parkinson, C. L. Arctic Sea Ice Variability and Trends, 1979-2010. *Cryosphere* **2012**, *6* (4), 881–889. https://doi.org/10.5194/tc-6-881-2012.

(60) Rhodes, R. H.; Yang, X.; Wolff, E. W. Sea Ice Versus Storms: What Controls Sea Salt in Arctic Ice Cores? *Geophysical Research Letters* **2018**, *45* (11), 5572–5580. https://doi.org/10.1029/2018GL077403.

(61) Rhodes, R. H.; Yang, X.; Wolff, E. W.; McConnell, J. R.; Frey, M. M. Sea Ice as a Source of Sea Salt Aerosol to Greenland Ice Cores: A Model-Based Study. *Atmospheric Chemistry and Physics* **2017**, *17* (15), 9417–9433. https://doi.org/10.5194/acp-17-9417-2017.

(62) Jourdain, B.; Preunkert, S.; Cerri, O.; Castebrunet, H.; Udisti, R.; Legrand, M. Year-Round Record of Size-Segregated Aerosol Composition in Central Antarctica (Concordia Station): Implications for the Degree of Fractionation of Sea-Salt Particles. *Journal of Geophysical Research Atmospheres* **2008**, *113* (14), 2007. https://doi.org/10.1029/2007JD009584.

(63) Wagenback, D.; Ducroz, F.; Mulvaney, R.; Keck, L.; Minikin, A.; Legrand, M.; Hall, J. S.; Wolff, E. W. Sea Salt Aerosol in Coastal Antarctic Regions. *Journal of Geophysical Research* **1998**, *103*, 10961–10794.

(64) Domine, F.; Sparapani, R.; Ianniello, A.; Beine, H. J. The Origin of Sea Salt in Snow on Arctic Sea Ice and in Coastal Regions. *Atmospheric Chemistry and Physics* **2004**, *4* (9–10), 2259–2271. https://doi.org/10.5194/acp-4-2259-2004.

(65) Yang, X.; Pyle, J. A.; Cox, R. A. Sea Salt Aerosol Production and Bromine Release: Role of Snow on Sea Ice. *Geophysical Research Letters* **2008**, *35* (16), 1–5. https://doi.org/10.1029/2008GL034536.

(66) Hannah, C. G.; Dupont, F.; Dunphy, M. D. Polynyas and Tidal Currents in the Canadian Arctic Archipelago. *Arctic* **2009**, *62* (1), 83–95. https://doi.org/10.14430/arctic115.

(67) Cai, M.; Yang, H.; Xie, Z.; Zhao, Z.; Wang, F.; Lu, Z.; Sturm, R.; Ebinghaus, R. Per- and Polyfluoroalkyl Substances in Snow, Lake, Surface Runoff Water and Coastal Seawater in Fildes Peninsula, King George Island, Antarctica. *Journal of Hazardous Materials* **2012**, *209–210*, 335–342. https://doi.org/10.1016/j.jhazmat.2012.01.030.

(68) Garnett, J.; Halsall, C.; Vader, A.; Joerss, H.; Ebinghaus, R.; Leeson, A.; Wynn, P. M. High Concentrations of Perfluoroalkyl Acids in Arctic Seawater Driven by Early Thawing Sea Ice. *Environmental Science and Technology* **2021**, *55* (16), 11049–11059. https://doi.org/10.1021/acs.est.1c01676.

(69) Garnett, J.; Halsall, C.; Thomas, M.; Crabeck, O.; France, J.; Joerss, H.; Ebinghaus, R.; Kaiser, J.; Leeson, A.; Wynn, P. M. Investigating the Uptake and Fate

of Poly- and Perfl Uoroalkylated Substances (PFAS) in Sea Ice Using an Experimental Sea Ice Chamber. *Environmental Science and Technology* **2021**.

(70) Stefanac, T.; McCrindle, R.; McAlees, A. J.; Riddell, N.; Brazeau, A. L.; Chittim, B. C. Characterization of Nine Isomers in Commercial Samples of Perfluoroethylcyclohexanesulfonate and of Some Minor Components Including PFOS Isomers. *Environmental Science and Technology* **2018**, *52* (17), 9937–9945. https://doi.org/10.1021/acs.est.8b02369.

(71) Lescord, G. L.; Kidd, K. A.; De Silva, A. O.; Williamson, M.; Spencer, C.; Wang, X.; Muir, D. C. G. Perfluorinated and Polyfluorinated Compounds in Lake Food Webs from the Canadian High Arctic. *Environmental Science and Technology* **2015**, *49* (5), 2694–2702. https://doi.org/10.1021/es5048649.

(72) Wang, Y.; Vestergren, R.; Shi, Y.; Cao, D.; Xu, L.; Cai, Y.; Zhao, X.; Wu, F. Identification, Tissue Distribution, and Bioaccumulation Potential of Cyclic Perfluorinated Sulfonic Acids Isomers in an Airport Impacted Ecosystem. *Environmental Science and Technology* **2016**, *50* (20), 10923–10932. https://doi.org/10.1021/acs.est.6b01980.

(73) Sullivan, R. C.; Guazzotti, S. A.; Sodeman, D. A.; Prather, K. A. Direct Observations of the Atmospheric Processing of Asian Mineral Dust. *Atmospheric Chemistry and Physics* **2007**, *7* (5), 1213–1236. https://doi.org/10.5194/acp-7-1213-2007.

(74) Mochizuki, T.; Kawamura, K.; Aoki, K.; Sugimoto, N. Long-Range Atmospheric Transport of Volatile Monocarboxylic Acids with Asian Dust over a High Mountain Snow Site, Central Japan. *Atmospheric Chemistry and Physics* **2016**, *16* (22), 14621–14633. https://doi.org/10.5194/acp-16-14621-2016.

(75) Zhao, X.; Huang, K.; Fu, J. S.; Abdullaev, S. F. Long-Range Transport of Asian Dust to the Arctic: Identification of Transport Pathways, Evolution of Aerosol Optical Properties, and Impact Assessment on Surface Albedo Changes. *Atmospheric Chemistry and Physics* **2022**, *22* (15), 10389–10407. https://doi.org/10.5194/acp-22-10389-2022.

(76) Huang, Z.; Huang, J.; Hayasaka, T.; Wang, S.; Zhou, T.; Jin, H. Short-Cut Transport Path for Asian Dust Directly to the Arctic: A Case Study. *Environmental Research Letters* **2015**, *10* (11). https://doi.org/10.1088/1748-9326/10/11/114018.

(77) Moody, C. A.; Field, J. A. Perfluorinated Surfactants and the Environmental Implications of Their Use in Fire-Fighting Foams. *Environmental Science and Technology* **2000**, *34* (18), 3864–3870. https://doi.org/10.1021/es991359u.

(78) Department of Defence. *Aqueous Film Forming Foam Report to Congress*. https://denix.osd.mil/derp/home/documents/aqueous-film-forming-foam-report-to-congress/.

(79) *DRAFT State of Per- and Polyfluoroalkyl Substances (PFAS) Report Environment and Climate Change Canada Health Canada May 2023*. https://www.canada.ca/en/environment-climate-change/services/evaluating-existing-substances/draft-state-per-polyfluoroalkyl-substances-report.html.

(80) *PFAS Contamination sites in Airports and Military bases in Canada*.

(81) Place, B. J.; Field, J. A. Identification of Novel Fluorochemicals in Aqueous Film-Forming Foams Used by the US Military. *Environmental Science and Technology* **2012**, *46* (13), 7120–7127. https://doi.org/10.1021/es301465n.

(82) Backe, W. J.; Day, T. C.; Field, J. A. Zwitterionic, Cationic, and Anionic Fluorinated Chemicals in Aqueous Film Forming Foam Formulations and Groundwater from U.S. Military Bases by Nonaqueous Large-Volume Injection HPLC-MS/MS. *Environmental Science and Technology* **2013**, *47* (10), 5226–5234. https://doi.org/10.1021/es3034999.

(83) Riedel, T. P.; Lang, J. R.; Strynar, M. J.; Lindstrom, A. B.; Offenberg, J. H. Gas-Phase Detection of Fluorotelomer Alcohols and Other Oxygenated Per- and Polyfluoroalkyl Substances by Chemical Ionization Mass Spectrometry. *Environmental Science and Technology Letters* **2019**, *6* (5), 289–293. https://doi.org/10.1021/acs.estlett.9b00196.

(84) Roth, J.; Abusallout, I.; Hill, T.; Holton, C.; Thapa, U.; Hanigan, D. Release of Volatile Per-and Polyfluoroalkyl Substances from Aqueous Film-Forming Foam. *Environmental Science and Technology Letters* **2020**, *7* (3), 164–170. https://doi.org/10.1021/acs.estlett.0c00052.

(85) Bourgeois, J. C. Seasonal and Annual Variation of Pollen Content in the Snow of a Canadian High Arctic Ice Cap. *Boreas* **1990**, *19* (4), 313–322. https://doi.org/10.1111/j.1502-3885.1990.tb00135.x.

(86) Clarke, G. K. C.; Jarosch, A. H.; Anslow, F. S.; Radić, V.; Menounos, B. Projected Deglaciation of Western Canada in the Twenty-First Century. *Nature Geoscience* **2015**, *8* (5), 372–377. https://doi.org/10.1038/ngeo2407.

(87) Lenaerts, J. T. M.; Van Angelen, J. H.; Van Den Broeke, M. R.; Gardner, A. S.; Wouters, B.; Van Meijgaard, E. Irreversible Mass Loss of Canadian Arctic Archipelago Glaciers. *Geophysical Research Letters* **2013**, *40* (5), 870–874. https://doi.org/10.1002/grl.50214.

CHAPTER 3

The Occurrence of Legacy Perfluoroalkyl Substances (PFAS) Deposited along a Latitudinal Transect in Newfoundland and Labrador, Canada

Daniel Persaud[1], Trevor C. VandenBoer[1,2*], Bryan K. Place[3,a], Kate A. Edwards[4,b], Susan E. Ziegler[2], Christine Spencer[5], Amila O. De Silva[5], and Cora J. Young[1,3*].

[1]Department of Chemistry, York University, Toronto, ON

[2]Department of Earth Science, Memorial University, St. John's, NL

[3]Department of Chemistry, Memorial University, St. John's, NL

[4]Canadian Forest Service, Natural Resources Canada, Corner Brook, NL

[5]Aquatic Contaminants Research Division, Environmental and Climate Change Canada, Burlington, ON

[a]now at: SciGlob Instruments & Services LLC, Columbia, MD, USA

[b]now at: Climate Change Impacts and Adaptation Division, Lands and Minerals Sector, Natural Resources Canada, Ottawa, ON, Canada

Author Contributions:

Susan E. Ziegler, Trevor C. VandenBoer, and Cora J. Young conceived of and designed the experiment. Trevor C. Vandenboer, Bryan K. Place and Kate A. Edwards built and deployed the samplers. Christine Spencer and Amila O De Silva performed the chemical analysis. Daniel Persaud analyzed the data and wrote the manuscript with input from all authors. Funding was acquired by Susan E. Ziegler, Trevor C. VandenBoer and Cora J. Young.

3.1 Introduction

Perfluoroalkyl acids (PFAAs), including perfluoroalkyl carboxylic acids (PFCAs) and perfluoroalkanesulfonic acids (PFSAs), are ubiquitous compounds that have been manufactured since the 1940s.[1] The carbon–fluorine bond imparts unique properties to molecules when compared to the hydrocarbon analogs, including the ability to form stable foams and exceptional chemical and thermal stability.[2] As such, PFAAs have found numerous industrial and commercial uses, including firefighting foams, non-stick applications, and performance chemicals.[3] Due to concerns over environmental persistence, toxicity, bioaccumulation potential, and long-range transport, several national and international regulatory agencies implemented regulations regarding PFAA production with more than six carbon atoms (>6C) and the use of that compound class.[4–7] This resulted in the introduction and increased use of alternative PFAAs such as short-chain substitutes (e.g., perfluorobutanoic acid, PFBA), which also have growing concerns about potential environmental and health risks, making them compounds of emerging concern.[8,9] Although efforts were made to minimize environmental release from manufacturing, and there is consideration of future regulation of all PFAS using a class-based approach,[10] continued inputs can occur through diverse ongoing and legacy sources (e.g., landfills), which are expected to continue to add to the environmental burden globally.[11,12] Furthermore, large natural reservoirs (e.g. oceans and glaciers) [13,14] and anthropogenic repositories including landfills[15] and contaminated sites[16] are likely to continue to act as vectors and sources of PFAAs due to their persistence and mobility.

Currently, the two main sources of PFAAs in the atmosphere are (i) direct release from anthropogenic sources (e.g., industrial and consumer applications)[17–19] and (ii) and indirect sources by the oxidation of precursor compounds in the gas phase, such as fluorotelomer alcohols (FTOHs) and N-alkyl perfluoroalkane sulfonamides/sulfonamidoethanols.[20–24] Other potential non-fluorotelomer sources include hydrofluorocarbons (HFCs) and hydrochlorofluorocarbons (HCFCs).[25–27] There is also compelling evidence from lab experiments that PFAAs can be remobilized from the ocean to the atmosphere through the formation of marine aerosols facilitated by wave breaking action.[28–30] However, direct field evidence of this transport pathway to PFAA

deposition is limited and site specific.[13,31,32] To confirm and quantify the role of marine aerosols, there is a need for more field measurement across coastal and inland transects.

The atmospheric lifetime and persistence of PFAAs are long enough that they can be globally transported,[33] with their ultimate removal from the atmosphere occurring through the wet and/or dry deposition processes. Wet deposition involves scavenging of gaseous compounds or particles by cloud water and subsequent transport to the surface of the earth through precipitation (e.g., snow and rain).[34] This removal mechanism is highly dependent on the physical–chemical properties of PFAAs, such as the air-water partition coefficient (K_{aw}), and their acid dissociation coefficients (PK_a).[35] The dry deposition mechanism involves the removal of particles and gases from the atmosphere by gravitational settling, impaction, interception, and/or diffusion.[36] While wet deposition is episodic, dry deposition is a continuous process for the loss of material from the atmosphere.[37] Since this mechanism does not depend on rainfall amount or intensity, this has important implications for understanding PFAA deposition.

The global detection of PFAAs in atmospheric deposition next to fluorochemical facilities,[34,38,39] in urban,[40–48] rural,[49,50] and remote locations[31,51–55] suggests that precipitation is an effective scavenger of gas phase and particle-associated PFAAs from the atmosphere. This leads to an amplified deposition and transport in hydrological compartments such as oceans, ground, and surface waters.[51] In fact, concentrations of PFAAs in precipitation frequently exceed the US Environmental Protection Agency, Danish, and European Union drinking water standards.[56] Despite this, measurements of PFAAs in North American precipitation are limited and often discontinuous.[42,48,57,58] Most previous studies measured PFAAs using total (bulk) deposition, usually collected on an event basis,[38,42,43,49,52,58–60], while a few have distinguished between measurements of wet and dry deposition.[34,58,61] Some separate efforts have been made to estimate the dry deposition contribution using chemical models [62–64] and gas-to-liquid distribution ratios.[65] In the current study, we aim to better understand the contribution of wet and dry deposition to the total deposition fluxes of PFAAs, which is crucial in understanding ecosystem sources and atmospheric transport mechanisms.

The Newfoundland and Labrador Boreal Ecosystem Latitudinal Transect (NL-BELT) consists of four forested watersheds in remote eastern Canada. The sites span five degrees of latitude (47 to 53°N) across western Newfoundland and south-eastern Labrador. The study sites within the NL-BELT are unique since each individual site differs in mean annual temperature (0 to 5.2 ºC) and mean annual precipitation (1074 to 1505 mm), with precipitation and temperature decreasing with increasing latitude.[66] All NL-BELT sites are marine-influenced, within ~30 km of the ocean. This transect provides a unique opportunity to examine the spatial distribution of PFAA deposition, as well as assess PFAA sources, including the contribution of marine aerosol remobilization.

The objective of the study was to assess the occurrence of PFAAs in precipitation across the NL-BELT. Sampling sites were selected due to their proximity to the open ocean, with the intent to assess the importance of marine aerosols as a mechanism of PFAS remobilization in this region. Integrated total and wet deposition samplers were deployed semi-continuously from 2013 to 2015 during the period from May to October. Fluxes in total deposition samples were fully continuous and used to assess spatial and temporal variations, as well as discern the sources and transport of PFAAs based on correlation analysis, molar concentration ratios, homologue profiles, and air mass back trajectory analysis. We also calculated the contribution of dry deposition to the total PFAA deposition in this region.

3.2 Methods

3.2.1 Study sites and sampling

Total and wet deposition samples were collected across the NL-BELT on a monthly or bi-monthly schedule from the end of snowmelt to the beginning of snowfall, corresponding to the period from May to October (summer and fall). Measurements commenced in October 2013 and concluded in August 2016, with total deposition collected continuously with integrated samples throughout the winter. Each site within the NL-BELT lies within an experimental forest dominated by mature balsam fir, located less than 800 km from a population center of approximately 250000 residents.[67] Total deposition was collected using an open polyvinylchloride (PVC) pipe (2.88 m height, 0.23 m diameter), whereas wet-only deposition was collected using custom-built off-grid

precipitation samplers.[68] All samplers were deployed in the open at a distance from the forest stand equal to or greater than the height of the trees, in accordance with Canadian Air and Precipitation Monitoring Network (CAPMoN) and National Atmospheric Deposition Program (NADP) guidelines.[69,70] This minimizes the probability of influence from the nearby canopy. Details of the collection apparatus are outlined in Section B-1 of the Supplemental Information (SI).

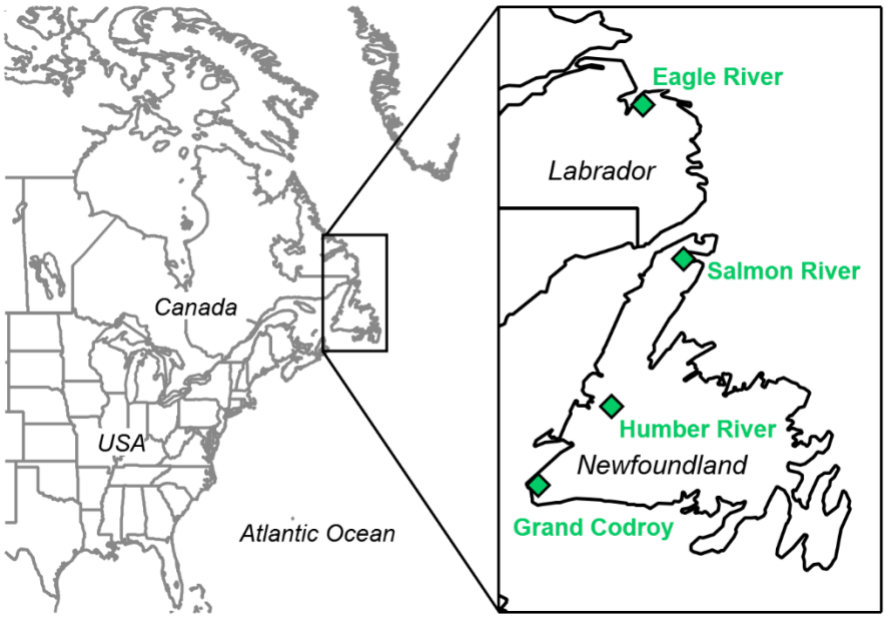

Figure 3-1: Locations of the NL-BELT sampling sites (green diamonds) in Newfoundland and Labrador, Canada, inset from eastern North America. From south to north, the watersheds and sites are: Grand Codroy O'Regan's Hill site (GC), Humber River Camp 10 site (HR), Salmon River Hare Bay site (SR), and Eagle River Muddy Pond site (ER).

The four sites were located across four watershed regions in the NL-BELT: Grand Codroy O'Regan's Hill site (GC; 47.893° N, 59.174° W), Humber River Camp 10 site (HR; 49.070° N, 57.643° W), Salmon River Hare Bay site (SR; 51.256° N, 56.138° W), and Eagle River Muddy Pond site (ER; 53.550° N, 56.987° W). In total we collected and analyzed 38 total deposition samples across the four sites (GC: n = 13, HR: n = 10, SR: n = 9 and ER: n = 6), and wet deposition samples (n = 11) were available for a smaller paired subset at each site (GC: n = 3, HR/PB n = 3, SR: n = 4 and ER n =1). The smaller

number of wet deposition samples is a practical reality from the larger collaborative undertaking across the NL-BELT: i) the samplers are custom built and had a later deployment than the simple total deposition samplers,[68] and ii) each collection period has a limited volume for all biogeochemical and PFAA analysis, where the latter was only possible after all other analyses for NL-BELT biogeochemical determinations were completed.[66,68,71] The volume of all precipitation collected during the integrated sampling period was measured for flux determinations, then filtered through a 0.45 µm pore size 45 mm polyether sulfone filter mounted on a 1L HDPE Nalgene vacuum filtration flask assembly (VWR, Mississauga, ON, CA). All samples were shipped to the laboratory and kept refrigerated at 4°C until subjected to chemical analysis. Temperature (T) and relative humidity (RH) probes and dataloggers (HOBO® U23 Pro v2, P/N U23-001) were installed at the Newfoundland sites in November 2014 and at the Labrador site in June 2016.

3.2.2 Sample preparation and extraction

A full analyte list with PFAA acronyms is provided in Table B-1. We name PFAAs using their carbon number for simplicity, which refers to the number of carbon atoms in the molecule (e.g., the C4 PFCA is PFBA). In the current study, we targeted C4-14, C16, and C18 PFCAs, C4, C6-C8, and C10 PFSAs, the cyclic PFSA perfluoroethylcyclohexane sulfonate (PFECHS), and perfluorooctanesulfonamide (FOSA). Details of sample extractions are described elsewhere.[42] Briefly, sealed samples were allowed to reach room temperature and aliquoted to 500 mL total volume. Sub-samples for extraction were spiked with 30 µL of a surrogate mixture (Table B-1), which functions as the internal standard (IS) to evaluate recoveries. Samples were shaken, sonicated for 10 minutes, and held for 30 minutes at room temperature.

Samples were extracted and target analytes concentrated using OASIS® weak anion exchange (WAX) solid phase extraction (SPE) cartridge (6 cm^3, 150 mg, 30 µm). Cartridges were preconditioned with 5 mL 1% ($^v/_v$) ammonium hydroxide in methanol, followed by 5 mL methanol and 5 mL SPE-precleaned HPLC grade water. After sample concentration, the cartridges were rinsed with 25 mM aqueous ammonium acetate buffer acidified to pH 4 with acetic acid and then centrifuged at 4000 rpm to remove any residual water. Samples were eluted into two fractions. The first fraction was eluted with 6 mL of MeOH for (FOSA), and the second fraction was eluted with 8 mL of 0.1 % ($^v/_v$) ammonium

hydroxide in methanol for other PFAAs. Both fractions were evaporated to dryness under a gentle stream of dry pure nitrogen gas in a 30 ºC water bath and then reconstituted in 0.5 mL using 50/50 methanol-water containing a second surrogate IS mixture (Table B-1) to account for matrix effects. Reconstituted samples were sonicated for 5 min, vortexed, and transferred to polypropylene vials for analysis.

3.2.3 Chemical analysis of PFAAs

Samples were analyzed by ultra performance liquid chromatography (Waters Acquity UPLC I-class) coupled with a tandem mass spectrometer (Waters Xevo® TQ-S, MS/MS) operated in electrospray negative ionization mode. Two analyses were conducted. For PFAA analysis (PFCAs > C4, PFSAs > C4 and FOSA), samples were separated using a C_{18} column (Waters Acquity UPLC® BEH, 2.1 x 50 mm, d_p=1.7 µm) with a water-methanol 2 mM ammonium acetate gradient method. Details of chromatographic and mass spectrometric conditions used to separate PFAAs can be found in Tables B-2 and B-3 in the SI. Analytes were quantified based on relative response to isotopically labelled IS (Table B-1; Wellington Laboratories, Guelph, Canada).

3.2.4 Quality Assurance and Quality Control

To prevent contamination, all glassware used for sample collection and extraction was rinsed twice with methanol before use. Nitrile gloves were used when handling samples and materials containing PFAS were avoided. Isotopically labelled internal standards were used to evaluate recovery and correct for matrix effects, and cartridge blanks were used to validate the integrity of the extraction method. Three samples were extracted in triplicate and one sample in duplicate to evaluate reproducibility. A composite mixture of the NL-BELT samples was prepared for three types of QA/QC measures conducted in triplicate: one sample was spiked with PFAAs before extraction, one sample was spiked with PFAAs after extraction, and the third sample was spiked with the internal standard and processed similarly to the more extensive sample set. The pre-extraction and post-extraction spiked samples were compared to evaluate recovery and matrix effects (Table B-4).

Matrix effects were further evaluated by comparing the peak area of the instrument performance (IP) standard spiked into the extracted sample matrix to the peak areas from

the same molecules at equivalent concentrations in a solvent standard (Table B-5). Recovery was evaluated by comparing the recovered analyte concentration in the spike and recovery sample to the theoretical spiked concentration measured in a solvent standard. Each sample concentration was quantified by correcting for recovery and matrix effects based on the relative response of target analytes to isotopically labelled IS added before extraction. A 15-level calibration curve was employed for quantification, ranging from 0.02 to 8.5 ng mL^{-1}, and included analytical blanks. Analytical blanks consisted of pure MeOH, and cartridge blanks were included in the method analysis to assess potential contamination sources. Any detected contamination in the blanks was subtracted from the analyte concentration to ensure accurate results. The method detection limit (LOD) was based on three times the standard deviation of any signal detected in the cartridge blanks. PFAA analytes were not detected in the method blanks with the exception of PFBA (0.046 ng mL^{-1}) and PFBS (0.013 ng mL^{-1}) and were therefore below the instrument detection limit (IDL; Table B-6). The instrument Limit of Detection (LOD) and Limit of Quantitation (LOQ) in such cases were then quantified based on signal-to-noise (S/N) ratios of 3 and 10, respectively.

Extensive care was taken to avoid contamination in the field that could potentially compromise the trace analysis of PFAAs. Due to the ubiquitous nature of PFAAs, obtaining a true blank sample is challenging. We transported ultrapure water (Barnstead™ Nanopure™, P/N D11901) to the field sites of the NL-BELT to perform apparatus cleaning. A subsample was used to rinse all cleaned material surfaces to obtain a blank relevant to sample collection. All blank samples were processed in the lab simultaneously alongside the collected samples. Because the ultrapure water itself contained small quantities of PFAAs, we used a t-test to determine if there were any significant differences between the PFAA levels in the ultrapure water transported to the field sites and the obtained rinse water. The null hypothesis was accepted for each homologue (p-values 0.09 – 0.97), which indicated that no significant difference exists and that there was no contamination from the sampling procedure.

3.2.5 Wet deposition estimation

Automated deposition samplers were deployed simultaneously with the total deposition samplers to quantify the magnitude of the dry deposition mechanism. The automated deposition samplers selectively collect only wet deposition during a precipitation event. When the rain sensor detects conductive precipitation, a motor is triggered via limit switches to open and close the lid that is resting over a funnel opening.[68] By subtracting the wet-only deposition from the total deposition fluxes (i.e., wet + dry), we can effectively estimate the contribution of the dry deposition mechanism. We determined dry deposition fluxes for a subset of samples (n=11) between 2015 to 2016, where enough sample volume was collected that a sufficient amount remained for PFAS analysis after all other analyses for collaborator targets were completed. The total deposition flux measured at HR and the wet deposition fluxes measured at PB were used to estimate dry deposition fluxes in the Humber River watershed region. This comparison was unavoidable since HR was initially planned for full use but became inaccessible in early 2015, stranding the initially deployed total deposition equipment and preventing the installation of the automated samplers. These two sites (HR and PB) share the same watershed, and the relative error between volumes collected between the two sites was ±15%, which was comparable to the reproducibility typically observed for replicates within a given site in the NL-BELT (±12.5%).[68]

3.2.6 Major Ion Analysis

Aqueous sub-samples were analyzed for a suite of elements (Na, Ca, Al, Fe, Mg, Mn, K, and Si) and anions (PO_4^{3-} and SO_4^{2-}), respectively. Elemental and total P determinations were made using inductively coupled plasma optical emission spectroscopy (ICP-OES) on an iCap 6500 series system (Thermo Scientific, Mississauga, ON, Canada). Detection limits ranged from 0.40 – 20 ppb. Anion analysis was performed on a Dionex ICS 2100 ion chromatography system coupled to a conductivity detector (Thermo Scientific, Mississauga, ON, Canada). Detection limits ranged from 0.079-27 ppb.

3.2.7 Air Mass Back Trajectories

To determine possible source region(s) or directionality of enriched air masses arriving at each sampling site for a given collection period, a back trajectory was performed utilizing the National Oceanic and Atmospheric Administration Hybrid Single-Particle Lagrangian Integrated Trajectory model (HYSPLIT).[72] The trajectory analysis was performed using the Global Data Assimilation System (GDAS) meteorology data set with a 0.5-degree resolution. The model commenced at noon on the date of sample collection and had a total run time of 120 hours, with a trajectory interval of three hours, and spanned the number of days in the collection period (maximum of 32 days). Frequency analysis using HYSPLIT modelling generated 256 trajectories at most. The frequency plot was generated using the percentages of trajectories that ended in each grid square. The raw endpoint output files for the entire sampling period were concatenated and sorted for sector assignments in Igor Pro 8 using a custom procedure (Figure B-3).

3.2.8 Statistical Analysis

Data visualization was done in Igor Pro 8, whereas statistical analysis was completed using RStudio (Version 1.4.1106) with R version 4.3.1. In this study, Pearson correlation (r) analysis was done using the lmodel2 package to correlate logarithm-transformed PFAA fluxes (i.e., $\log_{10}$ $PFAA_{flux}$) for comparison to major ion fluxes (Na^+, nss-Ca^{2+}, nss-Mg^{2+} and nss-K^+) and between homologue pairs. Analytical determinations below the instrument LOD were not included in any statistical interpretations. Associations between variables were considered statistically significant when p-values were less than 0.05. Comparisons between sites (Grand Codroy, n= 13, Humber River, n= 10, Salmon River, n= 9, and Eagle River, n=6) for total PFAAs were also evaluated using one-way ANOVA and post hoc Tukey's test or Newman-Keuls test. Both post hoc tests were used to balance the stringent control of type 1 error (finding differences when none exist) provided by Tukey's test, with the increased sensitivity of the Newman-Keuls test, ensuring a robust detection and cross-validation of site differences.

3.3 Results and Discussion

3.3.1 PFAA concentrations and fluxes in total deposition samples

A comprehensive analysis of PFAAs and FOSA was carried out on the total deposition samples (n=38). In general, PFCAs from perfluorobutanoic acid (PFBA, C4) to perfluorotetradecanoic acid (PFTeDA, C14) were detected in at least one sample at each location (Figure 3-2, Table B-7). The median summed PFCA homologue concentration across the sampling sites was 300 pg L^{-1}, with concentration values ranging from <LOD to 10000 pg L^{-1} (Figure 2B). The shortest chain homologue (PFBA, C4) was found to have the highest concentration, with a detection frequency of 82%. Perfluorooctanoic acid (PFOA, C8) was detected in all samples with a mean concentration of 729 pg L^{-1} across the sampling sites. Perfluorononanoic acid (PFNA, C9) and perfluorodecanoic acid (PFDA, C10) were both detected in all but one sample, equal to a detection frequency of 97%. The detection frequencies of perfluoropentanoic acid (PFPeA, C5), perfluorohexanoic acid (PFHxA, C6), perfluoroheptanoic acid (PFHpA, C7), and perfluoroundecanoic acid (PFUnDA, C11) were 47%, 74%, 89% and 87%, respectively. The other long-chain PFCAs, perfluorotridecanoic acid (PFTrDA, C13), PFTeDA and perfluorohexadecanoic acid (PFHxDA, C16) were detected in 45%, 18% and 8% of samples, respectively. Perfluorooctadecanoic acid (PFOcDA, C18) were below LOD for all samples analyzed and will not be discussed further.

The PFSA concentrations in total deposition samples were two orders of magnitude lower than the PFCAs, with a summed median PFSA concentration of 3 pg L^{-1} across the sampling sites (Figure 3-2C, Table B-8). Perfluorooctane sulfonate (PFOS, C8) had the highest detection frequency at 55%, with concentration ranging from <LOD to 173 pg L^{-1}. Detection of perfluorobutane sulfonate (PFBS, C4), perfluorohexane sulfonate (PFHxS, C6), and perfluoroheptane sulfonate (PFHpS, C7) was sporadic, with detection frequencies of 26%, 13%, and 5%, respectively. FOSA was only detected in five samples (13%) with a mean concentration of 20 pg L^{-1}. Perfluorodecane sulfonate (PFDS, C10) and PFECHS were sought but were <LOD for all the samples and will not be discussed further.

Concentrations (pg L^{-1}) of PFAAs were converted to flux (ng m^{-2} a^{-1}) using the volume of samples, the area of the sampler, and sampling duration (Tables S9 and S10).

All fluxes were further normalized to the sampling duration on an annual scale (units: per annum; a^{-1}) for comparisons, given the long duration of each integrated period and the extended duration of the study. This provides comparability to the magnitude of atmospheric deposition measured in ice cores and uses the relevant units for geochemical fluxes of other long-lived compounds or elements. The median PFCA flux was 170 ng m^{-2} a^{-1}, with PFBA accounting for the highest fluxes, ranging from <LOD to 9000 ng m^{-2} a^{-1} (Figure 3). The PFCA deposition fluxes across the sampling sites showed the following general homologue trend: PFBA (C4) > PFOA (C8) > PFHpA (C7) > PFNA (C9) > PFHxA (C6) > PFDA (C10) > PFUnDA (C11) > PFPeA (C5) > PFDoDA (C12). The median PFSA flux across the sampling sites was 33 ng m^{-2} $a^{-1,}$ with PFOS and PFBS being the major contributors. The median fluxes of PFOS and PFBS were 35 and 21 ng m^{-2} a^{-1}, respectively, with maximum fluxes of 180 and 300 ng m^{-2} a^{-1}. Overall, the reported fluxes are generally comparable to or lower previously reported fluxes in mid-latitude precipitation.[42,46,47,60,73,74]

We examined the temporal variations for each homologue during the period 2014–2016. Generally, fluxes showed no clear seasonal patterns, and we observed substantial variability between individual homologues and sampling periods. This was particularly evident for PFBA, where elevated levels were observed at GC (June and September 2014), late season enhancements at SR (October 2014 & 2015), an extreme event at HR (November 2015), and repeated late summer maxima at ER (August 2014 & 2015). A particular sample may result in undetectable analyte quantities where: air masses do not originate from source regions, the precipitation is very intense (diluting the analyte concentration), and both oxidant and precursor levels are low. Although precipitation studies report seasonal patterns of trifluoroacetic acid (TFA),[75,76] comparable seasonal deposition patterns for other PFAAs are limited. Deposition samples from the Arctic show strong seasonal patterns for PFCAs attributed to the complete absence of photochemical activity in winter.[77,78] In contrast, no substantive seasonal differences were observed in atmospheric measurements from mid-latitude regions of PFCAs with four carbons (i.e., PFBA) or more, though these PFCAs were attributed to atmospheric formation.[77–79]

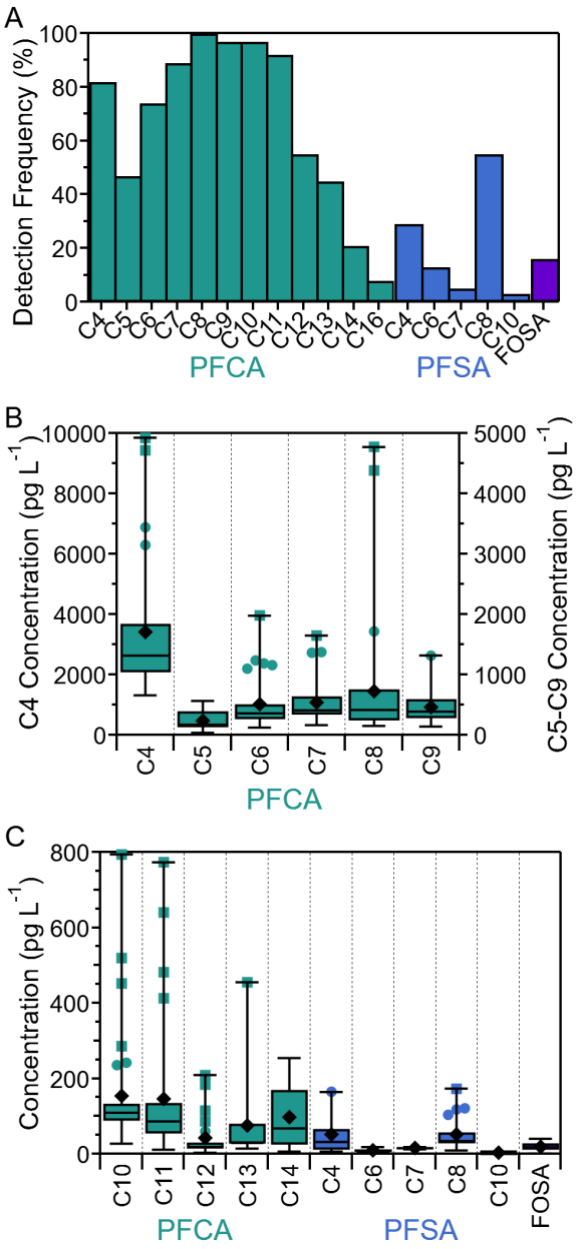

Figure 3-2: (A) Detection frequency of PFCAs (green), PFSAs (blue) and FOSA (purple) for the entire sampling period (2013 – 2016) (B) Boxplots of C4 (left axis) and C5 – C9 (right axis) PFCA homologue concentrations (pg L^{-1}) and (C) Boxplots of C10 – C14, PFSA, and FOSA concentrations (pg L^{-1}) across the sampling sites in the total deposition samplers. Boxplot limits represent the third and first quartiles of the data set, whiskers represent the range, solid coloured circles represent outliers, and solid coloured squares represent far outliers. The solid black line represents the median, and the mean is a solid black diamond.

3.3.2 Latitudinal trends in total deposition

To investigate the relative roles of local, regional, or long-range sources, we compared the mean fluxes within the NL-BELT study sites to understand the drivers of any latitudinal trends in PFAA deposition. In addition to latitudinal comparisons, deposition fluxes were also compared to other climate factors, including precipitation amount, temperature and relative humidity, to discern the role of climate effects. Results of the one-way ANOVA indicated no statistical differences between sites, and the null hypothesis was accepted for the majority of the PFAA homologues (PFCAs, C5-C8, C10-C14, p:0.24-0.99). This strongly suggests that there is no discernible deposition trend within the transect with latitude. Additionally, no statistically significant correlation was found between precipitation amount (r = -0.86-0.45, p=0.02-0.96), temperature (r = 0.01-0.99, p=0.0002-0.95) and relative humidity (r = 0.04-0.90, p=0.09-0.94), suggesting a minor role of climate effects on PFAA deposition in the NL-BELT region. However, the statistical analysis is likely impacted by the low sample size and uneven homogeneity of variance. The PFBA and PFNA homologues were notable exceptions, where the one-way ANOVA and both post hoc tests suggested that statistically significant (p: 0.01-0.04) differences exist between the sampling sites, which is discussed in detail below. Considering PFBA, the mean deposition fluxes measured at the three Newfoundland sites (GC, HR, and SR) were statistically higher by 70%, 58% and 77%, respectively, when compared to measurements at the more northern Labrador site (ER). A similar trend was observed with the PFNA homologue, where the deposition fluxes were enhanced by more than 80% at GC and SR when compared to ER. This suggests that selected PFAAs may vary spatially, and their local point sources may be important. Though Newfoundland and Labrador is sparsely populated (~500,000 total population, ~405,000 km^2), it is possible that some regional anthropogenic activities could present sources of PFAS.

Recently, eight federal contaminated sites were identified in the province of Newfoundland and Labrador (Figure B-4).[63,64] Non-federal contaminated sites may also exist within the region, including landfills, recycling centres and wastewater treatment plants.[65,66] The HR site is located ~20 km from one of the largest landfill sites in Newfoundland. Landfills are known to act as point sources for PFAS to the atmosphere,[65–68]which could lead to increased deposition levels. The significant difference in PFBA at

the island locations may reflect a current shift towards short-chain alternatives in consumer products, but neither region is extensively populated (SR is much less densely populated than HR). In addition, it is curious that landfills would only elevate one PFAA, given the legacy usage of other chain lengths. Thus, although point sources may exist for selected PFAA homologues, there is no strong grounding to justify local sources as major contributors at this time. Additionally, the lack of correlations between PFAA homologues and climate variables (precipitation volume, temperature and relative humidity) further supports the hypothesis that deposition is primarily influenced by other sources rather than local inputs. More targeted measurements in these areas, coupled with greater community identification of potential PFAS use, may help to reconcile this issue in future work. Overall, as there is a limited number of known point sources in this region, coupled with a relatively low population density in Newfoundland and Labrador, the drivers of PFAA deposition likely extend to larger spatial scales.

To expand the analysis of latitudinal trends, we extended the observed deposition fluxes by comparison to measurements made in the Canadian High Arctic at the Devon Ice Cap (75.2°N, 82.7°W, 2175 m above sea level) for 2014-2015 and Mt. Oxford icefield, Nunavut (82.19°N, 72.96°W, 1784 m above sea level) for 2014-2016 (Table B-11). The 2015 measurement from the Devon Ice Cap was a partial year of deposition and, therefore, is an underestimation of the annual PFAA flux. Generally, PFAA fluxes were lower at Devon Ice Cap and higher at Mt. Oxford icefield when compared to the NL-BELT sites. This trend is expected, as Mt. Oxford icefield is influenced less by North American air masses and instead receives inputs from Eurasia.[69] The more southern Devon Ice Cap is influenced to a greater extent by North American air masses[20,42] where efforts have been made to reduce emissions of PFAAs and their precursors, and is therefore a better comparison for atmospheric transport and deposition at the NL-BELT sites. Considering individual PFAA homologues, PFBA showed the greatest difference between the high Arctic and NL-BELT sites. The average PFBA flux in the NL-BELT was 2200 ng m^{-2} a^{-1}, whereas average fluxes at Devon Ice Cap and Mt. Oxford icefield were 30 and 185 ng m^{-2} a^{-1}, respectively. This trend suggests that sources other than fluorotelomer oxidation are responsible for PFBA deposition at lower latitudes, including the degradation of other precursor compounds and direct release. Both mechanisms are further discussed in

Section 3.3.4. The distinct behavior of PFBA highlights the need for future studies to better constrain its atmospheric sources and, therefore, its mechanism(s) of global distribution.

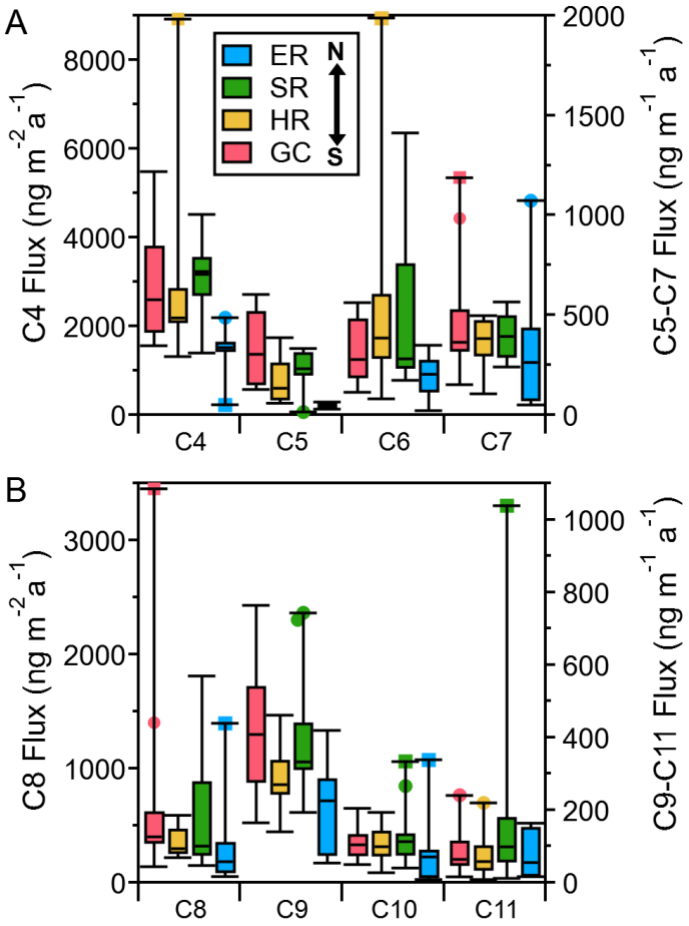

Figure 3-3: Boxplot of calculated deposition flux (ng m^{-2} a^{-1}) of (A) C4 – C7 PFCAs and (B) C8 – C11 PFCAs across the four sampling regions (from south to north: Grand Codroy, GC, pink; Humber River, HR, yellow; Salmon River, SR, green; Eagle River, ER, blue). Boxplot limits represent the third and first quartiles of the data set, whiskers represent the range, solid coloured circles represent outliers, and solid coloured squares represent far outliers. The median flux is indicated by a solid black line.

3.3.3 Wet and dry deposition

Although several prior efforts have been made to determine the concentrations and fluxes of various PFAS homologues in precipitation, there are limited reports that

have used measurements to explicitly assess the relative contributions of wet and dry deposition to the total deposition of PFAAs.[24,50,51] Efforts to constrain the two different removal mechanisms have involved samplers that selectively collect wet deposition and continuously collect dry deposition during rain-free periods.[24,70] In another approach, wet deposition was measured and dry deposition was estimated from measurements of gaseous and particulate PFAS.[50] In the current study, we use the same approach as the former studies and use the measurement of wet deposition. However, to determine dry deposition, we subtract wet deposition values from the total deposition, yielding a result that represents the sum of wet and dry deposition.

We assessed these deposition mechanisms for C4 (PFBA), C8 (PFOA), and C9 (PFNA) PFCAs, normalized to the sampling duration to facilitate effective comparison given the long duration of each sample and the extended duration of the entire dataset over multiple years. For all other analytes, the detection frequency was too low to conduct a meaningful analysis. Generally, we found that dry deposition was the predominant pathway for the removal of these three near-ubiquitous PFCAs from the atmosphere across the NL-BELT (Table B-12). The estimated dry deposition flux for PFBA ranged from 1000 – 3800 ng m^{-2} a^{-1}, while PFOA and PFNA ranged between 100 – 500 ng m^{-2} a^{-1} (Figure 3-4). There was considerable variability in the contribution of dry deposition between samples, as well as between homologues, where PFBA exhibited the largest fraction of dry deposition. The median fraction of total deposition attributed to dry deposition for PFBA was 95% (range 36 to 100%), 60% for PFOA (range 16 to 91%), and for PFNA was 66% (range 24 to 92%) (Figure B-5). Existing literature on the importance of dry versus wet deposition is inconsistent (Table B-13), as one may expect, because dry deposition will depend on the duration of rain-free conditions and the atmospheric abundance of the PFCAs. Comparisons between our results and those previously published are not straightforward because of the different approaches used to measure or calculate wet and dry deposition. Our findings generally agree with Xia et al.,[50] who showed that dry deposition dominated these loss mechanisms for PFBA and was less important for PFOA (with similar trends for the corresponding PFSAs). In contrast, Shimizu et al. made measurements that disagree with ours, where wet deposition removed PFAS by an order of magnitude greater than dry deposition.[24] These

measurements were made in a very polluted region, ~110 km from a known fluorotelomer manufacturer. Modelling of emissions from a point source by D'Ambro et al.,[51] showed that dry deposition was expected to dominate for total PFAS and hexafluoropropylene oxide dimer acid, and that dry deposition became more important as a function of distance from the point source. Thus, it is reasonable to expect disagreement between our measurements and those of Shimizu et al., as these deposition mechanisms are expected to depend on source proximity, atmospheric production rate from precursors, and the frequency and intensity of rain at a particular sampling location. Given the remote locations of the NL-BELT sampling sites, we would expect the atmosphere to be relatively well mixed and to have a low influence from local point sources. As a result, our observations are reliable in assigning dry deposition as an equivalent or dominant removal process for PFCAs from the remote atmosphere. Further spatial comparisons of total and wet deposition are needed, alongside reliable quantitative measurements of gaseous PFCAs, to discretely quantify dry deposition rates to various environmental compartments for use in chemical transport models.

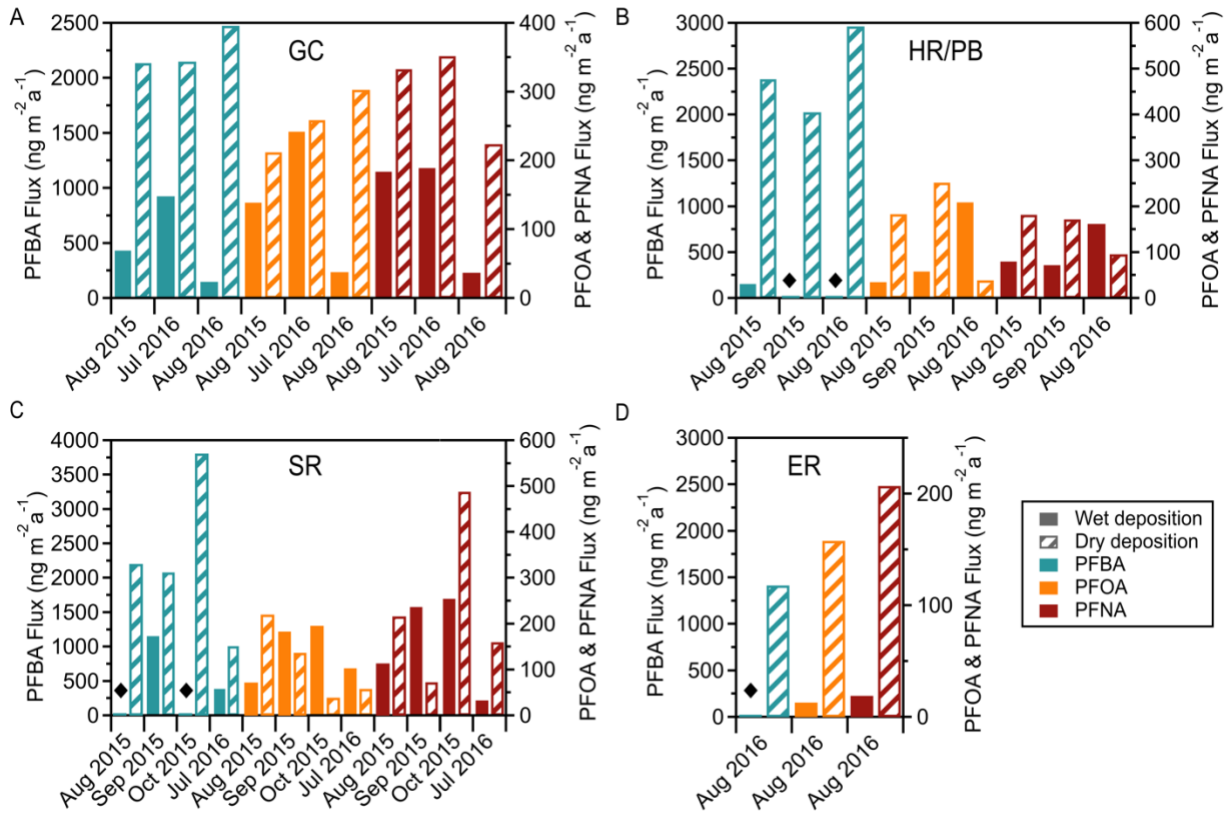

Figure 3-4: Measured wet (solid bars) and calculated dry (striped bars) deposition fluxes (ng m^{-2} a^{-1}) of PFBA (left axis), PFOA and PFNA (right axis) at (A) GC, (B) HR and PB, (C) SR, and (D) ER for selected months in 2015 and 2016. Fluxes were normalized to an annual interval for comparisons independent of sampling duration and for comparison to longer-term geochemical records with annual resolution, such as ice cores.[20,42] Dry deposition was estimated by subtracting the wet deposition fluxes from those measured in the total deposition samples. A solid diamond indicates where ½ LOD values were used to derive upper limit flux estimates. Note that the axes have different ranges for PFOA and PFNA at GC and ER.

3.3.4 Sources of PFAAs to the NL-BELT

The global distribution of PFAAs in the environment suggests that long-range transport may be a major contributor to levels observed in remote locations. Indirect sources have been identified as pathways for the formation of PFAAs, where volatile precursors such as FTOHs, perfluoroalkane sulfonamides, and N-alkane perfluoroalkane sulfonamidoethanols can undergo oxidation in the gas phase to produce PFAAs.[13] This has been confirmed by several studies that (i) detect the presence of precursor compounds in the gas phase,[71–73] (ii) use homologue correlations and/or molar ratios of PFAAs in atmospheric deposition samples,[23,31,42,44], and (iii) utilize chemical modelling.[74–

[76] The patterns of PFAA homologues are useful tools to examine the contribution that fluorotelomer compounds play in gas-phase atmospheric oxidation.[23] Conversely, direct transport mechanisms release PFAAs from manufacturing, dispersions, and the use of aqueous film-forming foams, consumer products and other industrial products.[2,51,77] We utilize correlation analysis, air mass back trajectories, molar flux ratios, and model comparisons to discern the role of direct and indirect sources of PFAAs across the NL-BELT.

3.3.5 Evidence of direct transport to the NL-BELT

To discern the role of direct transport on PFAA deposition, we explore the complementary information yielded from major ion determinations in the same samples. Herein, we correlated PFAA fluxes with Na^+ as a sea salt tracer, non-sea salt (nss) K^+ for biomass burning, and nss-Ca^{2+} and nss-Mg^{2+} for mineral dust transport. We also compared the observed deposition flux of selected PFAAs and Na^+ to a recent marine aerosol remobilization model to assess the role of direct transport of PFAAs by sea spray aerosols.

Generally, most PFAAs were not statistically correlated with major ions, and the degree of the correlations varied between the different sampling sites (Tables B-16–19). At the most southerly site (GC), a significant correlation was observed between PFDA and Na^+ and nss-Ca^{2+} ($r = 0.75$, $p = 0.02$). At the mid-latitude Newfoundland site (HR), PFBA and PFUnDA correlated with Na^+ ($r = 0.73$-0.78, $p < 0.05$), and PFOA correlated with nss-Ca^{2+} ($r = 0.72$, $p < 0.05$). At the highest-latitude Newfoundland site (SR), correlations were observed between PFHpA and nss-Ca^{2+} ($r = 0.90$, $p = 0.01$), as well as between PFBA and nss-K^+ ($r = 0.91$, $p = 0.02$). Lastly, strong correlations were observed between PFNA and PFDoDA with nss-Ca^{2+} ($r = 0.99$, $p < 0.05$) and PFHpA and PFDA with nss-K^+ ($r = 0.96$-0.99, $p < 0.03$) at the Labrador site (ER).

The results from the correlation analysis suggest that some PFAAs and major ions could be derived from a common source, from a mixture of sources along a common transport pathway to a given site and then undergo similar deposition processes. The correlation between selected PFAAs and Na^+ at GC and HR is suggestive of the presence of marine aerosols acting as a potential source for some PFAAs at some locations (Figure 3-5). Given the close proximity of the NL-BELT sites to the St. Lawrence Estuary, Atlantic

Ocean, and Labrador Sea (~6 to 30 km), we were surprised that correlations between PFAAs and Na^+ were not more widespread in our measurements. In contrast to our observations, Sha et al.[22] analyzed aerosol samples from two Norwegian coastal locations (~1.3 and ~20 km from the ocean) and found significant correlations ($r = 0.4$-0.8, $p < 0.05$) between Na^+ and several PFAAs.

The correlations between PFOA (GC), PFHpA (SR), PFNA (ER), PFDoDA (ER), and nss-Ca^{2+} (r:0.72-0.99, $p<0.05$) and PFBA (SR), PFHpA and PFDA (ER) and nss-K^+ (r: 0.91-0.99, $p<0.03$) suggest that mineral dust transport and biomass burning plumes may also be an important transport and source media to the sites denoted in brackets, respectively. These are not unreasonable hypotheses since mineral dust transport has been shown as a reactive mechanism facilitating long-range transport of other strong acids[78] ,and similar correlations were previously observed for PFAAs in two separate High Arctic Ice cores ($r = 0.30$-0.50, $p<0.05$).[20,42] Plants can also bioaccumulate PFAAs[28,79] and remobilization during biomass burning events is plausible.

To further assess the potential contribution of marine aerosols, we compared the observed deposition fluxes of PFOA, PFOS and Na^+ ion to a recent model estimate of PFAA remobilization by marine aerosols (Figure B-6).[21] Generally, the marine aerosol remobilization model predicts that a latitudinal dependence in PFAA deposition should exist, with fluxes decreasing with latitude. The model predictions estimated decreases of 143% and 183% in median PFOA and PFOS fluxes, respectively, between the lowest and highest latitude sites. This is contrary to our measurements, which show no significant differences in fluxes between our sampling sites. We further compared the estimated versus measured fluxes across the NL-BELT. This is not a simple comparison since the estimates were generated on 2.5° x 1.875° grid cells, whereas we measured deposition at a fixed location. We found that the estimates generally agree with the measured PFOA deposition but overestimate the PFOS deposition at the lower latitude sites (GC and HR) by more than 150%. This discrepancy is expected since the model estimates rely on accurate spatial and time-resolved measurements of PFAAs and Na^+, which are not always available. For instance, the mean sodium flux utilized in the estimates was generated using the Norwegian Earth System Model Version 2 (NorESM2), which estimates that 1.7 – 3.9 g m^{-2} a^{-1} is deposited across the NL-BELT region. However, our

measured mean sodium flux was 2–18 times lower than those predicted by the NorESM2 model, with the greatest discrepancy observed in the two northernmost sites (SR and ER). These findings highlight the complexities of accurately modelling PFAA deposition. The overestimation of PFOS fluxes suggests that limitations in current model parametrization exist. Similar challenges extend beyond PFAAs, as other surface-active compounds (e.g., lipids) also exhibit spatial variability in their air-sea exchange rates.[80,81] Future research should focus on extensive, temporal and spatially resolved measurements of PFAA homologues and the Na^+ ion, which will provide a more accurate understanding of PFAA deposition in this region and help to refine model representations of these processes in coastal environments.

We note that the lack of significant correlations between most PFAA homologues and major ions at the NL-BELT sites and the discrepancy between the model and our measurements suggest that other potential PFAA direct or indirect sources exist (e.g., oxidation of volatile precursors), including unknown direct industrial sources. To further assess the influence of direct transport, future work should be undertaken to expand the spatial resolution of PFAA deposition and incorporate long-term datasets that provide sufficient observation of temporal variations of PFAAs and major ions to better constrain inputs for models in a wide variety of coastal locations. Marine aerosols and mineral dust tracers are invaluable tools for source apportionment, but they require a large number of measurements to increase the statistical power of the correlations.

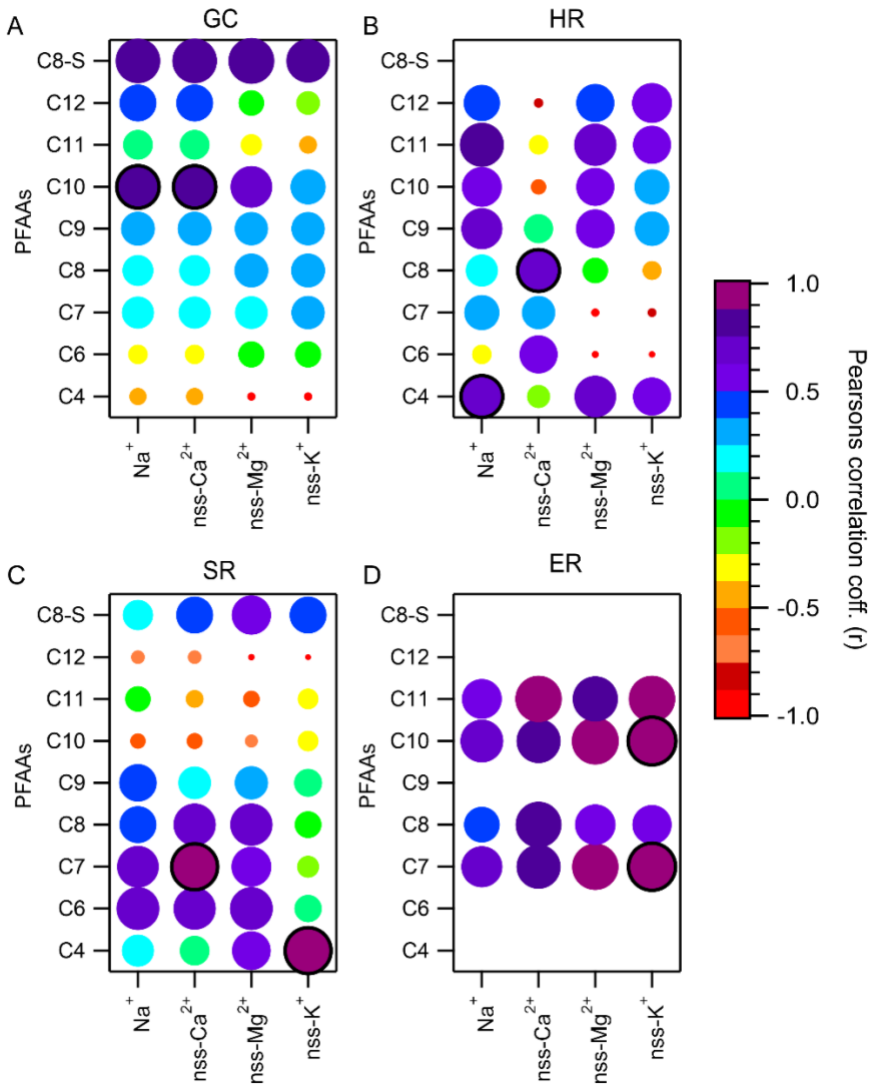

Figure 3-5: Correlation map of log-transformed PFAA deposition fluxes (C4-C12 PFCAs and PFOS as C8-S) (y-axis) at (A) GC, (B) HR, (C) SR, and (D) ER for the entire sampling period. The strength of the correlation is denoted by larger circles for a larger Pearson correlation coefficient, alongside the noted color scale shift. Where a black outline surrounds a circle, this represents a statistically significant correlation (p-value <0.05).

3.3.6 Air Mass Back Trajectory

Back trajectory analysis is useful to understand potential long-range atmospheric sources of PFAS in the NL-BELT. When applied to high-frequency or very long term measurements, such an approach can yield insights into the origins of detected pollutants and, as a result, the potential mechanisms governing their formation and/or fate in the atmosphere. As our sample dataset is limited, the analysis here can only consider broad

synoptic scale relationships. The geographical sector assignment of air mass source regions for each month was calculated for each sampling site for the period 2014 - 2016 (Table B-20). During the sampling period, the field sites across the NL-BELT were predominantly influenced by air masses originating from the northwest (NW) and southwest (SW) sectors. This is consistent with the prevailing westerlies across North America, where PFAS use and emissions from industrial activities and use/disposal of commercial products are expected. This transport pattern is known to intensify in the fall,[82], which is evident from our analysis, where the percentages of air masses arriving from the NW and SW sectors dominate during the months of September and October for the entire sampling period (2014-2016).

We further compared the sector assignments to periods where elevated levels of selected PFAAs were observed. We caution that the results from the air mass back trajectory are not an indication of PFAS origins since the lifetimes of PFAAs and their precursors can be much longer than the back trajectory timescales. We observed that the relationship between sector and deposition flux varied depending on the PFAA homologue, sampling site, and time. For instance, elevated levels of C4, C6 – C9 PFCAs were observed when the air mass originated from the NE and SE sectors (68%) in June 2014 at the southernmost site (GC). Whereas the opposite trend was observed in September 2014 when elevated levels of PFBA corresponded with airmasses arriving from the west (77%). At the same site, elevated levels of PFOS were observed in October 2014 and November 2015 when the air masses originated from the west (<67%). The trends observed here highlight the complexity of identifying PFAA sources through a small number of monthly deposition measurements, although these results are suggestive that short-range transport of air masses does not seem to be intercepting substantial local point sources. Back trajectory and similar source identification strategies benefit most from large numbers of measurements, preferably with other molecular tracers for source apportionment (e.g., to dust). Our findings from this work emphasize the need for long-term and/or high time resolution measurements with detection limits suitable for atmospheric mixing ratios (e.g., chemical ionization mass spectrometry (CIMS))[83] which can relate changing concentrations with other environmentally relevant variables (e.g., wind direction, other pollutants measured at the same timescale).

3.3.7 Examining the role of fluorotelomer oxidation as a major PFCA source

A correlation matrix was generated between PFAAs fluxes at the different sampling regions to determine whether any relationship existed within the group of molecules quantified. If PFAAs originate from a volatile precursor source, they would undergo similar subsequent atmospheric transport and deposition processes, and we would then expect the sequential pair to be correlated with one another. Homologues with a low detection frequency (< 50 %) were not included in the analysis. We performed a total correlation, which combined all four sampling sites (GC, HR, SR, and ER) as well as each site individually to discern any latitudinal trends. The full correlation matrix results can be found in Tables B-21–B-24 and Figure B-7.

We observed statistically significant correlations between selected PFAAs, suggesting a common source and similar deposition mechanisms. Considering the overall correlation, PFCAs from C6–C12 showed a statistically significant moderate to strong correlation between the PFAA homologues ($r = 0.61\text{-}0.87$, $p<0.001$), which strongly suggests that atmospheric PFCAs originate from a common precursor source(s). We also observed an unexpected moderate correlation between PFOS and C4 and C6– C8 PFCAs ($r = 0.54\text{-}0.64$, $p<0.05$) and a weak correlation between PFOS and C9-C12 PFCAs ($r = 0.37\text{-}0.39$, $p<0.11$). Correlations between PFOS and selected PFCAs would be expected from the oxidation of perfluoroalkane sulfonamido substances. For example, the oxidation of *N*-methyl perfluorooctane sulfonamido ethanol produces PFOS and any one of the C2 to C8 PFCAs and may explain why a moderate correlation was observed for the C4-C8 PFCAs.

At individual sites, selected PFCAs and PFSAs were also correlated with each other, further supporting the hypothesis that fluorotelomer oxidation is important for PFCA deposition. However, the correlations varied depending on the sampling site. For example, the C8:C9 pair was correlated at GC and ER ($r = 0.71\text{-}0.84$, $p<0.007$) but not at HR and SR ($r = -0.05\text{-}0.43$, $p>0.25$). Furthermore, the C9:C10 were correlated at HR and ER ($r = 0.66\text{-}0.99$, $p<0.03$) but not at the GC and SR site ($r = 0.46\text{-}0.43$, $p>0.12$). This spatial variability may reflect localized differences in emission sources, deposition mechanisms or the influence of other transport mechanisms (e.g., aerosols). Interestingly, the number and strength of the correlations also increase with latitude,

similar to previous observations in the Canadian Arctic.[20,42,44]

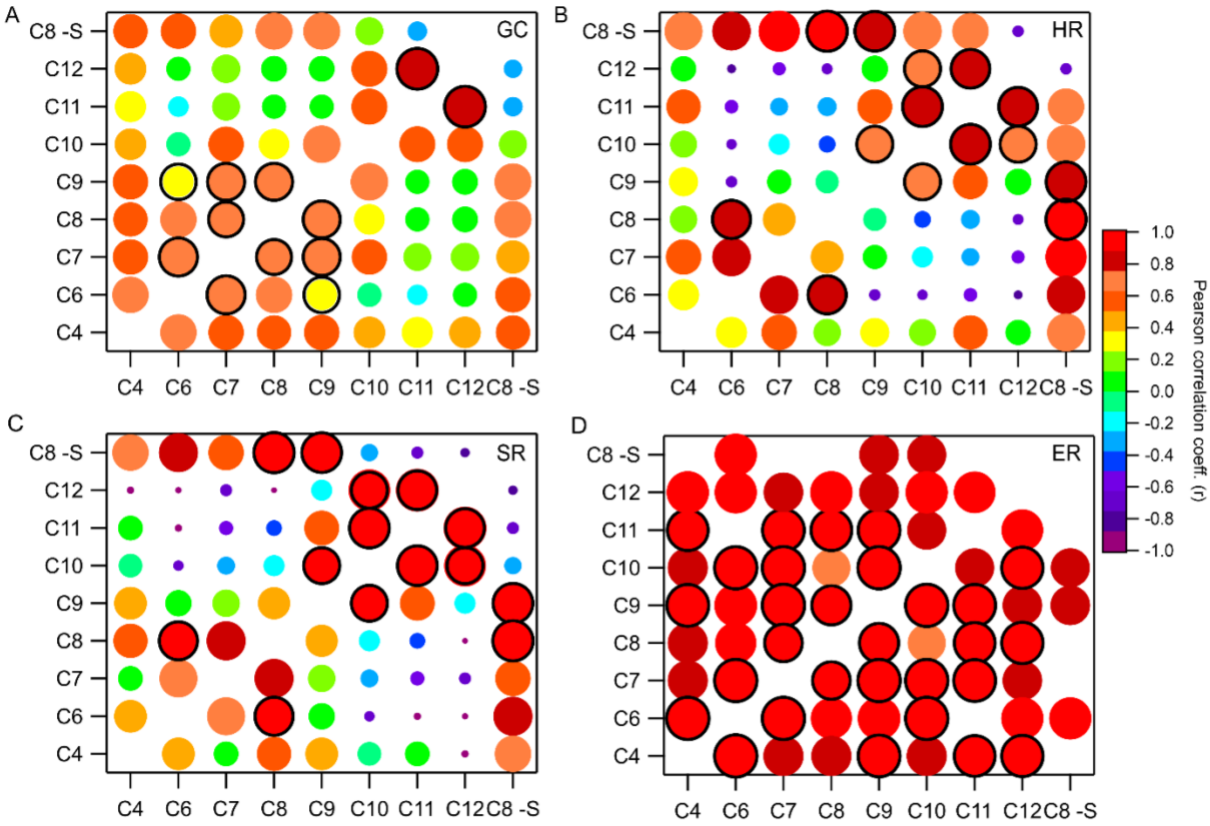

Figure 3-6: Pearson correlation map of log-transformed C4 – C12 PFCA and C8 PFSA deposition fluxes at (A) GC, (B) HR, (C) SR and (D) ER. The strength of the correlation is illustrated by the colour and size of the circle, where larger circles denote a strong correlation based on the magnitude of r. The black outline represents a statistically significant correlation (p-value <0.05).

Examining the even-odd molar flux ratios in precipitation is useful to determine the role of atmospheric oxidation of fluorotelomer compounds on PFCA deposition.[47,55,60] Molar flux ratios were calculated for four pairs of PFCAs: C4:C5, C6:C7, C8:C9 and C10:C11, which are used as a proxy for the oxidation of the 4:2, 6:2, 8:2 and 10:2 FTOHs, respectively (Figure 3-7). We observed that 61-78% of flux ratio measurements of C6:C7, C8:C9 and C10:C11 are within a factor of 2 and 91-96% are within a factor of 6. This strongly suggests that the oxidation of fluorotelomer precursors is a contributing source of C6-C11 PFCAs in the NL-BELT region, and potentially the dominant source.

Conversely, molar flux ratios of the C4:C5 pair are greater than ratios expected from the oxidation of fluorotelomer compounds (15 ± 9, mean and standard deviation), with 14% of the homologue pair within a factor of 6, suggesting oxidation of the 4:2 FTOH

may contribute to the observations but is not the dominant source of the observed PFBA. This is consistent with findings by several studies that observe higher molar flux ratios of C4:C5 when compared to other PFCA homologue pairs.[43,44,84,85]These findings suggest that other sources of PFBA exist other than fluorotelomer oxidation. It is known that PFBA was directly produced by at least one major fluorochemical manufacturer,[77,86] but there is no information available on emissions to the air prior to and during the observation time period. Other non-fluorotelomer gas phase sources, such as chlorofluorocarbon (CFC) replacement compounds, may be driving the PFBA formation and subsequent deposition in this region. There is extensive evidence that hydrofluoroethers (HFEs) such as HFE-7100 and HFE-7200, as well as hydrofluorocarbon-329 ($CF_3(CF_2)_3H$), can oxidize in the gas phase to produce PFBA.[14–16] This is expected to be a major source since HFEs and HFCs are present in greater atmospheric abundance (~5-200 pptv)[87] compared to fluorotelomer precursors (~0.0098-0.0195 pptv).[73,88,89]

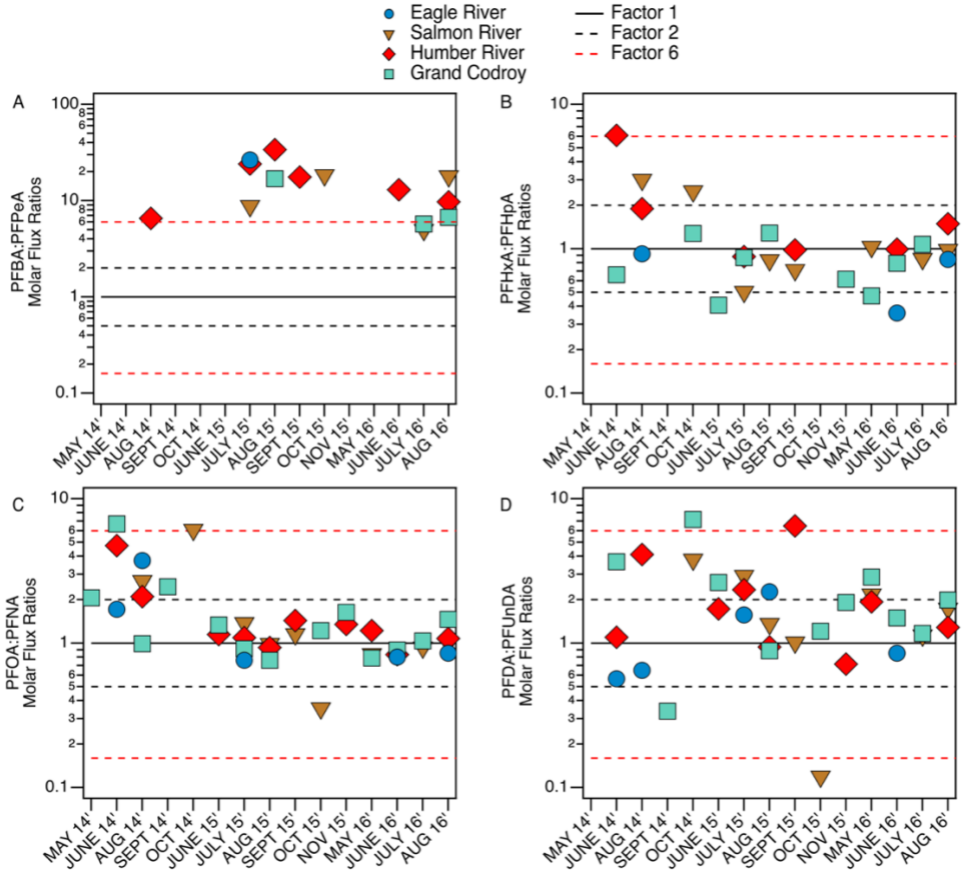

Figure 3-7: Molar Flux ratios of even-odd PFCA pairs: (A) PFBA: PFPeA, (B) PFHxA: PFHpA, (C) PFOA: PFNA and (D) PFDA: PFUnDA for GC (teal square), HR (red diamond), SR (brown

diamond) and ER (blue circle) for the period 2014 - 2016. The solid black line represents a ratio of 1, which indicates that equal amounts were deposited, whereas dashed black and red lines correspond to molar flux ratios within a factor of 2 and 6, respectively.

Comparisons were also made between deposition fluxes of PFCAs and a GEOS-CHEM model developed by Thackray et al.[74] This is an updated model for PFCA formation from the degradation of precursors, including fluorotelomer alcohols (FTOH), fluorotelomer olefins (FTOs) and fluorotelomer iodides (FTIs). The model also incorporates the deposition and transport of the precursors, intermediates, and PFCA end-products.[74] The comparisons were made between C4 – C12 PFCAs at each location for 2015 (see Table B-25 and Figure B-8). The observations show the expected variability and bias between modelled wet deposition and measured concentrations. This uncertainty is expected for modelled rainwater concentrations since any chemical model relies on accurate time-resolved emission inventories, the assumption that all sources and associated rates of all relevant reactions are known, and its capacity to predict the location and quantity of precipitation occurring at the measurement site. We assessed the contribution of the fluorotelomer derived pathway by comparing the minimum modelled to the minimum observed flux at each site. We found that the model generally underestimates the PFAA deposition but can account for more than 70% of the fluxes of C5, C6 and C8-C11 PFCAs measured across the sampling sites. These results confirm our hypothesis that fluorotelomer oxidation is an important source of PFCAS across the NL-BELT.

However, some disparities were observed for selected PFAAs. For instance, the model accounted for 58% and 49% of the observed C7 and C12 deposition. This was not surprising, as Thackray et al. found that the C7 homologue similarly underpredicted in the Canadian Arctic.[74] The authors attributed this to the uncertainty in the perfluorinated aldehyde hydration reaction, a key process in odd-chain PFCA formation and uncertainties in direct C7 emissions.[74] Meanwhile, the discrepancy of the C12 homologue could be attributed to the fact that this homologue detection was close to the method detection limits at all sites, with a detection frequency of only 55%. The greatest disparity between modelled-measured deposition fluxes was observed for the C4 homologue, with the model simulation accounting for 5-10% of the measured deposition across the sampling sites, at most. This further supports the results of the molar concentration ratios

that the C4 homologue is likely formed from sources other than fluorotelomer oxidation in the NL-BELT region.

3.4 Conclusion

The results of this study fill a significant gap in current knowledge of PFAA deposition, given that there are limited measurements in North American precipitation. The measurements demonstrated that PFAAs were ubiquitously detected in deposition samples across Newfoundland and Labrador, where deposition is dominated by the short-chain PFBA homologue. This is potentially a consequence of continued reduction in long chain PFAAs use and replacement by shorter homologues or additional non-fluorotelomer sources. The PFCA deposition could be attributed to oxidation and transport of precursor compounds, particularly evident at higher latitudes, further from more direct sources. Conversely, no clear source of PFSAs was identified. This calls for future research to focus on the transport and deposition of sulfonic acids and its precursors.

We found limited evidence of direct, short-range transport in this region. Trajectory analysis revealed that most of the airmass originates from the west, but there were no definite trends in elevated deposition with airmass origin. Additionally, there is limited evidence that marine aerosols were a major source of PFAA deposition in this region despite close proximity to the open ocean (6 – 30 km). If sea spray aerosols were the dominant deposition pathway, we would expect consistent statistically significant correlations with the Na^+ ion. This highlights the complex mechanisms that are responsible for PFAS deposition. In addition, it demonstrates the importance of temporal and spatial measurements of both PFAA homologues and major ions towards source elucidation.

This study also produces a unique finding that was not possible to assess in previous studies. We observed that gas-phase dry deposition can be a major deposition pathway for selected PFAAs. The median dry deposition contribution was 100 ng m^2 $a^{-1,}$ with PFBA dominating the deposition with values ranging from 1000 – 3800 ng m^2 a^{-1}. The magnitude of the dry deposition flux has previously been estimated by others to be a small fraction of the total deposition flux of PFAAs at other locations, but our measurements show that it could be equal to or greater than the wet deposition flux at these remote sites. We strongly recommend future measurements of PFAA deposition to

explicitly differentiate between total and wet-only deposition to further interrogate the relative role of the dry deposition process and improve our understanding of PFAA transport and fate. Further investigation into the role of different deposition mechanisms is also crucial for advancing our understanding of PFAA transport to remote regions and assessing the long-term environmental impacts of these persistent contaminants through parameterizations in global chemical transport models.

3.5 References

1 Z. Wang, J. C. DeWitt, C. P. Higgins and I. T. Cousins, A Never-Ending Story of Per- and Polyfluoroalkyl Substances (PFASs)?, *Environ. Sci. Technol.*, 2017, **51**, 2508–2518.

2 K. Prevedouros, I. T. Cousins, R. C. Buck and S. H. Korzeniowski, Sources, fate and transport of perfluorocarboxylates, *Environ. Sci. Technol.*, 2006, **40**, 32–44.

3 A. B. Lindstrom, M. J. Strynar and E. L. Libelo, Polyfluorinated compounds: Past, present, and future, *Environ. Sci. Technol.*, 2011, **45**, 7954–7961.

4 US EPA PFOA Stewardship Program Baseline Year Summary Report, https://www.epa.gov/assessing-and-managing-chemicals-under-tsca/pfoa-stewardship-program-baseline-year-summary-report#contents, (accessed 10 June 2022).

5 Environment and Climate Change Canada and Health Canada, State of per- and polyfluoroalkyl substances (PFAS) report, https://publications.gc.ca/collections/collection_2025/eccc/En84-395-2025-eng.pdf, (accessed 29 March 2025).

6 M. Land, C. A. De Wit, I. T. Cousins, D. Herzke, J. Johansson and J. W. Martin, What is the effect of phasing out long-chain per- and polyfluoroalkyl substances on the concentrations of perfluoroalkyl acids and their precursors in the environment? A systematic review protocol, *Environ. Evid.*, 2015, **4**, 1–13.

7 Government of Canada and Public Works and Government Services Canada, Canada Gazette, Part 1, Volume 159, Number 10, https://gazette.gc.ca/rp-pr/p1/2025/2025-03-08/html/reg2-eng.html, (accessed 29 March 2025).

8 M. Ateia, M. Arifuzzaman, S. Pellizzeri, M. F. Attia, N. Tharayil, J. N. Anker and T. Karanfil, Cationic polymer for selective removal of GenX and short-chain PFAS from surface waters and wastewaters at ng/L levels, *Water Res.*, 2019, **163**, 114874.

9 F. Xiao, Emerging poly- and perfluoroalkyl substances in the aquatic environment: A review of current literature, *Water Res.*, 2017, **124**, 482–495.

10 S.-K. Kim and K. Kannan, Perfluorinated Acids in Air, Rain, Snow, Surface Runoff, and Lakes: Relative Importance of Pathways to Contamination of Urban Lakes, *Environ. Sci. Technol.*, 2007, **41**, 8328–8334.

11 J. C. D'eon, M. D. Hurley, T. J. Wallington and S. A. Mabury, Atmospheric Chemistry of *N* -methyl Perfluorobutane Sulfonamidoethanol, $C_4F_9SO_2N(CH_3)CH_2CH_2OH$: Kinetics and Mechanism of Reaction with OH, *Environ. Sci. Technol.*, 2006, **40**, 1862–1868.

12 D. A. Ellis, J. W. Martin, A. O. De Silva, S. A. Mabury, M. D. Hurley, M. P. Sulbaek Andersen and T. J. Wallington, Degradation of Fluorotelomer Alcohols: A Likely Atmospheric Source of Perfluorinated Carboxylic Acids, *Environ. Sci. Technol.*, 2004, **38**, 3316–3321.

13 C. J. Young and S. A. Mabury, in *Reviews of Environmental Contamination and Toxicology Volume 208*, ed. P. De Voogt, Springer New York, New York, NY, 2010, vol. 208, pp. 1–109.

14 T. J. Wallington, W. F. Schneider, J. Sehested, M. Bilde, J. Platz, O. J. Nielsen, L. K. Christensen, M. J. Molina, L. T. Molina and P. W. Wooldridge, Atmospheric Chemistry of HFE-7100 (C4F9OCH3): Reaction with OH Radicals, UV Spectra and Kinetic Data for C4F9OCH2· and C4F9OCH2O2· Radicals, and the Atmospheric Fate of C4F9OCH2O· Radicals, *J. Phys. Chem. A*, 1997, **101**, 8264–8274.

15 C. J. Young, M. D. Hurley, T. J. Wallington and S. A. Mabury, Atmospheric chemistry of CF3CF2H and CF3CF2CF2CF2H: Kinetics and products of gas-phase reactions with Cl atoms and OH radicals, infrared spectra, and formation of perfluorocarboxylic acids, *Chem. Phys. Lett.*, 2009, **473**, 251–256.

16 L. Chen, T. Uchimaru, S. Kutsuna, K. Tokuhashi and A. Sekiya, Kinetics and mechanism of gas-phase reactions of n-C4F9OCH3, i-C4F9OCH3, n-C4F9OC(O)H, and i-C4F9OC(O)H with OH radicals in an environmental reaction chamber at 253–328K, *Chem. Phys. Lett.*, 2011, **514**, 207–213.

17 J. H. Johansson, M. E. Salter, J. C. Acosta Navarro, C. Leck, E. D. Nilsson and I. T. Cousins, Global transport of perfluoroalkyl acids via sea spray aerosol, *Environ. Sci. Process. Impacts*, 2019, **21**, 635–649.

18 M. Reth, U. Berger, D. Broman, I. T. Cousins, E. D. Nilsson and M. S. McLachlan, Water-to-air transfer of perfluorinated carboxylates and sulfonates in a sea spray simulator, *Environ. Chem.*, 2011, **8**, 381–388.

19 B. Sha, J. H. Johansson, J. P. Benskin, I. T. Cousins and M. E. Salter, Influence of Water Concentrations of Perfluoroalkyl Acids (PFAAs) on Their Size-Resolved Enrichment in Nascent Sea Spray Aerosols, *Environ. Sci. Technol.*, 2021, **55**, 9489–9497.

20 D. Persaud, A. S. Criscitiello, C. Spencer, I. Lehnherr, D. C. G. Muir, A. O. De Silva and C. J. Young, A 50 year record for perfluoroalkyl acids in the High Arctic: implications for global and local transport, *Environ. Sci. Process. Impacts*, 2024, **26**, 1543–1555.

21 B. Sha, J. H. Johansson, M. E. Salter, S. M. Blichner and I. T. Cousins, Constraining global transport of perfluoroalkyl acids on sea spray aerosol using field measurements, *Sci. Adv.*, 2024, **10**, eadl1026.

22 B. Sha, J. H. Johansson, P. Tunved, P. Bohlin-Nizzetto, I. T. Cousins and M. E. Salter, Sea Spray Aerosol (SSA) as a Source of Perfluoroalkyl Acids (PFAAs) to the Atmosphere: Field Evidence from Long-Term Air Monitoring, *Environ. Sci. Technol.*, 2022, **56**, 228–238.

23 C. J. Young, V. I. Furdui, J. Franklin, R. M. Koerner, D. C. G. Muir and S. A. Mabury, Perfluorinated Acids in Arctic Snow: New Evidence for Atmospheric Formation, *Environ. Sci. Technol.*, 2007, **41**, 3455–3461.

24 M. S. Shimizu, R. Mott, A. Potter, J. Zhou, K. Baumann, J. D. Surratt, B. Turpin, G. B. Avery, J. Harfmann, R. J. Kieber, R. N. Mead, S. A. Skrabal and J. D. Willey, Atmospheric Deposition and Annual Flux of Legacy Perfluoroalkyl Substances and Replacement Perfluoroalkyl Ether Carboxylic Acids in Wilmington, NC, USA, *Environ. Sci. Technol. Lett.*, 2021, **8**, 366–372.

25 C. A. Barton, M. A. Kaiser and M. H. Russell, Partitioning and removal of perfluorooctanoate during rain events: the importance of physical-chemical properties, *J. Environ. Monit.*, 2007, **9**, 839–846.

26 D. K. Farmer, E. K. Boedicker and H. M. DeBolt, Dry Deposition of Atmospheric Aerosols: Approaches, Observations, and Mechanisms, *Annu. Rev. Phys. Chem.*, 2021, **72**, 375–397.

27 D. A. Grantz, J. H. B. Garner and D. W. Johnson, Ecological effects of particulate matter, *Environ. Int.*, 2003, **29**, 213–239.

28 Z. Liu, Y. Lu, Y. Shi, P. Wang, K. Jones, A. J. Sweetman, A. C. Johnson, M. Zhang, Y. Zhou, X. Lu, C. Su, S. Sarvajayakesavaluc and K. Khan, Crop bioaccumulation and human exposure of perfluoroalkyl acids through multi-media transport from a mega fluorochemical industrial park, China, *Environ. Int.*, 2017, **106**, 37–47.

29 H. Chen, Y. Yao, Z. Zhao, Y. Wang, Q. Wang, C. Ren, B. Wang, H. Sun, A. C. Alder and K. Kannan, Multimedia Distribution and Transfer of Per- and Polyfluoroalkyl Substances (PFASs) Surrounding Two Fluorochemical Manufacturing Facilities in Fuxin, China, *Environ. Sci. Technol.*, 2018, **52**, 8263–8271.

30 J. H. Johansson, Y. Shi, M. Salter and I. T. Cousins, Spatial variation in the atmospheric deposition of perfluoroalkyl acids: source elucidation through analysis of isomer patterns, *Environ. Sci. Process. Impacts*, 2018, **20**, 997–1006.

31 K. A. Pike, P. L. Edmiston, J. J. Morrison and J. A. Faust, Correlation Analysis of Perfluoroalkyl Substances in Regional U.S. Precipitation Events, *Water Res.*, 2021, **190**, 116685.

32 G. Sammut, E. Sinagra, R. Helmus and P. de Voogt, Perfluoroalkyl substances in the Maltese environment – (I) surface water and rain water, *Sci. Total Environ.*, 2017, **589**, 182–190.

33 G. Shan, X. Chen and L. Zhu, Occurrence, fluxes and sources of perfluoroalkyl substances with isomer analysis in the snow of northern China, *J. Hazard. Mater.*, 2015, **299**, 639–646.

34 T. Han, L. Gao, J. Chen, X. He and B. Wang, Spatiotemporal variations, sources and health risk assessment of perfluoroalkyl substances in a temperate bay adjacent to metropolis, North China, *Environ. Pollut.*, 2020, **265**, 115011.

35 S. Taniyasu, N. Yamashita, H.-B. Moon, K. Y. Kwok, P. K. S. Lam, Y. Horii, G. Petrick and K. Kannan, Does wet precipitation represent local and regional atmospheric transportation by perfluorinated alkyl substances?, *Environ. Int.*, 2013, **55**, 25–32.

36 B. F. Scott, C. Spencer, S. A. Mabury and D. C. G. Muir, Poly and perfluorinated carboxylates in North American precipitation, *Environ. Sci. Technol.*, 2006, **40**, 7167–7174.

37 K. Y. Kwok, S. Taniyasu, L. W. Y. Yeung, M. B. Murphy, P. K. S. Lam, Y. Horii, K. Kannan, G. Petrick, R. K. Sinha and N. Yamashita, Flux of Perfluorinated Chemicals

through Wet Deposition in Japan, the United States, And Several Other Countries, *Environ. Sci. Technol.*, 2010, **44**, 7043–7049.

38 M. Filipovic, H. Laudon, M. S. McLachlan and U. Berger, Mass Balance of Perfluorinated Alkyl Acids in a Pristine Boreal Catchment, *Environ. Sci. Technol.*, 2015, **49**, 12127–12135.

39 S. B. Gewurtz, A. S. Auyeung, A. O. De Silva, S. Teslic and S. A. Smyth, Per- and polyfluoroalkyl substances (PFAS) in Canadian municipal wastewater and biosolids: Recent patterns and time trends 2009 to 2021, *Sci. Total Environ.*, 2024, **912**, 168638.

40 G. Casas, A. Martinez-Varela, M. Vila-Costa, B. Jiménez and J. Dachs, Rain Amplification of Persistent Organic Pollutants, *Environ. Sci. Technol.*, 2021, **55**, 12961–12972.

41 M. Chen, C. Wang, K. Gao, X. Wang, J. Fu, P. Gong and Y. Wang, Perfluoroalkyl substances in precipitation from the Tibetan Plateau during monsoon season: Concentrations, source regions and mass fluxes, *Chemosphere*, 2021, **282**, 131105.

42 H. M. Pickard, A. S. Criscitiello, C. Spencer, M. J. Sharp, D. C. G. Muir, A. O. De Silva and C. J. Young, Continuous non-marine inputs of per- and polyfluoroalkyl substances to the High Arctic: A multi-decadal temporal record, *Atmospheric Chem. Phys.*, 2018, **18**, 5045–5058.

43 H. M. Pickard, A. S. Criscitiello, D. Persaud, C. Spencer, D. C. G. Muir, I. Lehnherr, M. J. Sharp, A. O. De Silva and C. J. Young, Ice Core Record of Persistent Short-Chain Fluorinated Alkyl Acids: Evidence of the Impact From Global Environmental Regulations, *Geophys. Res. Lett.*, 2020, **47**, e2020GL087535.

44 J. J. Macinnis, K. French, D. C. G. Muir, C. Spencer, A. Criscitiello, A. O. De Silva and C. J. Young, Emerging investigator series: A 14-year depositional ice record of perfluoroalkyl substances in the High Arctic, *Environ. Sci. Process. Impacts*, 2017, **19**, 22–30.

45 I. T. Cousins, J. H. Johansson, M. E. Salter, B. Sha and M. Scheringer, Outside the Safe Operating Space of a New Planetary Boundary for Per- and Polyfluoroalkyl Substances (PFAS), *Environ. Sci. Technol.*, 2022, **56**, 11172–11179.

46 B. F. Scott, D. Mactavish, C. Spencer, W. M. J. Strachan and D. C. G. Muir, Haloacetic acids in Canadian lake waters and precipitation, *Environ. Sci. Technol.*, 2000, **34**, 4266–4272.

47 D. Pfotenhauer, E. Sellers, M. Olson, K. Praedel and M. Shafer, PFAS concentrations and deposition in precipitation: An intensive 5-month study at National Atmospheric Deposition Program – National trends sites (NADP-NTN) across Wisconsin, USA, *Atmos. Environ.*, 2022, **291**, 119368.

48 M. Guerra de Navarro, Y. Reyna and N. Quinete, It's raining PFAS in South Florida: Occurrence of per- and polyfluoroalkyl substances (PFAS) in wet atmospheric deposition from Miami-Dade, South Florida, *Atmospheric Pollut. Res.*, 2024, **15**, 102302.

49 S. Olney, M. Jones, C. Rockwell, R. D. Collins, J. D. Bryant and J. Occhialini, Influence of convective and stratiform precipitation types on per- and polyfluoroalkyl substance concentrations in rain, *Sci. Total Environ.*, 2023, **890**, 164051.

50 C. Xia, S. L. Capozzi, K. A. Romanak, D. C. Lehman, A. Dove, V. Richardson, T. Greenberg, D. McGoldrick and M. Venier, The Ins and Outs of Per- and Polyfluoroalkyl Substances in the Great Lakes: The Role of Atmospheric Deposition, *Environ. Sci. Technol.*, 2024, **58**, 9303–9313.

51 E. L. D'Ambro, H. O. T. Pye, J. O. Bash, J. Bowyer, C. Allen, C. Efstathiou, R. C. Gilliam, L. Reynolds, K. Talgo and B. N. Murphy, Characterizing the Air Emissions, Transport, and Deposition of Per- And Polyfluoroalkyl Substances from a Fluoropolymer Manufacturing Facility, *Environ. Sci. Technol.*, 2021, **55**, 862–870.

52 Z. Wang, Y. Wang, J. Li, S. Henne, B. Zhang, J. Hu and J. Zhang, Impacts of the Degradation of 2,3,3,3-Tetrafluoropropene into Trifluoroacetic Acid from Its Application in Automobile Air Conditioners in China, the United States, and Europe, *Environ. Sci. Technol.*, 2018, **52**, 2819–2826.

53 Z. Wang, Z. Xie, A. Möller, W. Mi, H. Wolschke and R. Ebinghaus, Estimating dry deposition and gas/particle partition coefficients of neutral poly-/perfluoroalkyl substances in northern German coast, *Environ. Pollut.*, 2015, **202**, 120–125.

54 F. Wang, W. Wang, D. Zhao, J. Liu, P. Lu, N. L. Rose and G. Zhang, Source apportionment and wet deposition of atmospheric poly- and per-fluoroalkyl

substances in a metropolitan city centre of southwest China, *Atmos. Environ.*, 2022, **273**, 118983.

55 S. E. Ziegler, R. Benner, S. A. Billings, K. A. Edwards, M. Philben, X. Zhu and J. Laganière, Climate Warming Can Accelerate Carbon Fluxes without Changing Soil Carbon Stocks, *Front. Earth Sci.*, DOI:10.3389/feart.2017.00002.

56 Government of Canada, 2021 Census of Population - Newfoundland and Labrador [Province], https://www12.statcan.gc.ca/census-recensement/2021/dp-pd/prof/index.cfm?Lang=E, (accessed 23 April 2025).

57 A. A. Colussi, D. Persaud, M. Lao, B. K. Place, R. F. Hems, S. E. Ziegler, K. A. Edwards, C. J. Young and T. C. VandenBoer, Cost-effective off-grid automatic precipitation samplers for pollutant and biogeochemical atmospheric deposition, *Atmospheric Meas. Tech.*, 2024, **17**, 3697–3718.

58 Canadian Air and Precipitation Monitoring Network, Site operations reference manual, https://publications.gc.ca/site/eng/9.883036/publication.html, (accessed 23 April 2025).

59 NADP Site Selection and Installation Manual, https://nadp.slh.wisc.edu/wp-content/uploads/2024/08/NADP-2010_Site_Selection_and_Installation_Manual_v_OB2.pdf, (accessed 23 April 2025).

60 A. F. Stein, R. R. Draxler, G. D. Rolph, B. J. B. Stunder, M. D. Cohen and F. Ngan, NOAA's HYSPLIT Atmospheric Transport and Dispersion Modeling System, *Bull. Am. Meteorol. Soc.*, 2015, **96**, 2059–2077.

61 X. Li, Y. Wang, J. Cui, Y. Shi and Y. Cai, Occurrence and Fate of Per- and Polyfluoroalkyl Substances (PFAS) in Atmosphere: Size-Dependent Gas-Particle Partitioning, Precipitation Scavenging, and Amplification, *Environ. Sci. Technol.*, 2024, **58**, 9283–9291.

62 H. Chen, L. Zhang, M. Li, Y. Yao, Z. Zhao, G. Munoz and H. Sun, Per- and polyfluoroalkyl substances (PFASs) in precipitation from mainland China: Contributions of unknown precursors and short-chain (C2 C3) perfluoroalkyl carboxylic acids, *Water Res.*, 2019, **153**, 169–177.

63 DRAFT State of Per- and Polyfluoroalkyl Substances (PFAS) Report Environment and Climate Change Canada Health Canada May 2023, https://www.canada.ca/en/environment-climate-change/services/evaluating-existing-substances/draft-state-per-polyfluoroalkyl-substances-report.html.

64 Government of Canada, Treasury Board of Canada: Federal Contaminated Sites Inventory, https://www.tbs-sct.gc.ca/fcsi-rscf/numbers-numeros-eng.aspx?qid=305787, (accessed 8 October 2024).

65 L. Ahrens, M. Shoeib, T. Harner, S. C. Lee, R. Guo and E. J. Reiner, Wastewater Treatment Plant and Landfills as Sources of Polyfluoroalkyl Compounds to the Atmosphere, *Environ. Sci. Technol.*, 2011, **45**, 8098–8105.

66 A. M. Lin, J. T. Thompson, J. P. Koelmel, Y. Liu, J. A. Bowden and T. G. Townsend, Landfill Gas: A Major Pathway for Neutral Per- and Polyfluoroalkyl Substance (PFAS) Release, *Environ. Sci. Technol. Lett.*, 2024, **11**, 730–737.

67 M. Zhang, X. Zhao, D. Zhao, T.-Y. Soong and S. Tian, Poly- and Perfluoroalkyl Substances (PFAS) in Landfills: Occurrence, Transformation and Treatment, *Waste Manag.*, 2023, **155**, 162–178.

68 E. S. Coffin, D. M. Reeves and D. P. Cassidy, PFAS in municipal solid waste landfills: Sources, leachate composition, chemical transformations, and future challenges, *Curr. Opin. Environ. Sci. Health*, 2023, **31**, 100418.

69 K. Goto-Azuma and R. M. Koerner, Ice core studies of anthropogenic sulfate and nitrate trends in the Arctic, *J. Geophys. Res. Atmospheres*, 2001, **106**, 4959–4969.

70 GenX Investigation | NC DEQ, https://www.deq.nc.gov/news/key-issues/genx-investigation, (accessed 17 December 2024).

71 A. Jahnke, L. Ahrens, R. Ebinghaus and C. Temme, Urban versus Remote Air Concentrations of Fluorotelomer Alcohols and Other Polyfluorinated Alkyl Substances in Germany, *Environ. Sci. Technol.*, 2007, **41**, 745–752.

72 Z. Xie, Z. Wang, W. Mi, A. Möller, H. Wolschke and R. Ebinghaus, Neutral Poly-/perfluoroalkyl Substances in Air and Snow from the Arctic, *Sci. Rep.*, 2015, **5**, 8912.

73 A. Saini, S. Chinnadurai, J. K. Schuster, A. Eng and T. Harner, Per- and polyfluoroalkyl substances and volatile methyl siloxanes in global air: Spatial and temporal trends, *Environ. Pollut.*, 2023, **323**, 121291.

74 C. P. Thackray, N. E. Selin and C. J. Young, A global atmospheric chemistry model for the fate and transport of PFCAs and their precursors, *Environ. Sci. Process. Impacts*, 2020, **22**, 285–293.

75 G. Yarwood, S. Kemball-Cook, M. Keinath, R. L. Waterland, S. H. Korzeniowski, R. C. Buck, M. H. Russell and S. T. Washburn, High-Resolution Atmospheric Modeling of Fluorotelomer Alcohols and Perfluorocarboxylic Acids in the North American Troposphere, *Environ. Sci. Technol.*, 2007, **41**, 5756–5762.

76 T. J. Wallington, M. D. Hurley, J. Xia, D. J. Wuebbles, S. Sillman, A. Ito, J. E. Penner, D. A. Ellis, J. Martin, S. A. Mabury, O. J. Nielsen and M. P. Sulbaek Andersen, Formation of $C_7F_{15}COOH$ (PFOA) and Other Perfluorocarboxylic Acids during the Atmospheric Oxidation of 8:2 Fluorotelomer Alcohol, *Environ. Sci. Technol.*, 2006, **40**, 924–930.

77 Z. Wang, I. T. Cousins, M. Scheringer, R. C. Buck and K. Hungerbuhler, Global emission inventories for C4-C14 perfluoroalkyl carboxylic acid (PFCA) homologues from 1951 to 2030, Part II: The remianing pieces of the puzzle, *Environ. Int.*, 2014, **69**, 166–176.

78 R. C. Sullivan, S. A. Guazzotti, D. A. Sodeman and K. A. Prather, Direct observations of the atmospheric processing of Asian mineral dust, *Atmospheric Chem. Phys.*, 2007, **7**, 1213–1236.

79 Y. Zhi, H. Lu, K. D. Grieger, G. Munoz, W. Li, X. Wang, Q. He and S. Qian, Bioaccumulation and Translocation of 6:2 Fluorotelomer Sulfonate, GenX, and Perfluoroalkyl Acids by Urban Spontaneous Plants, *ACS EST Eng.*, 2022, **2**, 1169–1178.

80 A. A. Frossard, V. Gérard, P. Duplessis, J. D. Kinsey, X. Lu, Y. Zhu, J. Bisgrove, J. R. Maben, M. S. Long, R. Y.-W. Chang, S. R. Beaupré, D. J. Kieber, W. C. Keene, B. Nozière and R. C. Cohen, Properties of Seawater Surfactants Associated with Primary Marine Aerosol Particles Produced by Bursting Bubbles at a Model Air–Sea Interface, *Environ. Sci. Technol.*, 2019, **53**, 9407–9417.

81 M. van Pinxteren, S. Zeppenfeld, K. W. Fomba, N. Triesch, S. Frka and H. Herrmann, Amino acids, carbohydrates, and lipids in the tropical oligotrophic Atlantic Ocean: sea-

to-air transfer and atmospheric in situ formation, *Atmospheric Chem. Phys.*, 2023, **23**, 6571–6590.

82 D. J. Jacob, *Introduction to atmospheric chemistry*, Princeton university press, Princeton, 1999.

83 C. J. Young, S. Joudan, Y. Tao, J. J. B. Wentzell and J. Liggio, High Time Resolution Ambient Observations of Gas-Phase Perfluoroalkyl Carboxylic Acids: Implications for Atmospheric Sources, *Environ. Sci. Technol. Lett.*, 2024, **11**, 1348–1354.

84 J. J. MacInnis, I. Lehnherr, D. C. G. Muir, K. A. St. Pierre, V. L. St. Louis, C. Spencer and A. O. De Silva, Fate and Transport of Perfluoroalkyl Substances from Snowpacks into a Lake in the High Arctic of Canada, *Environ. Sci. Technol.*, 2019, **53**, 10753–10762.

85 J. Garnett, C. Halsall, H. Winton, H. Joerss, R. Mulvaney, R. Ebinghaus, M. Frey, A. Jones, A. Leeson and P. Wynn, Increasing Accumulation of Perfluorocarboxylate Contaminants Revealed in an Antarctic Firn Core (1958–2017), *Environ. Sci. Technol.*, 2022, **56**, 11246–11255.

86 Z. Wang, I. T. Cousins, M. Scheringer, R. C. Buck and K. Hungerbühler, Global emission inventories for C4-C14 perfluoroalkyl carboxylic acid (PFCA) homologues from 1951 to 2030, Part I: Production and emissions from quantifiable sources, *Environ. Int.*, 2014, **70**, 62–75.

87 Intergovernmental Panel On Climate Change, Ed., in *Climate Change 2013 – The Physical Science Basis*, Cambridge University Press, 1st edn., 2014, pp. 659–740.

88 A. Dreyer and R. Ebinghaus, Polyfluorinated compounds in ambient air from ship- and land-based measurements in northern Germany, *Atmos. Environ.*, 2009, **43**, 1527–1535.

89 N. L. Stock, F. K. Lau, D. A. Ellis, J. W. Martin, D. C. G. Muir and S. A. Mabury, Polyfluorinated Telomer Alcohols and Sulfonamides in the North American Troposphere, *Environ. Sci. Technol.*, 2004, **38**, 991–996.

CHAPTER 4

Atmospheric removal of TFA by dry and wet deposition: a multi year analysis in Toronto

Daniel Persaud[1], Shira Joudan[1†], Trevor C. VandenBoer[1], and Cora J. Young[1*]

[1]Department of Chemistry, York University, Toronto, ON, M3J1P3

[†]Now at Department of Chemistry, University of Alberta, Edmonton, AB, T6G 2G2

Published: Reproduced with permission from Persaud, D.; Joudan, S.; VandenBoer, T. C.; et al. *Atmospheric Removal of Trifluoroacetic Acid by Dry and Wet Deposition: A Multiyear Analysis in Toronto*. *Environmental Science & Technology Letters* 2026.

Author Contributions:

Trevor C. VandenBoer and Cora J. Young conceived of and designed the experiment. Daniel Persaud collected and analyzed the samples with assistance from Shira Joudan. Daniel Persaud analyzed the data and wrote the manuscript with input from all authors. Funding was acquired by Trevor C. VandenBoer and Cora J. Young.

4.1 Introduction

Trifluoroacetic acid (CF_3COOH, TFA) is an ultrashort-chain perfluoroalkyl acid (PFAA), a subgroup of per- and polyfluoroalkyl substances (PFAS). TFA is an anthropogenic molecule that is mobile, phytotoxic, and persistent in the environment with an estimated lifetime longer than ten thousand years.[1,2] High persistence results in TFA accumulation in environmental compartments and has led to its widespread detection in oceans,[3,4] air,[5–7] precipitation, [8–18] plants,[19] soil,[20] and human serum.[21] Concentrations of TFA are consistently 1–2 orders of magnitude greater than other legacy PFAS.[22] Initial interest in the environmental fate and effects of TFA began in the 1990s, with the introduction of replacement compounds for stratospheric ozone-depleting chlorofluorocarbons. Replacement hydrofluorocarbons (HFCs) and hydrochlorofluorocarbons (HCFCs) had other environmental impacts, such as appreciable global warming potential, and selected compounds within these classes (e.g., HFC-134a) produce TFA as a degradation product.[23] Early risk assessment reported lower bioaccumulation and toxicity of TFA compared to other PFAAs.[2,24,25] However, these did not consider the accumulation of TFA in water resources and plants.[26] Although TFA does not bioaccumulate in the conventional sense, elevated levels in humans and the environment are cause for concern.[27]

Interest in TFA has reemerged due to increasing concentration in remote locations,[28] archived plant leaves,[19] groundwater[29] as well as detection in human blood and urine.[21,30,31] Additionally, the global TFA burden is expected to increase due to increasing emissions of hydrofluoroolefin (HFO) gases, like 2,3,3,3-tetrafluoropropene (HFO-1234yf), which reacts with hydroxyl radical to form TFA in 100 % yield,[32] which can be subsequently removed by wet and dry deposition.

Wet deposition scavenges gases and particles and transports them to the surface through precipitation (e.g., rain or snow), whereas dry deposition removes gas and particle phase species from the atmosphere by gravitational settling, impaction, interception, and/or diffusion.[33] While wet deposition is episodic and is dependent on precipitation amount and intensity, dry deposition is a continuous process. For a given parcel of air, strong and frequent rainfall can deplete TFA, reducing its downwind dry deposition until it remixes fully with background air or interacts with new sources.

Several measurements of TFA in precipitation were made from the mid-1990s to early 2000s.[8,10–13,19,34] These measurements were of total (bulk) deposition, which includes both wet and dry deposition, but cannot distinguish between them. Attempts have been made to estimate the dry deposition contribution of TFA using chemical models.[32,35–37] However, available models are limited by uncertain deposition parameters and remain unvalidated by observations. Our study aimed to (i) determine the temporal variation of TFA in total and wet deposition in an urban environment, (ii) calculate the dry deposition fraction of the total, and (iii) compare our measured values to available chemical models. To the best of our knowledge, this is the first study that quantifies TFA deposited in total, wet, and dry deposition fractions.

4.2 Materials and Methods

4.2.1 Sample Collection

Integrated total and wet deposition samples were collected continuously at the Air Quality Research Station, York University, Toronto, Canada (~25 m above ground; 43.7735 N, 79.5069 W) ~10 km northwest of downtown Toronto. The site is located in a mixed suburban–urban area with moderate vehicle traffic, residential areas and proximity to light industrial zones, without expected point sources based on the current state of knowledge. Wet deposition samples were collected from November 2018 to December 2024 using custom-built precipitation samplers, described previously.[38] The automated system features a motorized lid for selective collection of precipitation, excluding dry deposition. Total deposition samples were collected from May 2018 to December 2024 using a permanently open system, collecting both wet and dry deposition. To determine the dry deposition contribution, we subtract wet deposition values from total deposition. This method of calculating dry deposition contribution was previously validated.[38] After collection, all sample volumes were measured then stored at 4 ºC until analysis.

4.2.2 Sample Preparation and Analysis

Total and wet deposition samples were equilibrated at room temperature, then a 10 mL aliquot was withdrawn into a polypropylene syringe (P/N: 14-817-44. Fischer Scientific) and filtered through a 0.22 µm syringe filter (P/N: 76479-030, VWR) into a precleaned polypropylene conical tube (14-959-53A, Fisher Scientific). Then an 800 µL

sample was transferred along with 100 µL $^{13}C_2$ or $^{13}C_1$ TFA internal standard (20 µg L^{-1}) to a 1.0 mL polypropylene vial (5182-0567, Agilent). Analysis of TFA was done by direct injection of 750 µL into a concentrator column, followed by ion chromatography with mass spectrometry detection (IC-MS). TFA was separated by anion exchange using a hydroxide gradient (Table C-1) and detection was performed with a quadrupole MS operating in negative electrospray ionization mode (Table C-2).

4.2.3 Quality Assurance and Quality Control

Field blanks consisting of 1 L of deionized water were deployed simultaneously with the deposition samplers and opened for ~10 seconds during sample collection. TFA was below the method detection limit in all field blanks.

Sample concentrations were quantified based on relative response of TFA to the internal standard. A 12-level calibration curve was employed for quantification, ranging from 0.05 to 10 µg L^{-1}. Check standards (0.25 µg L^{-1}) were included every ten injections to assess reproducibility. Deionized water laboratory blanks were analyzed to monitor potential contamination and determine limit of detection and limit of quantification. Further QA/QC details are in Section B-2.4.

4.3 Results and Discussion

4.3.1 TFA concentration and fluxes

TFA was detected in 100 % of total (n=103) and wet (n=98) deposition samples collected between 2018–2024. Given the non-normal distribution and the presence of elevated levels of TFA, we report the median as a representative measure of central tendency. Measured total deposition concentrations ranged from 0.07–4.55 µg L^{-1} (median: 0.54 µg L^{-1}), whereas wet deposition ranged from 0.09–3.19 µg L^{-1} (median: 0.58 µg L^{-1}, Tables C-3 and C-4). The measurements are comparable to previously reported concentrations in mid-latitude precipitation (0.002–38 µg L^{-1}) collected between 1994–2023 (Table C-5).[4,8,10–13,34,39–41] Interestingly, the median TFA concentration measured in our total deposition samples (0.54 µg L^{-1}) is approximately two times greater than the maximum values reported during the 2003–2004 period in Toronto (0.27 µg L^{-1}). This agrees with recent gas-phase measurements in Toronto, which also increased by a

factor of approximately two between 2000 and 2022.[5,42] A similar increasing trend of TFA in atmospheric deposition over time was reported in the Canadian Arctic and in Germany.[28,41] Both studies concluded the increased deposition is likely due to higher atmospheric mixing ratios of precursor compounds (HFCs, HCFCs, HFOs). We propose that a similar precursor-driven mechanism is responsible for the observed TFA in the current study.

Direct comparison between concentrations in precipitation is problematic when thinking about environmental processes transferring pollutants between compartments. For rainwater, concentration is inversely proportional to volume, complicating spatial comparisons. Converting the concentration (μg L^{-1}) to deposition flux using the volume, area of the sampler, and sampling duration (μg m^{-2} d^{-1}) provides robust comparisons. Fluxes were normalized to an annual scale (μg m^{-2} a^{-1}, Table C-3 and C-4) to remove sample duration effects. Fluxes of TFA in total deposition ranged from 66–1500 μg m^{-2} a^{-1} (median: 300 μg m^{-2} a^{-1}), while wet deposition fluxes ranged from 24–610 μg m^{-2} a^{-1} (median: 200 μg m^{-2} a^{-1}; Figure 4-1 A). A moderate relationship between concentration and fluxes (Figure C-4, $R^2 = 0.48$) demonstrates that at most, concentration can account for ~50 % of the observed variance in deposition flux. This relationship implies that concentration is a moderate predictor of TFA deposition flux, but that deposition is also driven by other factors (e.g., gas phase abundance, temperature). Thus, comparison with other studies is not straightforward since only a few studies report fluxes and available fluxes are not always normalized for duration. Among studies that report duration-normalized flux, most predate the widespread use of modern TFA precursors and/or were taken from remote regions. Estimates of available TFA fluxes are summarized in Table C-5. Generally, our median total deposition flux (300 μg m^{-2} a^{-1}) is approximately two times lower than the median flux recently reported in Switzerland (2021–2023) (555 μg m^{-2} a^{-1})[40], but is comparable to the median fluxes observed in wet deposition across several sites in Germany in 2018 (193 μg m^{-2} a^{-1})[41] and to total atmospheric inputs reported in Guangzhou, China in 2007–2008 (229 μg m^{-2} a^{-1})[18] and Switzerland in 1996 (230 μg m^{-2} a^{-1}).[12] We call for a standardized reporting of normalized annual TFA fluxes (μg m^{-2} a^{-1}), which will allow for ongoing comparisons of deposition collected over any duration in different regions globally and into the future.

We compared our measured deposition fluxes to chemical transport models that predict TFA atmospheric deposition primarily from the degradation of HFO-1234yf under specified emission scenarios,[32,35–37,43] with earlier works simulating deposition from HCFCs and HFC-134a.[6,42,44] Existing models do not directly simulate deposition for our study area or time period. Instead, we compared the mean measured TFA deposition for the entire sampling period to the mean modelled levels in different regions. Generally, our total deposition fluxes were comparable to available model estimates (Table C-6). Interestingly, the mean total deposition flux measured in the current study (425 μg m^{-2} a^{-1}) was comparable to predicted future deposition in the US (500 μg m^{-2} a^{-1}) and the EU (540 μg m^{-2} a^{-1}) from HFO-1234yf alone and exceeds the predicted global average (180 μg m^{-2} a^{-1}) by 2030.[36] The agreement is notable because those scenarios consider TFA produced from HFO-1234yf and a limited set of other precursors, whereas our measurements integrate all sources. Our findings suggest that the increased use of HFO-1234yf could result in TFA deposition beyond levels considered in risk assessments. We call for other observational constraints to derive more benchmarks for evaluating and refining model TFA deposition.

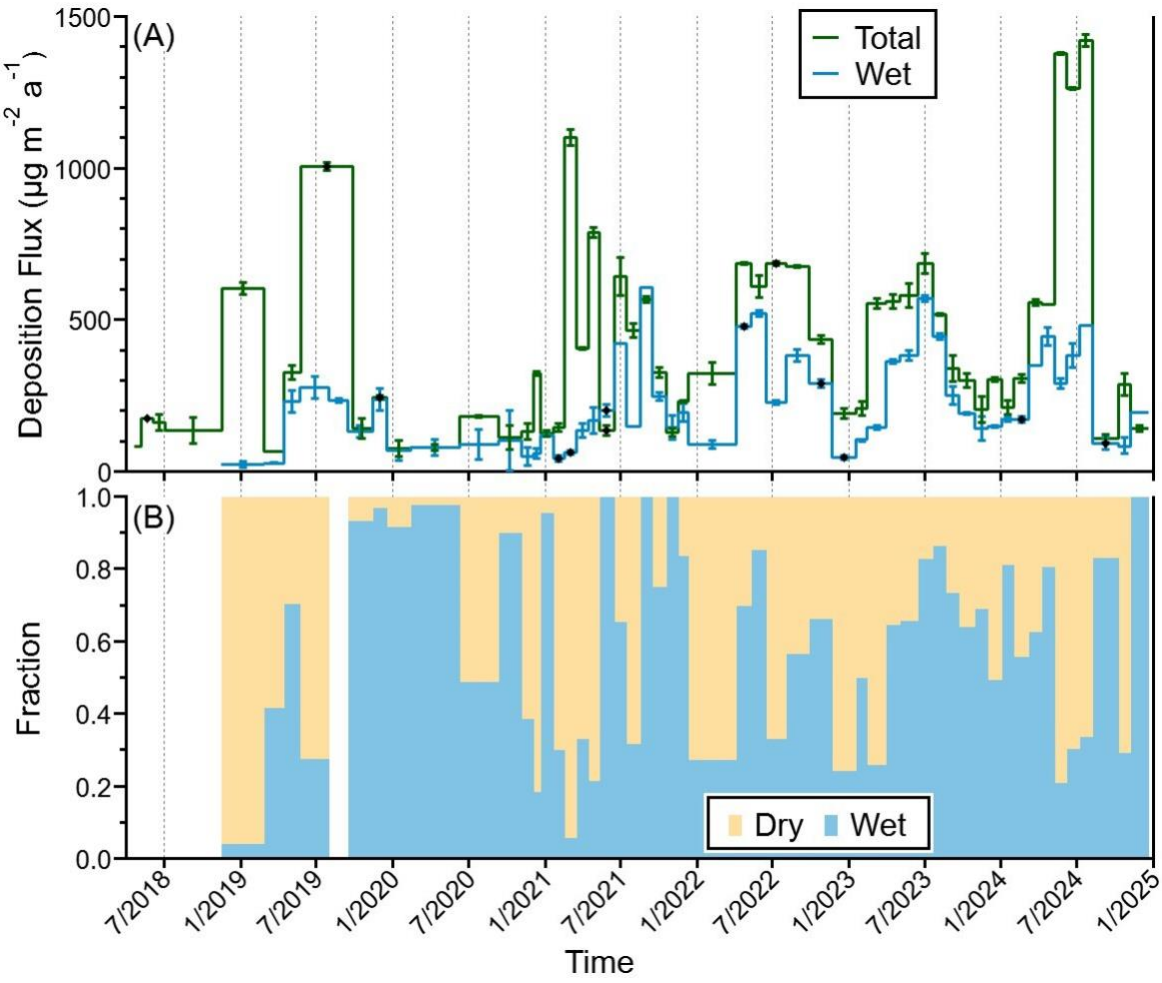

Figure 4-1: Time series of the average deposition flux (µg m^{-2} a^{-1}) of TFA in (A) total deposition (green trace) and wet-only deposition (blue trace) for the period 2018–2024, and (B) fraction of wet (blue) and dry deposition (orange) to the total deposition of TFA. The dry deposition contribution was only calculated for sample periods with matched start and end dates for total and wet samples. The blue and green error bars represent the relative error determined between two independent samples. In instances where we obtained a single sample (¨), we propagate errors from all measurements and analytical determinations to derive an estimated uncertainty.

4.3.2 Temporal and seasonal variations

We utilized the temporal record to look for trends in annual atmospheric deposition of TFA and did not find any increase from 2018 to 2024. This apparent discrepancy with the predicted TFA enhancement from increasing HFO-1234yf use likely reflect that deposition at our site represents contributions from multiple precursors with variability, which can obscure increasing trends expected from a single compound. This chemical

uncertainty combined with natural variability in atmospheric transport and precipitation dynamics complicates trend elucidation at this time. We used the Kruskal-Wallis test to evaluate differences in TFA deposition across years within the 2019–2024 period, followed by post-hoc Dunn's test with Bonferroni correction.[45,46] The post-hoc test revealed that the deposition flux in 2020 was statistically different from the other years ($p<0.05$), with median fluxes in 2019 and 2021–2024 approximately 2–5 times greater than the median flux measured in 2020 (Figure 4-2A). This anomaly coincides with the first year of the COVID-19 pandemic, which led to widespread reduction in many anthropogenic pollutant emissions, particularly nitrogen oxides (NO_x).[47,48] While lower NO_x would be expected to both increase the yield of TFA formation from some halocarbon precursors (e.g., HFCs, HCFCs, and HFOs)[49] and increase the rate of formation through increased hydroxyl radicals,[5] we observed a decrease in TFA deposition. Since the atmospheric abundances of long-lived TFA precursors (e.g., HFC-134a) are minimally affected by short-term changes in emissions,[50,51] our observations suggest that reduced emissions of short-lived precursors, including HFOs,[49] hydrochlorofluoroolefins,[52] and fluorotelomer compounds[49] may have contributed to the decline of TFA deposition. We acknowledge that annual differences in meteorology, including precipitation patterns and air mass origin can also modulate TFA deposition and can contribute to the observed decline in 2020. Disentangling these effects would require real time gas and particle measurements of TFA, combined with high resolution measurements of oxidants, meteorology, and all precursors.

Within a given year, seasonal variation of TFA deposition had fluxes peaking in the summer and minimizing in winter (Figure 4-2B). Elevated summer TFA is expected since the mixing ratios of atmospheric oxidants and TFA precursors are both known to be elevated during this time.[53] A similar seasonal trend was observed in German precipitation samples,[41] as well as gas-phase measurements in Beijing[6,7] and Toronto.[5] Modelling studies predict increased deposition in the summer compared to other seasons for the same chemical reasons.[36] Our observations are in agreement with a growing body of evidence suggesting the abundance of atmospheric TFA is primarily driven by atmospheric oxidation of precursors, while its deposition reflects its abundance.

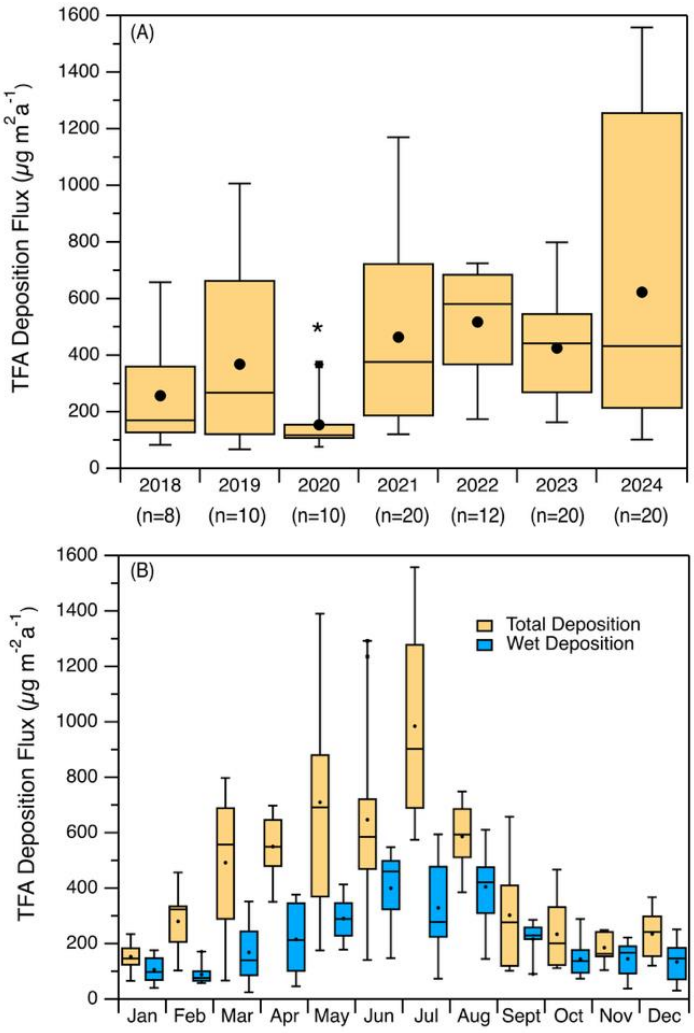

Figure 4-2: Boxplots of TFA deposition fluxes (μg m^{-2} a^{-1}) for 2018–2024. (A) Annual total deposition fluxes, where boxes represent the interquartile range (25^{th}–75^{th} percentile), horizontal lines indicate the median, filled circles represent means and whiskers denote the minimum and maximum values. Note that 2018 represents a partial year and (*) indicates that total deposition was significantly different in 2020 compared to 2019, 2021–2024. (B) Monthly distribution of TFA fluxes in total (orange) and wet (blue) deposition for the entire sampling period. Boxes, median, mean and whiskers are defined as in panel A. Fluxes spanning multiple months were assigned to the month containing the midpoint date

4.3.3 Dry deposition contribution

Although numerous studies have quantified the concentration and fluxes of TFA in precipitation, to the best of our knowledge, no study has used measurements to quantify the relative contribution of dry deposition to the total TFA flux. Quantifying the dry deposition contribution is essential for validating the assumptions in the modelled environmental fate of TFA.

Generally, we found that dry deposition contributed substantively to the removal of TFA from the atmosphere. The median calculated dry deposition of TFA was 106 μg m^{-2} a^{-1} for the entire sampling period, with a maximum value of 1088 μg m^{-2} a^{-1} occurring during the summer months (Table C-7). The median fraction of total deposition attributed to dry deposition for TFA was 37 % (Figure 4-1B). Although there was considerable variability in the contribution of dry deposition from 0 to 94 %, we observed that dry deposition exceeded wet deposition in 37 % of the samples, indicating that this pathway plays a role in total atmospheric removal. Consequently, relying on wet deposition measurements alone would regularly and substantially underestimate total inputs.

Although no previous measurements of TFA dry deposition exist, efforts have been made to estimate the dry deposition contribution using chemical transport models (CTM, Figure C-5,Table C-6). The wide range of measured dry deposition contributions (0–94 %) in Toronto unsurprisingly encompassed CTM estimates. For instance, Luecken et al. predicted that dry deposition accounts for 10–75 % of the total deposition in the Continental US.[32] It is important to note that this was a high emission scenario for the summertime, assuming that ~50 % of the annual HFO-1234yf emission was released.[32] Most other studies report mean deposition, which was compared to the mean contribution observed in our study. Generally, our observed mean of 45 % dry deposition is in reasonable agreement with two CTM estimates using air and particle measurements and the Atkinson Box Model of 50 % (Toronto)[42] and 40 % (Beijing)[6] but is higher than most other estimates made using CTMs, which mostly fall between 17-37 %.[35,43,54] These differences suggest a potential systematic underestimation of this deposition pathway. Discrepancies of TFA dry deposition contribution are expected since most models simulated large geographic areas over a single year, considered a sub-set of potential precursors, and assumed that nitric acid is an effective proxy for estimating the atmospheric behavior of TFA.[6,32,35–37,42–44] However, the key controls of nitric acid deposition through its gas-particle partitioning, heterogeneous uptake to coarse aerosol, and deposition velocity are poorly constrained themselves,[55,56] and though TFA has chemical similarities to nitric acid its partitioning may be quite different.[57]

While this is the first measurement of dry deposition of TFA, a few studies have attempted to quantify the deposition mechanism for other PFAAs. For instance, Xia et al.

concluded that one-third of perfluorooctane sulfonate (PFOS) was deposited via dry deposition.[58] Another study found that wet deposition removed PFAS by an order of magnitude greater than dry deposition.[59] These inconsistencies highlight the reality of atmospheric dynamics (e.g., transport pathways and precipitation frequency) and chemical properties (e.g., abundance, partitioning, reactivity, and deposition velocity) that drive complexity and variability in the relative roles of wet and dry deposition mechanisms as a function of time. Our findings suggest that dry deposition is a non-negligible and often dominant removal mechanism of TFA from the atmosphere, a factor that must be included in future risk assessments and CTMs.

4.4 Implications

This study provides a six-year wet and dry deposition record of TFA, addressing a critical data gap for this pollutant for the first time. We found that TFA is detected in 100 % of atmospheric deposition in Toronto, with a median flux of 300 $\mu g\ m^{-2}\ a^{-1}$ in total deposition samples and 200 $\mu g\ m^{-2}\ a^{-1}$ in wet deposition samples. The temporal record showed a seasonal variation of TFA, with maximum fluxes observed during the summer. This supports the hypothesis that the atmospheric oxidation of CFC replacement compounds is a major source of TFA in the atmosphere and that is removed in part by precipitation. The lower flux observed in 2020 likely reflects short-term changes in precursor emissions associated with COVID-19 restrictions, rather than a sustained reduction in TFA precursors relative to other sources. The consistent seasonal trends also highlight that selecting a representative time is important when reporting concentration and fluxes in the atmosphere to avoid bias in TFA levels.

This study also produced the first simultaneous measurements of wet and dry deposition of TFA. We observed that dry deposition is a highly variable process, but could be a substantial deposition mechanism for TFA, with a mean contribution of 106 $\mu g\ m^{-2}\ a^{-1}$ corresponding to 45 % (median 37%) of the total TFA deposition over individual sampling periods. We strongly recommend future measurements of TFA to explicitly differentiate between the wet and dry deposition processes to improve our understanding of PFAA transport and fate, but also to improve the accuracy of CTM deposition parameterizations.

4.5 References

(1) Scheurer, M.; Nödler, K.; Freeling, F.; Janda, J.; Happel, O.; Riegel, M.; Müller, U.; Storck, F. R.; Fleig, M.; Lange, F. T.; Brunsch, A.; Brauch, H.-J. Small, Mobile, Persistent: Trifluoroacetate in the Water Cycle – Overlooked Sources, Pathways, and Consequences for Drinking Water Supply. *Water Research* **2017**, *126*, 460–471. https://doi.org/10.1016/j.watres.2017.09.045.

(2) Boutonnet, J. C.; Bingham, P.; Calamari, D.; de Rooij, C.; Franklin, J.; Kawano, T.; Libre, J.-M.; McCulloch, A.; Malinverno, G.; Odom, J. M.; Rusch, G. M.; Smythe, K.; Sobolev, I.; Thompson, R.; Tiedje, J. M. Environmental Risk Assessment of Trifluoroacetic Acid. *Human and Ecological Risk Assessment: An International Journal* **1999**, *5* (1), 59–124. https://doi.org/10.1080/10807039991289644.

(3) Frank, H.; Christoph, E. H.; Holm-Hansen, O.; Bullister, J. L. Trifluoroacetate in Ocean Waters. *Environ. Sci. Technol.* **2002**, *36* (1), 12–15. https://doi.org/10.1021/es0101532.

(4) Scott, B. F.; Macdonald, R. W.; Kannan, K.; Fisk, A.; Witter, A.; Yamashita, N.; Durham, L.; Spencer, C.; Muir, D. C. G. Trifluoroacetate Profiles in the Arctic, Atlantic, and Pacific Oceans. *Environmental Science and Technology* **2005**, *39* (17), 6555–6560. https://doi.org/10.1021/es047975u.

(5) Young, C. J.; Joudan, S.; Tao, Y.; Wentzell, J. J. B.; Liggio, J. High Time Resolution Ambient Observations of Gas-Phase Perfluoroalkyl Carboxylic Acids: Implications for Atmospheric Sources. *Environ. Sci. Technol. Lett.* **2024**, *11* (12), 1348–1354. https://doi.org/10.1021/acs.estlett.4c00897.

(6) Wu, J.; Martin, J. W.; Zhai, Z.; Lu, K.; Li, L.; Fang, X.; Jin, H.; Hu, J.; Zhang, J. Airborne Trifluoroacetic Acid and Its Fraction from the Degradation of HFC-134a in Beijing, China. *Environmental Science and Technology* **2014**, *48* (7), 3675–3681. https://doi.org/10.1021/es4050264.

(7) Zhang, B.; Zhai, Z.; Zhang, J. Distribution of Trifluoroacetic Acid in Gas and Particulate Phases in Beijing from 2013 to 2016. *Science of The Total Environment* **2018**, *634*, 471–477. https://doi.org/10.1016/j.scitotenv.2018.03.384.

(8) Chen, H.; Zhang, L.; Li, M.; Yao, Y.; Zhao, Z.; Munoz, G.; Sun, H. Per- and Polyfluoroalkyl Substances (PFASs) in Precipitation from Mainland China:

Contributions of Unknown Precursors and Short-Chain (C2 C3) Perfluoroalkyl Carboxylic Acids. *Water Research* **2019**, *153*, 169–177. https://doi.org/10.1016/j.watres.2019.01.019.

(9) Pike, K. A.; Edmiston, P. L.; Morrison, J. J.; Faust, J. A. Correlation Analysis of Perfluoroalkyl Substances in Regional U.S. Precipitation Events. *Water Research* **2021**, *190*, 116685. https://doi.org/10.1016/j.watres.2020.116685.

(10) Scott, B. F.; Mactavish, D.; Spencer, C.; Strachan, W. M. J.; Muir, D. C. G. Haloacetic Acids in Canadian Lake Waters and Precipitation. *Environ. Sci. Technol.* **2000**, *34* (20), 4266–4272. https://doi.org/10.1021/es9908523.

(11) Von Sydow, L. M.; Grimvall, A. B.; Borén, H. B.; Laniewski, K.; Nielsen, A. T. Natural Background Levels of Trifluoroacetate in Rain and Snow. *Environmental Science and Technology* **2000**, *34* (15), 3115–3118. https://doi.org/10.1021/es9913683.

(12) Berg, M.; Müller, S. R.; Mühlemann, J.; Wiedmer, A.; Schwarzenbach, R. P. Concentrations and Mass Fluxes of Trifluoroacetic Acid in Rain and Natural Waters in Switzerland. *Environmental Science and Technology* **2000**, *34* (13), 2675–2683. https://doi.org/10.1021/es990855f.

(13) Frank, H.; Klein, A.; Renschen, D. Environmental Trifluoroacetate. *Nature* **1996**, *382*, 34. https://doi.org/10.1038/382034a0.

(14) Björnsdotter, M. K.; Yeung, L. W. Y.; Kärrman, A.; Jogsten, I. E. Mass Balance of Perfluoroalkyl Acids, Including Trifluoroacetic Acid, in a Freshwater Lake. *Environ. Sci. Technol.* **2022**, *56* (1), 251–259. https://doi.org/10.1021/acs.est.1c04472.

(15) Scott, B. F.; Spencer, C.; Martin, J. W.; Barra, R.; Bootsma, H. A.; Jones, K. C.; Johnston, A. E.; Muir, D. C. G. Comparison of Haloacetic Acids in the Environment of the Northern and Southern Hemispheres. *Environmental Science and Technology* **2005**, *39* (22), 8664–8670. https://doi.org/10.1021/es050118l.

(16) Scott, B. F.; Spencer, C.; Mabury, S. A.; Muir, D. C. G. Poly and Perfluorinated Carboxylates in North American Precipitation. *Environ. Sci. Technol.* **2006**, *40* (23), 7167–7174. https://doi.org/10.1021/es061403n.

(17) Wujcik, C. E.; Cahill, T. M.; Seiber, J. N. Determination of Trifluoroacetic Acid in 1996 - 1997 Precipitation and Surface Waters in California and Nevada.

Environmental Science and Technology **1999**, *33* (10), 1747–1751. https://doi.org/10.1021/es980697c.

(18) Wang, Q.; Wang, X.; Ding, X. Rainwater Trifluoroacetic Acid (TFA) in Guangzhou, South China: Levels, Wet Deposition Fluxes and Source Implication. *Science of The Total Environment* **2014**, *468–469*, 272–279. https://doi.org/10.1016/j.scitotenv.2013.08.055.

(19) Freeling, F.; Scheurer, M.; Koschorreck, J.; Hoffmann, G.; Ternes, T. A.; Nödler, K. Levels and Temporal Trends of Trifluoroacetate (TFA) in Archived Plants: Evidence for Increasing Emissions of Gaseous TFA Precursors over the Last Decades. *Environmental Science & Technology Letters* **2022**, *9*, 400–405. https://doi.org/10.1021/acs.estlett.2c00164.

(20) Cahill, T. M.; Benesch, J. A.; Gustin, M. S.; Zimmerman, E. J.; Seiber, J. N. Simplified Method for Trace Analysis of Trifluoroacetic Acid in Plant, Soil, and Water Samples Using Headspace Gas Chromatography. *Analytical Chemistry* **1999**, *71* (20), 4465–4471. https://doi.org/10.1021/ac990484l.

(21) Duan, Y.; Sun, H.; Yao, Y.; Meng, Y.; Li, Y. Distribution of Novel and Legacy Per-/Polyfluoroalkyl Substances in Serum and Its Associations with Two Glycemic Biomarkers among Chinese Adult Men and Women with Normal Blood Glucose Levels. *Environment International* **2019**, *134*. https://doi.org/10.1016/j.envint.2019.105295.

(22) Chen, H.; Yao, Y.; Zhao, Z.; Wang, Y.; Wang, Q.; Ren, C.; Wang, B.; Sun, H.; Alder, A. C.; Kannan, K. Multimedia Distribution and Transfer of Per- and Polyfluoroalkyl Substances (PFASs) Surrounding Two Fluorochemical Manufacturing Facilities in Fuxin, China. *Environ. Sci. Technol.* **2018**, *52* (15), 8263–8271. https://doi.org/10.1021/acs.est.8b00544.

(23) Wallington, T. J.; Hurley, M. D.; Fracheboud, J. M.; Orlando, J. J.; Tyndall, G. S.; Sehested, J.; Møgelberg, T. E.; Nielsen, O. J. Role of Excited CF3CFHO Radicals in the Atmospheric Chemistry of HFC-134a. *Journal of Physical Chemistry* **1996**, *100* (46), 18116–18122. https://doi.org/10.1021/jp9624764.

(24) Hanson, M. L.; Solomon, K. R. Haloacetic Acids in the Aquatic Environment. Part I: Macrophyte Toxicity. *Environmental Pollution* **2004**, *130* (3), 371–383. https://doi.org/10.1016/j.envpol.2003.12.016.

(25) Likens, G. E.; Tartowski, S. L.; Berger, T. W.; Richey, D. G.; Driscoll, C. T.; Frank, H. G.; Klein, A. Transport and Fate of Trifluoroacetate in Upland Forest and Wetland Ecosystems. *Proceedings of the National Academy of Sciences of the United States of America* **1997**, *94*, 4499–4503. https://doi.org/10.1073/pnas.94.9.4499.

(26) Arp, H. P. H.; Gredelj, A.; Glüge, J.; Scheringer, M.; Cousins, I. T. The Global Threat from the Irreversible Accumulation of Trifluoroacetic Acid (TFA). *Environ. Sci. Technol.* **2024**, *58* (45), 19925–19935. https://doi.org/10.1021/acs.est.4c06189.

(27) Joudan, S.; De Silva, A. O.; Young, C. J. Insufficient Evidence for the Existence of Natural Trifluoroacetic Acid. *Environmental Science: Processes and Impacts* **2021**, *23* (11), 1641–1649. https://doi.org/10.1039/d1em00306b.

(28) Pickard, H. M.; Criscitiello, A. S.; Persaud, D.; Spencer, C.; Muir, D. C. G.; Lehnherr, I.; Sharp, M. J.; De Silva, A. O.; Young, C. J. Ice Core Record of Persistent Short-Chain Fluorinated Alkyl Acids: Evidence of the Impact From Global Environmental Regulations. *Geophysical Research Letters* **2020**, *47* (10), e2020GL087535. https://doi.org/10.1029/2020GL087535.

(29) Albers, C. N.; Sültenfuss, J. A 60-Year Increase in the Ultrashort-Chain PFAS Trifluoroacetate and Its Suitability as a Tracer for Groundwater Age. *Environ. Sci. Technol. Lett.* **2024**, *11* (10), 1090–1095. https://doi.org/10.1021/acs.estlett.4c00525.

(30) Zheng, G.; Eick, S. M.; Salamova, A. Elevated Levels of Ultrashort- and Short-Chain Perfluoroalkyl Acids in US Homes and People. *Environ. Sci. Technol.* **2023**, *57* (42), 15782–15793. https://doi.org/10.1021/acs.est.2c06715.

(31) Muir, D. C. G.; Freeling, F.; Nilsson, S.; Bugsel, B.; Bowles, K.; Hobson, P.; Toms, L.-M.; Mueller, J. F. Trifluoroacetic Acid in Australian Human Urine Samples. *Environ. Sci. Technol. Lett.* **2025**, *12* (10), 1411–1417. https://doi.org/10.1021/acs.estlett.5c00678.

(32) Luecken, D. J.; Waterland, R. L.; Papasavva, S.; Taddonio, K. N.; Hutzell, W. T.; Rugh, J. P.; Andersen, S. O. Ozone and TFA Impacts in North America from Degradation of 2,3,3,3-Tetrafluoropropene (HFO-1234yf), a Potential Greenhouse

Gas Replacement. *Environmental Science and Technology* **2010**, *44* (1), 343–348. https://doi.org/10.1021/es902481f.

(33) Finlayson-Pitts, B. J.; Pitts, J. N. *Chemistry of the Upper and Lower Atmosphere: Theory, Experiments, and Applications*; Academic Press, 2000.

(34) Wujcik, C. E.; Cahill, T. M.; Seiber, J. N. Extraction and Analysis of Trifluoroacetic Acid in Environmental Waters. *Analytical Chemistry* **1998**, *70* (19), 4074–4080. https://doi.org/10.1021/ac9802123.

(35) Kazil, J.; McKeen, S.; Kim, S.-W.; Ahmadov, R.; Grell, G. A.; Talukdar, R. K.; Ravishankara, A. R. Deposition and Rainwater Concentrations of Trifluoroacetic Acid in the United States from the Use of HFO-1234yf. *Journal of Geophysical Research: Atmospheres* **2014**, *119* (24), 14,059-14,079. https://doi.org/10.1002/2014JD022058.

(36) Wang, Z.; Wang, Y.; Li, J.; Henne, S.; Zhang, B.; Hu, J.; Zhang, J. Impacts of the Degradation of 2,3,3,3-Tetrafluoropropene into Trifluoroacetic Acid from Its Application in Automobile Air Conditioners in China, the United States, and Europe. *Environ. Sci. Technol.* **2018**, *52* (5), 2819–2826. https://doi.org/10.1021/acs.est.7b05960.

(37) Henne, S.; Shallcross, D. E.; Reimann, S.; Xiao, P.; Brunner, D.; O'Doherty, S.; Buchmann, B. Future Emissions and Atmospheric Fate of HFC-1234yf from Mobile Air Conditioners in Europe. *Environmental Science and Technology* **2012**, *46* (3), 1650–1658. https://doi.org/10.1021/es2034608.

(38) Colussi, A. A.; Persaud, D.; Lao, M.; Place, B. K.; Hems, R. F.; Ziegler, S. E.; Edwards, K. A.; Young, C. J.; VandenBoer, T. C. Cost-Effective off-Grid Automatic Precipitation Samplers for Pollutant and Biogeochemical Atmospheric Deposition. *Atmospheric Measurement Techniques* **2024**, *17* (12), 3697–3718. https://doi.org/10.5194/amt-17-3697-2024.

(39) Taniyasu, S.; Kannan, K.; Yeung, L. W. Y.; Kwok, K. Y.; Lam, P. K. S.; Yamashita, N. Analysis of Trifluoroacetic Acid and Other Short-Chain Perfluorinated Acids (C2–C4) in Precipitation by Liquid Chromatography–Tandem Mass Spectrometry: Comparison to Patterns of Long-Chain Perfluorinated Acids (C5–C18). *Analytica Chimica Acta* **2008**, *619* (2), 221–230. https://doi.org/10.1016/j.aca.2008.04.064.

(40) Henne, S.; Storck, F. R.; Wöhrnschimmel, H.; Leuenberger, M.; Vollmer, M. K.; Reimann, S. Trifluoroacetate (TFA) in Precipitation and Surface Waters in

Switzerland: Trends, Source Attribution, and Budget. EGUsphere [Preprint] June 27, 2025. https://doi.org/10.5194/egusphere-2025-2861.

(41) Freeling, F.; Behringer, D.; Heydel, F.; Scheurer, M.; Ternes, T. A.; Nödler, K. Trifluoroacetate in Precipitation: Deriving a Benchmark Data Set. *Environ. Sci. Technol.* **2020**, *54* (18), 11210–11219. https://doi.org/10.1021/acs.est.0c02910.

(42) Martin, J. W.; Mabury, S. A.; Wong, C. S.; Noventa, F.; Solomon, K. R.; Alaee, M.; Muir, D. C. G. Airborne Haloacetic Acids. *Environ. Sci. Technol.* **2003**, *37* (13), 2889–2897. https://doi.org/10.1021/es026345u.

(43) David, L. M.; Barth, M.; Höglund-Isaksson, L.; Purohit, P.; Velders, G. J. M.; Glaser, S.; Ravishankara, A. R. Trifluoroacetic Acid Deposition from Emissions of HFO-1234yf in India, China, and the Middle East. *Atmospheric Chemistry and Physics* **2021**, *21* (19), 14833–14849. https://doi.org/10.5194/acp-21-14833-2021.

(44) Kanakidou, M.; Dentener, J.; Crutzen, P. J. A Global Three-Dimensional Study of the Fate of HCFCs and HFC-134a in the Troposphere. *Journal of Geophysical Research* **1995**, *100* (D9), 18781–18801. https://doi.org/10.1029/95jd01919.

(45) Gewurtz, S. B.; Auyeung, A. S.; De Silva, A. O.; Teslic, S.; Smyth, S. A. Per- and Polyfluoroalkyl Substances (PFAS) in Canadian Municipal Wastewater and Biosolids: Recent Patterns and Time Trends 2009 to 2021. *Science of The Total Environment* **2024**, *912*, 168638. https://doi.org/10.1016/j.scitotenv.2023.168638.

(46) Helsel, D. R. *Statistics for Censored Environmental Data Using Minitab and R*, Second Edition.; John Wiley & Sons: New Jersey, USA, 2011.

(47) Kroll, J. H.; Heald, C. L.; Cappa, C. D.; Farmer, D. K.; Fry, J. L.; Murphy, J. G.; Steiner, A. L. The Complex Chemical Effects of COVID-19 Shutdowns on Air Quality. *Nat. Chem.* **2020**, *12* (9), 777–779. https://doi.org/10.1038/s41557-020-0535-z.

(48) Zhao, X.; Fioletov, V.; Alwarda, R.; Su, Y.; Griffin, D.; Weaver, D.; Strong, K.; Cede, A.; Hanisco, T.; Tiefengraber, M.; McLinden, C.; Eskes, H.; Davies, J.; Ogyu, A.; Sit, R.; Abboud, I.; Lee, S. C. Tropospheric and Surface Nitrogen Dioxide Changes in the Greater Toronto Area during the First Two Years of the COVID-19 Pandemic. *Remote Sensing* **2022**, *14* (7), 1625. https://doi.org/10.3390/rs14071625.

(49) Young, C. J.; Mabury, S. A. Reviews of Environmental Contamination and Toxicology. In *Reviews of Enviromental Contamination and Toxicology*; edited by de Voogt, P., Ed.; Springer New York: New York, NY, 2010; Vol. 208.

(50) Thompson, R. L.; Montzka, S. A.; Vollmer, M. K.; Arduini, J.; Crotwell, M.; Krummel, P. B.; Lunder, C.; Mühle, J.; O'Doherty, S.; Prinn, R. G.; Reimann, S.; Vimont, I.; Wang, H.; Weiss, R. F.; Young, D. Estimation of the Atmospheric Hydroxyl Radical Oxidative Capacity Using Multiple Hydrofluorocarbons (HFCs). *Atmospheric Chemistry and Physics* **2024**, *24* (2), 1415–1427. https://doi.org/10.5194/acp-24-1415-2024.

(51) Dodangodage, R.; Bernath, P. F.; Boone, C.; Harrison, J. J.; Lecours, M.; Schmidt, M.; Montzka, S. A.; Vimont, I.; Crotwell, M. The First Satellite Measurements of HFC-125 by the ACE-FTS: Long-Term Trends and Distribution in the Earth's Upper Troposphere and Lower Stratosphere. *Journal of Quantitative Spectroscopy and Radiative Transfer* **2025**, *330*, 109218. https://doi.org/10.1016/j.jqsrt.2024.109218.

(52) Sulbaek Andersen, M. P.; Schmidt, J. A.; Volkova, A.; Wuebbles, D. J. A Three-Dimensional Model of the Atmospheric Chemistry of E and Z-CF3CH=CHCl (HCFO-1233(Zd) (E/Z)). *Atmospheric Environment* **2018**, *179*, 250–259. https://doi.org/10.1016/j.atmosenv.2018.02.018.

(53) Xiang, B.; Patra, P. K.; Montzka, S. A.; Miller, S. M.; Elkins, J. W.; Moore, F. L.; Atlas, E. L.; Miller, B. R.; Weiss, R. F.; Prinn, R. G.; Wofsy, S. C. Global Emissions of Refrigerants HCFC-22 and HFC-134a: Unforeseen Seasonal Contributions. *Proc. Natl. Acad. Sci. U.S.A.* **2014**, *111* (49), 17379–17384. https://doi.org/10.1073/pnas.1417372111.

(54) Kotamarthi, V. R.; Rodriguez, J. M.; Ko, M. K. W.; Tromp, T. K.; Sze, N. D.; Prather, M. J. Trifluoroacetic Acid from Degradation of HCFCs and HFCs: A Three-Dimensional Modeling Study. *Journal of Geophysical Research* **1998**, *103* (D5), 5747–5758. https://doi.org/10.1029/97JD02988.

(55) Vet, R.; Artz, R. S.; Carou, S.; Shaw, M.; Ro, C. U.; Aas, W.; Baker, A.; Bowersox, V. C.; Dentener, F.; Galy-Lacaux, C.; Hou, A.; Pienaar, J. J.; Gillett, R.; Forti, M. C.; Gromov, S.; Hara, H.; Khodzher, T.; Mahowald, N. M.; Nickovic, S.; Rao, P. S. P.; Reid, N. W. A Global Assessment of Precipitation Chemistry and Deposition of Sulfur, Nitrogen, Sea Salt, Base Cations, Organic Acids, Acidity and pH, and Phosphorus.

Atmospheric Environment **2014**, *93*, 3–100. https://doi.org/10.1016/j.atmosenv.2013.10.060.

(56) He, Y.; Liu, M.; Shang, F.; Sudo, K. Can CMIP6 Models Reproduce the Decadal-to-Seasonal Variabilities in Nitrogen Deposition Across Major Emission Hotspots? *Geophysical Research Letters* **2025**, *52* (18), e2025GL118824. https://doi.org/10.1029/2025GL118824.

(57) Tao, Y.; VandenBoer, T. C.; Ye, R.; Young, C. J. Exploring Controls on Perfluorocarboxylic Acid (PFCA) Gas–Particle Partitioning Using a Model with Observational Constraints. *Environ. Sci.: Processes Impacts* **2023**, *25* (2), 264–276. https://doi.org/10.1039/D2EM00261B.

(58) Xia, C.; Capozzi, S. L.; Romanak, K. A.; Lehman, D. C.; Dove, A.; Richardson, V.; Greenberg, T.; McGoldrick, D.; Venier, M. The Ins and Outs of Per- and Polyfluoroalkyl Substances in the Great Lakes: The Role of Atmospheric Deposition. *Environ. Sci. Technol.* **2024**, *58* (21), 9303–9313. https://doi.org/10.1021/acs.est.3c10098.

(59) Shimizu, M. S.; Mott, R.; Potter, A.; Zhou, J.; Baumann, K.; Surratt, J. D.; Turpin, B.; Avery, G. B.; Harfmann, J.; Kieber, R. J.; Mead, R. N.; Skrabal, S. A.; Willey, J. D. Atmospheric Deposition and Annual Flux of Legacy Perfluoroalkyl Substances and Replacement Perfluoroalkyl Ether Carboxylic Acids in Wilmington, NC, USA. *Environ. Sci. Technol. Lett.* **2021**, *8* (5), 366–372. https://doi.org/10.1021/acs.estlett.1c00251.

(60) Pan, Z.; Li, S.; Zhao, Q.; Li, J.; Dong, Y.; Borthwick, A. G. L.; Sun, W.; Xu, N. Anthropogenic PFAS or Natural Products? Natural Products Cause Overestimation of C2–C5 Perfluoroalkyl Carboxylic Acid Levels. *Environ. Sci. Technol.* **2025**, *59* (22), 11194–11204. https://doi.org/10.1021/acs.est.4c12934.

CHAPTER 5

Quantifying the Global Reach of Trifluoroacetic Acid: Contrasting Total Deposition between the Southern and Northern Hemispheres

Daniel Persaud[1], Heetasmin Singh,[2] Trevor C. VandenBoer[1], and Cora J. Young[1*].

[1]Department of Chemistry, York University, Toronto, ON, Canada.

[2]Department of Chemistry, University of Guyana, Turkeyen Campus, Guyana, South America.

Author Contributions:

Cora J. Young and Daniel Persaud conceived and designed the experiment. Heetasmin Singh, Cora J. Young and Trevor C. VandenBoer collected the samples. Daniel Persaud analyzed the sample and collected the data. Daniel Persaud wrote the manuscript with input from all authors. Funding was acquired by Trevor C. VandenBoer and Cora J. Young.

5.1 Introduction

Trifluoroacetic acid (CF_3COOH, TFA) is a highly persistent and water-soluble compound that is ubiquitous in the environment. In environmental systems, TFA exists almost exclusively in its deprotonated form, trifluoroacetate (CF_3COO^-), which is extremely persistent with an estimated lifetime on the order of tens of thousands of years.[1,2] This persistence has resulted in widespread accumulation in different environmental media, leading to detection in global oceans[3,4], air[5–7], precipitation[8–13] and human biological samples, including serum[14] and urine.[15] Additionally, TFA is typically detected at concentrations 1-2 orders of magnitude higher than those of other legacy per-and polyfluoroalkyl substances (PFAS) in several environmental media.[16,17] Although some authors suggest a natural source may exist, current levels are mainly attributed to anthropogenic activities.[18]

An initial interest in the fate and effects of TFA began in the 1990s, prompted by the Montreal Protocol's phase-out of ozone-depleting chlorofluorocarbon (CFC) compounds and their subsequent replacement with hydrofluorocarbons (HFCs), hydrochlorofluorocarbons (HCFCs), each of which produce TFA as a degradation product, with yields of 7-20% for HFC-134a.[19] However, these early assessments failed to anticipate the profound and widespread accumulation of TFA across global environmental matrices and in humans. It is noteworthy to mention that although TFA may not bioaccumulate in the conventional sense, the elevated levels in humans and environmental matrices are a cause for concern.[18] This prompted a renewed interest in TFA mainly due to observations of increasing concentrations in remote locations,[20] plants,[21] groundwater[22] and human blood.[14,23] The TFA burden is also expected to increase with the increased use of hydrofluoroolefin (HFO) gases, like HFO-1234yf, which degrade to TFA in 100% molar yield in the atmosphere.[24] In addition to the fluorinated gases, other sources contribute to enhancing TFA levels, including other HFOs,[25] pesticide use,[26,27] pharmaceuticals,[16] fluoropolymers,[18] and other PFAS.[27,28] Once released, TFA is rapidly removed from the atmosphere by wet and dry deposition.

Despite the known persistence and increasing documented ubiquity, critical gaps remain in our understanding of TFA in different regions. Current knowledge of TFA deposition is heavily based on the Northern Hemisphere and temperate regions.[9,13,21,29–32]

Measurements from the southern hemisphere, especially near the equator, are exceptionally limited. The last published measurements of TFA in South American precipitation were done over two decades ago,[33] and to the best of our knowledge, no studies have reported TFA deposition levels near the equatorial regions. Additionally, the environmental fate and deposition mechanism of TFA are likely influenced by other climate variables (e.g., OH concentration, precipitation volume) and atmospheric transport patterns, which can differ dramatically across hemispheres.

In the current study, we aim to address these critical knowledge gaps by presenting the first continuous measurements of TFA fluxes in atmospheric deposition samples from an equatorial region in Georgetown, Guyana and a rural site in Lambton County, Canada. Herein, we (i) quantified and compared TFA fluxes between these two distinct sampling locations; (ii) identified the major atmospheric processes controlling TFA deposition; and (iii) evaluate current model predictions against measurements.

5.2 Material and Methods

5.2.1 Sample collection

Integrated total deposition samplers were deployed at the University of Guyana, Turkeyen Campus, Georgetown, Guyana (GEO: 6.811ºN, 58.115ºW). Samples (n = 12) were collected between December 2021 to July 2023, generally on a monthly schedule with some exceptions. The sampling site is situated on the northern Atlantic coast of South America in a suburban setting with light vehicle traffic, residential areas, and light industrial zones. Given Guyana's low national population (~800,000), this location provides an ideal environment to study atmospheric deposition in a tropical coastal region. Samples (n = 9) were collected over a similar time frame (January 2022 to July 2023) in Lambton County, Ontario, Canada (LC: 43.222 ºN, 81.870ºW). This sampling site is located in southwestern Ontario, Canada, within a rural-agricultural area with a heavily industrialized corridor located ~ 50 km upwind of the sampling site adjacent to the St. Clair River and the US border (Figure 5-1).

Figure 5-1: Map showing the sampling locations at the University of Guyana, Guyana (GEO), on the northern Atlantic Coast of South America (pink circle) and in Lambton County, Canada (LC) in southwestern Ontario (blue circle).

The total deposition samples were collected using custom-built precipitation samplers, previously described in detail elsewhere.[34] The sampler consisted of an acrylic box, which housed a 10 L HDPE bottle connected to a funnel. To actively collect snow at the LC site, self-regulating heating cables (HEATIT JHFS 15 ft, Amazon.ca) were installed on each sampling funnel to melt any accumulated snow. The volume of precipitation samples collected during the integrated sampling period was measured for flux determinations. All samples were shipped to the laboratory and kept refrigerated at 4°C until chemical analysis.

5.2.2 Sample preparation and analysis

Details of sample preparation were described previously.[35] Total deposition samples were equilibrated at room temperature, then a 10 mL aliquot was withdrawn into a polypropylene syringe (P/N: 14-817-44. Fischer Scientific) and filtered through a 0.22 µm syringe filter (P/N: 76479-030, VWR) into a precleaned polypropylene conical tube (14-959-53A, Fisher Scientific). Then an 800 µL sample was transferred along with 100

µL $^{13}C_2$ or $^{13}C_1$ TFA internal standard (20 µg L^{-1}) to a 1.0 mL polypropylene vial (5182-0567, Agilent). Analysis of TFA was done by direct injection of 750 µL into a concentrator column, followed by ion chromatography with mass spectrometry detection (IC-MS). TFA was separated by anion exchange using a hydroxide gradient (Table D-1) and detection was performed with a quadrupole MS operating in negative electrospray ionization mode (Table D-2). Sub -samples were also analyzed for major cations (Li^+, Na^+, K^+, NH_4^+, Al^{3+}, Ca^{2+}, Mg^{2+}) by ion chromatography with conductivity detection.

5.2.3 Quality Assurance and Quality Control

We took extensive measures to avoid contamination during sample collection, preparation and analysis. All samplers were rinsed three times with deionized water and twice with HPLC grade methanol before use. Travel blanks (n=2) consisting of ultrapure deionized water were transported to Guyana to account for any contamination that could occur during transport or handling. Field blanks were also deployed simultaneously with the deposition samplers. During sample collection, field blanks were opened for ~10 seconds. We found that TFA was <LOD in all travel and field blanks, suggesting that there was minimal contamination during travel, deployment, and sample collection.

Each sample concentration was quantified based on the relative response of TFA to isotopically labelled TFA. A 12-level calibration curve was employed for quantification, ranging from 0.05 to 10 µg L^{-1}. Check standards (0.25 µg L^{-1}) were also included after ten injections to assess reproducibility. Analytical blanks consisting of deionized water were included in the method analysis to assess potential contamination sources.

5.3 Results and Discussion

5.3.1 TFA concentration and fluxes

TFA was detected in each total deposition sample from GEO (n = 12) and LC (n = 9) for the entire collection period. Individual concentrations in GEO ranged from 0.11 to 0.56 µg L^{-1} (median 0.15 µg L^{-1}, mean 0.18 µg L^{-1}), whereas concentrations in LC ranged from 0.28 to 0.99 µg L^{-1} (median 0.42 µg L^{-1}, mean 0.53 µg L^{-1}). Measured TFA concentrations are comparable to values observed in precipitation samples collected in different regions in the northern hemisphere (<LOD to 38 µg L^{-1}).[8–12,31,32,36–39] To the best

of our knowledge, the only other TFA measurement in South America was reported approximately two decades ago in two locations near Concepcion, Chile, ~ 5000 km southwest of our sampling site.[33] The mean concentration value reported in GEO (0.18 μg L^{-1}) is more than an order of magnitude greater than the mean value reported two decades ago in urban and rural Chile (0.012 and 0.014 μg L^{-1}). However, we caution that a direct comparison over locations and times using concentration may be misleading, as it is highly dependent on sample volume.

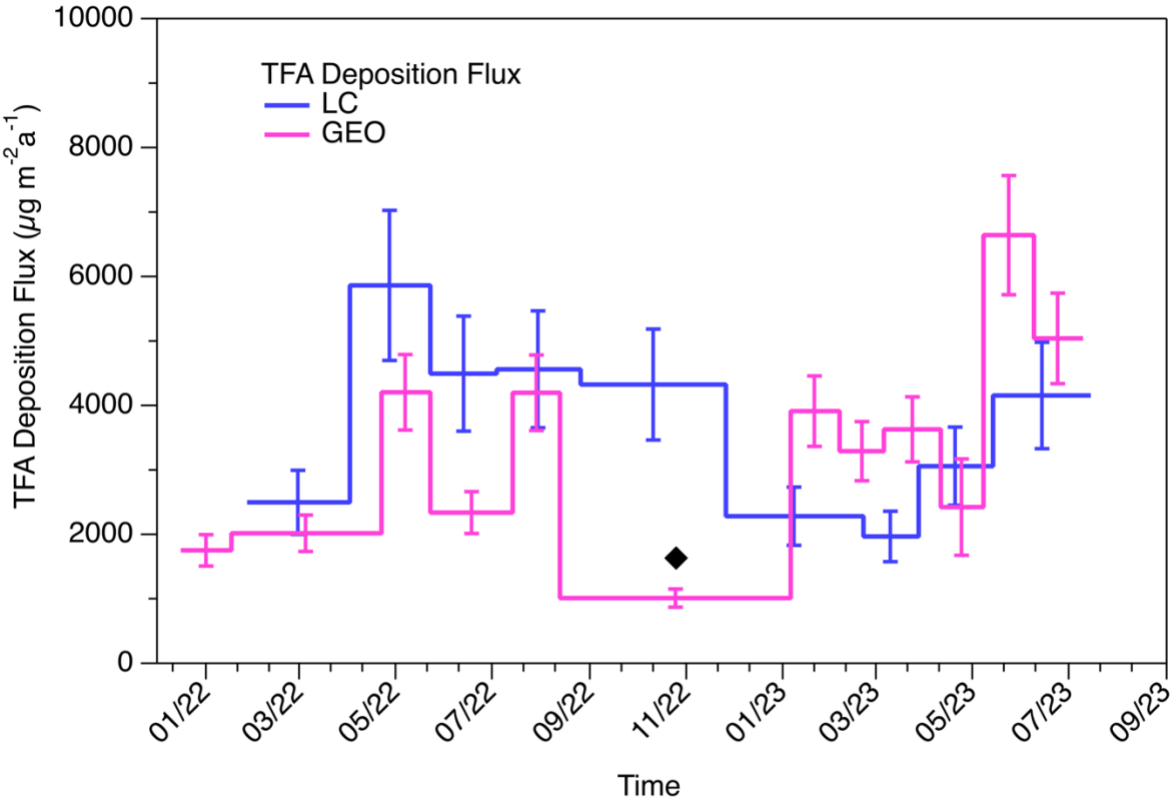

Figure 5-2: Time series of TFA deposition flux (μg m^{-2} a^{-1}) in total deposition at Lambton County (LC) (pink trace) and Georgetown, Guyana (GEO) (blue trace) for the entire sampling period. The cumulative error for deposition flux measurements was calculated using the error in the measurements in the check standard processing, errors in the precision and error in the volume collected by each sampler, where the error in each parameter is divided by the corresponding value, then squared and summed with the other terms. The solid diamond (♦) represent an underestimation of deposition flux

To enable robust spatial and temporal comparison, TFA concentrations (μg L^{-1}) were converted to deposition flux (μg m^{-2} d^{-1}) using the volume of samples, the area of

the sampler, and sampling duration (Figure 5-2, Tables D-3 and D-4). Resulting fluxes were further normalized to an annual scale (μg m^{-2} a^{-1}) to account for varying collection periods and to facilitate comparisons with other geochemical flux data and chemical models, which commonly report deposition fluxes in these units. We found that the deposition fluxes in GEO ranged from 1014 to 6641 μg m^{-2} a^{-1} (median: 3771 μg m^{-2} a^{-1}) and LC ranged from 1969 to 5863 μg m^{-2} a^{-1} (median: 4156 μg m^{-2} a^{-1}). These deposition fluxes can only be compared to a few previous measurements, since reports of fluxes in comparable units are rare. Median fluxes in the current study (3771 and 4156 μg m^{-2} a^{-1}) are at least an order of magnitude greater than median fluxes reported in Chapter 4 from Toronto, Canada (2018-2025, 300 μg m^{-2} a^{-1}),[35] Switzerland (2021-2023, 555 μg m^{-2} a^{-1})[36], Guangzhou China (2007 – 2008, 229 μg m^{-2} a^{-1}),[40] and in wet deposition across several sites in Germany in 2018 (193 μg m^{-2} a^{-1}). In each of these studies, atmospheric formation of TFA from oxidation of precursor molecules was suggested as the dominant source. Our results show that the median deposition fluxes were comparable (Welch two-sample t-test, $p = 0.19$) between LC (4156 μg m^{-2} a^{-1}) and GEO (3771 μg m^{-2} a^{-1}) (Figure 5-3). The fact that similar fluxes—both of which are substantially larger than other reported measurements—were observed from such fundamentally different regions raises important questions about the sources and controls of TFA deposition across diverse environments.

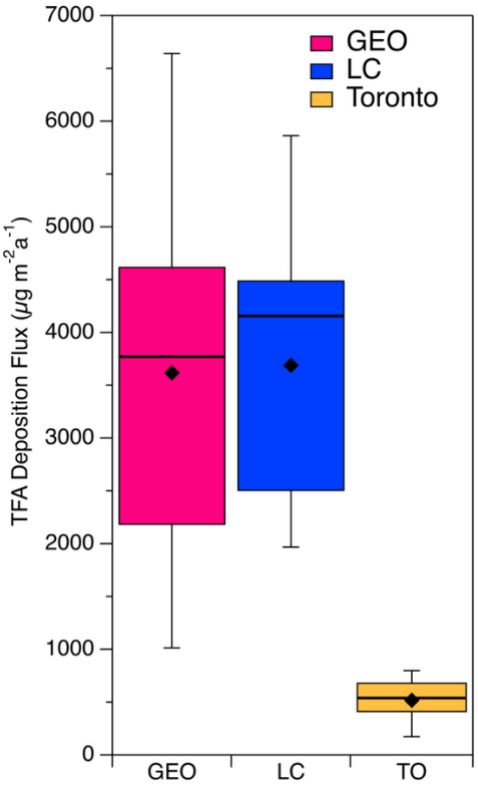

Figure 5-3: Boxplots of TFA deposition fluxes (µg m^{-2} a^{-1}) for Georgetown, Guyana (GEO)(2021 –2023), Lambton County, Canada (LC)(2021–2023) and Toronto, Canada (TO)(2021–2023; data from Chapter 4). The boxes represent the interquartile range (25^{th}-75^{th} percentile), the solid line represents the median, solid diamond (♦) represents the mean and whiskers denote the minimum and maximum values.

5.3.2 TFA source attribution for Lambton County, Canada

The elevated TFA deposition fluxes observed at LC may reflect regional influences associated with the industrialized Sarnia-Lambton area, which contains a large concentration of chemical manufacturing facilities and accounts for more than 40% of Canada's chemical industry.[41] However, these facilities are not located immediately adjacent to the sampling site and their influence on deposition at LC likely depends on regional transport patterns rather than proximately alone. Interestingly, the median TFA deposition at LC (4156 µg m^{-2} a^{-1}) is ~ 8 times greater than measurements in Toronto, Ontario (500 µg m^{-2} a^{-1},Chapter 4),[35] when compared for the same time period (Figure 5-3), despite the sites being separated by only ~ 200 km. This suggests that regional sources in LC may contribute to an enhanced TFA deposition. Although there are no fluorochemical facilities in the region, usage of fluorochemicals in the production of other

chemicals is expected. Other well-known TFA sources also exist within the regions, such as landfills (Safety-Kleen Inc.), and extensive agricultural pesticide use is present in the surrounding region.[42] Together, these sources may elevate the background atmospheric burden of TFA.

Although TFA is predicted,[43] and has been previously measured to be predominantly in the gas phase,[6,44] it is possible that transport on aerosols could contribute to the observed atmospheric deposition. We use particulate cations as markers for aerosol sources. The moderate correlation observed between K^+ and TFA (r: 0.39, p=0.07; Table 5-1), suggests a potential influence from biomass burning. This is consistent with regional studies identifying biomass burning as a persistent source of particulate matter in Ontario.[45] The significant 2023 wildfire season further demonstrates the potential for acute, large-scale biomass burning emissions across the province, including southwestern Ontario.[46] It is possible that TFA could be remobilized to the atmosphere through the burning of contaminated biomass.[21,47] Correlations between TFA and mineral dust tracers were moderate to strong (r: 0.56-0.72, p<0.07). Previous studies in the High Arctic have suggested a role of other PFAS long-range transport mediated by mineral dust.[48,49] At LC, a major dust source is likely to be local agricultural fields, which, if contaminated with TFA,[17,50] could remobilize it to the atmosphere. While these correlations indicate a possible direct source, it is also possible that TFA and mineral dust are simply being transported by the same airmass Future studies are required to constrain TFA remobilization from multiple sources. This would require direct measurements of TFA in both gas and particle phase, size resolved aerosol sampling and analysis of TFA in source materials such as contaminated soil, dust and vegetation. Coupling these measurements with source tracers and event-based sampling during biomass burning or dust mobilization episodes would determine whether TFA is directly remobilized or co-transported with polluted air masses.

5.3.3 TFA source attribution for Georgetown, Guyana

No point sources of fluorochemicals are known to exist in GEO. In this region, we hypothesize that increased TFA may be due to enhanced hydroxyl radical concentrations close to the equator, which could lead to an increase in TFA formation from precursors. This is supported by model and aircraft measurements, where OH maximum reaches ~2

to 9 x 10^6 molecules cm^{-3},[51,52] approximately double the global average of 1 x 10^6 molecules cm^{-3}. In addition, the tropical environment is also likely characterized by lower NO_x levels. This low-NO_x regime can increase the atmospheric yield of TFA from the oxidation of certain precursors (e.g., HFC-143a and fluorotelomers). [25,53] While we cannot directly identify the main TFA precursors, previous modelling studies suggest that elevated TFA deposition is expected in the tropics due to oxidation of HFCs and HCFCs.[54,55] Interestingly, Guyana has not ratified the Kigali Amendment,[56] which phases out and introduces hydrofluoroolefin (explicitly HFO-1234yf), which is a major TFA precursor source.[24]

A weak but statistically significant correlation was also observed between nss-K^+ and TFA (r:0.33, p = 0.05), suggesting that remobilization through biomass burning may be a potential source (Table 5-1). This is a plausible hypothesis given the local context. It is documented that agricultural burning, particularly of sugarcane and forest, is a common practice in Guyana.[57] A local exposure study confirmed the prevalence of sugarcane burning in the region, with 100% of households in one community reporting chronic exposure to smoke and soot. It is likely that TFA can be released during burning events and or transported by biomass burning plumes.[57]

No relationship was observed between Na^+ and TFA (r: 0.18, p = 0.17), which was somewhat surprising given the proximity of GEO (~1 km) to the Atlantic Ocean. This finding is consistent with our previous analysis in marine-influenced sites in Canada, where widespread correlations between PFAAs and Na^+ were unexpectedly absent. This contrasts with other coastal studies, including Sha et al., who observed statistically significant PFAA and Na^+ correlations at Norwegian coastal sites.[58] The overall pattern suggests that while direct transport from specific local sources may exist, the dominant source of TFA is atmospheric oxidation of precursors, which overwhelms these more localized signals.

This calls for explicit measurements of TFA and its precursors in regions that are not commonly investigated to understand the sources and deposition mechanisms and the need for expanded global monitoring of TFA and its precursors, particularly in underrepresented regions such as the southern hemisphere, to accurately constrain the source, transport pathway, and ultimate environmental fate.

Table 5-1: Pearson correlation coefficient (r), statistical significance (p) and number of data points (n) of TFA concentration with Na^+, K^+, Ca^{2+} and Mg^{2+} concentrations as tracers of sea spray, biomass burning and mineral dust at LC and GEO. Statistically significant p-values ($p \leq 0.05$) are highlighted in bold. The non sea spray (nss) concentration was used for comparison at GEO, whereas direct comparisons were made at LC

		Na^+	K^+	Mg^{2+}	Ca^{2+}	nss-K^+	nss-Mg^{2+}	nss-Ca^{2+}
LC	r	8.1×10^{-3}	0.39	**0.56**	**0.71**			
	p	0.99	0.07	**0.01**	**0.004**			
	n	9	9	**9**	**9**			
GEO	r	0.18	**0.32**	0.22	7.2×10^{-5}	**0.33**	0.01	0.01
	p	0.17	**0.06**	0.12	0.98	**0.05**	0.80	0.89
	n	12	**12**	12	12	**12**	12	12

5.3.4 Model Comparisons

To contextualize our empirical findings, we compared our measured TFA deposition fluxes with available chemical transport models that predict current and future TFA atmospheric deposition after oxidation of volatile precursors, including HCFCs, HFCs, and HFOs.[24,59–61] While these models were not configured for our specific sampling sites or sampling period, a comparison of spatial and temporal averages provides critical context for our empirical findings.

Generally, we found that all available models underestimate the TFA deposition measured in the current study (Table 5-2). The mean flux measured in LC (4156 μg m^{-2} a^{-1}) is ~ 23 times greater than the mean modelled global projection by 2030 (180 μg m^{-2} a^{-1}).[60] Similarly, the mean flux in GEO (3618 μg m^{-2} a^{-1}) is ~20 times greater than the projected 2030 global mean average and nearly twice the largest regional scale 2030 prediction for China (1850 μg m^{-2} a^{-1}).

This disparity between modelled and measured deposition flux is expected since all available models primarily simulate TFA primarily from the degradation of HFO-1234yf under specified emission scenarios,[24,59–62] with earlier works simulating deposition from HCFCs and HFC-134a.[6,44,55]. Consequently, these models omit contributions of other TFA

sources that may exist, including HFOs,[25] hydrochlorofluoroolefins,[63] and fluorotelomer compounds.[25] The omission of multiple source pathways provides a plausible explanation for systematic model underestimation. The smaller disparity in GEO may be due to the models more accurately representing well-mixed background precursors (e.g. HFCs and HCFCs), which can produce TFA in a smaller yield.

Furthermore, a direct comparison of mean values inherently fails to capture the impact of episodic deposition events or TFA remobilization. Our measurements recorded peak fluxes of 6641 μg m^{-2} a^{-1} and 5863 μg m^{-2} a^{-1} in GEO and LC, respectively – events that would be entirely obscured in mean comparisons. Therefore, we advocate for the urgent development of robust chemical models that account for all known TFA sources. Utilizing updated emission inventories can be constrained by empirical deposition measurements; these improved chemical transport models are essential for generating accurate risk assessment and informing future environmental policy.

Table 5-2: Comparisons of mean total deposition of TFA measured in the current study, to previous model estimates of TFA deposition across different regions. Ranges measured and estimated deposition are also included in brackets. All model estimates were based on the degradation of chlorofluorocarbon (CFC) replacement compounds.

Location	Time	TFA precursors	Model	Deposition Flux (μg m^{-2} a^{-1})	Ref.
Lambton County (LC)		-	-	3689	This study
Georgetown, Guyana		-	-	3618	
Beijing, China	May 2012-Apr 2013	HFC-134a	Atkinson Box Model	619	Wu et al.[6]
Tropics	2020	HCFC-22, HCFC-123, HCFC-124, HFC-134a, HCFC-141b	MOGUNTIA	228	Kanakidou et al.[55]
India	2020-2040	HFO-1234yf	GEOS-Chem	874	David et al.[62]
China				501	
Middle East				477	
India			WRF-Chem	802	
China				342	
Middle East				284	
China, annual	2016	HFO-1234yf	GEOS-Chem	960	Wang et al.[60]
US, annual				450	
EU, annual				520	
North Pole region, annual				80	
Globe, annual				120	
China, annual	2030			1850	
US, annual				500	
EU, annual				540	
Globe, annual				180	
US, Summer	Jun-Aug 2005	HFO-1234yf	CMAQ	240	Luecken et al.[24]
EU, annual	2020	HFO-1234yf	FLEXPART	370-650	Henne et al.[61]

5.4 Implications

This work provides the first deposition measurement of TFA in GEO, Guyana, with complementary measurements in a polluted region in southwestern Ontario. This addresses a significant data gap, as no prior deposition data exist near the equator and the last measurements in South America were made nearly two decades ago. Our findings reveal that TFA deposition fluxes in GEO are statistically comparable to measurements in LC. We show that the observed fluxes are driven by two different regimes. In LC, elevated fluxes are consistent with local sources, including proximity to chemical manufacturing, landfills, and intensive agriculture, which may enhance the local atmospheric burden of TFA and its precursors. In GEO, similar fluxes arise instead from enhanced oxidant levels, and high precipitation efficiently scavenge TFA formed from regional and hemispheric precursor emissions. This conceptual framework implies that TFA "hot spots" may emerge both uwind of industrial corridors and in tropical regions that may have limited direct sources but strong oxidative capacity and high rainfall.

Additionally, we observed discrepancies between measured and modelled deposition fluxes, where all available chemical models fail to account for the full complexity of TFA sources and deposition pathways. This discrepancy between observed and modelled fluxes highlights how existing chemical models cannot accurately assess TFA deposition, particularly in tropical ecosystems experiencing significant TFA deposition despite their remoteness from industrial sources.

These results highlight three immediate needs. First, expanded deposition monitoring networks are required in underrepresented regions, particularly in the southern hemisphere, which would better constrain the global distribution of TFA. In addition, targeted studies are needed to evaluate whether (or under what conditions) TFA may be remobilized after deposition (e.g., from soils, surface water, biomass) and subsequently redistributed in the atmosphere. Second, chemical transport models should be updated to include all known sources of TFA and its precursors. Models should also include more realistic deposition parameterizations and be evaluated against field measurements such as those presented here. Third, regulatory evaluations of current and future fluorinated substitutes should explicitly account for TFA formation and subsequent deposition and consider regions that may be subject to industrial emissions (e.g., near manufacturing,

use, and disposal hotspots) and remote regions. Collectively, our findings show that the environmental footprint of TFA is more extensive and complex than previously appreciated, and that policies governing fluorochemical use and replacement strategies must be informed by this broader perspective.

5.5 References

(1) Lifongo, L. L.; Bowden, D. J.; Brimblecombe, P. Photodegradation of Haloacetic Acids in Water. *Chemosphere* **2004**, *55* (3), 467–476. https://doi.org/10.1016/j.chemosphere.2003.11.006.

(2) Scheurer, M.; Nödler, K.; Freeling, F.; Janda, J.; Happel, O.; Riegel, M.; Müller, U.; Storck, F. R.; Fleig, M.; Lange, F. T.; Brunsch, A.; Brauch, H.-J. Small, Mobile, Persistent: Trifluoroacetate in the Water Cycle – Overlooked Sources, Pathways, and Consequences for Drinking Water Supply. *Water Res.* **2017**, *126*, 460–471. https://doi.org/10.1016/j.watres.2017.09.045.

(3) Frank, H.; Christoph, E. H.; Holm-Hansen, O.; Bullister, J. L. Trifluoroacetate in Ocean Waters. *Environ. Sci. Technol.* **2002**, *36* (1), 12–15. https://doi.org/10.1021/es0101532.

(4) Scott, B. F.; Macdonald, R. W.; Kannan, K.; Fisk, A.; Witter, A.; Yamashita, N.; Durham, L.; Spencer, C.; Muir, D. C. G. Trifluoroacetate Profiles in the Arctic, Atlantic, and Pacific Oceans. *Environ. Sci. Technol.* **2005**, *39* (17), 6555–6560. https://doi.org/10.1021/es047975u.

(5) Young, C. J.; Joudan, S.; Tao, Y.; Wentzell, J. J. B.; Liggio, J. High Time Resolution Ambient Observations of Gas-Phase Perfluoroalkyl Carboxylic Acids: Implications for Atmospheric Sources. *Environ. Sci. Technol. Lett.* **2024**, *11* (12), 1348–1354. https://doi.org/10.1021/acs.estlett.4c00897.

(6) Wu, J.; Martin, J. W.; Zhai, Z.; Lu, K.; Li, L.; Fang, X.; Jin, H.; Hu, J.; Zhang, J. Airborne Trifluoroacetic Acid and Its Fraction from the Degradation of HFC-134a in Beijing, China. *Environ. Sci. Technol.* **2014**, *48* (7), 3675–3681. https://doi.org/10.1021/es4050264.

(7) Zhang, B.; Zhai, Z.; Zhang, J. Distribution of Trifluoroacetic Acid in Gas and Particulate Phases in Beijing from 2013 to 2016. *Sci. Total Environ.* **2018**, *634*, 471–477. https://doi.org/10.1016/j.scitotenv.2018.03.384.

(8) Freeling, F.; Behringer, D.; Heydel, F.; Scheurer, M.; Ternes, T. A.; Nödler, K. Trifluoroacetate in Precipitation: Deriving a Benchmark Data Set. *Environ. Sci. Technol.* **2020**, *54* (18), 11210–11219. https://doi.org/10.1021/acs.est.0c02910.

(9) Chen, H.; Zhang, L.; Li, M.; Yao, Y.; Zhao, Z.; Munoz, G.; Sun, H. Per- and Polyfluoroalkyl Substances (PFASs) in Precipitation from Mainland China: Contributions of Unknown Precursors and Short-Chain (C2 C3) Perfluoroalkyl Carboxylic Acids. *Water Res.* **2019**, *153*, 169–177. https://doi.org/10.1016/j.watres.2019.01.019.

(10) Pike, K. A.; Edmiston, P. L.; Morrison, J. J.; Faust, J. A. Correlation Analysis of Perfluoroalkyl Substances in Regional U.S. Precipitation Events. *Water Res.* **2021**, *190*, 116685. https://doi.org/10.1016/j.watres.2020.116685.

(11) Scott, B. F.; Spencer, C.; Mabury, S. A.; Muir, D. C. G. Poly and Perfluorinated Carboxylates in North American Precipitation. *Environ. Sci. Technol.* **2006**, *40* (23), 7167–7174. https://doi.org/10.1021/es061403n.

(12) Wujcik, C. E.; Cahill, T. M.; Seiber, J. N. Determination of Trifluoroacetic Acid in 1996 - 1997 Precipitation and Surface Waters in California and Nevada. *Environ. Sci. Technol.* **1999**, *33* (10), 1747–1751. https://doi.org/10.1021/es980697c.

(13) Von Sydow, L. M.; Grimvall, A. B.; Borén, H. B.; Laniewski, K.; Nielsen, A. T. Natural Background Levels of Trifluoroacetate in Rain and Snow. *Environ. Sci. Technol.* **2000**, *34* (15), 3115–3118. https://doi.org/10.1021/es9913683.

(14) Duan, Y.; Sun, H.; Yao, Y.; Meng, Y.; Li, Y. Distribution of Novel and Legacy Per-/Polyfluoroalkyl Substances in Serum and Its Associations with Two Glycemic Biomarkers among Chinese Adult Men and Women with Normal Blood Glucose Levels. *Environ. Int.* **2019**, *134*. https://doi.org/10.1016/j.envint.2019.105295.

(15) Muir, D. C. G.; Freeling, F.; Nilsson, S.; Bugsel, B.; Bowles, K.; Hobson, P.; Toms, L.-M.; Mueller, J. F. Trifluoroacetic Acid in Australian Human Urine Samples. *Environ. Sci. Technol. Lett.* **2025**, acs.estlett.5c00678. https://doi.org/10.1021/acs.estlett.5c00678.

(16) Arp, H. P. H.; Gredelj, A.; Glüge, J.; Scheringer, M.; Cousins, I. T. The Global Threat from the Irreversible Accumulation of Trifluoroacetic Acid (TFA). *Environ. Sci. Technol.* **2024**, *58* (45), 19925–19935. https://doi.org/10.1021/acs.est.4c06189.

(17) Chen, H.; Yao, Y.; Zhao, Z.; Wang, Y.; Wang, Q.; Ren, C.; Wang, B.; Sun, H.; Alder, A. C.; Kannan, K. Multimedia Distribution and Transfer of Per- and Polyfluoroalkyl Substances (PFASs) Surrounding Two Fluorochemical Manufacturing Facilities in

Fuxin, China. *Env. Sci Technol* **2018**, *52* (15), 8263–8271. https://doi.org/10.1021/acs.est.8b00544.

(18) Joudan, S.; De Silva, A. O.; Young, C. J. Insufficient Evidence for the Existence of Natural Trifluoroacetic Acid. *Environ. Sci. Process. Impacts* **2021**, *23* (11), 1641–1649. https://doi.org/10.1039/d1em00306b.

(19) Wallington, T. J.; Hurley, M. D.; Fracheboud, J. M.; Orlando, J. J.; Tyndall, G. S.; Sehested, J.; Møgelberg, T. E.; Nielsen, O. J. Role of Excited CF3CFHO Radicals in the Atmospheric Chemistry of HFC-134a. *J. Phys. Chem.* **1996**, *100* (46), 18116–18122. https://doi.org/10.1021/jp9624764.

(20) Pickard, H. M.; Criscitiello, A. S.; Persaud, D.; Spencer, C.; Muir, D. C. G.; Lehnherr, I.; Sharp, M. J.; De Silva, A. O.; Young, C. J. Ice Core Record of Persistent Short-Chain Fluorinated Alkyl Acids: Evidence of the Impact From Global Environmental Regulations. *Geophys. Res. Lett.* **2020**, *47* (10), e2020GL087535. https://doi.org/10.1029/2020GL087535.

(21) Freeling, F.; Scheurer, M.; Koschorreck, J.; Hoffmann, G.; Ternes, T. A.; Nödler, K. Levels and Temporal Trends of Trifluoroacetate (TFA) in Archived Plants: Evidence for Increasing Emissions of Gaseous TFA Precursors over the Last Decades. *Environ. Sci. Technol. Lett.* **2022**, *9*, 400–405. https://doi.org/10.1021/acs.estlett.2c00164.

(22) Albers, C. N.; Sültenfuss, J. A 60-Year Increase in the Ultrashort-Chain PFAS Trifluoroacetate and Its Suitability as a Tracer for Groundwater Age. *Environ. Sci. Technol. Lett.* **2024**, *11* (10), 1090–1095. https://doi.org/10.1021/acs.estlett.4c00525.

(23) Zheng, G.; Eick, S. M.; Salamova, A. Elevated Levels of Ultrashort- and Short-Chain Perfluoroalkyl Acids in US Homes and People. *Environ. Sci. Technol.* **2023**, *57* (42), 15782–15793. https://doi.org/10.1021/acs.est.2c06715.

(24) Luecken, D. J.; Waterland, R. L.; Papasavva, S.; Taddonio, K. N.; Hutzell, W. T.; Rugh, J. P.; Andersen, S. O. Ozone and TFA Impacts in North America from Degradation of 2,3,3,3-Tetrafluoropropene (HFO-1234yf), a Potential Greenhouse Gas Replacement. *Environ. Sci. Technol.* **2010**, *44* (1), 343–348. https://doi.org/10.1021/es902481f.

(25) Young, C. J.; Mabury, S. A. Reviews of Environmental Contamination and Toxicology Perfluorinated Alkylated Substances. In *Reviews of Enviromental*

Contamination and Toxicology; edited by de Voogt, P., Ed.; Springer New York: New York, NY, 2010; Vol. 208.

(26) Joerss, H.; Freeling, F.; Van Leeuwen, S.; Hollender, J.; Liu, X.; Nödler, K.; Wang, Z.; Yu, B.; Zahn, D.; Sigmund, G. Pesticides Can Be a Substantial Source of Trifluoroacetate (TFA) to Water Resources. *Environ. Int.* **2024**, *193*, 109061. https://doi.org/10.1016/j.envint.2024.109061.

(27) Freeling, F.; Björnsdotter, M. K. Assessing the Environmental Occurrence of the Anthropogenic Contaminant Trifluoroacetic Acid (TFA). *Curr. Opin. Green Sustain. Chem.* **2023**, *41*, 100807. https://doi.org/10.1016/j.cogsc.2023.100807.

(28) Sun, M.; Cui, J.; Guo, J.; Zhai, Z.; Zuo, P.; Zhang, J. Fluorochemicals Biodegradation as a Potential Source of Trifluoroacetic Acid (TFA) to the Environment. *Chemosphere* **2020**, *254*, 126894. https://doi.org/10.1016/j.chemosphere.2020.126894.

(29) Scott, B. F.; Mactavish, D.; Spencer, C.; Strachan, W. M. J.; Muir, D. C. G. Haloacetic Acids in Canadian Lake Waters and Precipitation. *Env. Sci Technol* **2000**, *34* (20), 4266–4272. https://doi.org/10.1021/es9908523.

(30) Wujcik, C. E.; Cahill, T. M.; Seiber, J. N. Extraction and Analysis of Trifluoroacetic Acid in Environmental Waters. *Anal. Chem.* **1998**, *70* (19), 4074–4080. https://doi.org/10.1021/ac9802123.

(31) Berg, M.; Müller, S. R.; Mühlemann, J.; Wiedmer, A.; Schwarzenbach, R. P. Concentrations and Mass Fluxes of Trifluoroacetic Acid in Rain and Natural Waters in Switzerland. *Environ. Sci. Technol.* **2000**, *34* (13), 2675–2683. https://doi.org/10.1021/es990855f.

(32) Frank, H.; Klein, A.; Renschen, D. Environmental Trifluoroacetate. *Nature* **1996**, *382*, 34. https://doi.org/10.1038/382034a0.

(33) Scott, B. F.; Spencer, C.; Martin, J. W.; Barra, R.; Bootsma, H. A.; Jones, K. C.; Johnston, A. E.; Muir, D. C. G. Comparison of Haloacetic Acids in the Environment of the Northern and Southern Hemispheres. *Environ. Sci. Technol.* **2005**, *39* (22), 8664–8670. https://doi.org/10.1021/es050118l.

(34) Colussi, A. A.; Persaud, D.; Lao, M.; Place, B. K.; Hems, R. F.; Ziegler, S. E.; Edwards, K. A.; Young, C. J.; VandenBoer, T. C. Cost-Effective off-Grid Automatic

Precipitation Samplers for Pollutant and Biogeochemical Atmospheric Deposition. *Atmospheric Meas. Tech.* **2024**, *17* (12), 3697–3718. https://doi.org/10.5194/amt-17-3697-2024.

(35) Persaud, D.; Joudan, S.; VandenBoer, T.; Young, C. Atmospheric Removal of Trifluoroacetic Acid by Dry and Wet Deposition: A Multi Year Analysis in Toronto. ChemRxiv [Preprint] November 4, 2025. https://doi.org/10.26434/chemrxiv-2025-1x5nh.

(36) Henne, S.; Storck, F. R.; Wöhrnschimmel, H.; Leuenberger, M.; Vollmer, M. K.; Reimann, S. Trifluoroacetate (TFA) in Precipitation and Surface Waters in Switzerland: Trends, Source Attribution, and Budget. EGUsphere [Preprint] June 27, 2025. https://doi.org/10.5194/egusphere-2025-2861.

(37) Björnsdotter, M. K.; Yeung, L. W. Y.; Kärrman, A.; Jogsten, I. E. Mass Balance of Perfluoroalkyl Acids, Including Trifluoroacetic Acid, in a Freshwater Lake. *Environ. Sci. Technol.* **2022**, *56* (1), 251–259. https://doi.org/10.1021/acs.est.1c04472.

(38) Wang, Q.; Wang, X.; Ding, X. Rainwater Trifluoroacetic Acid (TFA) in Guangzhou, South China: Levels, Wet Deposition Fluxes and Source Implication. *Sci. Total Environ.* **2014**, *468–469*, 272–279. https://doi.org/10.1016/j.scitotenv.2013.08.055.

(39) Taniyasu, S.; Kannan, K.; Yeung, L. W. Y.; Kwok, K. Y.; Lam, P. K. S.; Yamashita, N. Analysis of Trifluoroacetic Acid and Other Short-Chain Perfluorinated Acids (C2–C4) in Precipitation by Liquid Chromatography–Tandem Mass Spectrometry: Comparison to Patterns of Long-Chain Perfluorinated Acids (C5–C18). *Anal. Chim. Acta* **2008**, *619* (2), 221–230. https://doi.org/10.1016/j.aca.2008.04.064.

(40) Wang, Q.; Wang, X.; Ding, X. Rainwater Trifluoroacetic Acid (TFA) in Guangzhou, South China: Levels, Wet Deposition Fluxes and Source Implication. *Sci. Total Environ.* **2014**, *468–469*, 272–279. https://doi.org/10.1016/j.scitotenv.2013.08.055.

(41) MacDonald, E. *Exposing Canada's Chemical Valley:An Investigation of Cumulative Air Pollution Emissions in the Sarnia, Ontario Area*; Ecojustise, 2007; pp 1–32. https://ecojustice.ca/wp-content/uploads/2015/09/2007-Exposing-Canadas-Chemial-Valley.pdf (accessed 2025-09-15).

(42) Atari, D. O.; Luginaah, I. N.; Gorey, K.; Xu, X.; Fung, K. Associations between Self-Reported Odour Annoyance and Volatile Organic Compounds in 'Chemical Valley',

Sarnia, Ontario. *Environ. Monit. Assess.* **2013**, *185* (6), 4537–4549. https://doi.org/10.1007/s10661-012-2887-3.

(43) Tao, Y.; VandenBoer, T. C.; Ye, R.; Young, C. J. Exploring Controls on Perfluorocarboxylic Acid (PFCA) Gas–Particle Partitioning Using a Model with Observational Constraints. *Environ. Sci. Process. Impacts* **2023**, *25* (2), 264–276. https://doi.org/10.1039/D2EM00261B.

(44) Martin, J. W.; Mabury, S. A.; Wong, C. S.; Noventa, F.; Solomon, K. R.; Alaee, M.; Muir, D. C. G. Airborne Haloacetic Acids. *Environ. Sci. Technol.* **2003**, *37* (13), 2889–2897. https://doi.org/10.1021/es026345u.

(45) Healy, R. M.; Sofowote, U.; Su, Y.; Debosz, J.; Noble, M.; Jeong, C.-H.; Wang, J. M.; Hilker, N.; Evans, G. J.; Doerksen, G.; Jones, K.; Munoz, A. Ambient Measurements and Source Apportionment of Fossil Fuel and Biomass Burning Black Carbon in Ontario. *Atmos. Environ.* **2017**, *161*, 34–47. https://doi.org/10.1016/j.atmosenv.2017.04.034.

(46) Chen, H.; Kaufman, J. S.; Chen, C.; Wang, J.; Maier, A.; van Dijk, A.; Slipp, N.; Rana, J.; MacIntyre, E.; Su, Y.; Kim, J.; Benmarhnia, T. Impact of the 2023 Wildfire Smoke Episodes in Ontario, Canada, on Asthma and Other Health Outcomes: An Interrupted Time-Series Analysis. https://doi.org/10.1503/cmaj.241506.

(47) Hawley, A. S.; Winne, M.; Cahill, T. M. Trifluoroacetic Acid Concentrations in Consumer Foods. *J. Agric. Food Chem.* **2025**, *73* (50), 32250–32254. https://doi.org/10.1021/acs.jafc.5c07390.

(48) Pickard, H. M.; Criscitiello, A. S.; Spencer, C.; Sharp, M. J.; Muir, D. C. G.; De Silva, A. O.; Young, C. J. Continuous Non-Marine Inputs of per- and Polyfluoroalkyl Substances to the High Arctic: A Multi-Decadal Temporal Record. *Atmospheric Chem. Phys.* **2018**, *18* (7), 5045–5058. https://doi.org/10.5194/acp-18-5045-2018.

(49) Persaud, D.; Criscitiello, A. S.; Spencer, C.; Lehnherr, I.; Muir, D. C. G.; De Silva, A. O.; Young, C. J. A 50 Year Record for Perfluoroalkyl Acids in the High Arctic: Implications for Global and Local Transport. *Environ. Sci. Process. Impacts* **2024**, *26* (9), 1543–1555. https://doi.org/10.1039/D4EM00219A.

(50) Scholl, J.; Meiers, E.; Mauch, T.; Lisec, J.; Sommerfeld, T.; Weinfurtner, K.; Haase, H.; Koch, M. Approaches towards Sensitive and Reliable Determination of

Trifluoroacetic Acid (TFA) from German Grass- and Farmland Soils. *Chemosphere* **2025**, *382*, 144496. https://doi.org/10.1016/j.chemosphere.2025.144496.

(51) Ringsdorf, A.; Edtbauer, A.; Vilà-Guerau De Arellano, J.; Pfannerstill, E. Y.; Gromov, S.; Kumar, V.; Pozzer, A.; Wolff, S.; Tsokankunku, A.; Soergel, M.; Sá, M. O.; Araújo, A.; Ditas, F.; Poehlker, C.; Lelieveld, J.; Williams, J. Inferring the Diurnal Variability of OH Radical Concentrations over the Amazon from BVOC Measurements. *Sci. Rep.* **2023**, *13* (1), 14900. https://doi.org/10.1038/s41598-023-41748-4.

(52) Lelieveld, J.; Butler, T. M.; Crowley, J. N.; Dillon, T. J.; Fischer, H.; Ganzeveld, L.; Harder, H.; Lawrence, M. G.; Martinez, M.; Taraborrelli, D.; Williams, J. Atmospheric Oxidation Capacity Sustained by a Tropical Forest. *Nature* **2008**, *452* (7188), 737–740. https://doi.org/10.1038/nature06870.

(53) Thackray, C. P.; Selin, N. E.; Young, C. J. A Global Atmospheric Chemistry Model for the Fate and Transport of PFCAs and Their Precursors. *Environ. Sci. Process. Impacts* **2020**, *22* (2), 285–293. https://doi.org/10.1039/C9EM00326F.

(54) Kotamarthi, V. R.; Rodriguez, J. M.; Ko, M. K. W.; Tromp, T. K.; Sze, N. D.; Prather, M. J. Trifluoroacetic Acid from Degradation of HCFCs and HFCs: A Three-Dimensional Modeling Study. *J. Geophys. Res. Atmospheres* **1998**, *103* (D5), 5747–5758. https://doi.org/10.1029/97JD02988.

(55) Kanakidou, M.; Dentener, J.; Crutzen, P. J. A Global Three-Dimensional Study of the Fate of HCFCs and HFC-134a in the Troposphere. *J. Geophys. Res.* **1995**, *100* (D9), 18781–18801. https://doi.org/10.1029/95jd01919.

(56) International Aerospace Environmental Group. *Alert 17.3: Phase Down of Hydrofluorocarbons (HFCs) – Update 2*. https://www.iaeg.com/binaries/content/assets/iaeg/wg9/kigali-amendment-and-hfcs_update2.pdf (accessed 2025-09-15).

(57) Gamell, M.; Mohammad, A.; Kakarla, K. K.; Ansari, A. Sugarcane Burning - A Potential Cause of Disease in Affected Individuals of Households in Uitvlugt and Ogle, Guyana. *Sch. Int. J. Biochem.* **2020**, *3* (9), 193–198. https://doi.org/10.36348/sijb.2020.v03i09.001.

(58) Sha, B.; Johansson, J. H.; Tunved, P.; Bohlin-Nizzetto, P.; Cousins, I. T.; Salter, M. E. Sea Spray Aerosol (SSA) as a Source of Perfluoroalkyl Acids (PFAAs) to the Atmosphere: Field Evidence from Long-Term Air Monitoring. *Environ. Sci. Technol.* **2022**, *56* (1), 228–238. https://doi.org/10.1021/acs.est.1c04277.

(59) Kazil, J.; McKeen, S.; Kim, S.-W.; Ahmadov, R.; Grell, G. A.; Talukdar, R. K.; Ravishankara, A. R. Deposition and Rainwater Concentrations of Trifluoroacetic Acid in the United States from the Use of HFO-1234yf. *J. Geophys. Res. Atmospheres* **2014**, *119* (24), 14,059-14,079. https://doi.org/10.1002/2014JD022058.

(60) Wang, Z.; Wang, Y.; Li, J.; Henne, S.; Zhang, B.; Hu, J.; Zhang, J. Impacts of the Degradation of 2,3,3,3-Tetrafluoropropene into Trifluoroacetic Acid from Its Application in Automobile Air Conditioners in China, the United States, and Europe. *Environ. Sci. Technol.* **2018**, *52* (5), 2819–2826. https://doi.org/10.1021/acs.est.7b05960.

(61) Henne, S.; Shallcross, D. E.; Reimann, S.; Xiao, P.; Brunner, D.; O'Doherty, S.; Buchmann, B. Future Emissions and Atmospheric Fate of HFC-1234yf from Mobile Air Conditioners in Europe. *Environ. Sci. Technol.* **2012**, *46* (3), 1650–1658. https://doi.org/10.1021/es2034608.

(62) David, L. M.; Barth, M.; Höglund-Isaksson, L.; Purohit, P.; Velders, G. J. M.; Glaser, S.; Ravishankara, A. R. Trifluoroacetic Acid Deposition from Emissions of HFO-1234yf in India, China, and the Middle East. *Atmospheric Chem. Phys.* **2021**, *21* (19), 14833–14849. https://doi.org/10.5194/acp-21-14833-2021.

(63) Sulbaek Andersen, M. P.; Schmidt, J. A.; Volkova, A.; Wuebbles, D. J. A Three-Dimensional Model of the Atmospheric Chemistry of E and Z-CF3CH=CHCl (HCFO-1233(Zd) (E/Z)). *Atmos. Environ.* **2018**, *179*, 250–259. https://doi.org/10.1016/j.atmosenv.2018.02.018.

CHAPTER 6

Summary and Future Directions

6.1 Conclusions

This thesis examined the spatial and temporal distribution of PFAS using atmospheric deposition samples across contrasting environments. Together, the results further constrain the sources, transport pathways and removal mechanism that govern PFAAs, as well as how regulatory actions and climate-related factors shape their environmental occurrence.

In Chapter 2, the 50-year ice core record from Mt. Oxford, icefield on Ellesmere Island show that both PFCAs, PFSAs and FOSA have been deposited in the High Arctic continuously since the 1960s. This record represents the longest Arctic PFCA record and the longest global PFSA archive to date, and captures the emergence, accumulation and decline of selected homologues following changes in global production and regulations. Homologue pair correlations, molar concentration ratios and model comparisons suggest that PFCAs are primarily formed through oxidation of volatile precursors. PFSAs showed no discernible trends, with concentrations at least an order of magnitude lower than PFCAs, however selected PFSAs (PFOS and PFBS) showed evidence of episodic events which may be linked to Arctic military activities. Tracer analysis suggests that marine aerosols and mineral dust are relevant as transport vectors for selected PFAAs during specific time periods. These observations highlight the complex mechanisms responsible for the transport and deposition of PFAAs in the High Arctic.

Chapter 3 extended the investigation on a coastal, forested mid-latitude region along the Newfoundland and Labrador Boreal Ecosystem Latitudinal Transect (NL-BELT). Precipitation samples were collected across four marine-influenced watersheds between 2014-2016. We detected PFAAs (C4-C12 PFCAs, C4-S, C8-S PFSAs) in both total and wet deposition samples, with the short chain PFCA homologue (PFBA) dominating deposition fluxes. Our measurements are among the first to separate the roles of wet and dry deposition, which could be quantified for perfluorobutanoic acid (PFBA), perfluorooctanoic acid (PFOA), and perfluorononanoic acid (PFNA). We found that the dry deposition contribution was equal to or greater than the wet deposition flux. Furthermore, our analysis of homologue correlations, molar concentration ratios, and model comparisons suggests that most PFCAs are formed indirectly through the oxidation

of precursor compounds. Air mass back trajectory and major ion analysis, conversely, indicate that direct transport and/or marine aerosol are minor contributors in this region, emphasizing the importance of atmospheric formation even in a marine influenced region.

Chapter 4 focused on the ultrashort chain PFAA homologue, TFA in a mixed suburban-urban environment. Here we present a record of TFA in total, wet, and dry deposition in Toronto, Canada, between 2018 and 2024. Samples were collected using custom-built total and automated wet deposition samplers. Contrary to expectations based on increasing use of HFO-1234yf, no clear increasing trend of TFA deposition was observed over the study period. Seasonal variation showed fluxes peaking in summer months, consistent with atmospheric oxidation of precursors as a major source. Fluxes in 2020 were statistically lower than other years by a factor of 2–5, coinciding with reduced anthropogenic activity during COVID-19 lockdowns. This provides compelling evidence that TFA sources in Toronto are mainly driven by short-lived precursors. A key outcome of this chapter is the first measurement-based estimate of the dry deposition removal pathway. We found that dry deposition can be equal or sometimes greater than wet deposition, suggesting that a reliance on wet-only measurements will systematically underestimate TFA deposition.

Chapter 5 compared further compared TFA deposition in a mid-latitude rural agricultural-industrial site in Lambton County, with an equatorial tropical site in Georgetown, Guyana. This work provides a hemispheric perspective on TFA deposition. Despite the absence of local point sources and delayed regulations, we found that TFA deposition in Georgetown, Guyana were comparable to or greater than measurements in Lambton County. Correlations between TFA and tracers of biomass burning and mineral dust suggest that these particular sources can modulate TFA formation, transport and removal, which may occur through co-transport or surface interaction. Together with the work in Chapter 4, the hemispheric comparison confirms that TFA deposition reflects large-scale precursor emissions and atmospheric chemistry, modulated by meteorology and precipitation patterns. This work also highlights the fact that existing models tend to underpredict observed TFA deposition across diverse climatic regimes.

6.2 Future directions

The findings of this thesis point to several avenues where further work is needed to improve our understanding of PFAA sources, deposition and transport mechanisms.

First, additional long term archives of PFAA deposition are needed across the Arctic and other remote regions. Ice cores improve our understanding of long-range transport sources and mechanisms of PFAAs, as well as the efficacy of regulation. However, this valuable resource is disappearing due to climate change. This underscores the urgency of collecting and analyzing new cores from vulnerable sites. There is a need to standardize the collection and analysis of ice cores across multiple sites, which would enable a spatial comparison in addition to the temporal records.

Second, there is a need to extend continuous total and wet deposition monitoring of PFAAs and mid and low latitude sites. The NL-BELT work demonstrates the usefulness of coordinated sampling along a climate gradient. However, limitations exist such as the lack of wintertime sampling. Extending the sampling times, including wintertime sampling and coordinating similar sampler networks in other coastal and continental regions would help to capture interannual variability, extreme deposition events and evolving emission patterns. Additionally, these deposition measurements would benefit from co-located measurements of precipitation characteristics, aerosol composition and meteorology. This would improve the interpretation of PFAA transport and deposition processes.

Third, mechanistic understanding and parametrization of dry deposition of PFAAs can be improved. The NL-BELT and Toronto studies highlight that dry deposition is an important removal mechanism, yet the processes driving this removal pathway remain sparse. Targeted field campaigns that measure both gas and particle phase PFAA is needed along with concurrent high resolution measurements of oxidants, meteorology and precursors.

Fourth, to confidently link observed deposition patterns to sources, future studies should couple deposition measurements with concurrent monitoring of key precursors. Co-located measurements of HFCs, HFOs, fluorotelomer alcohols and other volatile PFAA precursors alongside oxidant levels, would allow for a more quantitative

assessment of source receptor relationship and of the relative importance of long-lived versus short-lived precursors. Targeted work is needed to better constrain the role of aerosols and biomass burning in PFAS transport and deposition, including the extent to which marine aerosol processes mediate coastal inputs and whether biomass burning produces (or remobilize) PFAS in ways that influence atmospheric deposition. Combining such measurements with inverse modelling could help refine regional and global emissions estimates and test hypothesis regarding the drivers of observed changes in deposition, including the influence of regulatory actions and short term emission perturbations.

Finally, continued comparison of observations with chemical transport models is essential. However, these comparisons must be accompanied by targeted model development. Model efforts should incorporate updated emission inventories for both legacy and replacement PFAAs. There needs to be improved representation of precursor degradation pathways, more realistic wet and dry deposition parameterizations for PFAAs and between treatment of processes specific to the tropics and high latitude, including enhanced deposition volumes.

Taken together, these future directions emphasize the need for sustained, coordinated, and multi-disciplinary efforts that bridge field measurements, laboratory studies and modelling. Building on the measurements and insights presented in this thesis, such efforts will be vital for fully characterizing the environmental footprint of existing and emerging PFAA chemistries and for guiding the development of safter and more sustainable alternatives.

APPENDIX A

SUPPORTING INFORMATION FOR CHAPTER TWO

A 50-year record for perfluoroalkyl acids in the High Arctic: Implications for global and local transport

Section A-1: Method

List of PFAS analyzed in the current study.

Table A-1: Acronym, number of carbons, name/structure, and CAS No. of PFASs considered in this study.

Acronym	Number of carbons	Name / Structure	CAS. No
Perfluoroalkyl carboxylic acids (PFCAs)			
PFPeA	5	perfluoropentanoic acid	2706-90-3
PFHxA	6	perfluorohexanoic acid	307-24-4
PFHpA	7	perfluorohepTanoic acid	375-85-9
PFOA	8	perfluorooctanoic acid	335-67-1
PFNA	9	perfluorononanoic acid	375-95-1
PFDA	10	perfluorodecanoic acid	335-76-2
PFUnDA	11	perfluoroundecanoic acid	2058-94-8
PFDoDA	12	perfluorododecanoic acid	307-55-1
PFTrDA	13	perfluorotridecanoic acid	72629-94-8
PFTeDA	14	perfluorotetradecanoic acid	376-06-7
Perfluoroalkane sulfonic acids (PFSAs)			
PFBS	4	perfluorobutane sulfonic acid	375-73-5
PFHxS	6	perfluorohexane sulfonic acid	355-46-4
PFHpS	7	Perfluoroheptane sulfonic acid	
PFOS	8	perfluorooctane sulfonic acid	1763-23-1
PFDS	10	Perfluorodecane sulfonic acid	335-77-3
PFECHS	8	perfluoroethylcyclohexane sulfonate	646-83-3
Perfluorooctane sulfonamides/amidoethanols (xFOSA/Es)			
FOSA	8	$C_8F_{17}SO_2NH_2$	754-91-6
Emerging PFAS (per- and polyfluorinated ethers)			
HFPO-DA	6	$C_6HF_{11}O_3$	13252-13-6
ADONA	7	$CF_3OC_3F_6OCFHCF_2CO_2$-	
8Cl-PFOS	8	$ClC_8F_{16}SO_3$-	
9Cl-PF3ONS	8	$ClC_6F_{12}OC_2F_4SO_3$	Component of F-53B

Sample collection

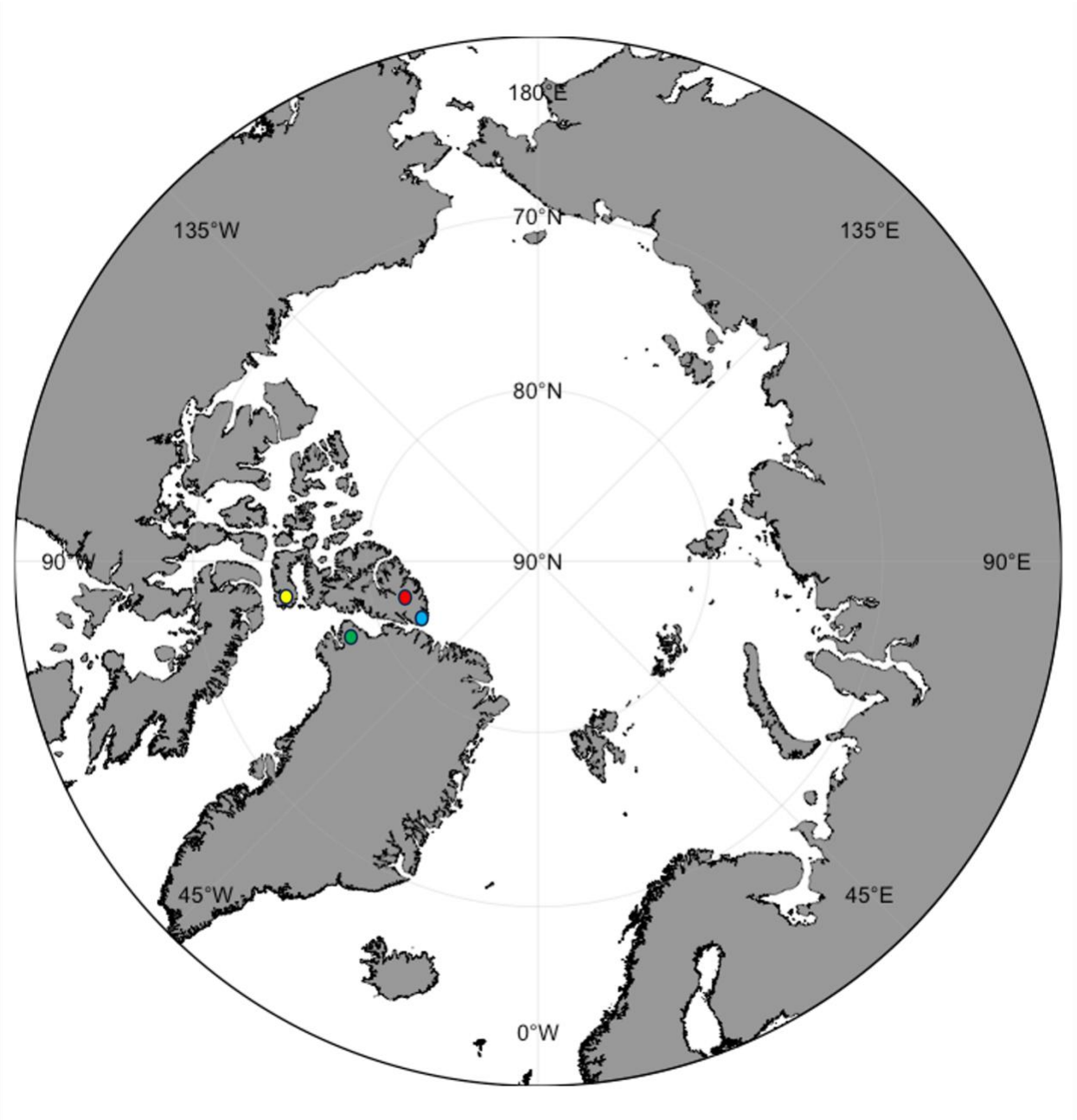

Figure A-4: Polar stereographic map of the Arctic region showing Mt. Oxford icefield, Canada (red circle), Thule Air Base, Qaanaaq, Greenland (green circle), Canada Forces Station (CFS) Alert (Blue Circle) and the Devon Ice Cap (yellow circle).

Ice core dating and sectioning

Dating of the ice core collected from Mt. Oxford icefield was done using oxygen stable isotope records and other glaciochemical records measured in a co-located core that was drilled simultaneously within a few metres from the core in the current study. A Picarro cavity ring – down spectroscopy analyzer was utilized to determine the oxygen isotope composition, the precision of $\delta^{18}O$ of water samples is ≤ 0.1 %. Sample isotope ratios were standardized using three working standards calibrated against the IAEA standards VSMOW and SLAP. Final $\delta^{18}O$ values are on the VSMOW/SLAP scale. The $\delta^{18}O$ time series were used to establish age-depth relationships by matching the $\delta^{18}O$ core records with local summer and winter solstice dates (linearly interpolating between solstices).[1] Elemental, ion, and H_2O_2 analyses for both cores were performed on an ICP-MS.[2] Where $\delta^{18}O$ records were ambiguous, we additionally used the non-sea salt sulfur/sodium (nssS/Na) summer peak (indicative of summer solstice) as well as H_2O_2 to ascertain the annual $\delta^{18}O$ maxima. We counted annual peaks in the remaining major ionic species to validate and confirm the accuracy of the age assignment (e.g., Figure A-2). Validation of the oxygen isotope-based dating was done using (in this order): nss-S, Na^+, H_2O_2, Mg^{2+}, Cl^-, and Ca^{2+}. Further confirmation of dating assignment was conducted using the Pb-enrichment time series wherein the 1979 spike in Pb enrichment was used as a tie-point. The total dating error for this method is ±1 year. The 16.5 – metre ice core was separated and packaged into 1-metre sections for transport.

Depths corresponding to a calendar year were determined as described above, and the dates of each 1-meter section were subsequently determined. To section the cores, we removed the samples from a -38°C storage freezer into a refrigerated vestibule (-10°C). We then removed each 1-metre section from the packaging and placed the firn and ice pieces onto aluminum foil that was previously cleaned with methanol. Each section was separated into a calendar year and placed in a labelled pre-cleaned polyethylene bottle. Using the aluminium foil underneath the firn and ice pieces ensured minimal loss and easy transfer to the polypropylene bottles. Samples were kept frozen at -38°C until extraction and analysis.

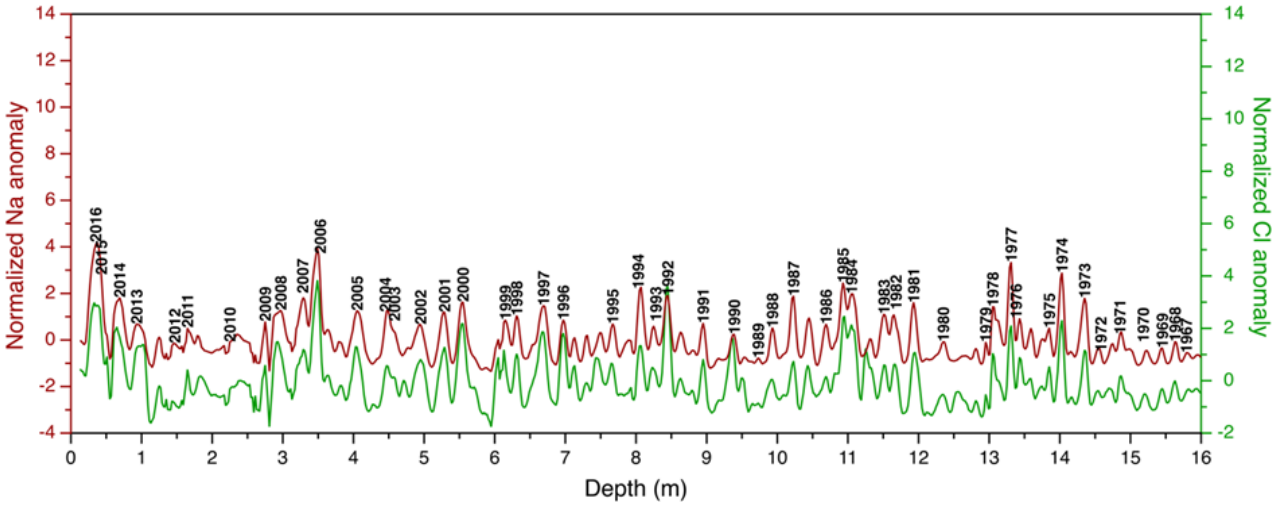

Figure A-2: Sodium (Na^+) and chloride (Cl^-) ions measured in 2 cm intervals in an ice core collected on Mt Oxford icefield co-located with the ice core examined in this study. Na and Cl are expressed as normalized anomaly* with labels corresponding to the winter maxima year. Normalized anomaly = $\frac{(X-m)}{s}$, where X is the data point, m *and* s are average and standard deviation, respectively. A three-point moving average smoother was also applied.

Controls for mitigating PFAS contamination in field sampling and lab processing

Extensive care was taken in handling the ice core to prevent contamination that could compromise the trace analysis of PFAAs. It is well established that PFAAs are extensively used consumer applications, therefore we specifically avoided products containing fluoropolymer coatings during the collecting, processing, and analysis of PFAAs. The ice core drill (Kovacs Mark II coring system, http://kovacsicedrillingequipment.com/coring-systems/mark-ii/) do not contain any material of concern which could potentially contaminate the ice core. It is also essential to note that the entire rind of the core is completely removed and discarded so that any firn or ice that was touching the inner circumference of the barrel is removed to mitigate contamination.

Additionally, we previously prepared field exposed blanks consisting of HPLC grade water that was transported to the field site, opened and exposed to the atmosphere in the Arctic location Resolute Bay Nunavut since 2010. These samples were shipped back to the lab, extracted, and analyzed with methods analogous to the ice core samples

and compared to HPLC water stored in the lab (See Pickard et al., 2018 for further details). The results from this exercise indicated that environmental exposure and shipping do not contribute to PFAS contamination. We acknowledge that these field blanks have limitations and are not identical to an ice core.

Contamination was also minimized during sectioning and analysis. Extensive planning was done to ensure that the ice core was handled minimally to reduce the risk of contamination. Sectioning itself was done in a refrigerated vestibule that is only used for ice core sectioning and has controlled temperature, humidity airflow and pressure. Only one person handled the actual core, everyone in the room wore nitrile gloves and lab coats. The ice core was placed on a stainless-steel table that was lined with pre-cleaned heavy duty aluminum foil sheets. We used a stainless-steel saw that was cleaned with solvent between each annual layer. After each cut the foil was discarded. The ability to constrain contamination during ice core collection and handling is an important area for future studies.

PFAS chemical extraction and analysis

The sample extraction procedure was adapted from Pickard et al.[1] Prior to extraction, sub-samples were spiked with internal standards (IS) to monitor recovery and matrix effects. Additionally, before instrument analysis, sample extracts were spiked with instrument performance standards (IP) to account for matrix effects and instrument drift. Table A-2 outlines the IS and IP standards used, the analyte ion transitions used are also included.

Chromatographic separation of targeted PFAS were separated using an Acquity UPLC BEH C18 column (Waters Acquity UPLC® BEH, 2.1 x 50 mm,1.7 μm) with a water – methanol gradient elution. An isolator column was employed to separate background contamination from the sample injection. The composition of the mobile phases was 98/2 SPE-cleaned water/ methanol containing 2 mM ammonium acetate (A) and MeOH (B). All solvents were HPLC grade. The method was a fifteen-minute run, at a flow rate of 0.3 mL min^{-1}. A summary of the chromatographic conditions for this gradient method is shown in Table A-3. The inlet and mass spectrometric conditions used for separation is summarized in Table A-4.

Table A-2: Analyte quantifier and qualifier ion transitions (m/z) and internal standards used for PFAAs analysis. Internal standards were used to evaluate recovery and matrix effects, whereas instrument performance standards were used to evaluate matrix effects only. Precursor ion/product ion transitions (m/z) are indicated in brackets.

PFAAs	Quantifier/Qualifier Ion Transitions (m/z)	Internal Standards	Instrument Performance Standards
PFPeA	263 > 219	$^{13}C_5$ PFPeA (268/223)	$^{13}C_3$ PFPeA (266/222)
PFHxA	313 > 269 / 313 > 119	$^{13}C_2$ PFHxA (315/270)	$^{13}C_5$ PFHxA (318/273)
PFHpA	363 > 319 / 363 > 169	$^{13}C_4$ PFHpA (367/322)	
PFOA	413 > 369 / 413 > 169	$^{13}C_4$ PFOA (417/372)	$^{13}C_2$ PFOA (415/370)
PFNA	463 > 419 / 463 > 219	$^{13}C_5$ PFNA (468/423)	$^{13}C_9$ PFNA (472/427)
PFDA	513 > 469 / 513 > 219	$^{13}C_2$ PFDA (515/470)	$^{13}C_6$ PFDA (519/474)
PFUnDA	563 > 519 / 563 > 269	$^{13}C_2$ PFUnDA (565/520)	$^{13}C_7$ PFUnDA (570/525)
PFDoDA	613 > 569 / 613 > 169	$^{13}C_2$ PFDoDA (615/570)	
PFTrDA	663 > 619 / 663 > 169	$^{13}C_2$ PFDoDA (615/570)	
PFTeDA	713 > 669 / 663 > 169	$^{13}C_2$ PFTeDA (715/670)	
PFHxDA	813 > 769 / 813 > 169	$^{13}C_2$ PFHxDA (815/770)	
PFBS	299 > 80 / 229 > 99	$^{13}C_3$ PFBS (302/99)	
PFHxS	399 > 80 / 399 > 99	$^{18}O_2$ PFHxS (403/103)	$^{13}_{C3}$ PFHxS (402/99)
PFHpS	449 > 80 / 449 > 99	$^{18}O_2$ PFHxS (403/103)	
PFOS	499 > 80 / 499 > 99	$^{13}C_4$ PFOS (503/99)	$^{13}C_8$ PFOS (507/99)
PFDS	599 > 80 / 599 > 99	$^{13}C_4$ PFOS (503/99)	
FOSA	498 > 78	$^{13}C_8$ FOSA (506/78)	
PFECHS	461 > 381 / 461 > 99	$^{18}O_2$ PFHxS (403/103)	
HFPO-DA	285>169	MHFPO-DA (287/ 169)	
ADONA	377>251, 377 > 85	$^{18}O_2$ PFHxS (403/103)	
8Cl-PFOS	515 > 80, 517 > 80	$^{13}C_4$ PFOS (503/99)	
9Cl-PF3ONS	531 > 83, 531 > 351	$^{13}C_4$ PFOS (503/99)	
11Cl-PF3OUdS	631 > 83, 631 > 451	$^{13}C_4$ PFOS (503/99)	

Table A-3: Summary of chromatographic conditions

Time (minutes)	Flow rate (mL min^{-1})	% A	% B
0	0.400	75	25
0.5	0.400	75	25
5.0	0.400	15	85
5.1	0.400	0	100
5.6	0.400	0	100
7.0	0.400	0	100
9.0	0.400	75	25
15.0	0.400	75	25

Table A-4: Summary of inlet and mass spectrometric conditions

Capillary Voltage (kV)	0.7
Source Offset (V)	50
Source Temperature (°C)	150
Desolvation Gas Temperature (°C)	450
Cone Gas Flow (L hr^{-1})	150
Desolvation Gas Flow (L hr^{-1})	800
Collision Gas Flow (mL min^{-1})	0.15
Nebulizer Pressure (bar)	7.0
Column Temperature (°C)	50
Injection Volume (µL)	9.0

Major Ion Analysis in melted ice core section

Sub samples of the sectioned ice core (15 mL) were analyzed for major anions and cations. Cation analysis was done using a Dionex 6000 Ion chromatography system coupled to a conductivity detector. Separation was achieved using a Dionex IonPac CS19 (4 x 250 mm) column equipped with a guard column (Dionex IonPac GS19, 4 x 50 mm) using an isocratic elution method with methanesulfonic acid at 1.0 mL min^{-1}. The eluent was supressed (CRDS 600 ion suppressor, 4 mm) before the analytes were measured. Calibration standards were prepared by serial dilution from the stock standard (Dionex 6

Cation I standard). In addition to calibration standards, two check standards and reagent blank were run every ten (10) samples.

Quality Control and Quality Assurance

The mean recoveries and standard errors for the IS and IP standards are provided in Tables A-5 and A-6. Recoveries are based on peak area comparisons to spiked solvent standards. The accuracy was evaluated by spiking an Arctic freshwater composite matrix (n=2) with native standards (final concentration in extract is 3 ng/mL) and treating analogous to a sample (see Table A-7). To obtain the composite matrix, excess melted sample from each discrete layer was combined. The final concentrations were then compared to the theoretical spiked concentrations. Similarly, two additional 500 mL aliquots were taken through the extraction method but only spiked with isotopically labeled standards just prior to the instrumental analysis (post extraction spikes).

Table A-5: Recovery of IS in sample extracts. Standards with number refers to the different ion transitions (m/z). Recovery is based on peak area in sample extracts compared to spiked solvent standard. Mean (standard deviation) recovery reported for n = 50 samples from the Mt. Oxford, icefield.

Internal Standards	Recovery (%)
$^{13}C_5$ PFPeA	63 (7.1)
$^{13}C_2$ PFHxA	64 (6.6)
$^{13}C_4$ PFHpA	69 (5.9)
$^{13}C_4$ PFOA	71 (5.6)
$^{13}C_5$ PFNA	72 (5.6)
$^{13}C_2$ PFDA	67 (8.9)
$^{13}C_2$ PFUnDA	57 (14)
$^{13}C_2$ PFDoDA	43 (14)
$^{13}C_2$ PFTeDA	56 (21)
$^{13}C_2$ PFHxDA	121 (60)
^{13}C8 FOSA	
$^{13}C_4$ PFOS	70(6.2)
$^{18}O_2$ PFHxS	76 (4.3)
$^{13}C_3$ PFBS	76 (4.4)
$^{13}C_3$ HFPO-DA	72 (6.7)

Table A-6: Recovery of isotopically labeled instrument performance (IP) standards in sample extracts. Recovery based on peak area in sample extract divided by peak area in spiked calibration standard at the same concentration. Mean (standard deviation) recovery reported for n = 50 samples from the Mt. Oxford icefield

Instrument Performance Standards	Recovery (%)
$^{13}C_3$ PFPeA	86 (6.2)
$^{13}C_5$ PFHxA	82 (5.0)
$^{13}C_2$ PFOA	84 (6.0)
$^{13}C_9$ PFNA	85 (6.5)
$^{13}C_6$ PFDA	88 (6.2)
$^{13}C_7$ PFUnDA	88 (7.2)
$^{13}C_8$ PFOS 80	84 (5.6)
$^{13}C_8$ PFOS 99	84 (5.5)

Table A-7: Calculated recoveries of Native PFAS analytes in spiked Arctic freshwater composite samples. Two samples were spiked before extraction and two samples were spiked after extraction. The range in calculated recovery is presented.

PFAAs	Recovery in sample spiked before extraction (%), n=2	Recovery in sample spiked after extraction (%), n=2
PFPeA	99-104	97-100
PFHxA	94-100	88-99
PFHpA	96-101	97-98
PFOA	78-90	78-81
PFNA	95-97	93-94
PFDA	99-103	92-100
PFUnDA	96-106	98-102
PFDoDA	97-103	92-97
PFTrDA	70-85	99-108
PFTeDA	102-113	98-100
PFHxDA	113-115	100-101
PFBS		
PFHxS	95-105	96-99
PFHpS	101-106	95-99
PFOS	87-95	94-102
PFDS	68-87	94-96
FOSA	96-103	100-100
PFECHS	92-101	93-97
HFPO-DA	95-103	94-95
ADONA	113-119	112-117
8Cl-PFOS	100-106	102-102
9Cl-PF3ONS	88-98	92-98
11Cl-PF3OUdS	NA	NA

Cartridge blanks (n=8) were included in the method analysis. Briefly, SPE conditioned water was spiked with the internal standard, extracted, and treated analogously as a sample. In addition, regular injections of MeOH and 1:1 MeOH/water were injected during the instrument batch to evaluate lab contamination and carryover. The method detection limit (MDL) is based on the average raw signal in method blanks plus 3 times the standard deviation. This concentration was transformed into sample units by multiplying by the final extract volume of 0.5 ml and dividing by a theoretical

sample volume of 0.5 L to obtain units relatable to sample reporting. The instrument detection limit was estimated using the IUPAC method, based on analysis of low-level calibration standards (near blank with signal to noise of less than 10) and the slope of the calibration curve (*m*):

$$\mathrm{LOD} = \frac{\mathrm{k}\, S_B}{\mathrm{m}}$$

Where S_B is the standard deviation of the raw signal in low level calibration standards and k = 3.

Table A-8: Instrument detection limit (LOD, ng/ml) based on calibration standard with S/N of 3 and method detection limit (MDL, ng/L) based on average + 3 times standard deviation of method blanks. Method detection limit is in units comparable to sample concentrations.

Internal Standards	LOD (ng/mL)	MDL (ng/L)
PFPeA	0.0032	0.0098
PFHxA	0.0120	0.0390
PFHpA	0.0039	0.0074
PFOA	0.0061	0.0130
PFNA	0.0054	0.0037
PFDA	0.0022	0.0045
PFUnDA	0.0099	0.0051
PFDoDA	0.0044	0.0025
PFTrDA	0.0014	0.0050
PFTeDA	0.0120	0.0075
PFHxDA	0.0590	0.0960
PFBS	0.0056	0.0080
PFHxS	0.0048	0.0074
PFHpS	0.0042	0.0055
PFOS	0.0081	0.0760
PFDS	0.0110	0.0034
PFECHS	0.0028	0.0330
FOSA	0.0010	0.0041
HFPO-DA	0.0360	0.0120
8Cl PFOS	0.0059	0.0032
ADONA	0.0063	0.0010
9Cl-PF3ONS	0.0102	0.0045
11Cl-PF3OUdS	0.0053	0.0028

Data Handling

Correlation Analysis

Correlation analysis was conducted on fluxes of PFAAs and major ions in ice sections. Only detected values were included (i.e. <LOD were excluded). The annual fluxes of PFAA and ions were logarithm-transformed [$\log_{10}$ PFAA,ions] to approximate normality, which was evaluated using Shapiro-Wilk tests of kurtosis and skewness. Significant correlations using Pearson correlation coefficient (r) was based on threshold of $p<0.05$. In addition, correlations were classified as very strong (0.90-1.0), strong (0.70-0.90), moderate (0.50-0.70) and weak (0.30-0.50).

Calculating Deposition Flux

Fluxes for each analyte were calculated for each calendar year. The analyte concentration (ng/L) was multiplied by the total ice volume per year (L/yr) and divided by the area (m^2).

$$\text{Flux} = \frac{\text{Analyte Concentration } \left(\frac{\text{ng}}{\text{L}}\right) \text{ x Total ice volume per year } \left(\frac{\text{L}}{\text{yr}}\right)}{\text{Area } (\text{m}^2)}$$

(Area = πr^2, where r = 3.85 cm)

Air Mass Transport Densities

Air mass back-trajectories were calculated to help characterize the probable marine moisture source regions and flow pathways of air masses reaching the ice core site. Annual air parcel back trajectories were calculated using the NOAA Hybrid Single-Particle Lagrangian Integrated Trajectory (HySPLIT) model.[3] HySPLIT has been used previously to assess the transport pathways of precipitation to Arctic ice core sites (e.g., Criscitiello et al., 2016; Criscitiello et al., 2021).[4,5] Ten-day back trajectories were calculated using National Centers for Environmental Protection and Atmospheric Research (NCEP/NCAR) global atmospheric reanalysis data sets, with a focus on low-elevation air masses (0–500 m above terrain) that are more likely to be representative of evaporation moisture sources.[6] We subsequently calculated air mass transport densities from single trajectories to derive more reliable airflow pathways and help discriminate

between local circulation patterns and regional-scale flow features.[5,7] The air mass transport density results are discussed in the context of ice core chemistry, and offer insight into probable airflow pathways arriving at the ice core site during time periods of interest in this study.

Section A-2: PFAA Concentration and Fluxes at the Mt. Oxford icefield

Table A-9:Depth profile (cm) of long chain PFCAs concentrations (ng L^{-1}) from Mt. Oxford icefield. Values <MDL are identified in red.

		Concentration (ng L^{-1})							
Depth(cm)	Year	PFPeA	PFHxA	PFHpA	PFOA	PFNA	PFDA	PFUnDA	PFDoDA
41	2016	0.254	0.465	0.951	0.857	1.147	0.118	0.084	0.011
63	2015	0.218	0.386	0.574	0.546	0.806	0.095	0.057	0.007
89	2014	0.280	0.509	0.882	0.976	1.147	0.113	0.087	0.014
138	2013	0.121	0.245	0.439	0.635	1.113	0.140	0.203	0.016
163	2012	0.104	0.288	0.533	0.862	2.330	0.191	0.276	0.025
191	2011	0.104	0.168	0.255	0.484	0.488	0.058	0.034	<0.0025
227	2010	0.230	0.422	0.324	0.530	0.745	0.159	0.119	0.020
279	2009	0.141	0.205	0.348	0.346	0.510	0.110	0.122	0.017
325	2008	0.279	0.420	0.526	0.651	0.778	0.109	0.093	0.012
353	2007	0.140	0.281	0.457	0.754	0.730	0.078	0.072	0.011
399	2006	0.186	0.390	0.539	0.905	0.949	0.106	0.090	0.014
413	2005	0.220	0.370	0.607	0.887	0.982	0.136	0.118	0.016
447	2004	0.118	0.165	0.257	0.434	0.543	0.078	0.092	0.018
490	2003	0.136	0.191	0.323	0.525	0.638	0.054	0.027	0.004
517	2002	0.137	0.208	0.368	0.552	0.677	0.123	0.099	0.012
545	2001	0.090	0.153	0.296	0.429	0.462	0.059	0.014	0.003
587	2000	0.123	0.218	0.316	0.464	0.589	0.086	0.081	0.016
615	1999	0.142	0.220	0.368	0.417	0.652	0.104	0.091	0.013
661	1998	0.115	0.228	0.333	0.391	0.386	0.064	0.051	<0.0025
687	1997	0.119	<0.0390	<0.0074	<0.0130	<0.0037	<0.0045	<0.0051	<0.0025
733	1996	0.102	0.234	0.377	0.404	0.583	0.081	0.060	0.011
775	1995	0.084	0.193	0.240	0.376	0.294	0.039	0.031	0.008
809	1994	0.058	0.165	0.160	0.282	0.218	0.034	0.027	<0.0025
835	1993	0.042	0.132	0.137	0.248	0.167	0.025	0.021	<0.0025
878	1992	0.048	0.111	0.130	0.268	0.158	0.026	0.013	<0.0025
920	1991	0.057	0.183	0.167	0.486	0.228	0.039	0.014	<0.0025
971	1990	0.037	0.091	0.078	0.263	0.071	0.015	0.006	<0.0025
987	1989	0.021	0.092	0.053	0.098	0.042	0.030	0.005	<0.0025
1010	1988	0.012	0.085	0.050	0.100	0.061	0.020	0.009	0.005
1057	1987	<0.0098	<0.0390	0.036	0.076	0.036	0.018	0.007	<0.0025
1079	1986	0.013	<0.0390	0.031	0.070	0.032	0.025	0.005	<0.0025
1103	1985	0.011	0.051	0.045	0.155	0.046	0.019	<0.0051	<0.0025
1138	1984	0.011	0.049	0.037	0.132	0.033	0.019	0.005	0.004
1172	1983	0.013	<0.0390	0.022	0.071	0.012	0.013	<0.0051	<0.0025
1190	1982	0.015	<0.0390	0.021	0.058	0.012	0.014	<0.0051	0.004
1233	1981	0.020	<0.0390	0.017	0.042	0.010	0.011	<0.0051	0.008
1277	1980	0.066	<0.0390	0.017	0.041	0.007	0.010	<0.0051	<0.0025
1300	1979	0.012	0.678	0.060	0.054	0.011	0.018	<0.0051	0.006
1318	1978	0.004	0.206	0.012	0.061	0.010	0.009	<0.0051	<0.0025
1332	1977	0.025	<0.0390	0.011	0.036	0.008	0.009	<0.0051	<0.0025
1363	1976	0.029	<0.0390	<0.0074	0.048	0.007	0.014	<0.0051	<0.0025
1389	1975	0.041	<0.0390	0.011	0.044	0.012	0.018	0.005	0.002
1410	1974	0.013	0.067	0.034	0.652	0.076	0.040	<0.0051	0.016
1438	1973	0.016	0.063	0.045	1.078	0.096	0.038	0.013	0.006
1461	1972	<0.0098	<0.0390	<0.0074	0.039	0.011	0.013	<0.0051	0.003
1482	1971	0.035	<0.0390	<0.0074	0.084	0.009	0.018	<0.0051	0.002
1515	1970	0.035	<0.0390	<0.0074	0.069	0.018	0.010	<0.0051	0.004
1547	1969	<0.0098	<0.0390	0.012	0.136	0.018	0.014	<0.0051	<0.0025
1575	1968	<0.0098	<0.0390	0.010	0.053	0.006	0.012	<0.0051	0.004
1588	1967	<0.0098	<0.0390	0.010	0.121	0.011	0.006	<0.0051	<0.0025

Table A-10: Depth profile (cm) of PFSA concentrations (ng L^{-1}) from Mt. Oxford icefield. Values <MDL are identified in red.

		Concentration (ng L^{-1})			
Depth(cm)	**Year**	**PFBS**	**PFOS**	**PFECHS**	**FOSA**
41	2016	0.037	0.267	0.065	0.008
63	2015	0.046	0.264	0.094	0.004
89	2014	0.008	<0.0760	<0.0330	0.008
138	2013	<0.0080	0.026	0.040	0.005
163	2012	0.021	0.076	0.045	0.009
191	2011	<0.0080	<0.0760	0.033	0.011
227	2010	0.015	0.077	0.067	0.009
279	2009	<0.0080	<0.0760	0.116	0.004
325	2008	0.017	0.082	0.117	0.012
353	2007	<0.0080	<0.0760	0.050	0.037
399	2006	<0.0080	<0.0760	<0.0330	0.059
413	2005	0.070	0.476	0.077	0.050
447	2004	<0.0080	<0.0760	0.048	0.044
490	2003	<0.0080	<0.0760	<0.0330	0.035
517	2002	0.021	<0.0760	<0.0330	0.064
545	2001	0.002	<0.0760	<0.0330	0.065
587	2000	0.029	0.213	0.053	0.059
615	1999	0.008	<0.0760	<0.0330	0.064
661	1998	0.017	0.087	<0.0330	0.056
687	1997	<0.0080	<0.0760	<0.0330	0.037
733	1996	0.008	0.079	0.065	0.041
775	1995	0.008	<0.0760	<0.0330	0.032
809	1994	<0.0080	<0.0760	<0.0330	0.030
835	1993	0.017	0.144	0.048	0.027
878	1992	0.015	0.114	0.104	0.028
920	1991	<0.0080	<0.0760	<0.0330	0.017
971	1990	<0.0080	<0.0760	0.039	0.004
987	1989	0.434	4.168	0.065	0.007
1010	1988	0.017	0.116	0.083	0.011
1057	1987	<0.0080	<0.0760	0.067	0.004
1079	1986	0.015	<0.0760	<0.0330	0.008
1103	1985	0.067	0.452	0.040	0.008
1138	1984	0.019	0.104	0.075	0.009
1172	1983	0.022	0.130	0.082	0.004
1190	1982	0.012	0.099	0.062	<0.0041
1233	1981	<0.0080	<0.0760	0.061	<0.0041
1277	1980	<0.0080	<0.0760	0.142	<0.0041
1300	1979	0.687	1.355	0.090	<0.0041
1318	1978	0.011	<0.0760	0.033	<0.0041
1332	1977	0.012	0.086	<0.0330	<0.0041
1363	1976	0.076	1.235	<0.0330	<0.0041
1389	1975	0.017	<0.0760	0.132	<0.0041
1410	1974	0.014	0.090	0.098	<0.0041
1438	1973	0.014	0.153	0.122	<0.0041
1461	1972	<0.0080	<0.0760	0.043	<0.0041
1482	1971	<0.0080	0.012	0.064	<0.0041
1515	1970	0.112	1.654	0.023	<0.0041
1547	1969	0.022	0.157	0.046	<0.0041
1575	1968	0.009	<0.0760	0.035	<0.0041
1588	1967	0.009	0.081	0.064	<0.0041

Table A-11: Depth profile (cm) of PFCA fluxes (ng m^{-2} a^{-1}) on the Mt Oxford icefield. Numbers in red indicate instances where ½ MDL was used for annual flux calculation.

		Flux (ng m^2 a^{-1})							
Depth(cm)	**Year**	**PFPeA**	**PFHxA**	**PFHpA**	**PFOA**	**PFNA**	**PFDA**	**PFUnDA**	**PFDoDA**
41	2016	37.27	68.24	139.56	125.76	168.32	17.32	12.33	1.61
63	2015	16.98	30.06	44.70	42.52	62.76	7.40	4.44	0.55
89	2014	34.00	61.82	107.12	118.53	139.30	13.72	10.57	1.70
138	2013	34.38	69.62	124.75	180.44	316.27	39.78	57.68	4.55
163	2012	9.87	27.32	50.56	81.77	221.03	18.12	26.18	2.37
191	2011	37.15	60.02	91.10	172.90	174.33	20.72	12.15	0.45
227	2010	21.03	38.59	29.63	48.47	68.13	14.54	10.88	1.83
279	2009	50.29	73.12	124.13	123.42	181.92	39.24	43.52	6.06
325	2008	64.29	96.78	121.20	150.01	179.27	25.12	21.43	2.77
353	2007	17.56	35.25	57.34	94.60	91.59	9.79	9.03	1.38
399	2006	43.52	91.26	126.12	211.76	222.06	24.80	21.06	3.28
413	2005	12.94	21.77	35.71	52.18	57.77	8.00	6.94	0.94
447	2004	18.93	26.47	41.24	69.64	87.13	12.52	14.76	2.89
490	2003	32.16	45.17	76.39	124.16	150.89	12.77	6.39	0.95
517	2002	22.51	34.18	60.48	90.71	111.26	20.21	16.27	1.97
545	2001	12.74	21.66	41.90	60.73	65.40	8.35	1.98	0.42
587	2000	26.99	47.84	69.35	101.83	129.27	18.87	17.78	3.51
615	1999	21.52	33.35	55.78	63.21	98.83	15.76	13.79	1.97
661	1998	30.27	60.01	87.65	102.91	101.60	16.85	13.42	0.33
687	1997	17.97	2.94	0.56	0.98	0.28	0.34	0.39	0.19
733	1996	26.41	60.59	97.62	104.61	150.96	20.97	15.54	2.85
775	1995	22.18	50.96	63.38	99.29	77.63	10.30	8.19	2.11
809	1994	12.13	34.51	33.47	58.99	45.60	7.11	5.65	0.26
835	1993	7.46	23.46	24.35	44.07	29.68	4.44	3.73	0.22
878	1992	12.78	29.55	34.61	71.35	42.07	6.92	3.46	0.33
920	1991	15.83	50.81	46.37	134.93	63.30	10.83	3.89	0.35
971	1990	11.99	29.49	25.27	85.22	23.01	4.86	1.94	0.41
987	1989	2.30	10.09	5.81	10.75	4.61	3.29	0.55	0.14
1010	1988	1.98	14.02	8.25	16.50	10.06	3.30	1.48	0.82
1057	1987	1.54	6.13	11.32	23.90	11.32	5.66	2.20	0.39
1079	1986	1.95	2.93	4.66	10.52	4.81	3.76	0.75	0.19
1103	1985	1.72	7.97	7.03	24.22	7.19	2.97	0.40	0.20
1138	1984	2.73	12.18	9.20	32.81	8.20	4.72	1.24	0.99
1172	1983	3.62	5.42	6.12	19.75	3.34	3.62	0.71	0.35
1190	1982	2.40	3.12	3.36	9.27	1.92	2.24	0.41	0.64
1233	1981	7.46	7.27	6.34	15.66	3.73	4.10	0.95	2.98
1277	1980	20.54	6.07	5.29	12.76	2.18	3.11	0.79	0.39
1300	1979	2.07	116.69	10.33	9.29	1.89	3.10	0.44	1.03
1318	1978	0.53	27.51	1.60	8.15	1.34	1.20	0.34	0.17
1332	1977	2.67	2.08	1.17	3.84	0.85	0.96	0.27	0.13
1363	1976	7.16	4.81	0.91	11.85	1.73	3.46	0.63	0.31
1389	1975	8.16	3.88	2.19	8.75	2.39	3.58	0.99	0.40
1410	1974	2.15	11.06	5.61	107.65	12.55	6.60	0.42	2.64
1438	1973	3.30	13.00	9.28	222.39	19.80	7.84	2.68	1.24
1461	1972	0.82	3.28	0.62	6.55	1.85	2.18	0.43	0.50
1482	1971	5.57	3.10	0.59	13.37	1.43	2.86	0.41	0.32
1515	1970	9.98	5.56	1.06	19.68	5.13	2.85	0.73	1.14
1547	1969	1.17	4.66	2.87	32.50	4.30	3.35	0.61	0.30
1575	1968	1.16	4.60	2.36	12.49	1.41	2.83	0.60	0.94
1588	1967	0.54	2.16	1.11	13.40	1.22	0.66	0.28	0.14

Table A-12: Depth profile (cm) of PFSA fluxes (ng m^{-2} a^{-1}) on the Mt Oxford icefield. Numbers in red indicate instances where ½ MDL was used for annual flux calculation.

Depth(cm)	Year	PFBS	PFOS	PFECHS	FOSA
41	2016	5.43	39.18	9.54	1.17
63	2015	3.58	20.56	7.32	0.31
89	2014	0.97	4.61	2.00	0.97
138	2013	1.14	7.39	11.37	1.42
163	2012	1.99	7.21	4.27	0.85
191	2011	1.43	13.58	11.79	3.93
227	2010	1.37	7.04	6.13	0.82
279	2009	1.43	13.55	41.38	1.43
325	2008	3.92	18.89	26.96	2.77
353	2007	0.50	4.77	6.27	4.64
399	2006	0.94	8.89	3.86	13.81
413	2005	4.12	28.00	4.53	2.94
447	2004	0.64	6.10	7.70	7.06
490	2003	0.95	8.99	3.90	8.28
517	2002	3.45	6.24	2.71	10.52
545	2001	0.28	5.38	2.34	9.20
587	2000	6.36	46.75	11.63	12.95
615	1999	1.21	5.76	2.50	9.70
661	1998	4.47	22.90	4.34	14.74
687	1997	0.60	5.74	2.49	5.59
733	1996	2.07	20.46	16.83	10.62
775	1995	2.11	10.03	4.36	8.45
809	1994	0.84	7.95	3.45	6.28
835	1993	3.02	25.59	8.53	4.80
878	1992	3.99	30.35	27.69	7.45
920	1991	1.11	10.55	4.58	4.72
971	1990	1.30	12.31	12.64	1.30
987	1989	47.60	457.10	7.13	0.77
1010	1988	2.80	19.14	13.69	1.81
1057	1987	1.26	11.95	21.07	1.26
1079	1986	2.26	5.71	2.48	1.20
1103	1985	10.47	70.63	6.25	1.25
1138	1984	4.72	25.85	18.64	2.24
1172	1983	6.12	36.16	22.81	1.11
1190	1982	1.92	15.82	9.91	0.33
1233	1981	1.49	14.17	22.74	0.76
1277	1980	1.25	11.83	44.20	0.64
1300	1979	118.24	233.20	15.49	0.35
1318	1978	1.47	5.08	4.41	0.27
1332	1977	1.28	9.18	1.76	0.22
1363	1976	18.76	304.85	4.07	0.51
1389	1975	3.38	7.56	26.26	0.41
1410	1974	2.31	14.86	16.18	0.34
1438	1973	2.89	31.56	25.17	0.42
1461	1972	0.67	6.38	7.22	0.34
1482	1971	0.64	1.91	10.18	0.33
1515	1970	31.94	471.69	6.56	0.58
1547	1969	5.26	37.52	10.99	0.49
1575	1968	2.12	8.96	8.25	0.48
1588	1967	1.00	8.97	7.09	0.23

Table A-13: PFAA fluxes (ng m^{-2} a^{-1}) comparisons with other selected Arctic, sub-Arctic, and lower latitude samp

		Flux (ng m^2 a^{-1})									
Matrix (Time)	**Site (Reference)**	**PFPeA**	**PFHxA**	**PFHpA**	**PFOA**	**PFNA**	**PFDA**	**PFUnDA**	**PFDoDA**	**PFBS**	**PFOS**
Ice Core (1967-2016)	Mt. Oxford icefield, Canadian Arctic (this study)	0.5 - 64	0.8 - 117	1 - 139	3.8 - 222	0.8 - 316	0.6 - 40	0.3 - 60	0.3 - 6	0.2 - 118	0.2 - 472
Ice Core (2006-2019)	Lomonsovfonna Ice Core, Svalbard	41-570	8 - 120	5 - 99	3 - 59	4 - 120	2 - 47	1-79	0.4 - 16		0.22- 70
Ice Core (1977-2015)	Devon Ice Cap, Canadian Arctic [8]	1 - 37	3 - 38	6 - 86	6 - 80.50	5 - 141	0.5 - 21	0.8 – 29	0.2 - 2	0.7 – 0.9	1 - 80
Snow Pit 1995 – 2007	Devon Ice Cap, Canadian Arctic [9]	7 – 68	5 – 60	21 - 99	25 – 97	25 – 219	9 - 35	4 – 38	0.1 – 4	14 - 42	1 – 4
Snow Pit 1966 – 2006	Devon Ice Cap, Canadian Arctic [10]	2.5 – 9			21 – 81	2 – 103	1 – 9	1 – 10			1 – 28
Surface Snow 2005	Melville Ice Cap, Canadian Arctic[10]				5	3	1				
Surface Snow 2005	Agassiz Ice Cap, Canadian Arctic[10]				4	3	1				
Snow Core 1980 - 2010	Mt. Muztagata, Tibetan Plateau [11]	20 - 90	7 - 63		15 – 154	3 – 26	2 – 32	2 - 6	4 - 21		208 - 195
Snow Core 1980 – 2010	Mt. Zuoqiupu, Tibetan Plateau [11]	32 - 46	6 – 45		27 – 188	2 – 22	30 – 56				
Firn Core 1996 - 2008	Colle Gnifetti, Swiss/Italian Border [12]				165 - 207	86 - 113		0 - 53			
Precipitation (2006-2007 & 2007-2008) [a]	Ksukuba, Japan [13]	686	1143	814	1955	2120	551	508	121		475
Precipitation (2006-2007 & 2007-2008)[a]	Kawaguchi, Japan[13]	817	1185	983.5	2475	2270	425	534	86	5880	1133
Precipitation (2006-2007)	Slingerlands, NY, US[13]	219	834	627	2050	2070	243	456	37	8	401
Precipitation (2006-2007) [b]	Downtown Albany, NY, US[13]	857	1050	534	2090	2032	297	794	5		255
Precipitation (1998-1999) [b]	Rural U.S. (Ithaca, New York)[14]	129	113	66	143	33					
Precipitation 2002 [b]	Remote Canada (Kejimkujik, NS)[14]	9	6	16	12	12					
Precipitation (2003-2004)[b]	Urban Canada (Toronto, ON)[14]	38	30	60	169	17					

Section A-3: PFAA deposition and temporal variations

The integrity of temporal trends could be affected by post-depositional processes, such as melting, percolation and refreezing. The propensity of PFAAs to percolate downwards during snowmelt depends on several factors including the specific snow surface area, PFAA chain length, and sorptive capacity of the snow grain surface.[15] Laboratory studies suggest that short chain PFAAs have a greater tendency to partition into meltwater whereas long chain compounds will sorb to snow surface or experience delayed release.[15,16]

If melting occurred within the last five decades, we expect the seasonal trends of PFAA deposition could be distorted but the annual interpretations should not be affected since any meltwater that percolates downward should refreeze within an interannual layer.[17] To circumvent errors associated with sectioning, dating and post depositional processes, we report fluxes as five year moving averages, which allows for a multidecadal temporal trend analysis of PFAS deposition to Mt Oxford icefield.

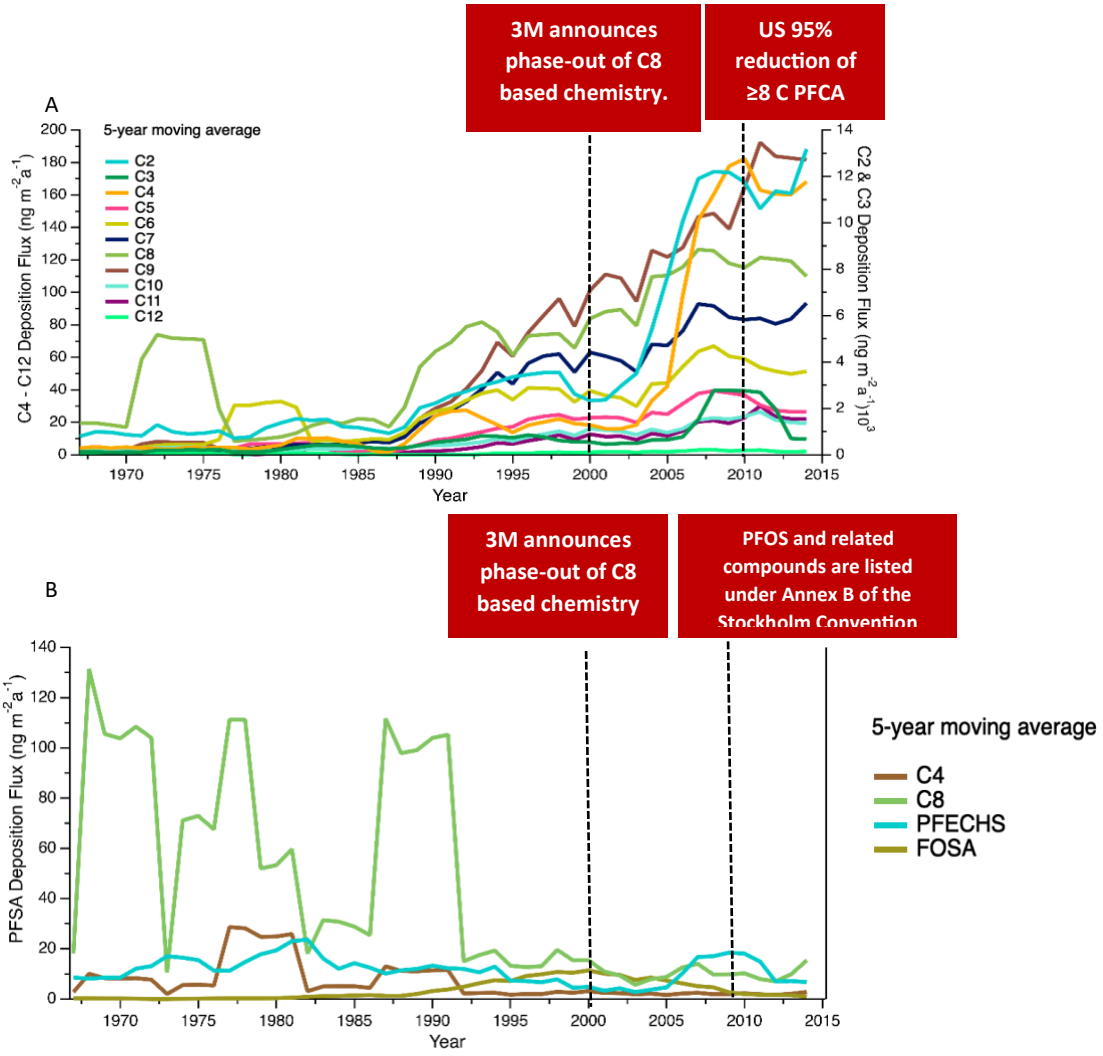

Figure A-3: Five year moving averages of (A) C2– C12 PFCA and (B) C4 PFSA, C8 PFSA, PFECHS and FOSA deposition fluxes on Mt. Oxford icefield for the entire sampling period. Regulatory and major industry changes are also included. Where applicable, ½ MDL values were used for temporal trend analysis.

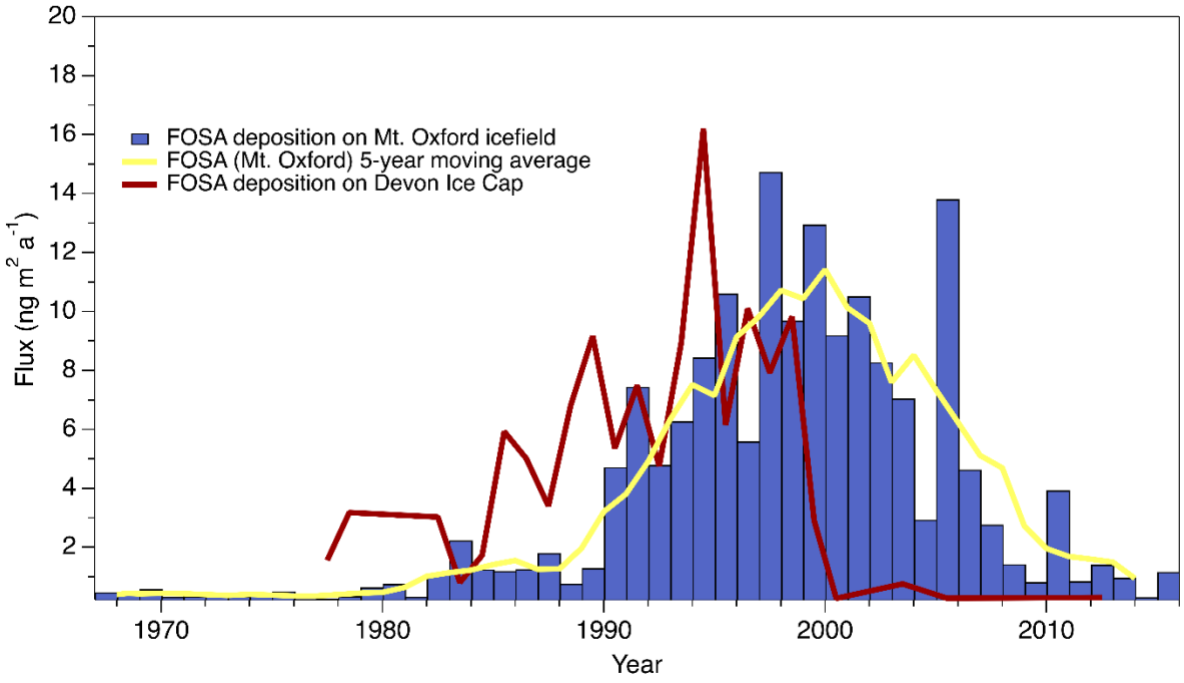

Figure A-4: FOSA fluxes (ng m^{-2} a^{-1}) at Mt. Oxford icefield annual fluxes as measured (blue bars) and with five-year moving average (yellow line). The 5-year moving average of FOSA flux to Devon Ice Cap from Pickard et al. is superimposed for comparison (red line).

Section A-4: Evidence of indirect sources of PFAAs on Mt. Oxford icefield

Table A-14: Pearson's correlation (r) matrix, and associated p-value for PFAS homologues. Weak correlations (r = 0.3-0.5) are shown in blue, moderate correlations (r= 0.5-0.7) shown in green, strong correlations (r= 0.7-0.9) are shown in red, and very strong correlations (0.9-1.0) are shown in purple. Statistically significant p-values (p<0.05) are also highlighted in bold. Data for C2-C4 PFCAs from Pickard et al.[3]

		TFA	PFPrA	PFBA	PFPeA	PFHxA	PFHpA	PFOA	PFNA	PFDA	PFUnDA	PFDoDA	PFBS	PFOS	PFECHS
TFA	r		0.77	0.91	0.64	0.83	0.84	0.76	0.80	0.75	0.73	0.48	-0.10	-0.12	-0.08
	p		1.E-14	1.E-14	5.E-6	3.E-13	1E-13	5E-10	2.E-11	3.E-09	1.E-06	0.02	0.50	0.41	0.60
PFPrA	r	0.77		0.77	0.58	0.70	0.77	0.70	0.75	0.71	0.60	0.60	-0.16	-0.09	0.05
	p	1.E-14		1.E-14	4.E-05	2.E-08	1.E-10	1.E-08	9.E-10	2.E-06	2.E-04	3.E-03	0.30	0.54	0.71
PFBA	r	0.91	0.70		0.74	0.75	0.73	0.53	0.69	0.64	0.58	0.42	0.08	-0.15	0.04
	p	1.E-14	3.E-06		1.E-06	4.E-07	7.E-7	0.001	7.E-06	5.E-5	8.E-04	0.07	0.66	0.40	0.78
PFPeA	r	0.64	0.58	0.74		0.66	0.78	0.70	0.79	0.82	0.71	0.56	-0.30	-0.02	**-0.32**
	p	5.E-6	4.E-05	1.E-06		1.E-06	5.E-10	2.E-07	1.E-09	7.E-12	4.E-06	0.007	0.06	0.88	**0.04**
PFHxA	r	0.83	0.70	0.75	0.66		0.90	0.77	0.82	0.75	0.77	0.72	0.10	0.03	-0.02
	p	3.E-13	2.E-08	4.E-07	1.E-06		2.E-18	1.E-10	2.E-12	1.E-09	1.E-07	4.E-06	0.50	0.83	0.84
PFHpA	r	0.84	0.77	0.73	0.78	0.90		0.87	0.96	0.90	0.80	0.60	-0.11	-0.13	-0.04
	p	1E-13	1.E-10	7.E-7	5.E-10	2.E-18		6.E-16	5.E-27	1.E-18	2.E-08	0.003	0.45	0.37	0.76
PFOA	r	0.76	0.70	0.53	0.70	0.77	0.87		0.90	0.87	0.68	0.53	-0.19	-0.13	0.03
	p	5E-10	1.E-08	0.001	2.E-07	1.E-10	6.E-16		6.E-19	1.E-15	1.E-05	0.010	0.20	0.40	0.83
PFNA	r	0.80	0.75	0.69	0.79	0.82	0.96	0.90		0.94	0.87	0.63	-0.21	-0.15	-0.19
	p	2.E-11	9.E-10	7.E-06	1.E-09	2.E-12	5.E-27	6.E-19		2.E-22	4.E-11	0.001	0.17	0.31	0.20
PFDA	r	0.75	0.71	0.64	0.80	0.75	0.90	0.87	0.94		0.93	0.76	-0.23	-0.18	-0.07
	p	3.E-09	2.E-06	5.E-5	9.E-10	1.E-09	1.E-18	1.E-15	2.E-22		1.E-15	3.E-05	0.11	0.25	0.62
PFUnDA	r	0.73	0.60	0.58	0.71	0.77	0.80	0.68	0.87	0.93		0.69	-0.04	0.02	0.03
	p	1.E-06	2.E-04	8.E-04	4.E-06	1.E-07	2.E-08	1.E-05	4.E-11	1.E-15		1.E-03	0.81	0.90	0.83
PFDoDA	r	0.48	0.60	0.42	0.56	0.72	0.60	0.53	0.63	0.76	0.69		**-0.46**	-0.37	-0.30
	p	0.02	3.E-03	0.07	0.007	4.E-06	0.003	0.010	0.001	3.E-05	1.E-03		**0.04**	0.10	0.09
PFBS	r	-0.10	-0.16	0.08	-0.30	0.10	-0.11	-0.19	-0.21	-0.23	-0.04	-0.46		0.90	0.23
	p	0.50	0.30	0.66	0.06	0.50	0.45	0.20	0.17	0.11	0.81	0.04		2.E-16	0.30
PFOS	r	-0.12	-0.09	-0.15	-0.02	0.03	-0.13	-0.13	-0.15	-0.18	0.02	-0.37	0.90		0.06
	p	0.41	0.54	0.399	0.88	0.83	0.37	0.40	0.31	0.25	0.90	0.10	2.E-16		0.66
PFECHS	r	-0.08	0.05	0.04	-0.32	-0.02	-0.04	0.03	-0.19	-0.07	-0.30	0.23	0.06	0.07	
	p	0.60	0.71	0.78	0.04	0.84	0.76	0.83	0.20	0.62	0.09	0.30	0.66	0.61	
FOSA	r	-9.E-03	0.11	-0.29	0.38	0.40	0.42	0.40	0.46	0.34	0.14	0.06	-0.17	0.19	-0.18
	p	0.96	0.53	0.13	0.03	0.03	0.02	0.02	0.01	0.05	0.47	0.82	0.41	0.35	0.37

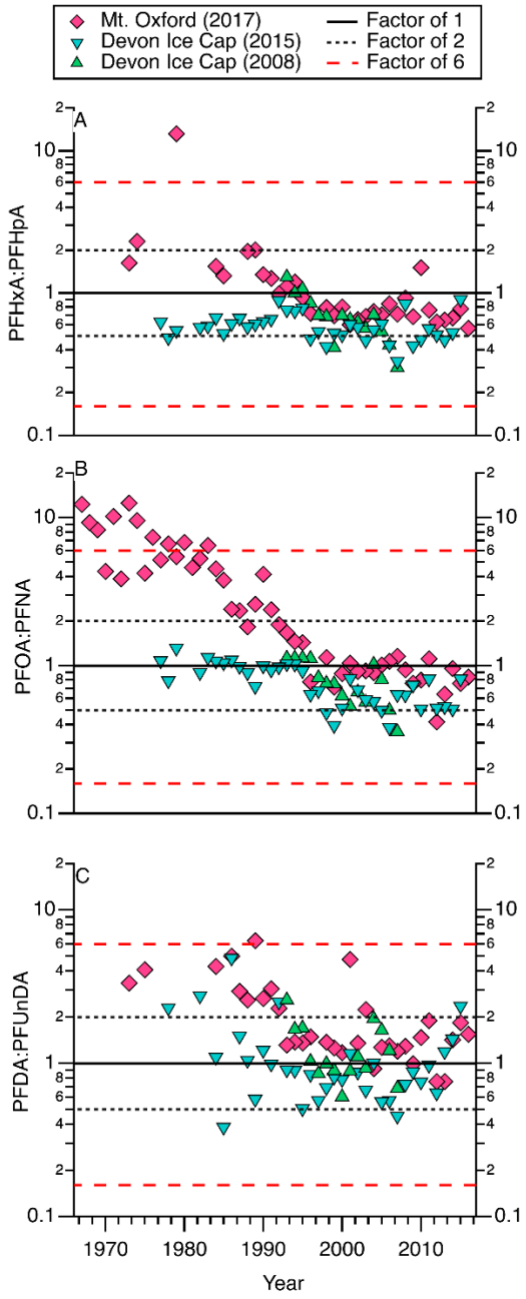

Figure A-5: Molar flux ratios of even-odd PFCA pairs: (A) PFHxA:PFHpA, (B) PFOA:PFNA and (C) PFDA:PFUnDA as a function of time. The ratios of previous studies at the Devon Ice cap (2015 and 2008) are also included for comparison. The solid black line represents molar flux ratio corresponding to 1 (i.e., equal molar amounts are deposited), whereas dashed black and red lines correspond to molar flux ratios within a factor of ± 2 and ± 6, respectively.

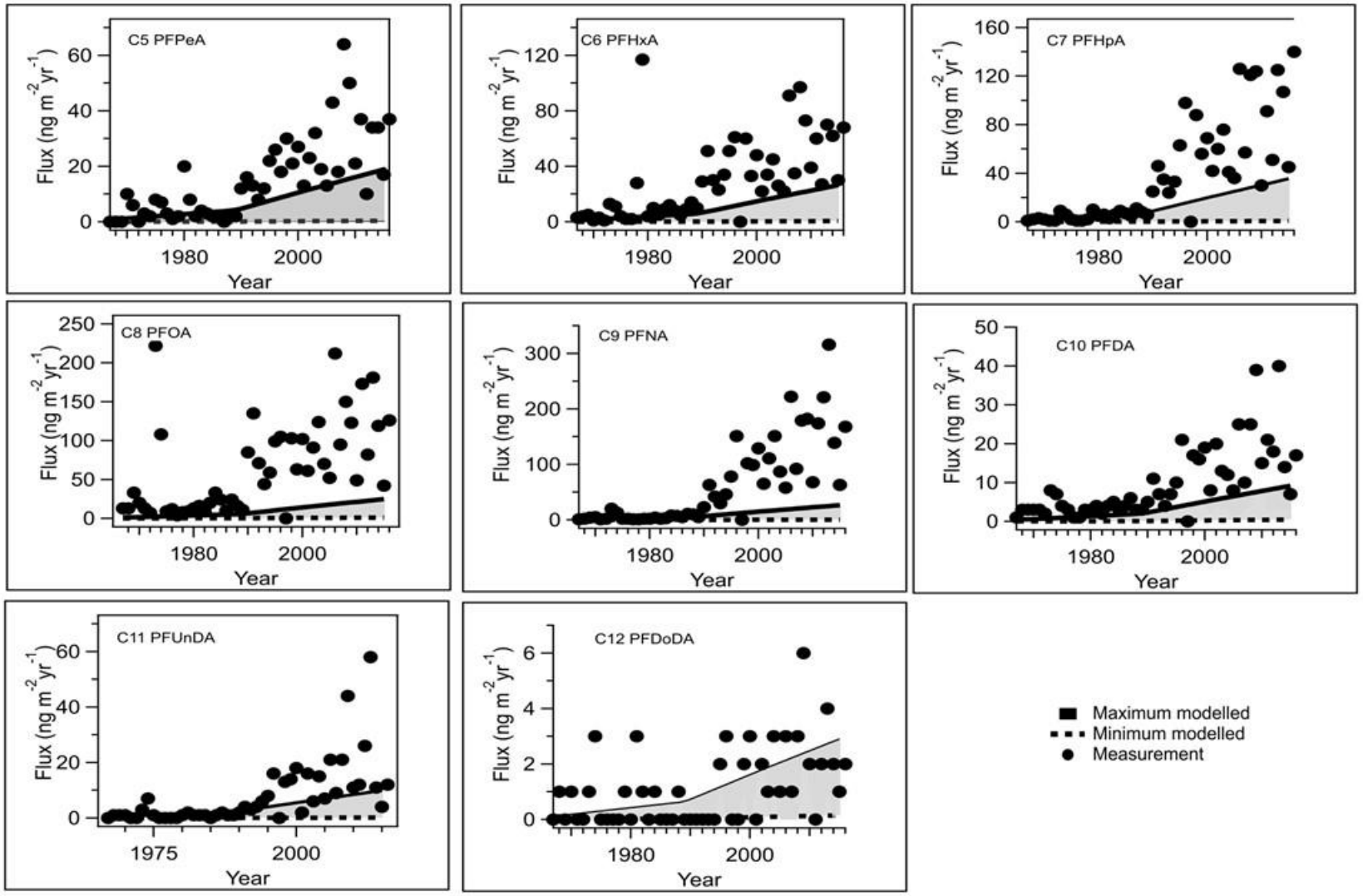

Figure A-6: Measured (symbols) and modeled comparisons of C5 – C12 PFCAs to the Mt. Oxford icefield over the years 1967 – 2016. The modeled maximum (black line) and minimum (broken line) are from Thackray et al.[18]

Section A-5: Evidence for aerosol transport of PFAAs

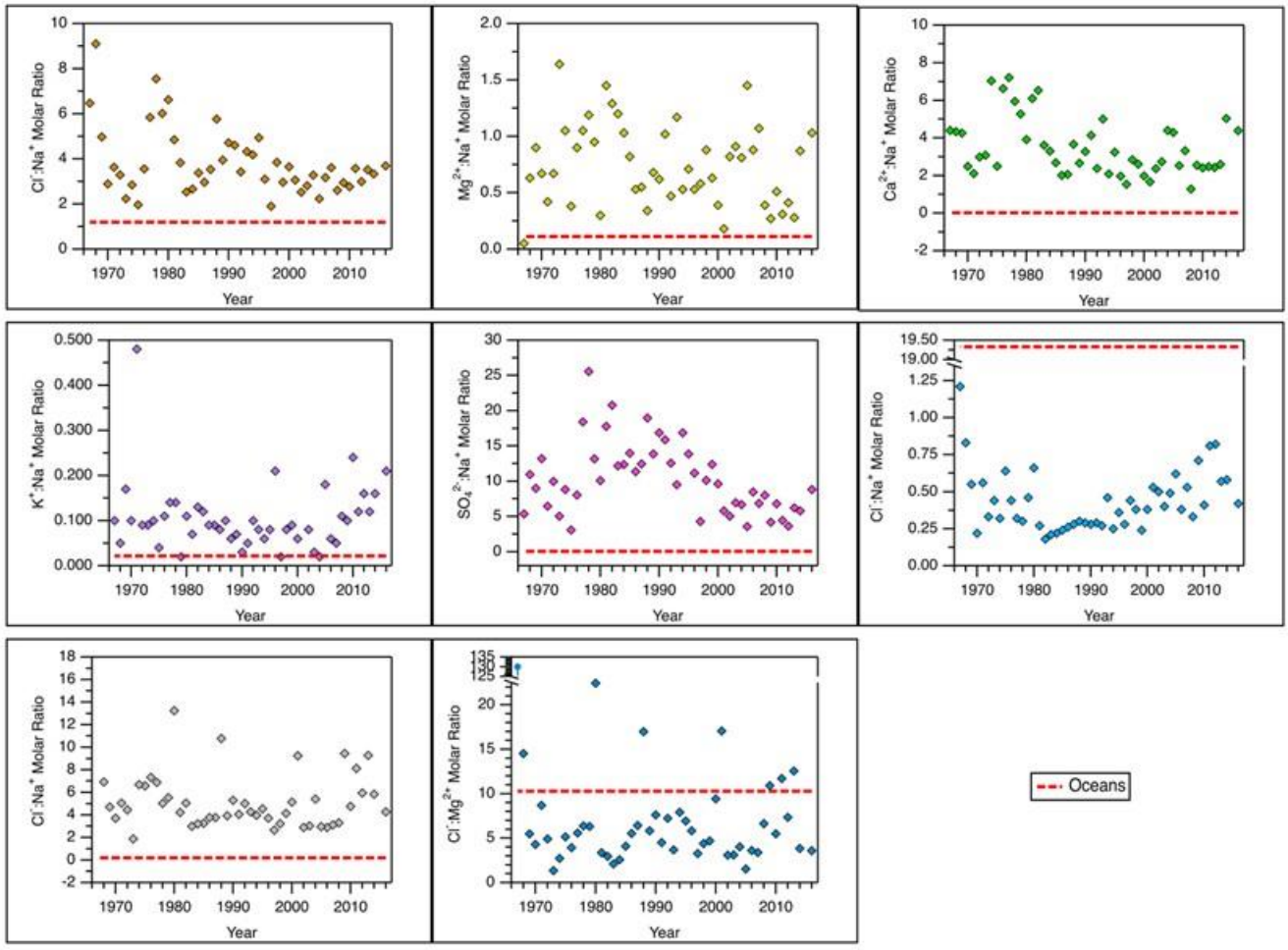

Figure A-7: Calculated molar ratios of major ions (y-axis) as a function of time from Mt. Oxford icefield (1967 – 2016). Molar ratio typical of bulk seawater is represented by the dashed red line.

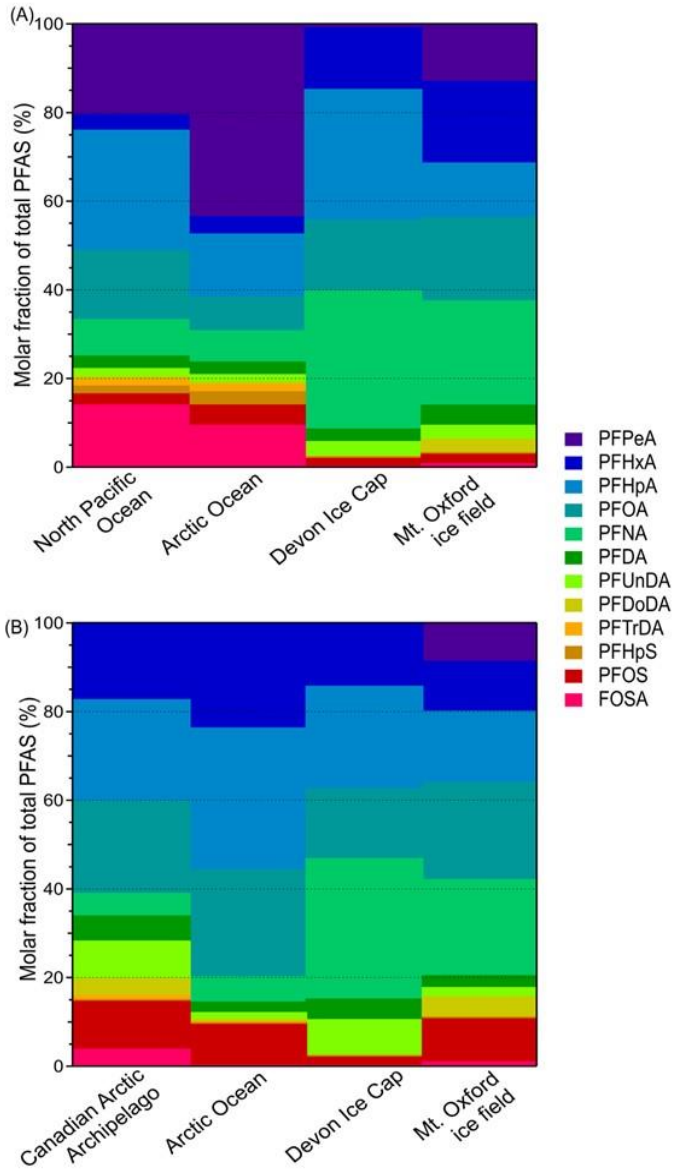

Figure A-8: Molar concentration fraction of selected PFAAs on the Mt. Oxford icefield compared to levels in the Canadian Arctic Archipelago,[19] Arctic Ocean,[19,20] North Atlantic Ocean[21] and North Pacific Ocean[20] in (A) 2010 and (B) 2005.

Table A-15: Depth profile (cm) of cations (ng mL^{-1}) on Mt. Oxford icefield. Values <LOD are identified in red. Due to insufficient volume of sample available for analysis, the year 2015 do not have concentration values. Lithium was <0.0087 for all samples analyzed.

LOD (ng mL^{-1})		0.0013	0.00035	0.01282	0.05107	0.06377
Depth	**Year**	**Sodium**	**Ammonium**	**Potassium**	**Magnesium**	**Calcium**
41	2016	23.28	13.70	8.13	25.28	181.14
89	2014	19.88	2.50	5.27	18.18	177.85
138	2013	15.59	4.19	3.12	4.62	71.97
163	2012	20.06	<0.00035	5.49	8.64	86.09
191	2011	17.73	<0.00035	3.62	5.74	78.19
227	2010	24.92	24.37	10.11	13.32	106.49
279	2009	24.78	0.61	4.00	7.08	112.34
325	2008	31.03	4.61	5.88	12.87	71.09
353	2007	12.66	0.00	1.03	14.32	74.63
399	2006	17.48	10.09	1.91	16.20	78.61
413	2005	19.31	19.78	5.93	29.63	146.89
447	2004	15.73	<0.00035	0.48	13.55	122.82
490	2003	16.55	<0.00035	0.76	15.86	80.53
517	2002	22.49	30.13	3.07	19.45	94.43
545	2001	14.52	0.03	< 0.01282	2.75	42.75
587	2000	16.48	16.03	1.58	6.74	58.01
615	1999	17.48	35.81	2.63	11.68	81.07
661	1998	16.27	30.66	2.08	15.12	82.09
687	1997	39.26	10.18	1.64	24.11	107.24
733	1996	19.77	15.65	7.20	11.12	69.28
775	1995	11.69	22.03	1.58	8.81	67.16
809	1994	15.09	56.88	1.58	8.43	56.08
835	1993	13.37	16.97	1.86	16.61	118.88
878	1992	18.09	31.00	2.96	9.06	76.28
920	1991	11.08	23.00	1.03	11.97	81.48
971	1990	9.98	37.39	0.42	6.52	57.99
987	1989	15.16	13.11	1.86	10.89	71.61
1010	1988	6.76	13.70	0.65	2.43	43.88
1057	1987	18.88	9.35	3.18	10.99	69.45
1079	1986	19.31	8.16	2.52	10.91	68.95
1103	1985	16.16	14.17	2.41	14.07	76.99
1138	1984	20.42	18.37	2.96	22.20	119.59
1172	1983	26.10	17.23	5.49	33.17	167.25
1190	1982	11.30	34.41	2.41	15.43	130.90
1233	1981	14.34	21.26	1.80	21.94	155.20
1277	1980	9.44	13.61	1.69	2.95	65.47
1300	1979	9.69	10.45	0.31	9.76	90.79
1318	1978	7.26	19.49	1.69	9.10	76.67
1332	1977	7.72	21.64	1.86	8.56	98.89
1363	1976	12.12	10.61	2.19	11.58	142.52
1389	1975	24.99	13.33	1.80	10.05	110.82
1410	1974	17.77	21.22	3.12	19.76	221.94
1438	1973	27.17	12.93	4.17	47.14	148.35
1461	1972	12.41	8.83	1.86	8.80	65.62
1482	1971	15.70	18.98	12.81	6.93	58.68
1515	1970	15.16	16.21	2.68	10.74	66.91
1547	1969	9.40	33.63	2.68	8.99	71.03
1575	1968	6.19	30.09	0.48	4.10	47.54
1588	1967	6.65	0.41	1.09	0.35	51.93

Table A-16: Depth profile (cm) of anions (ng mL^{-1}) detected on Mt. Oxford icefield. Due to insufficient volume of sample available for analysis, the year 2015 do not have concentration values. Bromide and Nitrite was <LOD for all samples analyzed.

LOD (ng mL^{-1})		0.22	1.93	5.70	11.90	23.49
Depth	**Year**	**Fluoride**	**Chloride**	**Sulfate**	**Phosphate**	**Nitrate**
41	2016	435.39	132.36	855.52	150.63	342.96
89	2014	56.08	102.04	479.53	150.74	405.73
138	2013	244.78	84.66	404.28	134.91	345.53
163	2012	241.63	92.34	303.89	153.25	129.45
191	2011	151.42	97.88	328.20	125.42	361.83
227	2010	326.08	106.48	708.00	111.56	550.02
279	2009	252.68	112.70	433.03	145.39	243.71
325	2008	295.14	124.51	1036.44	106.43	382.28
353	2007	348.49	70.48	362.86	102.18	177.22
399	2006	339.18	85.51	617.75	107.31	424.90
413	2005	142.50	66.32	288.25	94.43	297.20
447	2004	401.37	79.47	440.00	116.14	182.37
490	2003	273.51	71.65	479.53	108.94	119.44
517	2002	400.90	87.25	472.97	99.34	365.69
545	2001	353.94	68.52	351.45	106.65	90.42
587	2000	254.65	92.66	662.56	113.31	446.77
615	1999	245.49	79.90	905.61	180.96	427.76
661	1998	331.44	96.60	687.71	114.40	395.15
687	1997	99.72	114.94	702.08	119.53	205.82
733	1996	309.58	94.58	921.25	192.10	441.05
775	1995	29.24	89.03	676.51	108.40	469.94
809	1994	452.12	97.21	1062.44	94.87	418.75
835	1993	446.12	89.17	530.67	168.31	404.30
878	1992	124.58	95.50	949.79	114.83	503.83
920	1991	196.80	78.62	735.26	110.58	162.92
971	1990	220.00	72.43	702.29	140.70	100.00
987	1989	243.36	92.44	878.14	114.18	394.87
1010	1988	295.69	60.10	535.75	112.65	284.47
1057	1987	365.46	102.89	981.70	132.08	365.41
1079	1986	306.74	88.21	914.70	121.06	176.36
1103	1985	336.57	84.16	942.81	175.07	348.68
1138	1984	200.90	83.98	1055.04	98.47	338.24
1172	1983	311.08	102.01	1329.80	98.47	425.32
1190	1982	130.12	66.71	980.64	147.46	516.85
1233	1981	583.60	107.34	1064.97	128.48	488.10
1277	1980	219.61	96.35	397.52	144.41	262.87
1300	1979	255.75	89.99	532.36	127.60	154.62
1318	1978	244.07	84.55	775.63	112.43	185.80
1332	1977	273.67	69.55	593.87	122.47	280.89
1363	1976	362.30	66.53	406.19	115.16	170.93
1389	1975	354.96	75.35	321.43	130.00	85.41
1410	1974	345.02	77.98	653.47	130.88	88.99
1438	1973	473.11	93.48	571.89	118.33	176.36
1461	1972	410.37	62.94	515.67	110.47	252.86
1482	1971	33.98	87.86	423.10	124.55	94.28
1515	1970	283.06	67.49	834.60	110.58	359.11
1547	1969	241.00	72.01	352.50	107.85	233.27
1575	1968	361.99	86.79	282.55	122.04	269.45
1588	1967	410.62	66.32	148.67	136.32	102.16

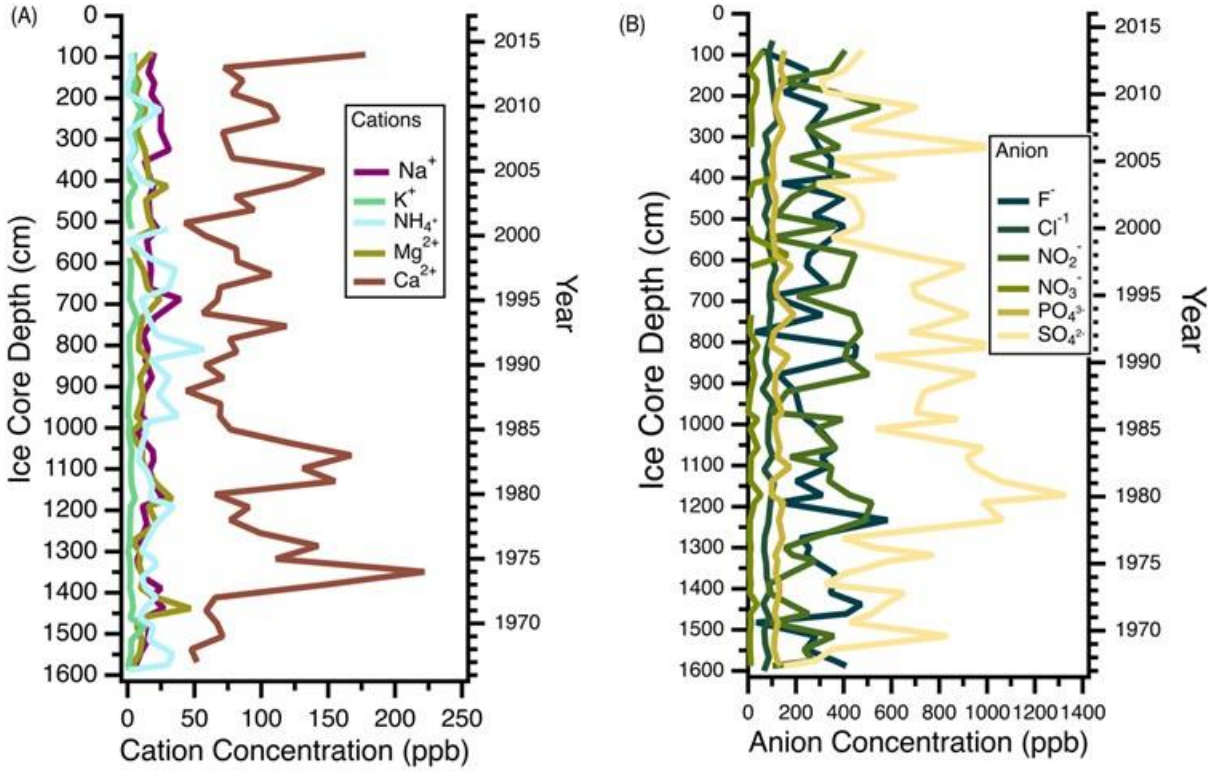

Figure A-9: Vertical profile of (A) cation and (B) anion concentrations (ng mL^{-1}) on Mt Oxford icefield.

To understand the contribution of sea salt and non-sea salt aerosols to the Mt. Oxford icefield, we calculated the contribution of each anion and cation that are commonly found in marine aerosols. Table A-17 is a summary of our findings. To calculate the nss-component, we first determined the average molar concentration of the ions in the core from 1967 – 2016. We then subtracted the individual ion molar concentration from the sodium molar concentration and multiplied this value by the expected ion to sodium ratio, taken from Libes, 2009.[22] Finally, the sea salt concentration and the percentage of non – sea salt were determined by taking the difference between the total average concentration and the average non-sea salt concentration.

The PFAAs detected were correlated with the cations and anions to determine if there were any statistically significant correlations. Ions were converted to flux as described earlier. For the entire period (1967-2016) only PFDoDA and PFECHS had weak correlations with sodium.

Table A-17: Non-sea salt and sea salt component concentrations (µmol/L) of selected ions in the ice core.

	Na^+	K^+	Mg^{2+}	Ca^{2+}	Cl^-	SO_4^{2-}	F^-
Average molar conc. in the ice core (µmol/L)	0.723	0.076	0.536	2.302	2.457	6.712	15.056
Average non – sea salt conc. (µmol/L)		0.060	0.450	2.240	1.590	6.530	14.750
Sea salt conc. (µmol/L)		0.016	0.086	0.062	0.867	0.182	0.306
Contribution of non – sea salt component (%)		77.63	83.11	97.33	64.68	97.36	98.00

Table A-18: Pearson's correlation coefficient (r) and associated p-value, including data points (n) of PFAA homologues with measured cations for the period 1967 – 2016 and 1967 – 1979. Weak correlations (r = 0.3-0.5) are shown in green, moderate correlations (r = 0.5-0.7) are shown in blue, and strong correlations (r = 0.7-1.0) are shown in red. Statistically significant p-values (p<0.05) are highlighted in bold. Cases where a Pearson correlation could not be calculated due to insufficient sample size are indicated by (-)

		1967 – 2016							1967-1979		
		Na^+	nss-K^+	nss-Mg^{2+}	nss-Ca^{2+}	nss-Cl^-	nss-SO_4^{2-}	PO_4^{3-}	Na^+	nss-Mg^{2+}	nss-Ca^{2+}
TFA	r	0.28	**0.30**	0.15	0.17	0.19	0.06	0.04			
	p	0.06	**0.04**	0.33	0.25	0.19	0.68	0.80			
	n	47	**46**	46	47	47	47	47			
PFPrA	r	**0.46**	**0.36**	0.17	0.28	**0.32**	0.28	0.12			
	p	**0.00**	**0.01**	0.26	0.05	**0.03**	0.05	0.42			
	n	**49**	**48**	48	49	**49**	49	49			
PFBA	R	0.29	**0.38**	-0.20	0.19	0.22	0.03	0.13	-0.08		0.05
	p	0.10	**0.03**	0.27	0.28	0.21	0.89	0.45	0.95		0.97
	n	34	**33**	33	34	34	34	34	3		3
PFPeA	r	**0.42**	0.30	0.002	0.11	**0.36**	0.01	0.23	**0.54**	-0.05	0.03
	p	**0.01**	0.06	0.99	0.48	**0.02**	0.93	0.14	**0.17**	0.91	0.95
	n	**43**	42	43	43	**43**	43	43	**8**	8	8
PFHxA	r	**0.35**	0.10	0.12	0.14	0.29	0.21	0.13	0.02	0.27	0.20
	p	**0.02**	0.49	0.42	0.35	0.05	0.16	0.37	0.95	0.42	0.54
	n	**47**	46	46	47	47	47	47	12	11	12
PFHpA	r	**0.41**	0.21	0.07	0.14	0.28	0.14	0.14	**0.38**	**0.60**	**0.55**
	p	**0.0053**	0.15	0.65	0.35	0.06	0.36	0.34	**0.21**	**0.04**	**0.05**
	n	**48**	47	47	48	48	0	48	**13**	**12**	**13**
PFOA	r	**0.49**	**0.32**	0.24	0.25	**0.31**	0.13	0.19	**0.56**	**0.84**	**0.59**
	p	**0.0004**	**0.03**	0.11	0.01	**0.03**	0.38	0.18	**0.05**	**0.0007**	**0.03**
	n	**48**	**47**	47	48	**48**	48	48	**13**	**12**	**13**
PFNA	r	**0.36**	0.24	0.01	0.06	0.14	0.03	0.03	**0.66**	**0.88**	**0.71**
	p	**0.01**	0.10	0.96	0.71	0.35	0.54	0.84	**0.02**	**0.0003**	**0.01**
	n	**47**	46	46	47	47	47	47	**12**	**11**	**12**
PFDA	r	**0.45**	**0.32**	0.05	0.13	0.23	-0.03	0.11	**0.70**	**0.73**	**0.76**
	p	**0.001**	**0.03**	0.72	0.40	0.12	0.86	0.46	**0.02**	**0.01**	**0.01**
	n	**46**	**45**	46	46	46	46	46	**11**	**11**	**11**
PFUnDA	r	0.11	0.28	-0.08	-0.06	0.04	-0.17	-0.02	-0.76	**0.39**	**0.99**
	p	0.54	0.12	0.65	0.00	0.82	0.35	0.90	0.45	0.74	0.09
	n	32	31	32	32	32	32	32	3	3	3
PFDoDA	r	**0.52**	0.36	-0.19	0.24	0.38	0.17	0.39	0.25	**0.33**	**0.81**
	p	**0.02**	0.10	0.41	0.27	0.08	0.45	0.07	0.69	0.58	0.09
	n	**22**	22	22	22	22	22	22	5	5	5
PFOS	r	0.03	-0.06	-0.24	0.11	-0.03	0.13	-0.05	**0.32**	**0.48**	**0.49**
	p	0.83	0.70	0.12	0.48	0.85	0.39	0.74	0.32	0.31	0.11
	n	43	43	42	43	43	43	43	12	11	12
PFBS	r	0.03	-0.18	0.14	0.07	-0.04	0.08	-0.09	**0.34**	0.27	**0.42**
	p	0.84	0.25	0.37	0.64	0.80	0.63	0.57	0.27	0.07	0.17
	n	42	42	41	43	42	42	42	12	0	12
PFECHS	r	**0.52**	0.29	0.18	**0.49**	**0.59**	**0.42**	**0.56**	**0.72**	**0.55**	**0.54**
	p	**0.0001**	0.05	0.25	**0.0005**	**1.6E-5**	**0.003**	**0.0001**	**0.01**	0.06	**0.05**
	n	**46**	46	45	**46**	**46**	**46**	**46**	**12**	12	**13**
FOSA	r	-0.04	-0.21	-0.04	-0.25	-0.05	-0.09	-0.08			
	p	0.83	0.28	0.82	0.18	0.77	0.64	0.68			
	n	30	0	30	30	30	30	30			

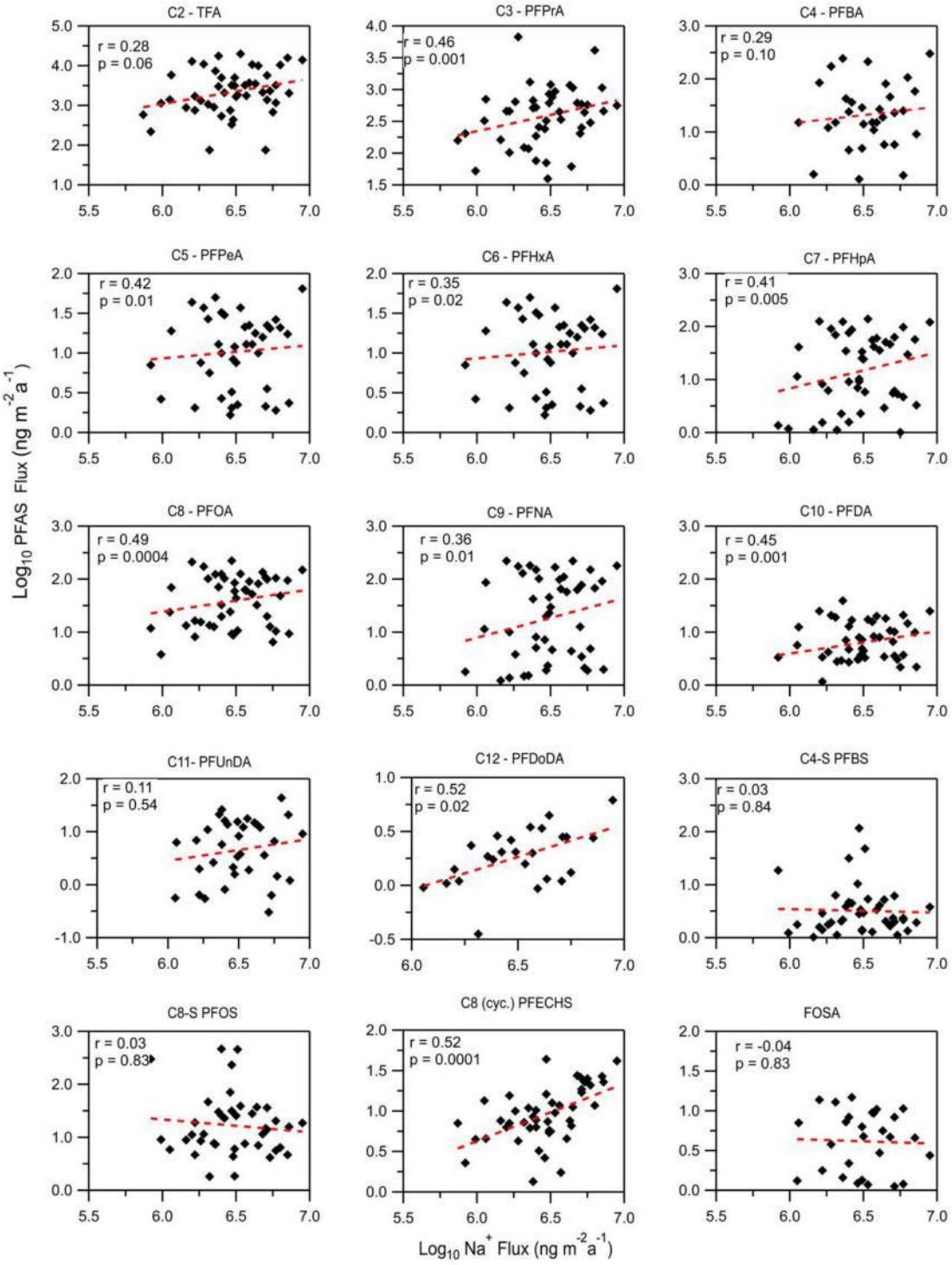

Figure A-10: Correlation between log-transformed fluxes of Na^+ and C2 – C12 PFCAs, PFSAs (C4, C8, cyclic C8)) and FOSA. The dashed red line represents a line of best fit (y = mx + b), the Pearson correlation (r) and p-value is also included.

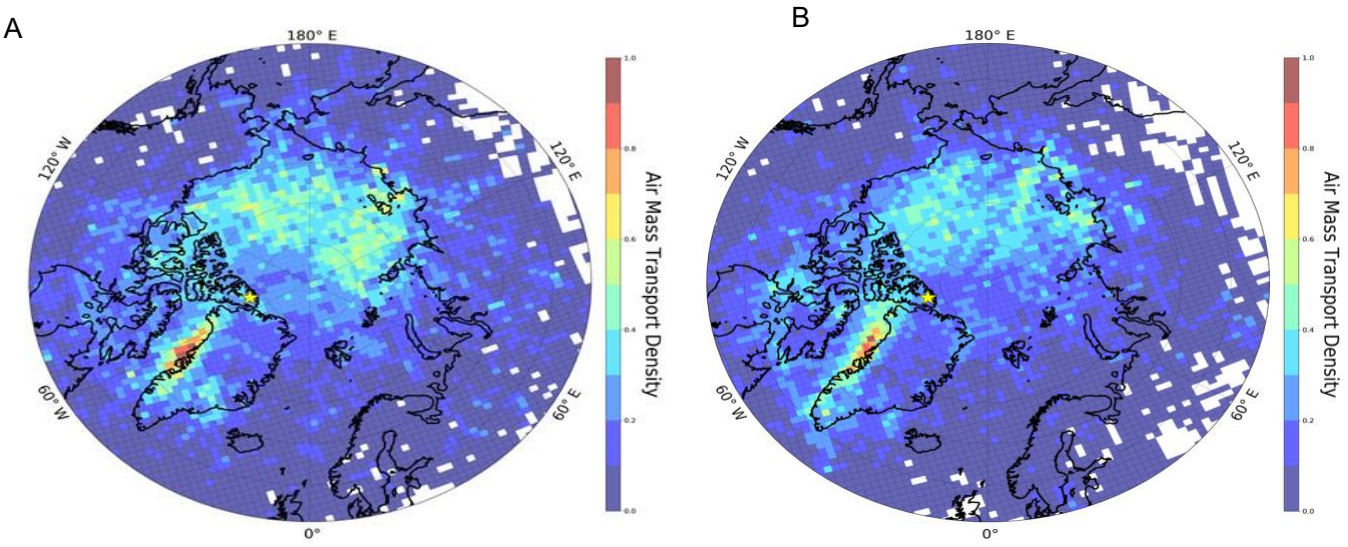

Figure A-11: Air mass transport density map for air parcels arriving at Mt. Oxford, icefield (yellow star) for (A) 2001 and (B) 2013.

References

(1) Criscitiello, A. S.; Das, S. B.; Karnauskas, K. B.; Evans, M. J.; Frey, K. E.; Joughin, I.; Steig, E. J.; McConnell, J. R.; Medley, B. Tropical Pacific Influence on the Source and Transport of Marine Aerosols to West Antarctica. *J. Clim.* **2014**, *27* (3), 1343–1363. https://doi.org/10.1175/JCLI-D-13-00148.1.

(2) McConnell, J. R.; Lamorey, G. W.; Lambert, S. W.; Taylor, K. C. Continuous Ice-Core Chemical Analyses Using Inductively Coupled Plasma Mass Spectrometry. *Environ. Sci. Technol.* **2002**, *36* (1), 7–11. https://doi.org/10.1021/es011088z.

(3) Draxler, R. R.; Hess, G. D. An Overview of the HYSPLIT_4 Modelling System for Trajectories, Dispersion and Deposition. *Aust. Meteorol. Mag.* **1998**, *47* (4), 295–308.

(4) Criscitiello, A. S.; Marshall, S. J.; Evans, M. J.; Kinnard, C.; Norman, A.-L.; Sharp, M. J. Marine Aerosol Source Regions to Prince of Wales Icefield, Ellesmere Island, and Influence from the Tropical Pacific, 1979–2001. *J. Geophys. Res. Atmos.* **2016**, *121* (16), 9492–9507. https://doi.org/https://doi.org/10.1002/2015JD024457.

(5) Criscitiello, A. S.; Geldsetzer, T.; Rhodes, R. H.; Arienzo, M.; McConnell, J.; Chellman, N.; Osman, M. B.; Yackel, J. J.; Marshall, S. Marine Aerosol Records of Arctic Sea-Ice and Polynya Variability From New Ellesmere and Devon Island Firn Cores, Nunavut, Canada. *J. Geophys. Res. Ocean.* **2021**, *126* (9), 1–20. https://doi.org/10.1029/2021JC017205.

(6) Stohl, A. Computation, Accuracy and Applications of Trajectories- a Review and Bibliography. *Atmospheic Environement* **1998**, *32* (6), 947–966. https://doi.org/10.1016/S1474-8177(02)80024-9.

(7) Dorling, S. R.; Davies, T. D. Extending Cluster Analysis-Synoptic Meteorology Links to Characterise Chemical Climates at Six Northwest European Monitoring Stations. *Atmos. Environ.* **1995**, *29* (2), 145–167. https://doi.org/10.1016/1352-2310(94)00251-F.

(8) Pickard, H. M.; Criscitiello, A. S.; Spencer, C.; Sharp, M. J.; Muir, D. C. G.; De Silva, A. O.; Young, C. J. Continuous Non-Marine Inputs of per- and Polyfluoroalkyl

Substances to the High Arctic: A Multi-Decadal Temporal Record. *Atmos. Chem. Phys.* **2018**, *18* (7), 5045–5058. https://doi.org/10.5194/acp-18-5045-2018.

(9) Macinnis, J. J.; French, K.; Muir, D. C. G.; Spencer, C.; Criscitiello, A.; De Silva, A. O.; Young, C. J. Emerging Investigator Series: A 14-Year Depositional Ice Record of Perfluoroalkyl Substances in the High Arctic. *Environ. Sci. Process. Impacts* **2017**, *19* (1), 22–30. https://doi.org/10.1039/c6em00593d.

(10) Young, C. J.; Furdui, V. I.; Franklin, J.; Koerner, R. M.; Muir, D. C. G.; Mabury, S. A. Perfluorinated Acids in Arctic Snow: New Evidence for Atmospheric Formation. *Environ. Sci. Technol.* **2007**, *41* (10), 3455–3461. https://doi.org/10.1021/es0626234.

(11) Wang, X.; Halsall, C.; Codling, G.; Xie, Z.; Xu, B.; Zhao, Z.; Xue, Y.; Ebinghaus, R.; Jones, K. C. Accumulation of Perfluoroalkyl Compunds in Tibetan Mountain Snow: Temporal Patterns from 1980 to 2010. *Environ. Sci. Technol.* **2014**, *48* (1), 173–181. https://doi.org/10.1021/es4044775.

(12) Kirchgeorg, T.; Dreyer, A.; Gabrieli, J.; Kehrwald, N.; Sigl, M.; Schwikowski, M.; Boutron, C.; Gambaro, A.; Barbante, C.; Ebinghaus, R. Temporal Variations of Perfluoroalkyl Substances and Polybrominated Diphenyl Ethers in Alpine Snow. *Environ. Pollut.* **2013**, *178* (3), 367–374. https://doi.org/10.1016/j.envpol.2013.03.043.

(13) Kwok, K. Y.; Taniyasu, S.; Yeung, L. W. Y.; Murphy, M. B.; Lam, P. K. S.; Horii, Y.; Kannan, K.; Petrick, G.; Sinha, R. K.; Yamashita, N. Flux of Perfluorinated Chemicals through Wet Deposition in Japan, the United States, and Several Other Countries. *Environ. Sci. Technol.* **2010**, *44* (18), 7043–7049. https://doi.org/10.1021/es101170c.

(14) Scott, B. F.; Spencer, C.; Mabury, S. A.; Muir, D. C. G. Poly and Perfluorinated Carboxylates in North American Precipitation. *Environ. Sci. Technol.* **2006**, *40* (23), 7167–7174.

(15) Plassmann, M. M.; Meyer, T.; Lei, Y. D.; Wania, F.; McLachlan, M. S.; Berger, U. Laboratory Studies on the Fate of Perfluoroalkyl Carboxylates and Sulfonates during Snowmelt. *Environ. Sci. Technol.* **2011**, *45* (16), 6872–6878. https://doi.org/10.1021/es201249d.

(16) Garnett, J.; Halsall, C.; Thomas, M.; Crabeck, O.; France, J.; Joerss, H.; Ebinghaus, R.; Kaiser, J.; Leeson, A.; Wynn, P. M. Investigating the Uptake and Fate of Poly- and Perfl Uoroalkylated Substances (PFAS) in Sea Ice Using an Experimental Sea Ice Chamber. *Environ. Sci. Technol.* **2021**.

(17) Moser, D. E.; Thomas, E. R.; Nehrbass-Ahles, C.; Eichler, A.; Wolff, E. Melt-Affected Ice Cores for (Sub-)Polar Research in a Warming World. *Egusph. Prepr.* **2023**, No. September, 1–48.

(18) Thackray, C. P.; Selin, N. E.; Young, C. J. A Global Atmospheric Chemistry Model for the Fate and Transport of PFCAs and Their Precursors. *Environ. Sci. Process. Impacts* **2019**, *22* (2), 285–293. https://doi.org/10.1039/c9em00326f.

(19) Benskin, J. P.; Muir, D. C. G.; Scott, B. F.; Spencer, C.; De Silva, A. O.; Kylin, H.; Martin, J. W.; Morris, A.; Lohmann, R.; Tomy, G.; Rosenberg, B.; Taniyasu, S.; Yamashita, N. Perfluoroalkyl Acids in the Atlantic and Canadian Arctic Oceans. *Environ. Sci. Technol.* **2012**, *46* (11), 5815–5823. https://doi.org/10.1021/es300578x.

(20) Cai, M. M.; Zhao, Z.; Yin, Z.; Ahrens, L.; Huang, P.; Cai, M. M.; Yang, H.; He, J.; Sturm, R.; Ebinghaus, R.; Xie, Z. Occurrence of Perfluoroalkyl Compounds in Surface Waters from the North Pacific to the Arctic Ocean. *Environ. Sci. Technol.* **2012**, *46* (2), 661–668. https://doi.org/10.1021/es2026278.

(21) Zhao, Z.; Xie, Z.; Möller, A.; Sturm, R.; Tang, J.; Zhang, G.; Ebinghaus, R. Distribution and Long-Range Transport of Polyfluoroalkyl Substances in the Arctic, Atlantic Ocean and Antarctic Coast. *Environ. Pollut.* **2012**, *170*, 71–77. https://doi.org/10.1016/j.envpol.2012.06.004.

(22) Libes, S. M. *Introduction to Marine Biogeochemistry*, 2nd ed.; Acedemic Press, 2009.

APPENDIX B

SUPPLEMENT FOR CHAPTER 3

The Occurrence of Legacy Perfluoroalkyl Substances (PFAS) Deposited along a Latitudinal Transect in Newfoundland and Labrador, Canada

Section B-1: Methods

Sample collection

Precipitation samples were collected on a regular monthly schedule from the end of snowmelt to the beginning of snowfall, and this translates to collection from May to October, with cumulative winter samples collected over the months that the sites were inaccessible. To collect samples, custom-built static and automated precipitation samplers were utilized. The static sampler was a 2.88 m long polyvinyl chloride (PVC) pipe with an internal diameter of 23 cm. The samplers were stood upright and secured to rebar anchors with nylon rope to maintain an upright position without presenting an injury hazard to regional wildlife (Figure S1). A liquid-tight cap is used to seal the bottom of the static precipitation sampler while the top is left open as the entrance for the deposited materials. This allows for the continuous collection of precipitation, gases and particulate matter from the atmosphere. To retrieve the samples, a 12 VDC battery-operated pump connected to a 0.95 cm (3/8-inch) diameter Norprene tubing is used, this tubing is lowered into the PVC pipe. This tubing material was explicitly selected since it is resistant to leaching and is intended for the unaltered transfer of ultrapure deionized water. The Norprene tube is also fitted with a 1 mm mesh size filter (47 mm ID) located 15 cm from the sampling end to prevent the intrusion of any large debris that accumulated in the sampling period. This is cleaned and rinsed with deionized water between collections.

Figure B-5: A photographic example of a custom-built Polyvinyl Chloride (PVC) static sampler, which was deployed at the NL-BELT field sites for the entire sampling campaign. Nylon ropes secured to rebar anchors are used to keep the sampler upright while also possible to break if interacting with large wildlife (e.g. moose) in the region without causing injury.

The custom-built automated precipitation samplers selectively collect wet deposition samples. When conductive precipitation is detected by a rain sensor, it triggers an electric motor via limit switches to open and close a lid resting over a funnel opening. The motors are controlled by a modular digital logic control board, which has low energy demands.

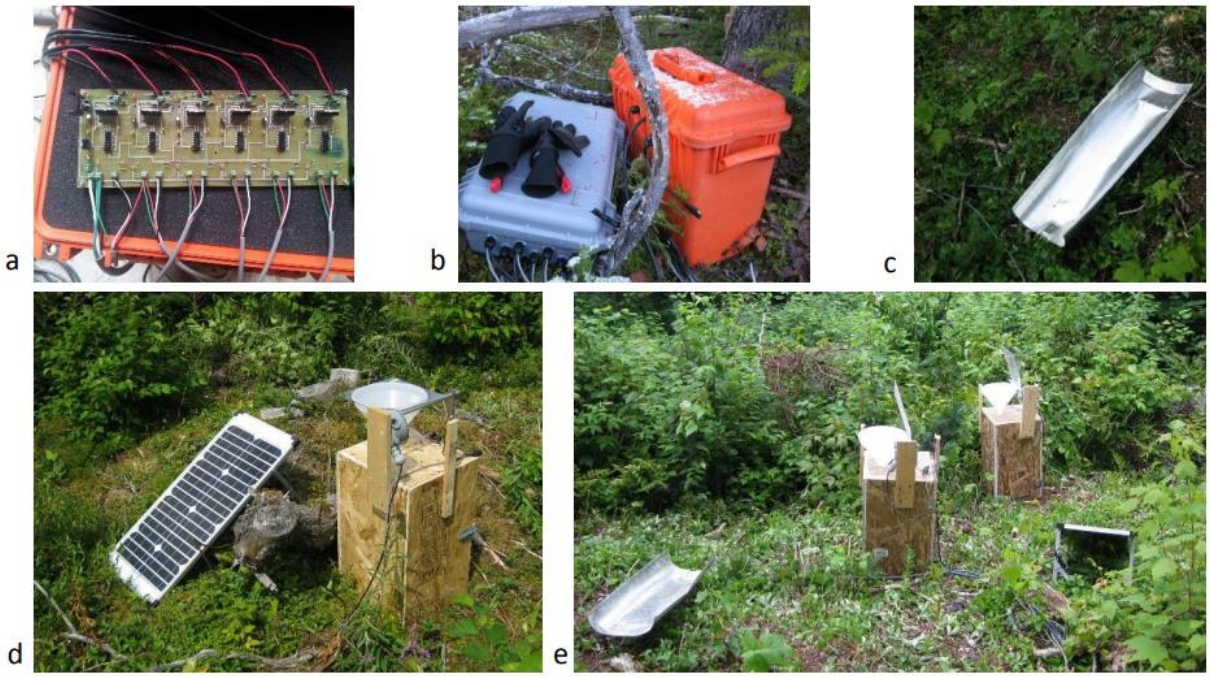

Figure B-2: Automated precipitation array stationed in the NL-BELT experimental forest sites in Newfoundland and Labrador, Canada consisting of (a) weatherproofed control board, (b) a deep cycle marine battery (orange case) to provide power to the control board and (c) a rain sensor with an enhanced sensitivity chute. To operate continuously off-grid, a (d) 40 W solar panel and a charge controller were integrated with the battery to retain charge. The completed package results in (e) automated collection units arranged in an array of replicates with solar panels and a rain sensor.

Section B-2. Methods - Sample preparation and analysis

Internal standards (IS) were added before extraction to monitor recovery and matrix effects. Instrument performance standards (IP) were also added to sub-samples immediately before analysis to account for matrix effects in the LC-MS/MS and/or ESI ionization efficiency and MS detection drift. All standards were purchased from Wellington Laboratories (Guelph, Canada).

Table B-3: Analyte quantifier and qualifier ion transitions (m/z), Internal standards (IS) and Instrument performance standards (IP) used for PFAA analysis. We used IS to assess recovery and matrix effects, whereas IP standards were used to only evaluate matrix effects. Precursor ion/products are indicated in brackets.

Analyte	Acronym	Carbon #	Quantifier/Qualifier Ion Transitions (m/z)	Internal Standards	Instrument Performance Standards
Perfluorobutanoic Acid	PFBA	4	213>169	$^{13}C_4$ PFBA(217/172)	$^{13}C_3$ PFBA (216/172)
Perfluoropentanoic Acid	PFPeA	5	263 > 219	$^{13}C_5$ PFPeA (268/223)	$^{13}C_3$ PFPeA (266/222)
Perfluorohexanoic Acid	PFHxA	6	313 > 269 / 313 > 119	$^{13}C_2$ PFHxA (315/270)	$^{13}C_5$ PFHxA (318/273)
Perfluoroheptonoic Acid	PFHpA	7	363 > 269 / 313 > 119	$^{13}C_4$ PFHpA (367/322)	
Perfluorooctanoic Acid	PFOA	8	413 > 369 / 414 > 169	$^{13}C_4$ PFOA (417/372)	$^{13}C_2$ PFOA (415/370)
Perfluorononanoic Acid	PFNA	9	462 > 419 / 463 > 219	$^{13}C_5$ PFNA (468/423)	$^{13}C_9$ PFNA (472/427)
Perfluorodecanoic Acid	PFDA	10	513 > 469 / 513 > 219	$^{13}C_2$ PFDA (515/470)	$^{13}C_6$ PFDA (519/474)
Perfluoroundecanoic Acid	PFUnDA	11	563 > 519 / 563 > 319, 269	$^{13}C_2$ PFUnDA (565/520)	$^{13}C_7$ PFUnDA (570/525)
Perfluorododecanoic Acid	PFDoDA	12	613 > 569 / 613 > 169	$^{13}C_2$ PFDoDA (615/570)	
Perfluorotridecanoic Acid	PFTrDA	13	663 > 619 / 663 > 169	$^{13}C_2$ PFDoDA (615/570)	
Perfluorotetradecanoic Acid	PFTeDA	14	713 > 669 / 663 > 169	$^{13}C_2$ PFTeDA (715/670)	
Perfluorohexadecanoic Acid	PFHxDA	16	813 > 769 / 813 > 169	$^{13}C_2$ PFHxDA (815/770)	
Perfluorooctadecanoic Acid	PFOcDA	18	913 > 869 / 913 > 169	$^{13}C_2$ PFHxDA (815/770)	
Perfluorobutanesulfonioc Acid	PFBS	4	299 > 80 / 229 > 99	$^{13}C_3$ PFBS (302/99)	
Perfluorohexanesulfonic Acid	PFHxS	6	399 > 80 / 399 > 99	$^{18}O_2$ PFHxS (403/103)	$^{13}C_3$ PFHxS (402/99)
Perfluoroheptanesulfonic Acid	PFHpS	7	499 > 80 / 449 > 99	$^{18}O_2$ PFHxS (403/103)	
Perfluorooctanesulfonic Acid	PFOS	8	449 > 80 / 499 > 99	$^{13}C_4$ PFOS (503/99)	$^{13}C_8$ PFOS (507/99)
Perfluorodecanesulfonic Acid	PFDS	10	599 > 80 / 599 > 99	$^{13}C_4$ PFOS (503/99)	
Perfluorooctanesulfonamide	FOSA	8	498 > 78	$^{13}C_8$ FOSA (506/78)	
Perfluoroethylcyclehexane Sulfonate	PFECHS	8	461 > 318 / 461 > 99	$^{18}O_2$ PFHxS (403/103)	

B-2.1 Summary of Chromatographic Conditions

To separate and quantify PFAAs and FOSA, two analytical methods were utilized. In the first analysis, the separation was conducted so that concentrations of PFCA > C4 and PFSA could be determined. A summary of the chromatographic conditions for the gradient program of the mobile phase is summarized in Table B-2. The electrospray conditions, ion inlet, and mass spectrometric conditions for this analysis are summarized in Table B-3. In the second method, the short-chain PFCA <C8 and PFOS were monitored. The two methods had similar chromatographic features; both runs have a run time of 15 minutes at a flow rate of 0.400 mL min^{-1}. The only notable difference is the column temperature, which was 50°C for the first method and 40°C for the second.

Table B-4: Summary of chromatographic conditions used to separate PFAAs and FOSA.

Time (minutes)	Flow rate (mL min^{-1})	% Water	% Methanol
0	0.400	75	25
0.5	0.400	75	25
5.0	0.400	15	85
5.1	0.400	0	100
5.6	0.400	0	100
7.0	0.400	0	100
9.0	0.400	75	25
12.0	0.400	75	25

Table B-5: Summary of inlet and mass spectrometric conditions used to separate PFAAs in all samples.

Capillary voltage (kV)	1.7
Cone Voltage (V)	10
Source Offset (V)	50
Source Temperature (°C)	150
Desolvation Gas Temperature (°C)	450
Cone Gas Flow (L hr^{-1})	150
Desolvation Gas Flow (L hr^{-1})	800
Collision Gas Flow (mL min^{-1})	0.15
Nebulizer Pressure (bar)	7.0

B-2.2 Quality Assurance and Quality Control

To prevent contamination, all glassware used for sample collection and extraction was rinsed twice with methanol before use. Nitrile gloves were used when handling samples and materials containing PFAS were avoided. Isotopically labelled internal standards were used to evaluate recovery and correct for matrix effects, and cartridge blanks were used to validate the integrity of the extraction method. Three samples were extracted in triplicate and one sample in duplicate to evaluate reproducibility. Mean recoveries, reported in Tables S4 and S5, were calculated based on peak area comparison between spike samples and solvent standards. Each sample was spiked with 30 µL of an internal standard mix (35 ng/mL) prior to extraction and compared to peak area in calibration standards (Table B1). Additionally, sample extracts were spiked with instrument performance (IP) standard post-extraction to account for matrix effects and instrumental drift (Table B1). In some instances, we monitored multiple transitions (different precursor to product ion pairs) from the same molecule to mitigate matrix effects and provide a more robust confirmation.

Matrix effects were further evaluated by comparing the peak area of the instrument performance (IP) standard spiked into the extracted sample matrix to the peak areas from the same molecules at equivalent concentrations in a solvent standard (Table B5). Recovery was evaluated by comparing the recovered analyte concentration in the spike and recovery sample to the theoretical spiked concentration measured in a solvent standard. Each sample concentration was quantified by correcting for recovery and matrix effects based on the relative response of target analytes to isotopically labelled IS added before extraction. A 15-level calibration curve was employed for quantification, ranging from 0.02 to 8.5 ng mL^{-1}, and included analytical blanks. Analytical blanks consisted of pure MeOH, and cartridge blanks were included in the method analysis to assess potential contamination sources. Any detected contamination in the blanks was subtracted from the analyte concentration to ensure accurate results. The method detection limit (LOD) was based on three times the standard deviation of any signal detected in the cartridge blanks. PFAA analytes were not detected in the method blanks with the exception of PFBA (0.046 ng mL^{-1}) and PFBS (0.013 ng mL^{-1}) and were therefore below the instrument detection limit (IDL; Table B-6). The instrument Limit of Detection

(LOD) and Limit of Quantitation (LOQ) in such cases were then quantified based on signal-to-noise (S/N) ratios of 3 and 10, respectively.

Table B-6: Mean Recoveries of internal standards (IS) in sample extracts. Analytes with multiple transition ions (m/z) are also included.

Internal Standards	Transition (m/z)	Recovery (%)
$^{13}C_4$ PFBA		89
$^{13}C_5$ PFPeA		79
$^{13}C_2$ PFHxA		90
$^{13}C_4$ PFHpA		94
$^{13}C_4$ PFOA		96
$^{13}C_5$ PFNA		102
$^{13}C_2$ PFDA		104
$^{13}C_7$ PFUnDA		99
$^{13}C_2$ PFDoDA		70
$^{13}C_2$ PFTeDA		31
$^{13}C_2$ PFHxDA		61
$^{13}C_4$ PFOS	80	101
$^{13}C_4$ PFOS	99	101
$^{18}O_2$ PFHxS	103	101
$^{18}O_2$ PFHxS	84	100
$^{13}C_3$ PFBS	80	101
$^{13}C_3$ PFBS	99	102

Table B-7: Mean recoveries of instrument performance (IP) standards in sample extracts. Analytes with multiple transition ions (m/z) are also included.

Instrument Performance Standards	Recovery (%)
$^{13}C_3$ PFBA	110
$^{13}C_3$ PFPeA	96
$^{13}C_5$ PFHxA	105
$^{13}C_2$ PFOA	104
$^{13}C_9$ PFNA	108
$^{13}C_6$ PFDA	111
$^{13}C_2$ PFUnDA	109
$^{13}C_8$ PFOS	104
$^{13}C_3$ PFHxS	104

B-2.3 Limit of Detection (LOD) and Limit of Quantitation (LOQ)

The limit of detection (LOD) and limit of quantitation (LOQ) represent the lowest quantity distinguishable from the blank and the lowest quantity accurately quantified, respectively. These values were determined using two sets of MeOH blanks and three sets of standard calibration curves. The average noise from the calibration standards was subtracted from the maximum peak value to calculate the signal, which was then divided by the average of the two standard deviations (SD) from the blanks to obtain signal-to-noise (S/N) ratios for each standard. A linear regression was performed for S/N versus calculated concentration (ng/mL), and LOD and LOQ were calculated from the slope using the equations: LOD = 3/m and LOQ = 10/m, where m is the slope (y = mx).

Table B-8: Instrument limit of detection (LOD) and limit of quantitation (LOQ) for PFAAs and FOSA.

Perfluoroalkyl Acids	LOD (ng/L)	LOQ (ng/L)
PFBA	0.005	0.020
PFPeA	0.008	0.010
PFHxA	0.002	0.003
PFHpA	0.001	0.002
PFOA	0.001	0.002
PFNA	0.002	0.004
PFDA	0.001	0.002
PFUnDA	0.003	0.005
PFDoDA	0.002	0.004
PFTrDA	0.003	0.005
PFTeDA	0.006	0.010
PFHxDA	0.08	0.100
PFOcDA	0.0002	0.0003
PFBS	0.0002	0.004
PFHxS	0.001	0.06
PFHpS	0.0001	0.0002
PFOS	0.0002	0.0003
PFDS	0.0004	0.001
PFECHS	0.0004	0.001
FOSA	0.0002	0.0004

B-2.4 Air Mass Back Trajectory Sector Assignments

Back trajectories were generated using the National Oceanic and Atmospheric Administration Hybrid Single-Particle Lagrangian Integrated Trajectory model (HYSPLIT).[1] The trajectory analysis was performed using the Global Data Assimilation System (GDAS) meteorology data set with a 0.5-degree resolution. The model commenced at noon on the date of sample collection and had a total run time of 120 hours, with a trajectory interval of three hours, and spanned the number of days in the collection period (maximum of 32 days). Frequency analysis using HYSPLIT modelling generated 256 trajectories at most. The frequency plot was generated using the percentages of trajectories that ended in each grid square. The raw endpoint output files

for the entire sampling period were concatenated and sorted for sector assignments in Igor Pro 8 using a custom procedure

The trajectory endpoints are then assigned to one of four quadrants (NE, NW, SW, SE) surrounding the coordinates centered on the desired NL-BELT field site (Figure S3). Any trajectory endpoints directly on top of the field site were not counted in the analysis. The procedure takes in 3 waves (columns) named latitude_points, longitude_points, and site_coordinates and creates the wave sector_points. The wave latitude_points contains all the latitude coordinates of the air mass trajectory endpoints for a given sampling period, while longitude_points contains all of the matching longitude coordinates. The wave site_coordinates contains the latitude and longitude points in that order within the wave for the field site of interest (ie, GC, HR, SR or ER). The procedure then takes each longitude and latitude trajectory endpoint and decides whether it is greater than or less than the corresponding site coordinate. It outputs the final result in the wave sector_points, which is a counting-based wave that contains the following rows: northwest points, northeast points, southwest points, southeast points, and total points. The procedure adds a value of one to the quadrant in which the trajectory endpoint lies and then adds a value of one to the total points. The probability density for air transit duration in each sector is calculated later by dividing the quadrant points by the total points counted.

```
#pragma rtGlobals=3

function assign_sector(latitude_points, longitude_points, site_coordinates)
        wave latitude_points, longitude_points, site_coordinates

        make/N=5/D sector_points

        variable i=0

        for(i=0;i<(numpnts(latitude_points));i+=1)
                if(latitude_points[i] > site_coordinates[0] && longitude_points[i] > site_coordinates[1])
                        sector_points[0]= sector_points[0]+1
                        sector_points[4]=sector_points[4]+1
                elseif(latitude_points[i] > site_coordinates[0] && longitude_points[i] < site_coordinates[1])
                        sector_points[1]= sector_points[1]+1
                        sector_points[4]=sector_points[4]+1
                elseif(latitude_points[i] < site_coordinates[0] && longitude_points[i] > site_coordinates[1])
                        sector_points[2]= sector_points[2]+1
                        sector_points[4]=sector_points[4]+1
                elseif(latitude_points[i] < site_coordinates[0] && longitude_points[i] < site_coordinates[1])
                        sector_points[3]= sector_points[3]+1
                        sector_points[4]=sector_points[4]+1
                endif
        endfor

        AppendToTable sector_points

end
```

Figure B-6: Procedure developed for geographical sector assignment of air mass back trajectory endpoints for use with Igor Pro by Place et al.[2]

Section B-3. PFAA concentration and fluxes at various sampling sites.

Table B-9: Summary of PFCA (C4 – C14) concentrations (ng/L) at the Grand Codroy O'Regan's site, Salmon River Hare Bay site, Humber River camp 10 site, and Eagle River muddy pond site. Values <LOD are identified in red bolded text. All samples are <LOQ for PFHxDA and PFOcDA and are therefore not shown here.

		Concentration (ng/L)										
Site	**Time**	**PFBA**	**PFPeA**	**PFHxA**	**PFHpA**	**PFOA**	**PFNA**	**PFDA**	**PFUnDA**	**PFDoDA**	**PFTrDA**	**PFTeDA**
Grand Codroy	**May 14'**	**<0.005**	**<0.008**	**<0.002**	**<0.001**	0.844	0.459	**<0.001**	0.061	**<0.002**	**<0.003**	**<0.006**
	Jun 14'	6.290	**<0.008**	0.777	1.363	4.771	0.799	0.120	0.036	0.006	**<0.003**	<0.006
	Sept 14'	9.436	**<0.008**	0.360	**<0.001**	0.620	0.702	0.127	0.413	0.183	**<0.003**	0.254
	Oct 14'	**<0.005**	**<0.008**	0.409	0.372	0.852	0.388	0.131	0.020	**<0.002**	**<0.003**	**<0.006**
	Jun 15'	1.919	**<0.008**	0.199	0.567	0.718	0.602	0.235	0.098	**<0.002**	**<0.003**	**<0.006**
	Jul 15'	**<0.005**	0.137	0.122	0.163	0.150	0.184	0.077	**<0.003**	**<0.002**	**<0.003**	**<0.006**
	Aug 15'	1.936	0.128	0.304	0.274	0.265	0.39	0.079	0.098	**<0.002**	**<0.003**	**<0.006**
	Oct 15'	**<0.005**	**<0.008**	**<0.002**	0.308	0.318	0.292	0.088	0.080	0.026	0.047	0.057
	Nov 15'	**<0.005**	**<0.008**	0.179	0.337	0.391	0.268	0.115	0.066	0.015	0.026	**<0.006**
	May 16'	1.615	**<0.008**	0.384	0.944	0.222	0.316	0.123	0.047	**<0.002**	0.027	**<0.006**
	Jun 16'	2.659	**<0.008**	0.396	0.579	0.753	0.940	0.109	0.080	0.023	0.075	**<0.006**
	Jul16'	2.098	0.411	0.356	0.385	0.341	0.369	0.102	0.096	0.014	0.028	**<0.006**
	Aug 16'	2.357	0.393	**<0.002**	0.384	0.306	0.235	0.098	0.054	0.015	0.029	**<0.006**
Humber River	**Jun 14'**	2.056	**<0.008**	1.976	0.376	0.586	0.139	0.027	**<0.003**	**<0.002**	**<0.003**	<0.006
	Aug 14'	3.293	0.564	1.184	0.725	0.756	0.404	0.045	**<0.003**	0.003	**<0.003**	<0.006
	Jun 15'	2.219	**<0.008**	**<0.002**	0.522	0.518	0.506	0.187	0.119	**<0.002**	**<0.003**	<0.006
	Jul 15'	2.043	0.095	0.125	0.164	0.442	0.454	0.192	0.090	0.03	0.018	<0.006
	Aug 15'	2.596	0.086	**<0.002**	0.292	0.223	0.268	0.09	0.105	0.018	0.028	0.009
	Sept 15'	2.629	0.167	0.502	0.594	0.388	0.303	0.242	0.041	0.018	0.014	**<0.006**
	Nov 15'	5.487	0.036	**<0.002**	**<0.001**	0.291	0.242	0.088	0.135	0.009	0.08	**<0.006**
	May 16'	3.785	**<0.008**	0.304	**<0.001**	0.331	0.304	0.095	0.054	**<0.002**	**<0.003**	**<0.006**
	Jun 16'	1.893	0.163	0.297	0.346	0.225	0.303	0.095	0.063	**<0.002**	**<0.003**	**<0.006**
	Aug 16'	2.887	0.333	0.374	0.291	0.241	0.251	0.089	0.076	**<0.002**	0.061	**<0.006**
Salmon River	**Aug 14'**	**<0.005**	**<0.008**	1.239	0.478	0.930	0.387	0.065	**<0.003**	**<0.002**	**<0.003**	0.078
	Oct 14'	4.282	**<0.008**	1.157	0.536	1.716	0.315	0.038	0.011	0.004	**<0.003**	**<0.006**
	Jul 15'	3.551	0.451	0.295	0.677	1.205	0.981	0.452	0.169	**<0.002**	**<0.003**	**<0.006**
	Aug 15'	9.851	0.044	0.516	0.715	0.868	0.981	0.794	0.640	0.087	0.108	**<0.006**
	Sept 15'	2.339	**<0.008**	0.197	0.32	0.231	0.224	0.098	0.106	0.025	0.027	**<0.006**
	Oct 15'	2.841	0.172	**<0.002**	0.213	0.175	0.553	0.084	0.773	**<0.002**	0.455	0.040
	May 16'	4.168	**<0.008**	0.372	0.417	0.227	0.303	0.133	0.067	**<0.002**	**<0.003**	**<0.006**
	Jul 16'	1.314	0.296	0.272	0.37	0.152	0.182	0.065	0.063	**<0.002**	**<0.003**	**<0.006**
	Aug 16'	3.582	0.223	0.338	0.398	0.425	0.477	0.13	0.082	0.018	0.017	**<0.006**
Eagle River	**Jun 14'**	**<0.005**	0.419	**<0.002**	0.724	1.198	0.782	0.122	0.236	0.114	**<0.003**	0.112
	Aug 14'	6.884	**<0.008**	1.096	1.375	4.387	1.317	0.285	0.482	0.209	**<0.003**	0.227
	Jul 15'	3.139	0.133	**<0.002**	0.507	0.404	0.594	0.163	0.114	**<0.002**	**<0.003**	**<0.006**
	Aug 15'	2.532	**<0.008**	**<0.002**	1.647	0.547	**<0.002**	0.519	0.251	0.059	0.123	**<0.006**
	Jun 16'	2.131	**<0.008**	0.198	0.64	0.491	0.686	0.118	0.152	0.016	0.118	**<0.006**
	Aug 16'	1.749	**<0.008**	0.251	0.345	0.211	0.278	0.077	**<0.003**	0.012	**<0.003**	**<0.006**
Detection Frequency (%)		82	47	74	89	100	97	97	87	55	45	18
Median (ng/L)		2.629	0.170	0.358	0.408	0.415	0.387	0.109	0.090	0.018	0.029	0.078

Table B-10: PFSA concentrations (ng/L) at the Grand Codroy O'Regan's site, Salmon River Hare Bay site, Humber River camp 10 site, and Eagle River muddy pond site. Values <LOD are identified in red bolded text. All samples are <LOQ for PFECHS and PFDS and are not reported.

		Concentration (ng/L)				
Site	**Time**	**PFBS**	**PFHxS**	**PFHpS**	**PFOS**	**FOSA**
Grand Codroy	**May 14'**	**<0.0002**	**<0.0001**	**<0.0001**	**<0.0002**	**<0.0002**
	Jun 14'	**<0.0002**	**<0.0001**	**<0.0001**	**<0.0002**	**<0.0002**
	Sept 14'	**<0.0002**	**<0.0001**	**<0.0001**	**<0.0002**	**<0.0002**
	Oct 14'	**<0.0002**	**<0.0001**	**<0.0001**	0.1170	0.0400
	Jun 15'	**<0.0002**	**<0.0001**	**<0.0001**	**<0.0002**	**<0.0002**
	July 15'	**<0.0002**	**<0.0001**	**<0.0001**	0.0280	**<0.0002**
	Aug 15'	**<0.0002**	**<0.0001**	**<0.0001**	0.0330	**<0.0002**
	Oct 15'	**<0.0002**	**<0.0001**	**<0.0001**	**<0.0002**	**<0.0002**
	Nov 15'	**<0.0002**	**<0.0001**	**<0.0001**	0.0600	**<0.0002**
	May 16'	**<0.0002**	**<0.0001**	**<0.0001**	0.0450	**<0.0002**
	Jun 16'	0.0660	**<0.0001**	<0.0001	0.0190	**<0.0002**
	July 16'	0.0090	**<0.0001**	0.0120	**<0.0002**	**<0.0002**
	Aug 16'	0.0320	0.0070	**<0.0001**	**<0.0002**	**<0.0002**
Humber River	**June 14'**	**<0.0002**	**<0.0001**	**<0.0001**	**<0.0002**	0.0280
	Aug 14'	**<0.0002**	**<0.0001**	**<0.0001**	**<0.0002**	**<0.0002**
	Jun 15'	**<0.0002**	**<0.0001**	**<0.0001**	**<0.0002**	**<0.0002**
	July 15'	**<0.0002**	**<0.0001**	**<0.0001**	**<0.0002**	**<0.0002**
	Aug 15'	**<0.0002**	0.0120	**<0.0001**	0.0340	**<0.0002**
	Sept 15'	<0.0002	<0.0001	**<0.0001**	0.0570	**<0.0002**
	Nov 15'	0.1640	0.0040	**<0.0001**	0.0550	**<0.0002**
	May 16'	0.0060	**<0.0001**	**<0.0001**	0.0280	**<0.0002**
	Jun 16'	**<0.0002**	**<0.0001**	**<0.0001**	**<0.0002**	**<0.0002**
	Aug 16'	**<0.0002**	**<0.0001**	**<0.0001**	0.0260	**<0.0002**
Salmon River	**Aug 14'**	**<0.0002**	**<0.0001**	**<0.0001**	**<0.0002**	0.0110
	Oct 14'	**<0.0002**	**<0.0001**	**<0.0001**	0.1730	0.0230
	July 15'	**<0.0002**	**<0.0001**	**<0.0001**	0.0480	**<0.0002**
	Aug 15'	**<0.0002**	0.0180	**<0.0001**	0.1030	**<0.0002**
	Sept 15'	**<0.0002**	**<0.0001**	**<0.0001**	0.0390	**<0.0002**
	Oct 15'	**<0.0002**	0.0050	**<0.0001**	0.0160	**<0.0002**
	May 16'	**<0.0002**	**<0.0001**	**<0.0001**	**<0.0002**	**<0.0002**
	July 16'	**<0.0002**	**<0.0001**	**<0.0001**	0.0150	**<0.0002**
	Aug 16'	0.0110	**<0.0001**	0.0180	0.0300	**<0.0002**
Eagle River	**Jun 14'**	**<0.0002**	**<0.0001**	**<0.0001**	**<0.0002**	0.0110
	Aug 14'	0.0310	**<0.0001**	**<0.0001**	**<0.0002**	**<0.0002**
	July 15'	**<0.0002**	**<0.0001**	**<0.0001**	0.0320	**<0.0002**
	Aug 15'	**<0.0002**	**<0.0001**	**<0.0001**	0.1210	**<0.0002**
	June 16'	0.0330	**<0.0001**	**<0.0001**	0.0090	**<0.0002**
	Aug 16'	0.1330	**<0.0001**	**<0.0001**	**<0.0002**	**<0.0002**
Detection Frequency (%)		26	13	5	55	13
Median		0.0315	0.0070	0.02290	0.0340	0.0230

Section B-3.1 Flux Estimations

Concentration of PFAAs in precipitation is influenced by volume and is not very useful for determining trends related to depositional inputs at the atmosphere-surface interface. To account for deposition volume, we calculated deposition fluxes (ng m^2 a^{-1}) for each homologue using the following formula:

$$\text{Deposition Flux} = \left[\frac{\text{analyte concentration } \left(\frac{\text{ng}}{\text{L}}\right) \text{x volume of sample(L)}}{\text{Area of static sampler } (\text{m}^2) \text{ / number of sampling days}} \text{ x } 365 \frac{\text{days}}{\text{year}} \right]$$

Area = πr^2 where r = 0.115 m

We normalize the deposition rates based on the sampling days and scale them to an annual basis equivalence. This method ensures consistency across different sampling periods and facilitates direct comparisons of atmospheric deposition trends. In instances where concentrations were below the LOD, we used ½ LOD for flux calculation and comparisons.

Table B-11: PFCA (C4-C14) fluxes (ng m^{-2} a^{-1}) at the Grand Codroy O'Regan's site, Salmon River Hare Bay site, Humber River camp 10 site, and Eagle River muddy pond site. Numbers in bolded red indicate instances where ½ LOD was used for annual flux calculation.

		Flux (ng m^{-2} a^{-1})										
Site	**Time**	**PFBA**	**PFPeA**	**PFHxA**	**PFHpA**	**PFOA**	**PFNA**	**PFDA**	**PFUnDA**	**PFDoDA**	**PFTrDA**	**PFTeDA**
Grand Codroy	**May 14'**	**8.32**	**6.65**	**1.66**	**0.83**	1404.03	763.56	**0.83**	101.48	1.66	**2.50**	**4.99**
	June 14'	4549.70	**2.89**	562.02	985.89	3450.98	577.94	86.80	26.04	4.34	**1.08**	**2.17**
	Sept 14'	5482.00	**2.32**	209.15	**0.29**	360.20	407.84	73.78	239.94	106.32	**0.87**	147.57
	Oct 14'	**3.94**	**3.16**	322.60	293.42	672.02	306.04	103.33	15.78	**0.79**	**1.18**	**2.37**
	Jun 15'	1669.72	**3.48**	173.15	493.35	624.73	523.80	204.47	85.27	**0.87**	**1.31**	**2.61**
	July 15'	**4.64**	127.19	113.26	151.33	139.26	170.83	71.49	**1.39**	**0.93**	**1.39**	**2.79**
	Aug 15'	2568.41	169.81	403.30	363.50	351.56	517.40	104.81	130.01	**1.33**	**1.99**	**3.98**
	Oct 15'	**2.82**	**2.26**	**0.56**	173.66	179.30	164.64	49.62	45.11	14.66	26.50	32.14
	Nov 15'	**5.13**	**4.10**	183.51	345.50	400.86	274.76	117.90	67.66	15.38	26.66	**3.08**
	May 16'	2031.59	**5.03**	483.05	1187.51	279.27	397.51	154.73	59.12	**1.26**	33.96	**3.77**
	Jun 16'	1558.38	**2.34**	232.09	339.34	441.32	550.91	63.88	46.89	13.48	43.96	**1.76**
	July 16'	3078.42	603.07	522.36	564.92	500.35	541.44	149.67	140.86	20.54	41.08	**4.40**
	Aug 16'	2621.75	437.14	**1.11**	427.13	340.37	261.40	109.01	60.07	16.68	32.26	**3.34**
Humber River	**Jun 14'**	2067.91	**4.02**	1987.44	378.18	589.39	139.80	27.16	**2.01**	**1.01**	**1.51**	**3.02**
	Aug 14'	2257.31	386.62	811.62	496.98	518.23	276.94	30.85	**8.23**	2.06	**1.03**	**2.06**
	Jun 15'	2021.78	**3.64**	**0.91**	475.60	471.96	461.03	170.38	108.42	**0.91**	**1.37**	**2.73**
	July 15'	1314.21	61.11	80.41	105.50	284.33	292.05	123.51	57.89	19.30	11.58	**1.93**
	Aug 15'	2542.18	84.22	**0.97**	285.95	218.38	262.44	88.13	102.82	17.63	27.42	8.81
	Sept 15'	2099.52	133.37	400.90	474.37	309.86	241.98	193.26	32.74	14.37	11.18	**2.40**
	Nov 15'	8918.64	58.51	**1.62**	**0.81**	473.00	393.35	143.04	219.43	14.63	130.03	**4.88**
	May 16'	2859.56	**3.02**	229.67	**0.38**	250.07	229.67	71.77	40.80	**0.76**	**1.13**	**2.27**
	Jun 16'	2112.16	181.87	331.38	386.06	251.05	338.08	106.00	70.29	**1.12**	**1.67**	**3.35**
	Aug 16'	2970.43	342.62	384.81	299.41	247.96	258.25	91.57	78.20	**1.03**	62.76	**3.09**
Salmon River	**Aug 14'**	**5.70**	**4.56**	1411.86	544.69	1059.75	440.99	74.07	2.28	**1.14**	**1.71**	88.88
	Oct 14'	4517.25	**4.22**	1220.56	565.45	1810.28	332.31	40.09	11.60	4.22	**1.51**	**3.16**
	July 15'	2617.64	332.46	217.46	499.06	888.27	723.15	333.19	124.58	0.74	**1.11**	**2.21**
	Aug 15'	3306.21	14.77	173.18	239.97	291.32	329.25	266.48	214.80	29.20	36.25	**1.01**
	Sept 15'	3236.72	**5.54**	272.61	442.82	319.66	309.97	135.61	146.68	34.60	37.36	**8.30**
	Oct 15'	3814.85	230.96	**1.34**	286.01	234.99	742.56	112.79	1037.97	1.34	610.97	53.71
	May 16'	2743.09	**2.63**	244.82	274.44	149.40	199.41	87.53	44.09	0.66	0.99	**1.97**
	July 16'	1394.74	314.19	288.71	392.73	161.34	193.18	68.99	66.87	1.06	1.59	**3.18**
	Aug 16'	3159.48	196.70	298.13	351.05	374.87	420.74	114.67	72.33	15.88	14.99	**2.65**
Eagle River	**Jun 14'**	**0.34**	28.85	**0.07**	49.85	82.49	53.85	**8.40**	16.25	7.85	**0.10**	**7.71**
	Aug 14'	2190.42	**1.27**	348.74	437.51	1395.90	419.06	90.68	153.37	66.50	**0.48**	72.23
	July 15'	1517.78	64.31	**0.48**	245.15	195.34	287.21	78.81	55.12	**0.48**	**0.73**	**1.45**
	Aug 15'	1650.00	**2.61**	**0.65**	1073.28	356.46	**0.65**	338.21	163.57	38.45	80.15	**1.95**
	Jun 16'	228.04	**0.43**	21.19	68.49	52.54	73.41	12.63	16.27	1.71	12.63	**0.32**
	Aug 16'	1417.15	**3.24**	203.38	279.54	170.97	225.25	62.39	**1.62**	9.72	**1.22**	**2.43**

Table B-12: PFSA fluxes (ng m^{-2} a^{-1}) at the Grand Codroy O'Regan's site, Salmon River Hare Bay site, Humber River camp 10 site, and Eagle River muddy pond site**.** Numbers in bolded red indicate instances where ½ LOD was used for annual flux calculation.

		Flux (ng m^{-2} a^{-1})				
Site		**PFBS**	**PFHxS**	**PFHpS**	**PFOS**	**FOSA**
Grand Codroy	**May 14'**	**2.50**	**0.83**	**0.50**	**0.17**	**1.66**
	Jun 14'	**1.08**	**0.36**	**0.22**	**0.07**	**0.72**
	Sept 14'	**0.87**	**0.29**	**0.17**	**0.06**	**0.58**
	Oct 14'	**1.18**	**0.39**	**0.24**	92.28	31.55
	June 15'	**1.31**	**0.44**	**0.26**	**0.09**	**0.87**
	July 15'	**1.39**	**0.46**	**0.28**	26.00	**0.93**
	Aug 15'	**1.99**	**0.66**	**0.40**	43.78	**1.33**
	Oct 15'	**0.85**	**0.28**	**0.17**	0.06	**0.56**
	Nov 15'	**1.54**	**0.51**	**0.31**	61.51	**1.03**
	May 16'	**1.89**	**0.63**	**0.38**	56.61	**1.26**
	Jun 16'	38.68	**0.29**	**0.18**	11.14	**0.59**
	July 16'	13.21	**0.73**	17.61	**0.15**	**1.47**
	Aug 16'	35.59	7.79	**0.33**	**0.11**	**1.11**
Humber River	**Jun 14'**	**1.51**	**0.50**	**0.30**	**0.10**	28.16
	Aug 14'	**1.03**	**0.34**	**0.21**	**0.07**	**0.69**
	Jun 15'	**1.37**	**0.46**	**0.27**	**0.09**	**0.91**
	July 15'	**0.96**	**0.32**	**0.19**	**0.06**	**0.64**
	Aug 15'	**1.47**	11.75	**0.29**	33.30	**0.98**
	Sept 15'	**1.20**	**0.40**	**0.24**	45.52	**0.80**
	Nov 15'	266.56	6.50	**0.49**	89.40	**1.63**
	May 16'	4.53	**0.38**	**0.23**	21.15	**0.76**
	Jun 16'	**1.67**	**0.56**	**0.33**	**0.11**	**1.12**
	Aug 16'	**1.54**	**0.51**	**0.31**	26.75	**1.03**
Salmon River	**Aug 14'**	28.48	**0.57**	**0.34**	**0.11**	12.53
	Oct 14'	**1.58**	**0.53**	**0.32**	182.51	24.26
	July 15'	**1.11**	**0.37**	**0.22**	35.38	**0.74**
	Aug 15'	**0.50**	6.04	**0.10**	34.57	**0.34**
	Sept 15'	**2.08**	**0.69**	**0.42**	53.97	**1.38**
	Oct 15'	**2.01**	6.71	**0.40**	21.49	**1.34**
	May 16'	**0.99**	**0.33**	**0.20**	**0.07**	**0.66**
	July 16'	**1.59**	**0.53**	**0.32**	15.92	**1.06**
	Aug 16'	9.70	**0.44**	15.88	26.46	**0.88**
Eagle River	**Jun 14'**	**0.10**	**0.03**	**0.02**	**0.01**	25.65
	Aug 14'	9.86	**0.16**	**0.10**	**0.03**	**0.32**
	July 15'	**0.73**	**0.24**	**0.15**	15.47	**0.48**
	Aug 15'	**0.98**	**0.33**	**0.20**	78.85	**0.65**
	Jun 16'	3.53	**0.05**	**0.03**	0.96	**0.11**
	Aug 16'	107.76	**0.41**	**0.24**	**0.08**	**0.81**

Section B-4. Latitudinal trends in total deposition

To assess the relative roles of local, regional or long-range sources, we compared the mean fluxes of PFAA deposition within the NL-BELT sites. We also extended the analysis to include deposition fluxes with measurements previously made in the Canadian High Arctic at the Devon Ice Cap (75.2°N, 82.7°W, 2175 m above sea level) for 2014-2015[3] and Mt. Oxford icefield, Nunavut (82.19°N, 72.96°W, 1784 m above sea level) for 2014-2016 (Table B-11).[4] We caution that the 2015 measurement from the Devon Ice Cap was a partial year of deposition and, therefore is an underestimation of the annual PFAA flux.

Table B-13: Comparison of PFAA deposition between the mean total deposition samples at the NL-BELT sites and measurements made at the Devon Ice Cap and Mt. Oxford icefield, Nunavut, for the period 2014–2016.[3,4] The 2015 data from the Devon Ice Cap is an underestimation of PFAA deposition since this represents a partial year of deposition. Values in bolded red indicate cases where fluxes set to ½ LOD were included in the mean calculations

	Deposition Flux (ng m^2 a^{-1})										
Site, time	**PFBA**	**PFPeA**	**PFHxA**	**PFHpA**	**PFOA**	**PFNA**	**PFDA**	**PFUnDA**	**PFDoDA**	**PFBS**	**PFOS**
Mt. Oxford, 2014	237	34	62	107	119	139	14	11	2	3	1
Mt. Oxford, 2015	104	17	30	45	42	63	7	4	1	21	7
Mt. Oxford, 2016	213	37	68	140	126	168	17	12	2	39	10
Devon Ice Cap, 2014	35		7	15	21	46	9	7			15
Devon Ice Cap, 2015	26		5	6	11	15	2	1		1	6
Eagle River, 2014	**1095**	**15**	**174**	244	739	236	**50**	85	37		40
Eagle River, 2015	1584	**33**	**1**	659	276	144	209	109	**19**	40	2
Eagle River, 2016	823	**2**	112	174	112	149	38	**9**	6	7	1
Salmon River, 2014	**2261**	**4**	1316	555	1435	387	57	**7**	**3**	2	46
Salmon River, 2015	3499	**118**	**377**	**407**	709	487	178	307	**14**	137	14
Salmon River, 2016	2432	**171**	277	339	229	271	90	61	**6**	6	3
Humber River, 2014	2163	195	1400	438	554	208	29	**5**	**2**	1	3
Humber River, 2015	3379	**68**	**97**	**268**	352	330	144	104	**13**	36	4
Humber River, 2016	2647	**176**	315	**229**	250	275	90	63	**1**	22	3
Grand Codroy, 2014	**2511**	**4**	**274**	**320**	1472	514	**66**	96	**28**	1	39
Grand Codroy, 2015	**850**	**61**	**175**	305	339	330	110	**66**	**7**	12	9
Grand Codroy, 2016	2323	262	310	630	390	438	119	77	13	38	3

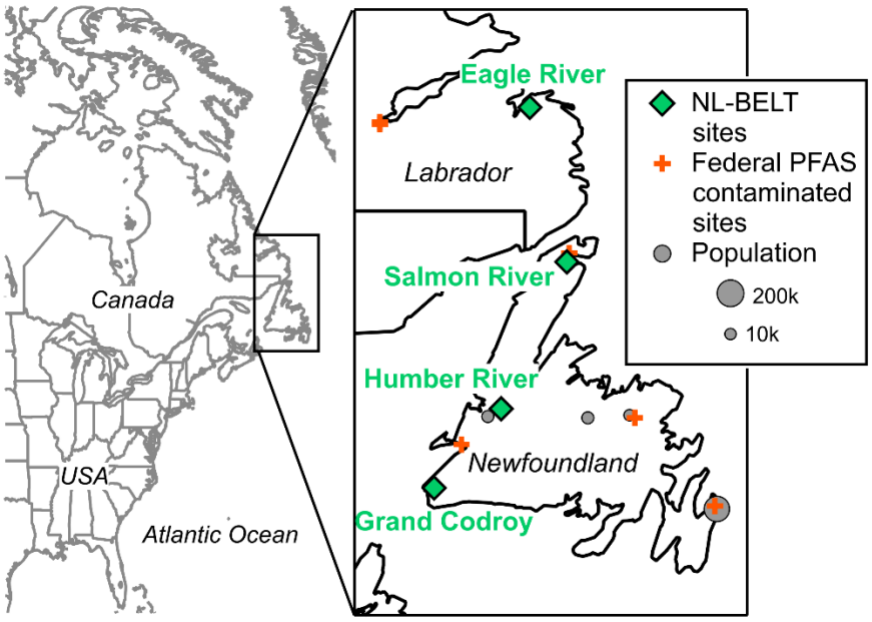

Figure B-7: Map showing the NL-BELT sampling sites (green diamonds) in Newfoundland and Labrador, Canada. From south to north: Grand Codroy O'Regan's site (GC), Humber River Camp 10 site (HR), Salmon River Hare Bay (SR), and Eagle River Muddy Pond (ER). The orange marker highlights the confirmed or suspected PFAS contamination sites. The grey circles represent population density.

Section B-5. Wet and Dry Deposition Mechanism

Although several studies have quantified PFAS homologues in precipitation, there is limited focus on distinguishing between the wet and dry deposition mechanisms. Herein, the dry deposition fluxes for C4 (PFBA), C8 (PFOA), and C9 (PFNA) were determined by subtracting measured wet deposition from total deposition (Table B-12). We also calculated the wet and dry fraction of each homologue (Figure S5) and compared our findings with previous literature that attempted to quantify the dry deposition contribution (Table B-13)

Table B-14: Measured total and wet deposition fluxes for selected months at GC, HR/PB, SR and ER. The dry deposition contribution was estimated by subtracting the wet deposition flux from the total (wet + dry) fluxes. ½ LOD values were used to estimate the fluxes in wet deposition for PFBA and are highlighted in bolded red. Total deposition fluxes were measured at HR and compared to wet deposition fluxes measured at PB. This comparison was unavoidable since HR was initially planned for full use but became inaccessible in 2015. These two sites (HR and PB) share the same watershed, and there was good agreement between the volumes collected between the two sites.

		Deposition (ng m^2 a^{-1})								
		PFBA			PFOA			PFNA		
Site	Time	Total	Wet	Dry	Total	Wet	Dry	Total	Wet	Dry
GC	Aug 2015	2568	432	2137	352	139	212	517	184	333
	Jul 2016	3078	927	2151	500	242	259	541	189	352
	Aug 2016	2622	148	2474	340	38	303	261	37	224
HR/PB	Aug 2015	2542	155	2387	218	35	183	262	80	182
	Sept 2015	2031	**2**	**2029**	310	58	252	242	72	172
	Aug 2016	2970	**7**	**2963**	248	209	39	258	162	96
SR	Aug 2015	2206	**1**	**2205**	291	72	220	329	114	216
	Sept 2015	3236	1155	2081	320	183	137	310	237	73
	Oct 2015	3815	**3**	**3812**	235	196	39	743	255	488
	Jul 2016	1395	387	1008	161	103	58	193	33	160
ER	Aug 2016	1417	**1**	**1416**	171	13	158	225	19	207

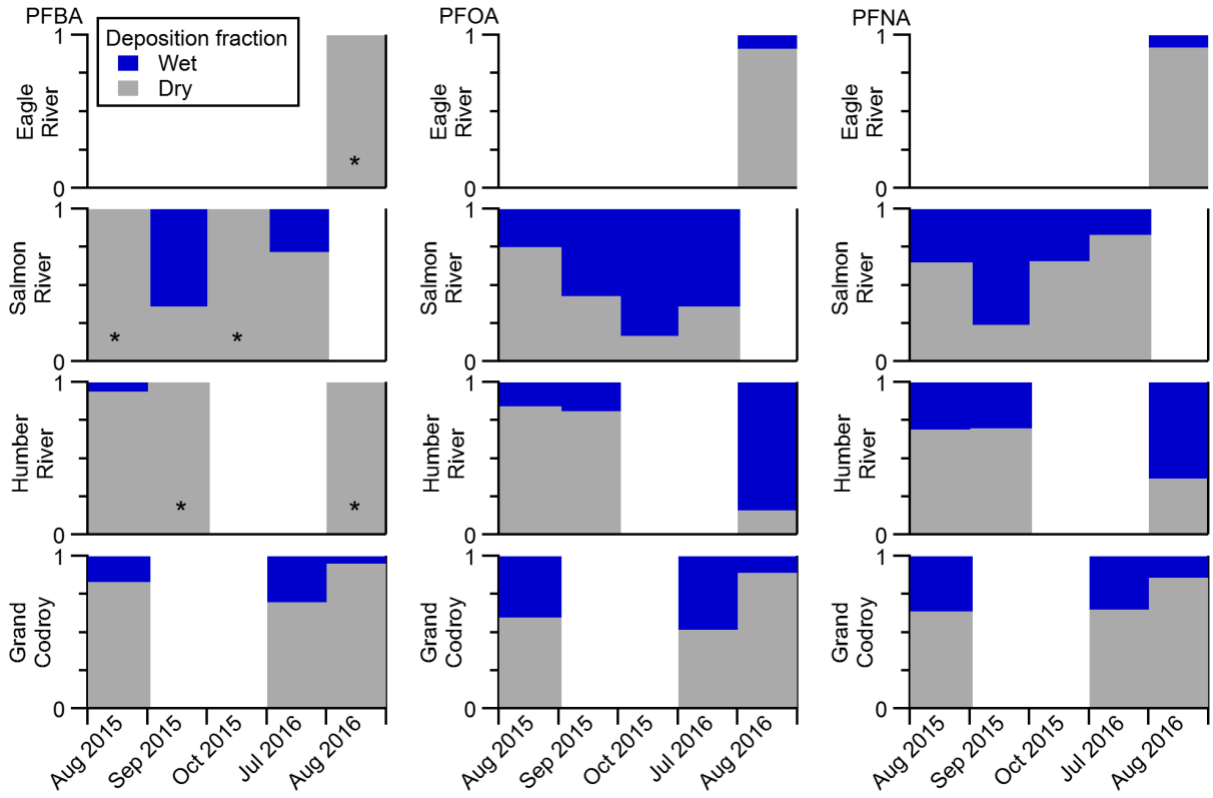

Figure B-8: Dry and wet deposition fractions for PFBA, PFOA, and PFNA. Samples where PFBA in wet deposition was <LOD are indicated with "*". In these cases, the wet deposition flux was used 1/2LOD.

Table B-15: Comparison of our measured fraction of total deposition contributed by dry deposition to previous literature reports. Only reports based on measurements in which both wet and dry deposition were reported are included.

		Fraction deposited by dry deposition (%)									
		This study			Xia et al., 2024[5]			Shimizu et al., 2021[6]	NC DEQ GenX[7]		
Compound		Median	Min	Max	Median	Min	Max		Median	Min	Max
Targeted in this study	PFBA	95 %	36 %	100 %	71 %	55 %	84 %				
	PFOA	52 %	16 %	91 %	39 %	35 %	46 %	4 %			
	PFNA	66 %	24 %	92 %							
Other PFAS	GenX							3 %	79 %	34 %	99 %
	PFBS				89 %	86 %	92 %				
	PFOS				51 %	16 %	71 %	2 %			

[5]From Xia et al., 2024. Five reports for each analyte. Wet deposition determined from direct precipitation measurements. Dry deposition calculated from measured particulate and gaseous measurements.
[6]From Shimizu et al., 2021. Wet and dry deposition both measured, with 39 wet and 25 dry deposition measurements. A single summed deposition fraction is reported.
[7]NC DEQ GenX Investigation measurements as reported in D'Ambro et al., 2021. Ten paired wet and dry deposition measurements.

Section B-6. Sources of PFAAs to the NL-BELT

Major ion analysis

Table B-16: Summary of cation and sulphate concentration (µg L^{-1}) at Grand Codroy, Humber River, Salmon River and Eagle River. Values <LOD are identified in bolded red. Ion concentrations are only available for 2014 and 2015. We assumed that phosphate and sulphate were measured as phosphorus and sulphur

		Concentration µg L^{-1}									
		Aluminium	**Calcium**	**Iron**	**Potassium**	**Magnesium**	**Manganese**	**Sodium**	**Phosphate**	**Sulphate**	**Silicon**
	LOD	**15**	**10**	**3**	**100**	**5**	**0.6**	**10**	**7**	**10**	**20**
	LOQ	**25**	**20**	**5**	**100**	**10**	**1**	**20**	**11**	**10**	**30**
Grand Codroy	May 14'	8	20	**< 3**	**<100**	**< 5**	2	**<10**	**< 7**	**<10**	20
	Jun 14'	**<15**	6000	6	520	310	1	320	31	270	30
	Sept 14'	5	5600	10	480	430	74	1600	17	470	710
	Oct 14'	9	4970	15	3350	1250	1340	1890	132	300	200
	Jun 15'	5	3960	5	480	690	12	2890	81	300	190
	July 15'	**<15**	2800	3	690	280	508	270	229	220	**<20**
	Aug 15'	1	1950	1	270	170	522	200	149	160	**<20**
	Oct 15'	8	5060	32	2650	960	692	2530	648	530	40
	Nov 15'	8	2640	6	2330	790	685	2200	191	260	40
Humber River	Jun 14'	**<15**	8670	5	110	160	16	170	12	460	150
	Aug 14'	5	16520	3	240	220	59	120	38	850	80
	Jun 15'	5	12560	3	150	330	29	1210	**< 7**	320	20
	July 15'	2	7680	6	820	430	140	310	214	320	90
	Aug 15'	3	3580	2	310	190	31	150	139	180	**<20**
	Sept 15'	7	3070	8	240	250	25	340	66	250	40
	Nov 15'	14	2740	12	590	550	186	2480	72	360	20
Salmon River	Aug 14'	**<15**	9290	7	170	330	35	1500	**< 7**	340	500
	Oct 14'	14	8410	10	580	380	143	1100	20	360	270
	July 15'	**<15**	11280	6	370	410	4	1390	99	310	30
	Aug 15'	26	7450	5	860	400	223	520	402	410	20
	Sept 15'	3	4650	3	190	160	50	530	58	190	0
	Oct 15'	4	4430	7	370	270	64	1070	102	190	10
Eagle River	Jun 14'	**<15**	11970	6	210	370	17	500	**< 7**	230	40
	Aug 14'	**<15**	26050	6	340	320	**< 0.6**	420	**< 7**	7780	350
	July 15'	**<15**	8770	3	250	280	46	630	27	200	**<20**
	Aug 15 '	16	6100	**<3**	530	200	17	230	51	190	10

Marine inputs

To elucidate possible sources, the contribution of non-sea salt was calculated for cations and anions that are common ions in marine aerosols and summarized in Table B-15. The average molar concentration of major ions was determined. To find the average non-sea salt concentration, we subtracted the individual ion molar concentration from the sodium molar concentration multiplied by the expected ion-to-sodium ratio. The ratio values used in the calculations were taken from Libes 2009.[8] The sea salt concentration and percentage of non-sea salt were determined by taking the difference between the total average concentration and the average non-sea salt concentration.

Table B-17: Average molar concentration (µmol/L) of selected ions predominantly found in marine aerosols. The non-sea salt and sea salt concentration (µmol/L) is reported along with the percent contribution of the non-sea salt component (%).

Grand Codroy	**Na^+**	**K^+**	**Mg^{2+}**	**Ca^{2+}**	**SO_4^{2-}**
Average Molar concentration (µmol/L)	57.51	30.61	25.10	91.49	2.90
Non-sea salt concentration (µmol/L)		29.35	17.81	90.23	-0.56
Sea salt concentration (µmol/L)		1.26	7.29	1.26	3.46
Contribution of non-sea salt component (%)		95.91	70.97	98.62	-19.21
Humber River	**Na^+**	**K^+**	**Mg^{2+}**	**Ca^{2+}**	**SO_4^{2-}**
Average Molar concentration (µmol/L)	29.70	8.99	12.52	195.40	4.07
Non-sea salt concentration (µmol/L)		8.34	9.18	194.75	2.29
Sea salt concentration (µmol/L)		0.65	3.34	0.65	1.78
Contribution of non-sea salt component (%)		92.81	73.29	99.67	56.13
Salmon River	**Na^+**	**K^+**	**Mg^{2+}**	**Ca^{2+}**	**SO_4^{2-}**
Average Molar concentration (µmol/L)	44.29	10.83	13.37	189.26	3.12
Non-sea salt concentration (µmol/L)		9.86	13.37	188.29	0.46
Sea salt concentration (µmol/L)		0.97	0.00	0.97	2.66
Contribution of non-sea salt component (%)		91.09	62.70	99.49	14.65
Eagle River	**Na^+**	**K^+**	**Mg^{2+}**	**Ca^{2+}**	**SO_4^{2-}**
Average Molar concentration (µmol/L)	19.36	8.50	12.04	329.92	21.86
Non-sea salt concentration (µmol/L)		8.08	9.86	329.50	20.70
Sea salt concentration (µmol/L)		0.42	2.18	0.42	1.16
Contribution of non-sea salt component (%)		95.04	81.89	99.87	94.67

Table B-18: Pearson correlation coefficient (r), statistical significance (p) and number of data points (n) of PFAA homologues comparison with Na+, nss-Ca^{2+}, nss-Mg^{2+} and K^+ as tracers of sea spray, mineral dust and biomass burning at Grand Codroy. Weak correlation (r = 0.3-0.5) shown in blue, moderate correlations (r = 0.5-0.7) in green and strong correlation (r = 0.7-0.90) are shown in red. Statistically significant p-values (p <0.05) are highlighted in bold.

		Na^+	nss-Ca^{2+}	nss-Mg^{2+}	K^+
PFBA	r	-0.46	0.35	-0.91	-0.42
	p	0.53	0.64	0.09	0.57
	n	4	4	4	4
PFPeA	r				
	p				
	n				
PFHxA	r	-0.34	0.57	-0.06	-0.11
	p	0.44	0.17	0.88	8.00E-01
	n	7	7	7	7
PFHpA	r	0.23	0.58	0.27	0.0001
	p	0.62	0.17	5.50E-01	0.99
	n	7	7	7	7
PFOA	r	0.16	0.54	0.31	0.12
	p	0.71	0.16	0.44	7.70E-01
	n	8	8	8	8
PFNA	r	0.30	0.64	0.28	-0.08
	p	0.47	0.08	0.49	8.30E-01
	n	8	8	8	8
PFDA	r	**0.75**	0.60	0.65	0.34
	p	**0.02**	0.11	0.07	0.39
	n	**8**	8	8	8
PFUnDA	r	0.09	0.02	-0.28	-0.43
	p	0.83	0.95	0.54	0.32
	n	7	7	7	7
PFDoDA	r	0.43	0.02	-0.09	-0.15
	p	0.56	0.97	0.9	0.84
	n	4	4	4	4
PFOS	r	-0.29	0.54	-0.38	-0.12
	p	0.62	0.16	0.52	0.83
	n	5	8	5	5

Table B-19: Pearson correlation coefficient (r), statistical significance (p) and number of data points (n) of PFAA homologues comparison with Na+, nss-Ca^{2+}, nss-Mg^{2+} and K^+ as tracers of sea spray, mineral dust and biomass burning at Humber River. Weak correlation (r = 0.3-0.5) shown in blue, moderate correlations (r = 0.5-0.7) in green, strong correlation (r = 0.7-0.90) in red, and very strong correlations are shown in purple (r = 0.90-1.0). Statistically significant p-values (p <0.05) are highlighted in bold.

		Na^+	nss-Ca^{2+}	nss-Mg^{2+}	K^+
PFBA	r	**0.73**	-0.19	0.67	0.51
	p	**0.05**	0.67	0.09	0.23
	n	**7**	7	7	7
PFPeA	r	-0.60	0.61	-0.75	-0.84
	p	0.27	0.27	0.13	0.06
	n	5	5	5	5
PFHxA	r	-0.36	0.50	**-0.95**	**-0.98**
	p	0.63	0.49	**0.04**	**0.01**
	n	4	4	**4**	**4**
PFHpA	r	0.15	0.27	-0.88	-0.84
	p	0.77	0.6	0.01	0.03
	n	6	6	6	6
PFOA	r	0.23	**0.72**	-0.08	-0.39
	p	0.61	**0.05**	0.85	0.37
	n	7	**7**	7	7
PFNA	r	0.63	0.07	0.51	0.32
	p	0.12	0.87	0.23	0.47
	n	7	7	7	7
PFDA	r	0.59	-0.55	0.50	0.36
	p	0.15	0.29	0.24	0.41
	n	7	7	7	7
PFUnDA	r	**0.78**	-0.35	0.70	0.50
	p	**0.03**	0.43	0.07	0.24
	n	**7**	7	7	7
PFDoDA	r	0.40	-0.84	0.49	0.58
	p	0.49	0.07	0.40	0.3
	n	5	5	5	5
PFOS	r	-0.64	-0.88	-0.88	**-0.98**
	p	0.35	0.11	0.11	**0.01**
	n	4	4	4	**4**

Table B-20: Pearson correlation coefficient (r), statistical significance (p) and number of data points (n) of PFAA homologues comparison with Na+, nss-$Ca^{2+,}$ nss-Mg^{2+} and K^+ as tracers of sea spray, mineral dust and biomass burning at Salmon River. Weak correlation (r = 0.3-0.5) shown in blue, moderate correlations (r = 0.5-0.7) in green, strong correlation (r = 0.7-0.90) in red, and very strong correlations are shown in purple (r = 0.90-1.0). Statistically significant p-values (p <0.05) are highlighted in bold.

		Na^+	nss-Ca^{2+}	nss-Mg^{2+}	K^+
PFBA	r	0.22	0.10	0.53	**0.91**
	p	0.71	0.86	0.35	**0.02**
	n	5	5	5	**5**
PFPeA	r	0.96	0.98	0.98	0.13
	p	0.16	0.11	0.12	0.91
	n	3	3	3	3
PFHxA	r	0.72	0.70	0.71	0.01
	p	0.16	0.18	0.17	0.98
	n	5	5	5	5
PFHpA	r	0.66	**0.90**	0.59	-0.24
	p	0.14	**0.01**	0.21	0.64
	n	6	**6**	6	6
PFOA	r	0.44	0.70	0.70	-0.03
	p	0.37	0.11	0.11	0.94
	n	6	6	6	6
PFNA	r	0.46	0.24	0.28	0.02
	p	0.34	0.64	0.59	0.96
	n	6	6	6	6
PFDA	r	-0.55	-0.53	-0.67	-0.30
	p	0.25	0.26	0.13	0.56
	n	6	6	6	6
PFUnDA	r	-0.07	-0.43	-0.50	-0.29
	p	0.90	0.46	0.38	0.62
	n	5	5	5	5
PFDoDA	r	-0.62	-0.64	-0.96	-0.99
	p	0.56	0.55	0.16	0.08
	n	3	3	3	3
PFOS	r	0.24	0.19	0.01	-0.60
	p	0.68	0.75	0.97	0.27
	n	5	5	5	5

Table B-21: Pearson correlation coefficient (r), statistical significance (p) and number of data points (n) of PFAA homologues comparison with Na+, nss-Ca^{2+}, nss-Mg^{2+} and K^+ as tracers of sea spray, mineral dust and biomass burning at Eagle River. Weak correlation (r = 0.3-0.5) shown in blue, moderate correlations (r = 0.5-0.7) in green, strong correlation (r = 0.7-0.90) in red, and very strong correlations are shown in purple (r = 0.90-1.0). Statistically significant p-values (p <0.05) are highlighted in bold.

		Na^+	nss-Ca^{2+}	nss-Mg^{2+}	K^+
PFBA	r	-0.76	0.88	-0.97	-0.41
	p	0.44	0.3	0.15	0.72
	n	3	3	3	3
PFPeA	r				
	p				
	n				
PFHxA	r				
	p				
	n				
PFHpA	r	0.64	0.78	0.87	**0.96**
	p	0.35	0.21	0.12	**0.03**
	n	4	4	4	**4**
PFOA	r	0.40	0.87	0.60	0.56
	p	0.60	0.12	0.40	0.43
	n	4	4	4	4
PFNA	r	0.83	**0.99**	0.94	0.97
	p	0.37	**0.03**	0.2	0.15
	n	3	**3**	3	3
PFDA	r	0.72	0.77	0.92	**0.99**
	p	0.27	0.22	0.07	**0.005**
	n	4	4	4	**4**
PFUnDA	r	0.59	0.87	0.84	0.89
	p	0.40	0.12	0.15	0.1
	n	4	4	4	3
PFDoDA	r	0.94	**0.99**	0.91	0.81
	p	0.20	**0.04**	0.25	0.39
	n	3	**3**	3	3
PFOS	r	0.70	0.38	-0.14	-0.86
	p	0.49	0.75	0.90	0.32
	n	3	3	3	3

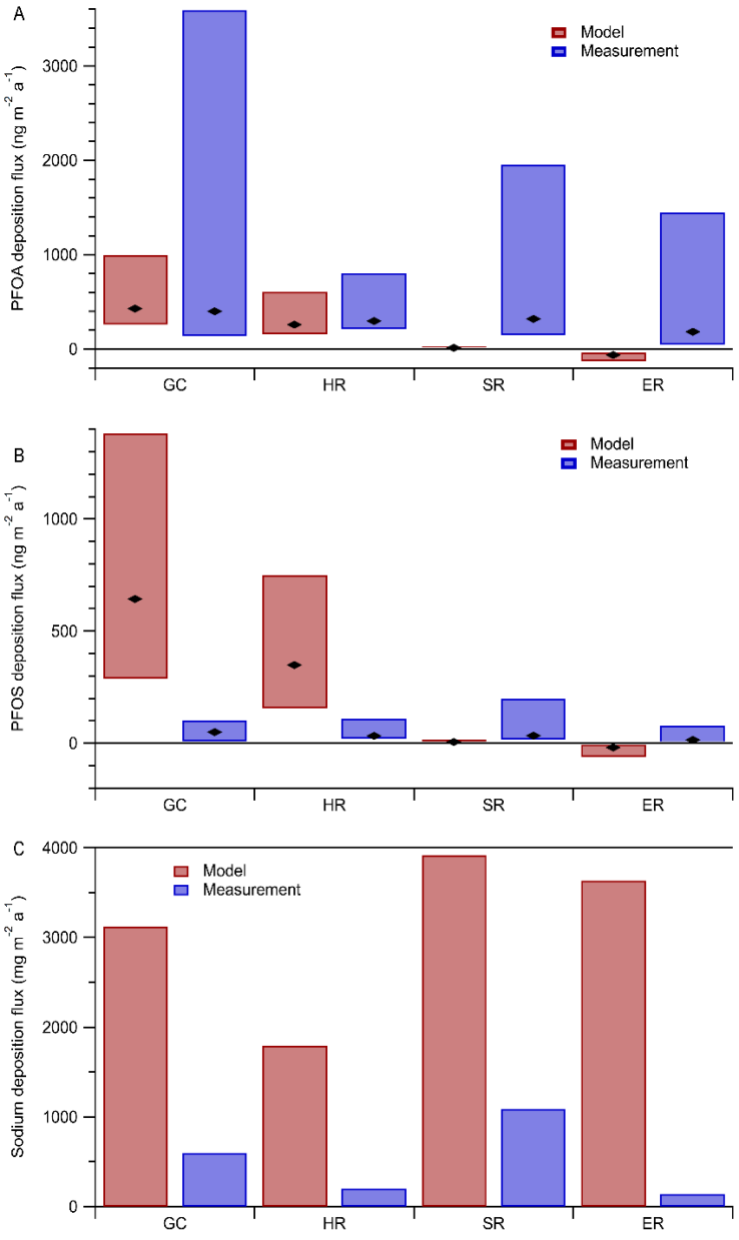

Figure B-9: Modeled (red bars) versus measured (Blue bars) deposition fluxes of (A) PFOA, (B) PFOS, and (C) sodium across the four sampling sites from north to south. The limits of the bars represent the range, whereas a solid diamond indicates the median values.

Table B-22: Geographical grid sector assignment of air mass source regions for each month of the study period for Grand Codroy, Humber River, Salmon River and Eagle River.

Time	Grand Codroy				Humber River				Salmon River				Eagle River			
	NE	NW	SE	SW	NE	NW	SE	SW	NE	NW	SE	SW	NE	NW	SE	SW
Jun. 2014	43%	18%	25%	14%	20%	23%	14%	43%								
Aug. 2014					28%	11%	18%	43%	37%	20%	34%	9%	25%	27%	23%	25%
Sept. 2014	5%	27%	18%	50%												
Oct. 2014	3%	27%	28%	42%					37%	20%	34%	9%				
Jul. 2015	22%	38%	11%	29%	33%	27%	14%	26%								
Aug. 2015	16%	14%	25%	45%	31%	18%	18%	33%	30%	19%	21%	30%	31%	21%	28%	20%
Sept. 2015	15%	54%	6%	25%	13%	51%	9%	27%	15%	53%	10%	22%				
Oct. 2015	10%	59%	8%	23%	14%	63%	7%	16%	7%	62%	2%	29%				
Nov. 2015	26%	58%	7%	9%	14%	63%	7%	16%	14%	72%	4%	10%				
Jun. 2016	30%	27%	18%	24%	32%	33%	13%	22%	33%	43%	8%	16%				
Jul. 2016	24%	27%	16%	33%	24%	27%	11%	38%	33%	19%	9%	39%				
Aug. 2016	17%	37%	16%	30%	17%	37%	10%	36%	11%	33%	19%	39%	30%	34%	13%	23%
Sept 2016	15%	53%	6%	26%	16%	53%	7%	24%	12%	67%	4%	17%	12%	69%	3%	16%
Oct 2016	16%	62%	4%	18%	14%	62%	3%	21%	15%	60%	2%	23%				

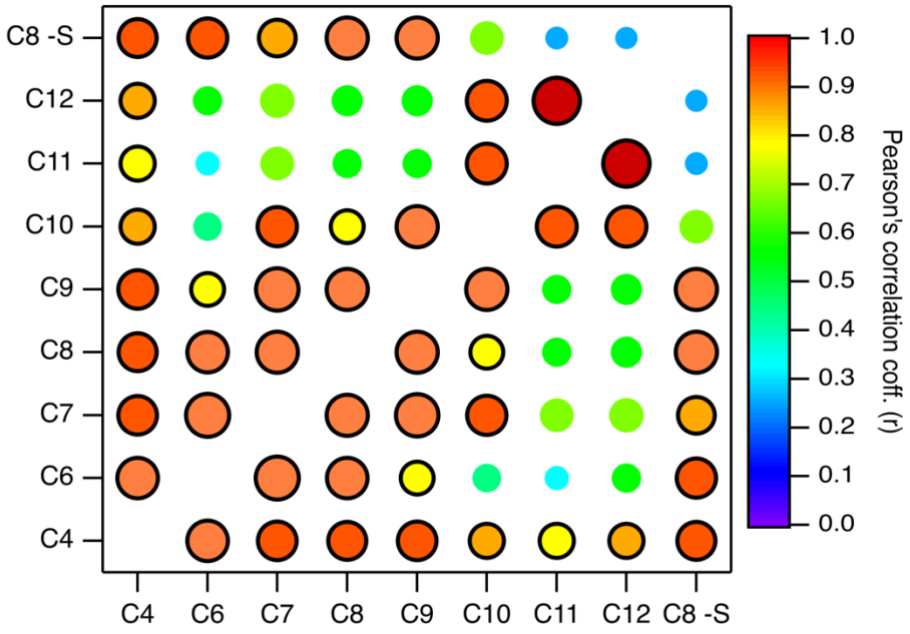

Figure B-10: Pearson correlation map of log-transformed C4 – C12 PFCA and C8 PFSA deposition fluxes across the NL-BELT sites. The strength of the correlation is illustrated by the colour and size of the circle, where larger circles denote a strong correlation based on the magnitude of r. The black outline represents a statistically significant correlation (p-value <0.05).

Table B-23: Pearson correlation coefficients (r), statistical significance (p) and number of data points (n) of PFAA homologues at Grand Codroy. Weak correlation (r = 0.3-0.5) shown in blue, moderate correlations (r = 0.5-0.7) in green, strong correlation (r = 0.7-0.90) in red, and very strong correlations (r: 0.90-1.0) are shown in purple. Statistically significant p-values (p <0.05) are highlighted in bold.

		PFBA	PFPeA	PFHxA	PFHpA	PFOA	PFNA	PFDA	PFUnDA	PFDoDA
PFPeA	r	0.77								
	p	0.44								
	n	3								
PFHxA	r	0.29	0.76							
	p	0.53	0.45							
	n	7	3							
PFHpA	r	0.42	0.87	**0.77**						
	p	0.35	0.13	**0.02**						
	n	7	4	**9**						
PFOA	r	0.37	0.80	0.55	**0.62**					
	p	0.36	0.20	0.10	**0.04**					
	n	8	4	10	**11**					
PFNA	r	-0.07	0.47	**0.64**	**0.71**	**0.72**				
	p	0.86	0.53	**0.05**	**0.01**	**0.01**				
	n	8	4	**10**	**11**	**13**				
PFDA	r	-0.37	0.88	-0.53	-0.60	-0.57	0.46			
	p	0.37	0.37	0.35	0.21	0.18	0.13			
	n	8	8	5	6	7	12			
PFUnDA	r	0.27	-0.18	-0.20	0.08	-0.28	0.30	-0.04		
	p	0.51	0.89	0.60	0.83	0.38	0.34	0.93		
	n	8	3	9	10	12	12	7		
PFDoDA	r	0.30		-0.53	-0.60	-0.57	-0.11	0.19	**0.92**	
	p	0.63		0.35	0.21	0.18	0.81	0.56	**0.00**	
	n	5		5	6	7	7	11	**7**	
PFOS	r	0.82		0.38	0.27	0.34	-0.23	-0.04	-0.26	
	p	0.39		0.45	0.60	0.52	0.66	0.93	0.67	
	n	3		6	6	6	6	7	5	

Table B-24: Pearson correlation coefficients (r), statistical significance (p) and number of data points (n) of PFAA homologues at Humber River. Weak correlation (r = 0.3-0.5) shown in blue, moderate correlations (r = 0.5-0.7) in green and strong correlations (r = 0.7-0.90) are shown in red. Statistically significant p-values (p <0.05) are highlighted in bold.

		PFBA	PFPeA	PFHxA	PFHpA	PFOA	PFNA	PFDA	PFUnDA	PFDoDA
PFPeA	r	-0.22								
	p	0.64								
	n	7								
PFHxA	r	0.37	**0.90**							
	p	0.41	**0.04**							
	n	7	**5**							
PFHpA	r	0.59	0.68	0.76						
	p	0.13	0.14	0.08						
	n	8	6	6						
PFOA	r	0.17	0.10	**0.78**	0.43					
	p	0.64	0.84	**0.04**	0.29					
	n	10	7	**7**	8					
PFNA	r	0.25	-0.42	-0.68	0.01	-0.06				
	p	0.48	0.35	0.10	0.98	0.88				
	n	10	7	7	8	10				
PFDA	r	0.14	-0.64	-0.72	-0.16	-0.40	**0.67**			
	p	0.70	0.12	0.07	0.70	0.26	**0.04**			
	n	10	7	7	8	10	**10**			
PFUnDA	r	0.52	-0.68	-0.55	-0.33	-0.27	0.55	**0.87**		
	p	0.16	0.14	0.26	0.47	0.49	0.13	**0.05**		
	n	9	6	6	7	9	9	**5**		
PFDoDA	r	0.06	**-0.92**	-0.82	-0.59	-0.70	0.12	**0.68**	**0.81**	
	p	0.92	**0.03**	0.39	0.41	0.19	0.84	**0.04**	**0.10**	
	n	5	**5**	3	4	5	5	**9**	**5**	
PFOS	r	0.73	-0.77	0.76	0.89	**0.90**	**0.87**	0.75	0.63	-0.68
	p	0.17	0.23	0.45	0.31	**0.04**	**0.06**	0.15	0.25	0.52
	n	5	4	3	3	**5**	**5**	5	5	3

Table B-25: Pearson correlation coefficients (r), statistical significance (p) and number of data points (n) of PFAA homologues at Salmon River. Weak correlation (r = 0.30-0.5) shown in blue, moderate correlations (r = 0.50-0.70) in green, strong correlation (r = 0.7-0.90) in red, and very strong correlations (r: 0.90-1.0) are shown in purple. Statistically significant p-values (p <0.05) are highlighted in bold.

		PFBA	PFPeA	PFHxA	PFHpA	PFOA	PFNA	PFDA	PFUnDA	PFDoDA
PFPeA	r	-0.39								
	p	0.52								
	n	5								
PFHxA	r	0.43	0.77							
	p	0.33	0.23							
	n	7	4							
PFHpA	r	0.03	0.79	0.71						
	p	0.94	0.11	0.05						
	n	8	5	8						
PFOA	r	0.52	0.14	**0.72**	**0.79**					
	p	0.19	0.83	**0.04**	**0.01**					
	n	8	5	**8**	**9**					
PFNA	r	0.45	0.22	0.11	0.17	0.42				
	p	0.26	0.72	0.79	0.65	0.25				
	n	8	5	8	9	9				
PFDA	r	-0.03	-0.44	**-0.72**	-0.34	-0.16	0.44			
	p	0.94	0.46	**0.04**	0.37	0.68	0.24			
	n	8	5	**8**	9	9	9			
PFUnDA	r	0.04	-0.16	-0.90	-0.52	-0.45	0.56	0.57		
	p	0.93	0.80	0.01	0.19	0.27	0.10	0.14		
	n	8	5	7	8	8	8	8		
PFDoDA	r	-0.90		**-0.94**	-0.65	**-0.96**	-0.15	**0.91**	**0.98**	
	p	0.10		**0.06**	0.35	**0.09**	0.85	**0.09**	**0.02**	
	n	4		**4**	4	**4**	4	**4**	**4**	
PFOS	r	0.65	-0.49	0.79	0.59	0.85	-0.07	-0.37	-0.65	-0.77
	p	0.11	0.40	0.06	0.16	0.02	0.89	0.42	0.12	0.23
	n	7	5	6	7	7	7	7	7	4

Table B-26: Pearson correlation coefficients (r), statistical significance (p) and number of data points (n) of PFAA homologues at Eagle River. Strong correlations (0.70-0.90) in red, and very strong correlations (r: 0.90-1.0) are shown in purple. Statistically significant p-values (p <0.05) are highlighted in bold.

		PFBA	PFHxA	PFHpA	PFOA	PFNA	PFDA	PFUnDA
PFPeA	r							
	p							
	n							
PFHxA	r							
	p							
	n							
PFHpA	r	**0.99**						
	p	**2.4×10^{-3}**						
	n	**3**						
PFOA	r	0.84	**0.99**					
	p	0.08	**0.03**					
	n	5	**3**					
PFNA	r	0.83	0.88	**0.76**				
	p	0.08	0.32	**0.08**				
	n	5	3	**6**				
PFDA	r	**0.98**	0.98	**0.99**	**0.85**			
	p	**0.02**	0.12	**1.5×10^{-3}**	**0.01**			
	n	**4**	3	**5**	**5**			
PFUnDA	r	0.83	**0.99**	**0.99**	0.71	**0.99**		
	p	0.08	**2.6×10^{-3}**	**1.0×10^{-3}**	0.11	**1.1×10^{-3}**		
	n	5	**3**	**6**	6	**5**		
PFDoDA	r	**0.92**		**0.97**	**0.91**	**0.96**	0.77	
	p	**0.08**		**0.01**	**0.03**	**0.04**	0.13	
	n	**4**		**5**	**5**	**4**	5	
PFOS	r	**0.94**	0.93	0.79	**0.94**	0.79	**0.94**	0.91
	p	**0.06**	0.23	0.11	**0.02**	0.21	**0.02**	0.09
	n	**4**	3	5	**5**	4	**5**	4

Table B-27: Model comparisons for C4-C13 PFCAs at GC, HR, SR and ER. We assessed the contribution of the fluorotelomer-derived pathway by comparing the minimum modelled to the minimum observed flux at each site.

		GC	HR	SR	ER
PFBA	Model Min	5	4	4	2
	Model Max	166	136	139	92
	Observed Min	1670	1314	2618	1518
	Observed Max	2568	8919	3815	1650
PFPeA	Model Min	6	5	5	3
	Model Max	224	186	191	127
	Observed Min	127	59	15	64
	Observed Max	170	133	332	64
PFHxA	Model Min	8	6	6	4
	Model Max	299	251	261	174
	Observed Min	113	80	173	
	Observed Max	403	401	273	
PFHpA	Model Min	9	7	8	5
	Model Max	381	323	337	220
	Observed Min	151	105	240	245
	Observed Max	493	476	499	1073
PFOA	Model Min	12	10	10	7
	Model Max	392	303	292	200
	Observed Min	139	218	235	195
	Observed Max	625	473	888	356
PFNA	Model Min	4	4	4	3
	Model Max	277	223	239	166
	Observed Min	165	242	310	287
	Observed Max	524	461	743	287
PFDA	Model Min	5	4	5	3
	Model Max	95	80	85	60
	Observed Min	50	88	113	79
	Observed Max	204	193	333	338
PFUnDA	Model Min	1	1	1	1
	Model Max	103	83	89	62
	Observed Min	45	33	125	55
	Observed Max	130	219	1038	164
PFDoDA	Model Min	2	1	1	1
	Model Max	30	25	27	19
	Observed Min	15	14	29	38
	Observed Max	15	19	35	38
PFTeDA	Model Min	0	0	0	0
	Model Max	30	24	26	18
	Observed Min	26	11	14	12
	Observed Max	43	130	610	80

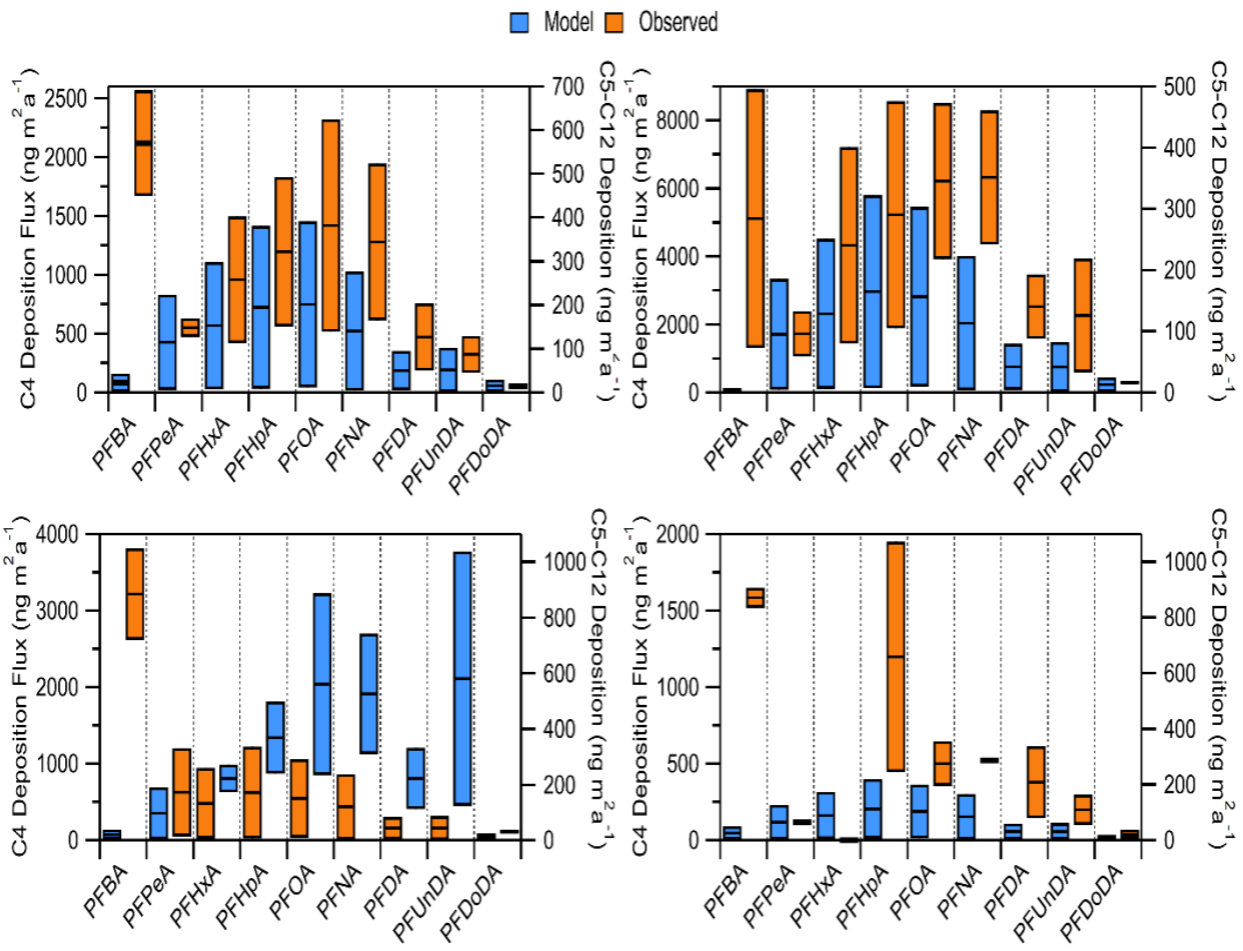

Figure B-11: Measurement-model comparison of PFCAs (C4) left axis and (C5-C12) right axis at (A) GC, (B) HR, (C) SR and (D) ER. The limits of the boxes represent the minimum and maximum modelled and observed values. The solid line represents the median.

References

1A. F. Stein, R. R. Draxler, G. D. Rolph, B. J. B. Stunder, M. D. Cohen and F. Ngan, NOAA's HYSPLIT Atmospheric Transport and Dispersion Modeling System, *Bulletin of the American Meteorological Society*, 2015, **96**, 2059–2077.

2B. Place, Masters Thesis, Memorial University of Newfoundland, 2017.

3H. M. Pickard, A. S. Criscitiello, C. Spencer, M. J. Sharp, D. C. G. Muir, A. O. De Silva and C. J. Young, Continuous non-marine inputs of per- and polyfluoroalkyl substances to the High Arctic: a multi-decadal temporal record, *Atmospheric Chemistry and Physics*, 2018, **18**, 5045–5058.

4D. Persaud, A. S. Criscitiello, C. Spencer, I. Lehnherr, D. C. G. Muir, A. O. De Silva and C. J. Young, Ice Core record of Legacy Fluorinated Alkyl Acids in the Canadian High Arctic: a 50 – year deposition record from Ellesmere Island, *In Prep*.

5C. Xia, S. L. Capozzi, K. A. Romanak, D. C. Lehman, A. Dove, V. Richardson, T. Greenberg, D. McGoldrick and M. Venier, The Ins and Outs of Per- and Polyfluoroalkyl Substances in the Great Lakes: The Role of Atmospheric Deposition, *Environ. Sci. Technol.*, 2024, **58**, 9303–9313.

6M. S. Shimizu, R. Mott, A. Potter, J. Zhou, K. Baumann, J. D. Surratt, B. Turpin, G. B. Avery, J. Harfmann, R. J. Kieber, R. N. Mead, S. A. Skrabal and J. D. Willey, Atmospheric Deposition and Annual Flux of Legacy Perfluoroalkyl Substances and Replacement Perfluoroalkyl Ether Carboxylic Acids in Wilmington, NC, USA, *Environ. Sci. Technol. Lett.*, 2021, **8**, 366–372.

7GenX Investigation | NC DEQ, https://www.deq.nc.gov/news/key-issues/genx-investigation, (accessed 17 December 2024).

8S. M. Libes, *Introduction to Marine Biogeochemistry*, Acedemic Press, 2009.

APPENDIX C

SUPPLEMENT FOR CHAPTER 4

Atmospheric removal of trifluoroacetic acid by dry and wet deposition: A multi-year analysis in Toronto

Section C-1: Methods – Sample collection

Integrated precipitation samples were collected from the roof of the Petrie Science and Engineering Building located at York University, Toronto, ON, Canada. This corresponds to the total of all precipitation events collected continuously. The custom-built automated precipitation samplers selectively collect wet deposition samples. When conductive precipitation is detected by a rain sensor, it triggers an electric motor via limit switches to open and close a lid resting over a funnel opening. The motors are controlled by a modular digital logic control board, which has low energy demands. Total deposition samples were collected using an identical setup but without the automated lid, allowing for continuous exposure to both wet and dry deposition. Further details of the sampler design and operation are provided elsewhere.[1]

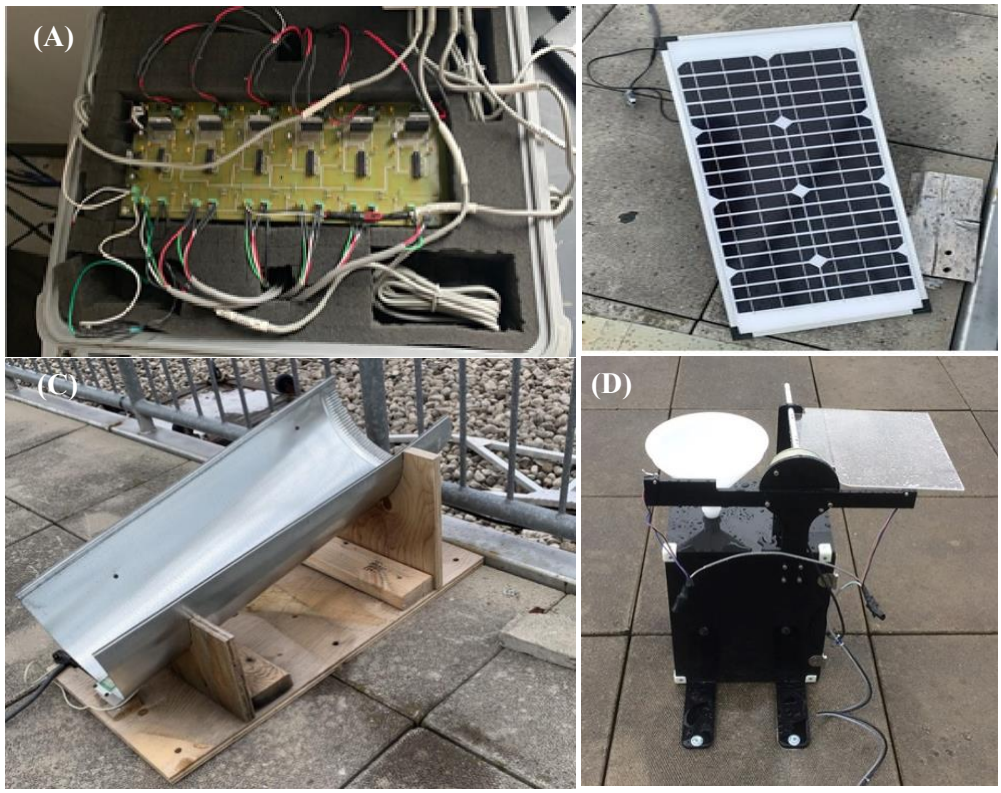

Figure C-1: Automated precipitation array installed at the Air Quality Research Station, York University (Toronto), showing (A) a weather-proofed control board, (B) a 40 W solar panel, (C) a rain sensor with an enhanced-sensitivity chute, and (D) an automated collection unit secured to concrete during a rain event.

Section C-2: Materials and Methods

2.1 Sample Preparation

All apparatus was rinsed three times with deionized water (DIW; 18.2 MΩ·cm at 25 ºC, Direct 8; EMP Millipore) and twice with ≥ 99.8 % HPLC grade methanol before use. After collection, all sample volumes were measured for flux calculations, transferred to precleaned HDPE bottles and kept refrigerated until analysis. Before analysis, all samples were allowed to equilibrate at room temperature for at least 30 minutes, then a 10 mL aliquot was withdrawn into a polypropylene syringe (P/N: 14-817-44. Fisher Scientific) and filtered through a 0.22 µm nylon syringe filter (P/N: 76479-030, VWR) into a precleaned polypropylene conical tube (14-959-53A, Fisher Scientific). Then an 800 µL sample was transferred to a 1.0 mL polypropylene vial (5182-0567, Agilent) along with 100 µL $^{13}C_2$ or $^{13}C_1$ (20 µg L^{-1}) TFA internal standard (IS), purchased from Toronto Research Chemicals.

2.2 Sample analysis

TFA was quantified using an ICS-6000 ion chromatography system coupled to an ISQEC single quadrupole mass spectrometer (Thermo Fisher Scientific). A sample volume of 750 µL was injected into a Dionex™ IonPac Low Pressure Trace Anion Concentrator Column (5 mm x 23 mm), and separation was performed on a Dionex IonPac AS24 microbore analytical column (2 x 250 mm) and Dionex™ IonPac AG24A guard column (4 x 50 mm) set to 35 ºC. The flow was suppressed using Dionex ADRS 600 Dynamically Regenerated Suppressor (2 mm) in legacy mode at 87 mA with external water supplied at 1 mL min^{-1} using an auxiliary pump. Chromatographic conditions are further summarized in Table C-1. In the effluent from the suppressor, external methanol was teed in at 0.20 mL min^{-1} using another auxiliary pump before the flow entered the MS electrospray source. The MS has unit mass resolution and was operated in selected ion mode to quantify TFA (m/z 113), $^{13}C_1$ TFA (m/z 114), and $^{13}C_2$ TFA (m/z 115). Mass spectrometric conditions are summarized in Table C-2.

Table C-1: Instrumental Method Details

Column Temperature	35 °C	
Mobile Phase A	DIW	
Mobile Phase B	100 mM NaOH	
Flow Rate	0.350 mL/min	
Gradient Program	**Time (min)**	**%B**
	0.0	10.0
	7.0	10.0
	10.0	27.0
	16.5	32.0
	20.0	50.0
	22.0	60.0
	25.0	60.0
	25.1	10.0
Injection Volume	750 µL	
Length of Method	30 min	

Table C-2: Mass spectrometry method details for TFA analysis.

Instrument	ISQEC single quadrupole mass spectrometer
Scan Type	Selected Ion Monitoring
Vaporizer Temperature	450 ºC
Ion Transfer Temperature	250 ºC
Source Voltage	-3000 V
Sheath gas pressure	45 psi
Auxiliary gas pressure	5 psi

2.3 Limit of Detection (LOD) and Limit of Quantitation (LOQ)

The limit of detection (LOD) and limit of quantitation (LOQ) represent the lowest signal distinguishable from the blank and the lowest quantity determination, respectively. The signal-to-noise ratio was found using three sets of DIW blanks and three sets of calibration curves. The average and standard deviation of detector signal from the deionized water blanks, along with the peak heights and their standard deviations from the calibration curve standards, were used to calculate the signal-to-noise (S/N) ratio for

the blanks and each standard. As opposed to the typical signal vs concentration plot, a S/N ratio vs calibration level was plotted to obtain a slope where the line is forced through the origin. The LOD and LOQ with mass of TFA per volume units were calculated from the slope using the equations: LOD = 3/m and LOQ = 10/m, where m is the slope (y = mx). The LOD and LOQ for TFA were determined by this method as 6 and 21 ng L^{-1} respectively.

2.4 Quality Control and Quality Assurance

Extensive care was taken throughout sample collection, handling and analysis to minimize the risk of contamination that could compromise our trace analysis of TFA.[2] The total and wet deposition samplers were thoroughly cleaned with DIW (18.2 MΩ·cm at 25 ºC, Direct 8; EMP Millipore) and twice with ³ 99.8% HPLC grade methanol before deployment. All personnel avoided the use of commercial or personal care products that may contain TFA and other PFAS during collection and sample processing.

The samplers were installed on an exposed rooftop ~25 m above ground and away from overhanging vegetation. During sample collection, samples were visually inspected and large debris such as leaves or insects was rarely observed. The design and deployment choices minimize the likelihood of large plant materials entering the sampling collectors. We know that fine particulates (e.g., dust, pollen) will enter the samples as they are true components of the atmosphere and will be included in the reported fluxes. These processes cannot be explicitly quantified within the present dataset and are considered as a minor, unquantified source of uncertainty in our flux estimates, while also being considered part of the atmospheric processes that remove TFA from the atmosphere.

Comprehensive QA/QC procedures were applied during sample preparation and instrumental analyses to assess random and systematic error. Isotopically labelled standards ($^{13}C_2$ or $^{13}C_1$) were used for analyte quantification. Figure S2 shows an example chromatogram of a rainwater sample compared with the $^{13}C_2$ TFA IS, a 1 μg L^{-1} standard and blank, demonstrating consistent signal shape and retention time. Method precision was assessed using the percent relative standard deviation (% RSD) derived from the slopes of replicate linear calibration curves (n=6) and was 13%. Accuracy was

determined by calculating the percent relative error (%RE) of 0.25 μg L^{-1} check standards, which ranged from 0.34 – 23% across analytical batches. To ensure continuous data quality, method blanks and check standards were systematically analyzed after every ten sample injections. The stability of the instrument throughout a sequence is demonstrated in Figure S3, which shows a consistent response of check standards at the beginning, middle and the end of a sequence.

There has been recent discussion about potential isobaric interference when determining TFA in complex matrices.[3,4] For instance, Muir et al.[3] quantified TFA in human urine by ion chromatography tandem mass spectrometry and subsequently verified the absence of co-eluting ions through complementary high resolution mass spectrometry instrument. They reported that urine, a considerably more complex matrix than rainwater, showed no co-eluting ions at the TFA retention time, and only minor fragments near m/z 69 that would (at most) elevate the baseline. In contrast, Pan et al.[4] demonstrated that interferences from a carboxylic acid natural product primary occur in biotic matrices (serum, tissue and fish) and noted that such interferences were not evident in abiotic samples such as water and soil. We note that our analytical approach inherently minimizes such risk. Our method employs ion-exchange chromatography, comparable to that used by Muir et al.,[3] and Freeling et al.,[5] which provides strong chromatographic separations based on anion charge and acidity. Under these conditions, carboxylic acids including TFA, other anions and organic acids elute in distinct, reproducible retention windows. In all samples, the retention times of TFA were consistent with the internal standard and no co-eluting peaks were observed. The chromatographic separation confirms that the detected signals arise solely from TFA rather than any isobaric interference. Nevertheless, coupling ion chromatography with a more selective detector (e.g., HRMS) in future work would provide additional selectivity and further reduce the possibility of undetected interferences.

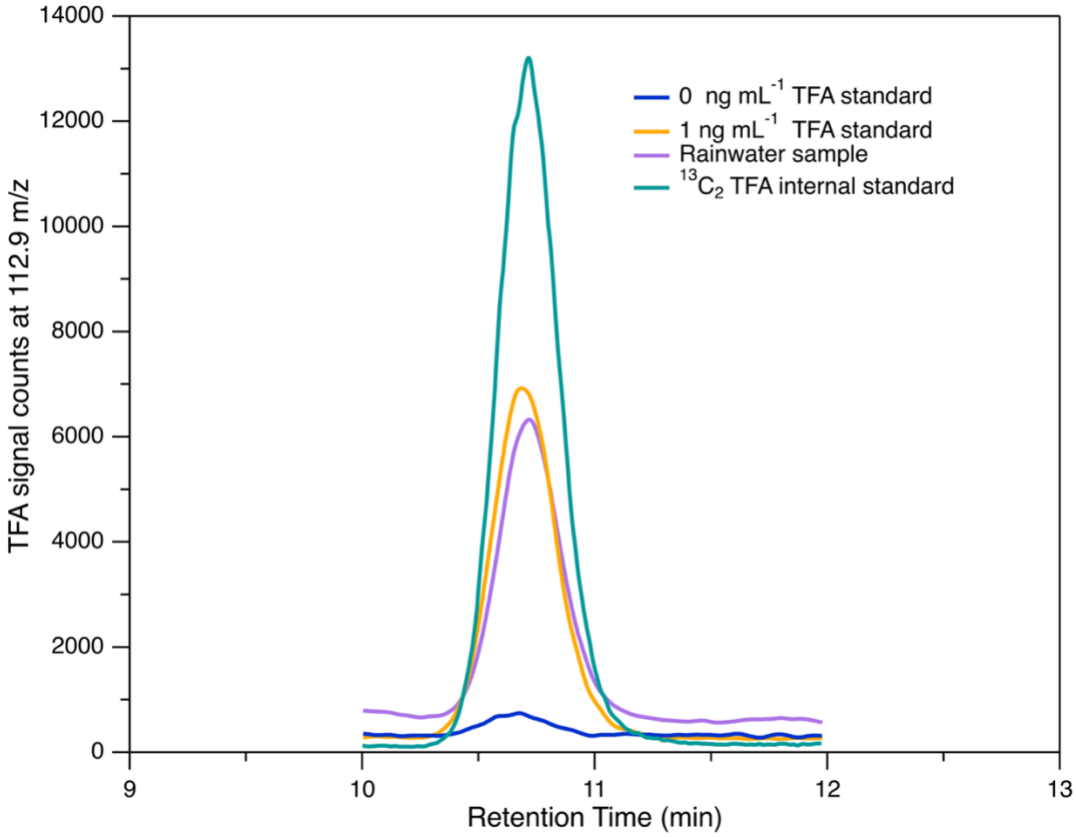

Figure C-2: Chromatograms showing the detection of TFA in a representative a total deposition sample. and corresponding standards. The blue, orange and purple trace represent the 0 ng mL^{-1} standard, 1 ng mL^{-1} standard and rainwater sample, while the teal trace shows the response of the $^{13}C_2$ TFA IS. All signals were monitored at m/z 112.9. The consistent retention time and identical peak shapes between the rainwater samples and TFA standards confirms chromatographic alignment and the absence of inferences.

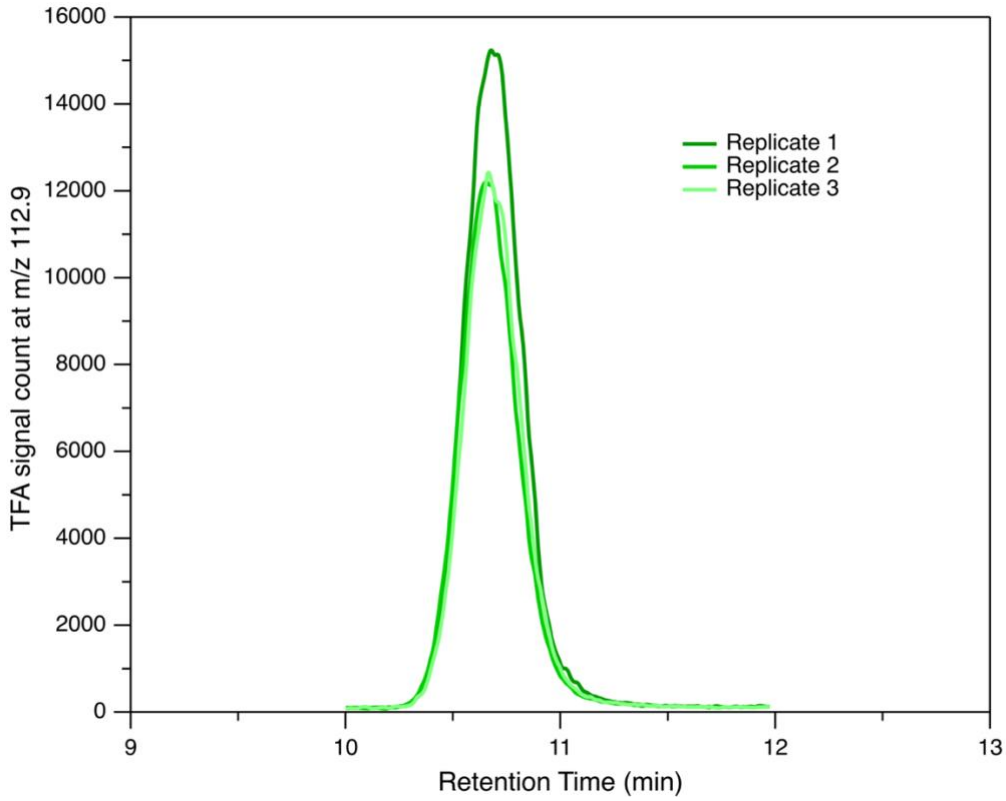

Figure C-3: Chromatographic reproducibility of TFA detection across replicate analyses of 0.250 ng mL^{-1} TFA check standards conducted over a sequence of 100 injections. Replicate 1, 2, and 3 correspond to injections performed at the beginning, middle, and end of the analytical sequence, respectively.

Section C-3: Concentration and Fluxes of TFA

Concentration of PFAAs in precipitation is influenced by volume and is not useful for determining trends related to depositional inputs at the atmosphere-surface interface. To normalize the effect of deposition volume and sample collection duration, we calculated deposition fluxes (μg m^{-2} a^{-1}) for TFA using the following formula:

$$\text{Deposition Flux} = \left[\frac{\text{analyte concentration } \left(\frac{\mu g}{L}\right) \text{x volume of sample(L)}}{\text{Area of static sampler } (m^2) \text{ / number of sampling days}} \text{ x } 365 \frac{\text{days}}{\text{year}}\right]$$

We normalize the deposition rates based on the sampling days and scale them to an annual basis equivalence. This method ensures consistency of comparison across different sampling periods and facilitates robust comparisons of atmospheric deposition trends.

Table C-3: Mean TFA concentration (µg L^{-1}) and deposition flux (µg m^{-2} a^{-1}) in total deposition samples (2018-2024). The error for concentration and flux were determined as relative error between two independent samples. For samples where n = 1, concentration error (0.08 ug L^{-1}) was calculated by propagating the calibration curve uncertainty and carried through the flux calculation ([a]), these single-sample standard errors are highlighted in red.

Sampling Start	Sampling End	Mean Concentration (µg/L)	Error (%)	Mean Flux (µg m^{-2} a^{-1})	Error (%)
07-05-2018	04-06-2018	0.44	0.08	176	15[a]
04-06-2018	03-07-2018	0.61	11	161	25
03-07-2018	16-11-2018	0.18	45	136	42
15-11-2018	27-02-2019	0.08	4	602	19
27-02-2019	15-04-2019	0.08	24	67	1
15-04-2019	26-05-2019	0.18	0	328	23
26-05-2019	27-09-2019	0.61	0.08	1006	12[a]
27-09-2019	13-11-2019	0.13	30	142	34
13-11-2019	18-12-2019	0.35	0.08	245	5[a]
18-12-2019	13-02-2020	0.14	30	76	28
13-02-2020	10-06-2020	0.11	4	80	8
10-06-2020	11-09-2020	0.95	14	298	1
11-09-2020	05-11-2020	0.35	6	113	2
05-11-2020	03-12-2020	0.15	49	131	41
03-12-2020	22-12-2020	1.18	18	323	28
22-12-2020	20-01-2021	0.57	1	125	7
20-01-2021	17-02-2021	1.46	9	146	10
17-02-2021	17-03-2021	1.41	29	1101	13
17-03-2021	15-04-2021	0.79	10	404	26
15-04-2021	12-05-2021	4.48	3	790	2
12-05-2021	16-06-2021	0.46	0.08	136	17[a]
16-06-2021	15-07-2021	0.70	12	643	18
15-07-2021	17-08-2021	1.35	0.08	466	14[a]
17-08-2021	16-09-2021	0.39	65	567	6
16-09-2021	19-10-2021	0.21	6	328	24
19-10-2021	16-11-2021	0.25	18	128	11
16-11-2021	10-12-2021	0.27	19	231	15
10-12-2021	05-04-2022	0.26	25	324	14
05-04-2022	12-05-2022	1.41	6	686	3
12-05-2022	16-06-2022	1.00	26	611	37
16-06-2022	03-08-2022	1.48	34	686	6
03-08-2022	27-09-2022	1.05	5	677	4
27-09-2022	22-11-2022	0.74	17	436	14
22-11-2022	17-01-2023	0.18	73	190	17
17-01-2023	14-02-2023	0.30	1	207	25
14-02-2023	30-03-2025	0.70	19	554	18
30-03-2023	04-05-2023	0.42	20	561	23
04-05-2023	16-06-2023	0.80	10	581	38
16-06-2023	21-07-2023	0.61	20	687	33
21-07-2023	22-08-2023	0.56	6	516	3
22-08-2023	22-09-2023	0.91	12	340	43
22-09-2023	31-10-2023	0.62	18	299	22
31-10-2023	30-11-2023	0.44	38	206	42
30-11-2023	02-01-2024	0.42	22	302	7
02-01-2024	01-02-2024	0.21	21	211	23
01-02-2024	08-03-2024	0.74	19	307	12
08-03-2024	08-04-2024	0.56	9	557	11
08-04-2024	08-05-2024	0.61	1	550	12
08-05-2024	07-06-2024	1.20	3	1378	2
07-06-2024	08-07-2024	1.27	1	1264	5
08-07-2024	08-08-2024	1.78	15	1420	20
08-08-2024	08-10-2024	0.31	11	109	13
08-10-2024	08-11-2024	0.27	38	288	36
08-11-2024	20-12-2024	0.39	17	143	11

Table C-4: Mean TFA concentration (µg L^{-1}) and deposition flux (µg m^{-2} a^{-1}) in wet deposition samples (2018-2024). Error for concentration and flux were determined as relative error between two independent samples. For samples where n = 1, concentration error (0.08 ug L^{-1}) was calculated by propagating the calibration curve uncertainty and carried through the flux calculation ([a]), these single-sample standard errors are highlighted in red.

Sampling Start	Sampling End	Mean Concentration (µg/L)	Error (%)	Mean Flux (µg m^{-2} a^{-1})	Error (%)
15-11-2018	27-02-2019	0.15	48	24	5
27-02-2019	24-05-2019	0.25	12	46	11
27-02-2019	15-04-2019	0.41	45	28	17
15-04-2019	24-05-2019	1.53	71	231	11
24-05-2019	01-08-2019	1.07	45	278	1
01-08-2019	16-09-2019	0.67	36	234	35
16-09-2019	13-11-2019	0.37	39	132	36
13-11-2019	18-12-2019	1.14	2	238	8
18-12-2019	13-02-2020	0.15	11	70	19
13-02-2020	10-06-2020	0.17	35	78	37
10-06-2020	11-09-2020	1.74	59	88	34
11-09-2020	05-11-2020	1.04	81	102	27
05-11-2020	03-12-2020	0.25	24	51	50
03-12-2020	22-12-2020	0.30	76	60	10
22-12-2020	20-01-2021	0.40	93	119	29
20-01-2021	17-02-2021	0.36	87	44	17
17-02-2021	17-03-2021	0.43	18	63	2
17-03-2021	15-04-2021	0.93	0.08	134	8[a]
15-04-2021	12-05-2021	1.26	0.08	169	6[a]
12-05-2021	16-06-2021	2.35	71	202	23
16-06-2021	15-07-2021	0.80	11	421	42
15-07-2021	17-08-2021	0.38	0.08	148	21[a]
17-08-2021	16-09-2021	0.53	21	607	1
16-09-2021	19-10-2021	0.36	1	246	13
19-10-2021	16-11-2021	0.45	4	145	39
16-11-2021	10-12-2021	0.76	51	193	30
10-12-2021	05-04-2022	0.18	63	88	12
05-04-2022	12-05-2022	2.20	0.08	479	6[a]
12-05-2022	16-06-2022	1.43	10	522	10
16-06-2022	03-08-2022	0.49	64	228	6
03-08-2022	27-09-2022	1.05	19	382	19
27-09-2022	22-11-2022	0.76	58	289	14
22-11-2022	17-01-2023	0.11	0.08	46	7[a]
17-01-2023	14-02-2023	0.53	1	104	3
14-02-2023	30-03-2023	0.95	6	144	6
30-03-2023	04-05-2023	1.66	5	363	8
04-05-2023	16-06-2023	1.34	28	382	17
16-06-2023	21-07-2023	0.68	12	569	9
21-07-2023	22-08-2023	0.53	3	446	10
22-08-2023	22-09-2023	0.80	5	249	29
22-09-2023	31-10-2023	0.48	13	192	4
31-10-2023	30-11-2023	0.46	40	142	39
30-11-2023	02-01-2024	0.67	14	149	4
02-01-2024	01-02-2024	0.20	4	171	6
01-02-2024	08-03-2024	0.92	0.08	171	9[a]
08-03-2024	08-04-2024	0.73	7	349	1
08-04-2024	08-05-2024	1.01	28	444	31
08-05-2024	07-06-2024	0.40	10	289	16
07-06-2024	08-07-2024	0.70	42	384	40
08-07-2024	08-08-2024	0.84	54	480	1
08-08-2024	08-10-2024	0.36	0.08	91	21[a]
08-10-2024	08-11-2024	0.11	29	84	26
08-11-2024	20-12-2024	0.73	6	194	1

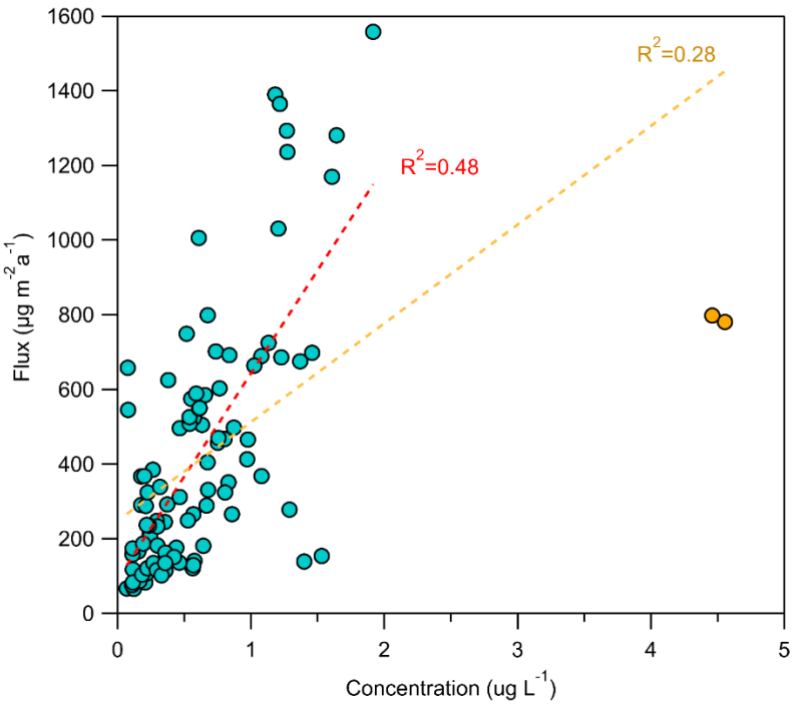

Figure C-4: Plot of total deposition flux (µg m^{-2} a^{-1}) versus concentration (µg L^{-1}) for the entire sampling period. Two linear fits are shown (i) a fit using all data (orange dashed line) and a fit excluding extreme outliers from a single sampling event (red dashed line). A Grubbs test (µ 0.05) identified the two highest concentration points as significant outliers. Their exclusion strengthens the positive concentration-flux relationship, as indicated by the increased slope and R^2 value. The outliers may reflect episodic deposition events or changes in the typical seasonal patterns including changes in the local meteorology, transport pathways or precursor abundances, which could enhance TFA deposition.

Table C-5: Comparisons of trifluoroacetic acid (TFA) concentrations (μg L^{-1}) and deposition fluxes measured in total deposition samples and precipitation from various geographic regions, including this work. Fluxes are reported as both flux per interval (μg m^{-2}) and normalized on annual period (μg $m^{-2}a^{-1}$).[a]Concentration values represent only wet deposition. [b]Denotes fluxes reported over daily intervals

Location	Time	TFA concentration (μg L^{-1})	TFA fluxes μg m^{-2}	TFA fluxes μg m^{-2} a^{-1}	Reference
Toronto, ON	2018-2024	0.07 – 4.6		66-1558	This work
Switzerland	2021-2023	0.04 – 5.7		410-1280	Henne et al.[6]
Lake Vattern, Sweden	December 2018 – February 2019	0.018 – 0.3		[b]0.3-16	Maria K. Björnsdotter[7]
Germany	2018-2019	[a]<LOD-38		91.4-401	Freeling et al.[5]
Mainland China	May – September 2016	0.0088–1.8		[b]0.1-16	Chen et al.[8]
Shaker Heights, OH	Summer, 2019	0.05 – 1.2			Pike et al.[9]
Willoughby, OH		0.07 – 0.17			
Wooster, OH		0.06 – 1.1			
Ashland, OH		0.06 – 1.1			
Rockford OH		0.08 – 0.75			
Whitestown, IN		0.004 – 1.7			
Jackson Hole, WY		0.27 – 0.85			
Guangzhou, China	April 2007-March 2008	0.045 – 0.17		229	Wang et al. [10]
Tsukuba City, Japan	May – July 2007	0.064 – 0.075			Taniyasu et al.[11]
Kawaguchi City, Japan		0.039 – 0.065			
Maryland (MD)	1998	0.023 – 0.62	1.9		Scott et al. [12]
	1999	0.021 – 0.2	3.7		
Delaware (DE)	1998	0.01 – 0.17	2.1		
	1999	0.017 – 2.4	5.5		
New York (NY)	1998	0.013 – 1.1	7.5		
	1999	0.009 – 0.36	10.1		
Vermont (VT)	1999	0.008 – 0.25	4.7		
Nova Scotia (NS)	2002	0.004 – 0.1	0.4		
Algoma (ON)	2002	0.008 – 0.25	0.8		
British Columbia (BC)	2002	0.005 – 0.14	0.9		
Ontario (Egbert)	2003-04	0.043 – 0.17	1.6		
Toronto (ON)	2003-04	0.087 – 0.27	4.6		
Burnt Island, Canada	1998-1999		<0.003-2.3		Scott et al.[13]
Point Petre, Canada			1.5-3.3		
Chile (urban)	1999	0.006 – 0.015	0.1-1.3		Scott et al.[14]
Chile (Rural)		0.005 – 0.021	0.1		
Senga Bay, Malawi		0.004 – 0.015	0.01-0.2		
Saturna, Canada		0.003 – 0.037	0.001-0.8		
Algoma, Canada		0.012 – 0.35	0.02-0.3		
Chapais, Canada		0.0005 – 0.054	0.20-9.0		
California, USA	1996	0.02 – 0.46			Wujcik et al.[15]
Nevada, USA	1994-1996	0.11 – 0.76			
Mace Head, Ireland	Feb – March 1996	0.002 – 0.092			Von Sydow et al.[16]
Gdansk, Poland	May 1996	0.026 – 1.1			
Switzerland	1996-1997	0.033 – 0.22			Berg et al.[17]
Hanoi, Vietnam	1996	0.004 – 0.15		230	
Baikal, Siberia	1996	0.03 – 0.22			
Bayreuth, Germany	March – December 1995	0.025 – 0.28			Frank et al.[18]

Table C-6: Comparisons of mean total, wet, and estimated dry deposition of TFA measured in the current study to previous model estimates of TFA deposition across different regions. Ranges measured and estimated deposition are also included in brackets. All model estimates were based on the degradation of chlorofluorocarbon (CFC) replacement compounds.

				TFA deposition (μg m^2 a^{-1})			
Location	**Time**	**TFA precursors considered**	**Model**	**Total**	**Wet**	**Dry**	**Ref.**
Toronto, Canada	2018-2024	-	-	425 (66-1558)	220 (13-611)	218 (2-1088)	Current Study
Beijing, China	May 2012-Apr 2013	HFC-134a	Atkinson Box Model	619		247	Wu et al.[18]
Tropics	2020	HCFC-22, HCFC-123, HCFC-124, HFC-134a, HCFC-141b	MOGUNTIA	228			Kanakidou et al.[19]
Guelph, Canada	2000	N/A	Box Model		120	120	Martin et al[20]
India	2020-2040	HFO-1234yf	GEOS-Chem	874	558	316	David et al.[21]
China				501	297	204	
Middle East				477	282	195	
India			WRF-Chem	802	641	161	
China				342	300	41	
Middle East				284	258	26	
China, annual	2016	HFO-1234yf	GEOS-Chem	960			Wang et al.[22]
US, annual				450			
EU, annual				520			
North Pole region, annual				80			
Globe, annual				120			
China, annual	2030			1850			
US, annual				500			
EU, annual				540			
Globe, annual				180			
US, Summer	Jun-Aug 2005	HFO-1234yf	CMAQ	240			Luecken et al.[23]
EU, annual	2020	HFO-1234yf	FLEXPART	370-650	1700	700	Henne et al.[24]

[a]Luecken et al stimulated US results for the high emission scenario for three months, June – August. The TFA deposition values were scaled up during the summertime, assuming that ~50% of the annual HFO-1234yf emission was released. [b] Maximum value observed in Northern Italy. [c] Maximum value observed in Western Europe

Table C-7: Mean calculated dry deposition of TFA for the entire sampling period (2018 – 2024). The dry deposition calculation was made by subtracting the mean wet deposition flux from the mean total deposition fluxes. For periods where this calculation yielded a negative value (n = 3) the dry deposition contribution was set to zero (red). These arise due to propagating sampling and analytical uncertainties.

Sampling Start	Sampling End	Estimated Dry Deposition ($\mu g\ m^{-2}\ a^{-1}$)
15-11-2018	27-02-2019	577
27-02-2019	15-04-2019	39
15-04-2019	24-05-2019	97
24-05-2019	01-08-2019	728
16-09-2019	13-11-2019	9
13-11-2019	18-12-2019	7
18-12-2019	13-02-2020	6
13-02-2020	10-06-2020	2
10-06-2020	11-09-2020	92
11-09-2020	05-11-2020	11
05-11-2020	03-12-2020	80
03-12-2020	22-12-2020	263
22-12-2020	20-01-2021	6
20-01-2021	17-02-2021	102
17-02-2021	17-03-2021	1038
17-03-2021	15-04-2021	270
15-04-2021	12-05-2021	620
12-05-2021	16-06-2021	0
16-06-2021	15-07-2021	222
15-07-2021	17-08-2021	318
17-08-2021	16-09-2021	0
16-09-2021	19-10-2021	82
19-10-2021	16-11-2021	0
16-11-2021	10-12-2021	38
10-12-2021	05-04-2022	236
05-04-2022	12-05-2022	207
12-05-2022	16-06-2022	89
16-06-2022	03-08-2022	458
03-08-2022	27-09-2022	294
27-09-2022	22-11-2022	147
22-11-2022	17-01-2023	144
17-01-2023	14-02-2023	103
14-02-2023	30-03-2023	410
30-03-2023	04-05-2023	197
04-05-2023	16-06-2023	199
16-06-2023	21-07-2023	118
21-07-2023	22-08-2023	70
22-08-2023	22-09-2023	90
22-09-2023	31-10-2023	107
31-10-2023	30-11-2023	64
30-11-2023	02-01-2024	152
02-01-2024	01-02-2024	40
01-02-2024	08-03-2024	135
08-03-2024	08-04-2024	208
08-04-2024	08-05-2024	106
08-05-2024	07-06-2024	1088
07-06-2024	08-07-2024	880
08-07-2024	08-08-2024	939
08-08-2024	08-10-2024	18
08-10-2024	08-11-2024	204

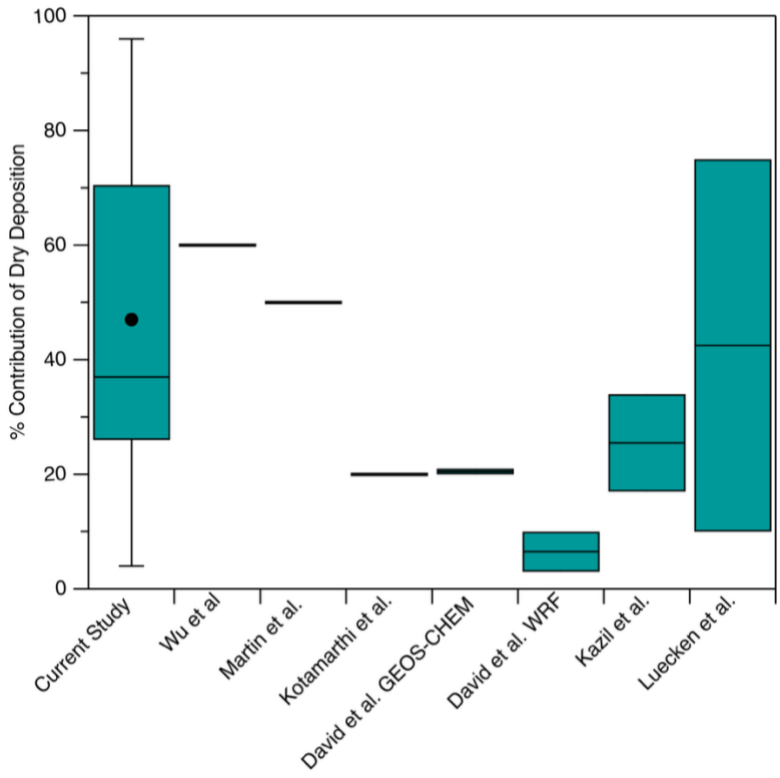

Figure C-5: Comparison of the percent contribution of dry deposition to the total deposition of TFA from the current study and mean estimated contributions from existing literature. Box and whisker (n=42) show the observed distribution across the sampling period for the current study, with the solid circle representing the mean value. Boxes (n=2) indicate modeled ranges reported by Kazil et al.,[26] Luecken et al.,[24] David et al. (WRF) and David et al. (GEOS-CHEM).[22], with the thick horizontal line indicating the median; single horizontal bars (n=1) are reported values from Kotamarthi et al,[27] Wu et al.,[19] and Martin et al.[21] We observed that the current study shows a higher median contribution and substantially greater variability than the box models, GEOS-CHEM and WRF estimates.

References

(1) Colussi, A. A.; Persaud, D.; Lao, M.; Place, B. K.; Hems, R. F.; Ziegler, S. E.; Edwards, K. A.; Young, C. J.; VandenBoer, T. C. Cost-Effective off-Grid Automatic Precipitation Samplers for Pollutant and Biogeochemical Atmospheric Deposition. *Atmospheric Measurement Techniques* **2024**, *17* (12), 3697–3718. https://doi.org/10.5194/amt-17-3697-2024.

(2) Muir, D. C. G.; Freeling, F.; Nilsson, S.; Bugsel, B.; Bowles, K.; Hobson, P.; Toms, L.-M.; Mueller, J. F. Trifluoroacetic Acid in Australian Human Urine Samples. *Environ. Sci. Technol. Lett.* **2025**, *12* (10), 1411–1417. https://doi.org/10.1021/acs.estlett.5c00678.

(3) Pan, Z.; Li, S.; Zhao, Q.; Li, J.; Dong, Y.; Borthwick, A. G. L.; Sun, W.; Xu, N. Anthropogenic PFAS or Natural Products? Natural Products Cause Overestimation of C2–C5 Perfluoroalkyl Carboxylic Acid Levels. *Environ. Sci. Technol.* **2025**, *59* (22), 11194–11204. https://doi.org/10.1021/acs.est.4c12934.

(4) Freeling, F.; Behringer, D.; Heydel, F.; Scheurer, M.; Ternes, T. A.; Nödler, K. Trifluoroacetate in Precipitation: Deriving a Benchmark Data Set. *Environ. Sci. Technol.* **2020**, *54* (18), 11210–11219. https://doi.org/10.1021/acs.est.0c02910.

(5) Henne, S.; Storck, F. R.; Wöhrnschimmel, H.; Leuenberger, M.; Vollmer, M. K.; Reimann, S. Trifluoroacetate (TFA) in Precipitation and Surface Waters in Switzerland: Trends, Source Attribution, and Budget. Gases/Field Measurements/Troposphere/Chemistry (chemical composition and reactions) June 27, 2025. https://doi.org/10.5194/egusphere-2025-2861.

(6) Björnsdotter, M. K.; Yeung, L. W. Y.; Kärrman, A.; Jogsten, I. E. Mass Balance of Perfluoroalkyl Acids, Including Trifluoroacetic Acid, in a Freshwater Lake. *Environ. Sci. Technol.* **2022**, *56* (1), 251–259. https://doi.org/10.1021/acs.est.1c04472.

(7) Chen, H.; Zhang, L.; Li, M.; Yao, Y.; Zhao, Z.; Munoz, G.; Sun, H. Per- and Polyfluoroalkyl Substances (PFASs) in Precipitation from Mainland China: Contributions of Unknown Precursors and Short-Chain (C2 C3) Perfluoroalkyl Carboxylic Acids. *Water Research* **2019**, *153*, 169–177. https://doi.org/10.1016/j.watres.2019.01.019.

(8) Pike, K. A.; Edmiston, P. L.; Morrison, J. J.; Faust, J. A. Correlation Analysis of Perfluoroalkyl Substances in Regional U.S. Precipitation Events. *Water Research* **2021**, *190*, 116685. https://doi.org/10.1016/j.watres.2020.116685.

(9) Wang, Q.; Wang, X.; Ding, X. Rainwater Trifluoroacetic Acid (TFA) in Guangzhou, South China: Levels, Wet Deposition Fluxes and Source Implication. *Science of The Total Environment* **2014**, *468–469*, 272–279. https://doi.org/10.1016/j.scitotenv.2013.08.055.

(10) Taniyasu, S.; Kannan, K.; Yeung, L. W. Y.; Kwok, K. Y.; Lam, P. K. S.; Yamashita, N. Analysis of Trifluoroacetic Acid and Other Short-Chain Perfluorinated Acids (C2–C4) in Precipitation by Liquid Chromatography–Tandem Mass Spectrometry: Comparison to Patterns of Long-Chain Perfluorinated Acids (C5–C18). *Analytica Chimica Acta* **2008**, *619* (2), 221–230. https://doi.org/10.1016/j.aca.2008.04.064.

(11) Scott, B. F.; Spencer, C.; Mabury, S. A.; Muir, D. C. G. Poly and Perfluorinated Carboxylates in North American Precipitation. *Environ. Sci. Technol.* **2006**, *40* (23), 7167–7174. https://doi.org/10.1021/es061403n.

(12) Scott, B. F.; Mactavish, D.; Spencer, C.; Strachan, W. M. J.; Muir, D. C. G. Haloacetic Acids in Canadian Lake Waters and Precipitation. *Environ. Sci. Technol.* **2000**, *34* (20), 4266–4272. https://doi.org/10.1021/es9908523.

(13) Scott, B. F.; Spencer, C.; Martin, J. W.; Barra, R.; Bootsma, H. A.; Jones, K. C.; Johnston, A. E.; Muir, D. C. G. Comparison of Haloacetic Acids in the Environment of the Northern and Southern Hemispheres. *Environmental Science and Technology* **2005**, *39* (22), 8664–8670. https://doi.org/10.1021/es050118l.

(14) Wujcik, C. E.; Cahill, T. M.; Seiber, J. N. Determination of Trifluoroacetic Acid in 1996 - 1997 Precipitation and Surface Waters in California and Nevada. *Environmental Science and Technology* **1999**, *33* (775), 1747–1751. https://doi.org/10.1021/es980697c.

(15) Von Sydow, L. M.; Grimvall, A. B.; Borén, H. B.; Laniewski, K.; Nielsen, A. T. Natural Background Levels of Trifluoroacetate in Rain and Snow. *Environmental Science and Technology* **2000**, *34* (15), 3115–3118. https://doi.org/10.1021/es9913683.

(16) Berg, M.; Müller, S. R.; Mühlemann, J.; Wiedmer, A.; Schwarzenbach, R. P. Concentrations and Mass Fluxes of Trifluoroacetic Acid in Rain and Natural Waters in Switzerland. *Environmental Science and Technology* **2000**, *34* (13), 2675–2683. https://doi.org/10.1021/es990855f.

(17) Frank, H.; Klein, A.; Renschen, D. Environmental Trifluoroacetate. *Nature* **1996**, *382*, 34. https://doi.org/10.1038/382034a0.

(18) Wu, J.; Martin, J. W.; Zhai, Z.; Lu, K.; Li, L.; Fang, X.; Jin, H.; Hu, J.; Zhang, J. Airborne Trifluoroacetic Acid and Its Fraction from the Degradation of HFC-134a in Beijing, China. *Environmental Science and Technology* **2014**, *48* (7), 3675–3681. https://doi.org/10.1021/es4050264.

(19) Kanakidou, M.; Dentener, J.; Crutzen, P. J.; Dentener, F. J.; Crutzen, P. J. A Global Three-Dimensional Study of the Fate of HCFCs and HFC-134a in the Troposphere. *Journal of Geophysical Research* **1995**, *100* (D9), 18781–18801. https://doi.org/10.1029/95jd01919.

(20) Martin, J. W.; Mabury, S. A.; Wong, C. S.; Noventa, F.; Solomon, K. R.; Alaee, M.; Muir, D. C. G. Airborne Haloacetic Acids. *Environ. Sci. Technol.* **2003**, *37* (13), 2889–2897. https://doi.org/10.1021/es026345u.

(21) David, L. M.; Barth, M.; Höglund-Isaksson, L.; Purohit, P.; Velders, G. J. M.; Glaser, S.; Ravishankara, A. R. Trifluoroacetic Acid Deposition from Emissions of HFO-1234yf in India, China, and the Middle East. Atmospheric Chemistry and Physics 2021, 21 (19), 14833–14849. https://doi.org/10.5194/acp-21-14833-2021.

(22) Wang, Z.; Wang, Y.; Li, J.; Henne, S.; Zhang, B.; Hu, J.; Zhang, J. Impacts of the Degradation of 2,3,3,3-Tetrafluoropropene into Trifluoroacetic Acid from Its Application in Automobile Air Conditioners in China, the United States, and Europe. *Environ. Sci. Technol.* **2018**, *52* (5), 2819–2826. https://doi.org/10.1021/acs.est.7b05960.

(23) Luecken, D. J.; Waterland, R. L.; Papasavva, S.; Taddonio, K. N.; Hutzell, W. T.; Rugh, J. P.; Andersen, S. O. Ozone and TFA Impacts in North America from Degradation of 2,3,3,3-Tetrafluoropropene (HFO-1234yf), a Potential Greenhouse Gas Replacement. *Environmental Science and Technology* **2010**, *44* (1), 343–348. https://doi.org/10.1021/es902481f.

(24) Henne, S.; Shallcross, D. E.; Reimann, S.; Xiao, P.; Brunner, D.; O'Doherty, S.; Buchmann, B. Future Emissions and Atmospheric Fate of HFC-1234yf from Mobile Air Conditioners in Europe. *Environmental Science and Technology* **2012**, *46* (3), 1650–1658. https://doi.org/10.1021/es2034608.

(25) Kazil, J.; McKeen, S.; Kim, S.-W.; Ahmadov, R.; Grell, G. A.; Talukdar, R. K.; Ravishankara, A. R. Deposition and Rainwater Concentrations of Trifluoroacetic Acid in the United States from the Use of HFO-1234yf. *Journal of Geophysical Research: Atmospheres* **2014**, *119* (24), 14,059-14,079. https://doi.org/10.1002/2014JD022058.

(26) Kotamarthi, V. R.; Rodriguez, J. M.; Ko, M. K. W.; Tromp, T. K.; Sze, N. D.; Prather, M. J. Trifluoroacetic Acid from Degradation of HCFCs and HFCs: A Three-Dimensional Modeling Study. *Journal of Geophysical Research* **1998**, *103* (D5), 5747–5758. https://doi.org/10.1029/97JD02988.

APPENDIX D

SUPPLEMENT FOR CHAPTER 5

Quantifying the Global Reach of Trifluoroacetic Acid: Contrasting Total Deposition between the Southern and Northern Hemispheres.

Section D-1: Methods

Sample collection

Precipitation samples were collected at the University of Guyana, Turkeyen Campus, Guyana (GEO: 6.811ºN, 58.115ºW) from December 2021 to July 2023 and a complementary sampling site was also deployed in Lambton County, Ontario, Canada (LC: 43.222 ºN, 81.870ºW) from January 2022 to July 2023. Total deposition samplers details are provided elsewhere.[1]

Figure D-1: Total deposition samples installed at (A) Georgetown, Guyana and (B) Lambton County.

Sample Preparation

All apparatus was rinsed three times with deionized water (DIW; 18.2 MΩ·cm at 25 ºC, Direct 8; EMP Millipore) and twice with ³ 99.8 % HPLC grade methanol before use. After collection, all sample volumes were measured for flux calculations, transferred to precleaned HDPE bottles and kept refrigerated until analysis. Before analysis, all

samples were allowed to equilibrate at room temperature for at least 30 minutes, then a 10 mL aliquot was withdrawn into a polypropylene syringe (P/N: 14-817-44. Fischer Scientific) and filtered through a 0.22 µm nylon syringe filter (P/N: 76479-030, VWR) into a precleaned polypropylene conical tube (14-959-53A, Fisher Scientific). Then an 800 µL sample was transferred to a 1.0 mL polypropylene vial (5182-0567, Agilent) along with 100 µL $^{13}C_2$ or $^{13}C_1$ (20 µg L^{-1}) TFA internal standard (IS), purchased from Toronto Research Chemicals.

Sample analysis

TFA was quantified using an ICS-6000 ion chromatography system coupled to an ISQEC single quadrupole mass spectrometer (Thermo Fisher Scientific). A sample volume of 750 µL was injected into a Dionex™ IonPac Low Pressure Trace Anion Concentrator Column (5 mm x 23 mm), and separation was performed on a Dionex IonPac AS24 microbore analytical column (2 x 250 mm) and Dionex™ IonPac AG24A guard column (4 x 50 mm) set to 35 ºC. The flow was suppressed using Dionex ADRS 600 Dynamically Regenerated Suppressor (2 mm) in legacy mode at 87 mA with external water supplied at 1 mL min^{-1} using an auxiliary pump. Chromatographic conditions are further summarized in Table D-1. In the effluent from the suppressor, external methanol was teed in at 0.20 mL min^{-1} using another auxiliary pump before the flow entered the MS electrospray source. The MS has unit mass resolution and was operated in selected ion mode to quantify TFA (m/z 113), $^{13}C_1$ TFA (m/z 114), and $^{13}C_2$ TFA (m/z 115). Mass spectrometric conditions are summarized in Table D-2

Table D-1: Instrumental Method Details

Column Temperature	35 °C	
Mobile Phase A	DIW	
Mobile Phase B	100 mM NaOH	
Flow Rate	0.350 mL/min	
Gradient Program	Time (min)	%B
	0.0	10.0
	7.0	10.0
	10.0	27.0
	16.5	32.0
	20.0	50.0
	22.0	60.0
	25.0	60.0
	25.1	10.0
Injection Volume	750 µL	
Length of Method	30 min	

Table D-2: Mass spectrometry method details for TFA analysis.

Instrument	ISQEC single quadrupole mass spectrometer
Scan Type	Selected Ion Monitoring
Vaporizer Temperature	450 ºC
Ion Transfer Temperature	250 ºC
Source Voltage	-3000 V
Sheath gas pressure	45 psi
Auxiliary gas pressure	5 psi

Limit of Detection (LOD) and Limit of Quantitation (LOQ)

The limit of detection (LOD) and limit of quantitation (LOQ) represent the lowest signal distinguishable from the blank and the lowest quantity determination, respectively. The signal-to-noise ratio was found using three sets of DIW blanks and three sets of calibration curves. The average and standard deviation of detector signal from the deionized water blanks, along with the peak heights and their standard deviations from the calibration curve standards, were used to calculate the signal-to-noise (S/N) ratio for the blanks and each standard. As opposed to the typical signal vs concentration plot, a S/N ratio vs calibration level was plotted to obtain a slope where the line is forced through the origin. The LOD and LOQ with mass of TFA per volume units were calculated from the slope using the equations: LOD = 3/m and LOQ = 10/m, where m is the slope (y = mx). The LOD and LOQ for TFA were determined by this method as 6 and 21 ng L^{-1} respectively.

Quality Control and Quality Assurance

Extensive care was taken throughout sample collection, handling and analysis to minimize the risk of contamination that could compromise our trace analysis of TFA. The samplers were thoroughly cleaned with DIW (18.2 MΩ·cm at 25 ºC, Direct 8; EMP Millipore) and twice with ³ 99.8% HPLC grade methanol before deployment. All personnel avoided the use of commercial or personal care products that may contain TFA and other PFAS during collection and sample processing.

Comprehensive QA/QC procedures were applied during sample preparation and instrumental analyses to assess random and systematic error. Isotopically labelled TFA standards were used for analyte quantification. Method precision was assessed using the percent relative standard deviation (% RSD) derived from the slopes of replicate linear calibration curves (n=6) was 13%. Accuracy was determined by calculating the percent relative error (%RE) of 0.25 µg L^{-1} check standards, which was 5%. To ensure continuous data quality, method blanks and check standards were systematically analyzed after every ten sample injections.

Section D-2: Concentration and Fluxes of TFA

Flux Estimation

Concentration of PFAAs in precipitation is influenced by volume and is not useful for determining trends related to depositional inputs at the atmosphere-surface interface. To normalize the effect of deposition volume and sample collection duration, we calculated deposition fluxes (μg m^{-2} a^{-1}) for TFA using the following formula:

$$\text{Deposition Flux} = \left[\frac{\text{analyte concentration } \left(\frac{\mu g}{L}\right) \text{x volume of sample(L)}}{\text{Area of static sampler } (m^2) \text{ / number of sampling days}} \text{ x } 365 \frac{\text{days}}{\text{year}}\right]$$

We normalize the deposition rates based on the sampling days and scale them to an annual basis equivalence. This method ensures consistency of comparison across different sampling periods and facilitates robust comparisons of atmospheric deposition trends.

Table D-3: Mean TFA concentration (µg L^{-1}) and deposition flux (µg m^{-2} a^{-1}) in total deposition samples collected from GEO for the entire sampling period. The cumulative error for deposition flux measurements was calculated using the error in the measurements in the check standard processing, errors in the precision and error in the volume collected by each sampler, where the error in each parameter is divided by the corresponding value, then squared and summed with the other terms. The measurements highlighted in red highlights an instance when the sampler overflowed, resulting in an underestimation of deposition flux.

Sampling Start	Sampling End	Concentration (µg/L)	Deposition Flux (µg m^{-2} a^{-1})	Deposition Flux Error (µg m^{-2} a^{-1})
16-12-2021	17-01-2022	0.12	1753	244
17-01-2022	22-04-2022	0.17	2019	281
22-04-2022	23-05-2022	0.12	4205	586
23-05-2022	14-07-2022	0.11	2337	325
14-07-2022	13-08-2022	0.13	4199	585
13-08-2022	01-06-2023	0.13	1014	141
01-06-2023	02-06-2023	0.17	3912	545
02-06-2023	03-06-2023	0.13	3291	458
03-06-2023	04-11-2023	0.56	3629	506
04-11-2023	05-08-2023	0.18	5374	749
05-08-2023	06-09-2023	0.19	6641	925
06-09-2023	07-10-2023	0.17	5039	702

Table D-4: Mean TFA concentration (µg L^{-1}) and deposition flux (µg m^{-2} a^{-1}) in total deposition samples collected from LC for the entire sampling period. The cumulative error for deposition flux measurements was calculated using the error in the measurements in the check standard processing, errors in the precision and error in the volume collected by each sampler, where the error in each parameter is divided by the corresponding value, then squared and summed with the other terms.

Sampling Start	Sampling End	Concentration (µg/L)	Deposition Flux (µg m-2 a-1)	Deposition Flux Error (µg m^{-2} a^{-1})
27/01/2022	04-02-2022	0.37	2499	348
04-02-2022	23/05/2022	0.99	5863	817
23/05/2022	07-04-2022	0.88	4493	626
07-04-2022	26/08/2022	0.33	4560	636
26/08/2022	26/11/2022	0.43	4324	603
26/11/2022	21/02/2023	0.41	2281	318
21/02/2023	28/03/2023	0.34	1969	275
28/03/2023	14/05/2023	0.28	3057	426
14/05/2023	15/07/2023	0.92	4156	579
15/07/2023	13/08/2023	0.41	15242	2124
13/08/2023	27/08/2023	0.51	19451	2711
27/08/2023	15/10/2023	0.49	3300	460